Energy

FOSSIL

MEASUREMENT AND CORRELATION OF CONDITIONS FOR ENTRAPMENT AND MOBILIZATION OF RESIDUAL OIL

Final Report for the Period January 1981—March 1984

October 1984
Date Published

New Mexico Institute of Mining and Technology
Socorro, New Mexico

Technical Information Center
Office of Scientific and Technical Information
United States Department of Energy

DISCLAIMER

MEASUREMENT AND CORRELATION OF CONDITIONS
FOR ENTRAPMENT AND MOBILIZATION OF RESIDUAL OIL

Final Report
January 1981--March 1984

Norman R. Morrow--Principal Investigator

Contributors:

Research Engineers	Ioannis Chatzis
	Murty Kuntamukkula
Research Chemist	Jill Ward
Visiting Scientists	Vladimir Hornof
	Geoffrey Mason
Research Associate	Hau Lim
Technicians	Earl Barber
	Mary Graham
	Mary Paneral
	Shangshi Shu
Undergraduates	Dana Hope
	Margaret Ward

New Mexico Petroleum Recovery Research Center
New Mexico Institute of Mining and Technology

Fred Burtch--Technical Project Officer
Bartlesville Project Office
P.O. Box 1398
Bartlesville, Oklahoma 74005

MASTER

TABLE OF CONTENTS

LIST OF TABLES

ABSTRACT

This is the final report of a two-year project which had four major task areas. Work is reported according to task. A substantial portion of work carried out under this project has been reported in detail in journals, the First Annual Report to the Department of Energy or in manuscripts which have been submitted for publication and are available on request. In such cases only major conclusions are reported, along with reference to the detailed accounts.

The first task was to investigate the limits of reliability of laboratory waterflooding as an evaluation tool. In systematic study of the influence of various factors on residual oil saturation, wettability was identified as a key variable. Task 1 consists of two parts. Part 1.a. reports results for residual oil saturation attained by waterflooding. Part 1.b. reports contact angle measurements made during the course of investigating wettability changes induced by crude oil.

A systematic study was made of factors which might affect residual oil. These included end effects, core size, viscosity ratio, core lithology, overburden pressure and wetting conditions. Wettability was identified as a key variable. Supplementary contact angle studies were made on typical laboratory fluids and the effect of crude oil on wettability. One particular crude, Moutray, was selected, mainly on the basis of its surface activity, for detailed study and was subsequently used as a wettability alteration agent in core flooding studies. With Moutray crude as the oil phase, results as compared with a clean mineral (Soltrol) were as follows: initial water saturations tended to be lower, residual oil saturations were about 5% lower, and microscopic displacement efficiencies increased by 25%. Further work is planned for testing the generality of these results. This would include investigation of the mechanism of wettability alteration which appears to lead to improved recovery.

The second task concerns the effects of high capillary number flows on trapping phenomena and residual oil saturation. Correlations of capillary number and relative permeability behavior at reduced residual saturations have been developed for displacement in sandstones. One application of the correlations is to provide corrections for flushing of residual oil in the region of the wellbore where pressure gradients are abnormally high. Results have also been obtained for two distinctly different types of carbonate rock. For one of these, a sucrosic (Baker) dolomite, the capillary number curves differed little from the general correlation developed for sandstones. However, for a suite of Caddo limestones, capillary numbers for mobilization of residual oil were about 10 to 100 times lower than was observed for sandstones and the sucrosic carbonate. For the Caddo formation, requirements for enhanced recovery will be much less stringent than normally expected. However, wellbore flushing could be a serious problem with respect to its effect on in situ determination of residual oil. Corrections to residual saturation for flushing around the wellbore for systems giving capillary number behavior comparable to the Caddo limestone are presented.

The effect of wettability on capillary number relationships has also been investigated using Berea sandstone. Wettability change was induced by means of the Moutray crude oil identified as a wettability alteration agent under Task 1.

It was found that crude oil induced wettability increased the capillary number required for mobilization by a factor of about five.

Another aspect of residual oil, investigated during the course of these experiments, was the relationship between electrical conductivity and reduced residual oil saturation, achieved both by high flow rates and by lowering of interfacial tensions. A large amount of data was taken partly because results showed considerable scatter. However, confidence limits were generally not much worse than those on which accepted log analysis relationships are based. The main conclusion of this work was that the Archie exponent for the reduced residual oil regime was close to 1, as compared with values closer to 2 which are typical for higher water saturations.

The third task, reported in three parts, deals with the mechanism of entrapment and mobilization and associated fundamental capillary phenomena. A detailed account of work under Task 3.a. on factors which influence the magnitude and detailed structure of residual oil has been presented and published. Comparison of the effects of extreme types of pore structure with aspect ratio identified as a key variable has been made.

A study of the stability of displacement fronts in micromodels formed from sintered bead packs of about 10 layers thickness is reported under Task 3.b. The thin models permitted the effects of varying interfacial tension, coalescence time, viscosity ratios and density differences to be followed directly and recorded on videotape. At low tensions, effects of gravity segregation are particularly severe even in thin layer models.

A theoretical and experimental study of the effect of pore geometry and wettability on displacement curvatures was also prepared under the third task. A theory forwarded by Mayer and Stowe and also by Princen has been found to be remarkably powerful in application over a wide range of circumstances. Extensions of the theory are proposed for application to pore shapes found in random sphere packs under varying contact angle. Theory and experiment were found to be in good agreement for systems of zero contact angle. Circumstances under which the theory serves as a good approximation for displacement curvatures in pore throats formed by spheres are discussed.

The fourth task involved study of the detailed structure of residual oil and the changes that take place during recovery. To this end, the technique of using a nonwetting phase which will solidify and can be separated from the rock has been applied. The size distribution of residual oil blobs, obtained under various displacement conditions, is being measured by various size-analysis methods. Detailed account is given of the application of the Coulter Counter method to this unusual problem in size analysis. This work provides insight into the mechanisms by which residual oil can be moved, and more quantitative understanding of why the difficulty of recovering oil increases as the amount which remains is reduced. The technique has also been applied to determining residual oil structure in carbonate rock.

TASK 1. RESIDUAL SATURATION MEASURED BY LABORATORY CORE FLOODING

BACKGROUND

The need for accurate determination of residual oil saturation in the swept zone of a waterflood in reservoir evaluation for tertiary oil recovery is now widely recognized.[1.1] Estimates of the amount of residual oil remaining after waterflooding are often derived from results of laboratory waterflood tests. Incentive for the development of tertiary methods was, for the most part, based on these estimates. When surfactant processes were first field tested, recoveries fell considerably below expectations; low waterflood residuals in the formation were one suspected cause. Results of 76 single well tracer tests[1.2] show that over one-third of the tested reservoirs have residual saturations in the range of 10 to 15%. These values, in general, are unusually low compared with those typically obtained by laboratory waterflooding.

The main reasons why laboratory waterflood residuals were generally accepted prior to the advent of tertiary recovery methods, were: (1) apart from estimates of recoverable reserves related to proration allowances, the amount of oil remaining after waterflood was of little economic significance compared to that produced; and (2) it was generally believed that most reservoirs were strongly water-wet and that their condition could be readily simulated in the laboratory in displacements that involved use of suitable brine and a light mineral oil.

Attempts to duplicate displacement in the reservoir are now commonly made by carrying out reservoir-condition laboratory waterfloods. However, unless reliable in situ measurements of residual oil are available, there is essentially no standard against which laboratory results can be checked. Examples of extreme differences in laboratory waterflood and field measurements of residual oil, which could not be wholly ascribed to problems in sampling, caused loss of acceptance of laboratory measurements as a reliable means of estimating residual oil. For many practical reasons, laboratory-established residual oil saturations must continue to be used in testing tertiary oil processes, even though these saturations may not be representative of the target formation with respect to either magnitude or distribution. In this respect, test results obtained using Berea outcrop sandstone could be misleadingly optimistic because residual oil saturations in this type of rock appear to be relatively high.

The uncertainties that exist in relating laboratory testing results to the reservoir point to the need for investigation of factors which might affect the magnitude of residual oil saturation in laboratory flooding tests. The broad objective of this work is to determine the variation of residual oil that can occur in a given core. This will help to identify problems that can arise in core testing and indicate limits of reliability of laboratory flooding as an evaluation tool for secondary and tertiary recovery. Results of this work are presented under section 1.a.

Wettability variation has been identified as a dominant but poorly understood variable in core flooding behavior. In the first stage of this study,

the likely wettability conditions pertaining to most laboratory flooding tests were investigated through contact angle studies. Details of this work have been presented.[1,3] An important conclusion with respect to laboratory systems commonly regarded as water-wet was that advancing and receding contact angles were low ($\theta_R < \theta_A < 30°$) but the systems would not generally be completely wetted ($\theta_R = \theta_A = 0°$). Systems giving low angles on smooth surfaces also gave low angles on rough surfaces including samples of sandstone, carbonate and talc. In the past year, attention has been turned to study of wetting conditions induced by crude oil. Results of this work are presented under section 1.b.

1.a. CORE FLOODING EXPERIMENTS

The reliability of laboratory waterflooding as an evaluation tool has been examined by studying the sensitivity of laboratory-measured residual saturations to the manner in which the displacement tests are carried out. Test procedures were chosen which provided reproducible results. Variables investigated included core material, core dimensions, properties of displaced and displacing fluids (including viscosities and viscosity ratios), overburden pressure, flooding rate, and wetting conditions.

In reporting core displacement results, we first presented displacements carried out using systems which provide strongly wetted conditions. This is followed by results of a study of crude oil induced wettability alteration and its effect on laboratory waterflood residual oil saturation.

Core Material and Preparation

Core plugs for these experiments were cut from quarried rock slabs and full diameter cores of 1.5, 1.0 and 0.75 inches. Diamond core drills, cooled with tap water, and an electric diamond-blade saw were used to cut and trim cores. The cores were then dried in an oven at 100°C for 24 hours, followed by cooling in a dessicator. Some cores were fired in a muffle furnace at 800°C for about 2 hours and then allowed to cool slowly to room temperature in the furnace. Vugular materials received as core plugs were usually encased in epoxy resin to facilitate mounting in the core holder.

Test Procedures, Initial-Residual Relations, and Reuse of Cores

Cores were mounted in one of three types of core holders: Hassler core holders; end-plate core holders (for epoxied cores); and Amoco-design core holders (designed for confining pressures of up to 10,000 psi). After

2

determination of specific permeability to gas, the sample was transferred to a stainless steel core saturator, and vacuum was applied until a reading of about 200 millitorr was reached. Previously degased 2% $CaCl_2$ brine was then introduced, and the core was left immersed overnight. Pore volume and porosity were calculated from the difference in weight between the dry and brine-saturated core. Absolute permeability to brine was measured for a range of pressure differences. Then the core was flooded with oil at about 250 to 350 psi/ft to establish an equivalent connate water saturation. Direction of flooding was reversed in order to alleviate end effects. Waterflood displacement pressures were generally lower than 10 psi/ft. If very low pressure gradients were required, the apparatus was modified so that flooding pressure was controlled by hydrostatic head. The test sample was weighed before and after each displacement to determine initial and residual oil saturations.

To repeat the experiment or carry out further work on the same core, high initial oil saturation in the sample was reestablished by one of the following techniques: 1) oilflooding the core at high pressure gradients; 2) cleaning the sample with 15 PV of IPA (isopropyl alcohol) followed by 15 PV of 2% $CaCl_2$ brine and finally flooding with oil; or 3) cleaning the core sample with IPA, oven drying, remeasuring air and water permeabilities, and then flooding with oil. Experience showed that Berea cores, fired at 800°C, gave better reproducibility than unfired cores in repeated high capillary number flooding experiments.[1,4] This practice was therefore generally followed in the course of measuring waterflood residual oils, particularly when the flooded-out core was subsequently used in high capillary number displacement tests, results of which are presented under Task 2.

Macroscopic Distribution of Residual Fluids

A set of experiments was conducted to see whether a saturation gradient results from the process of oilflooding and waterflooding described above. A Berea sandstone core of 3.80 cm diameter and 5.87 cm length was cut into two pieces of 3.64 and 2.22 cm length. With the position of the cores in the Hassler core holder identified, a Millipore prefilter pad soaked in brine was placed between the two pieces of core. The composite core was oilflooded in one direction at high pressure gradient to connate water saturation. The cores were weighed to determine initial oil saturations, S_{oi}, and replaced in the core holder with an oil-soaked pad at the contact. An oil flood in the opposite direction was run by reversing the position of the core holder. The cores were again weighed to determine S_{oi}. Waterflooding displacements were conducted in a similar manner.

This procedure was used in two sets of displacements, one with Soltrol 130/2% $CaCl_2$ brine and the second with Soltrol 220/2% $CaCl_2$ brine. The following observations were made: 1) after flooding in one direction, there was a significant difference in nonwetting phase saturation between the upstream and downstream sections of cores tested, presumably because of capillary end effect. Upstream oil saturations were about 5 to 9% higher than those in the downstream section; 2) uniform distribution of initial oil saturation, S_{oi}, could be

attained by flooding the core and then reversing the direction of flooding; and 3) core segments initially at comparable values of initial oil saturation did not, after waterflooding, show any significant differences in residual oil saturations. Thus, significant gradients in residual oil saturation are unlikely for the experiments described below for which initial oil saturations have been established by flooding in both directions.

The effect of using very short cores was tested using Berea sandstone 1.59 cm (diameter 1.91 cm) long. Values of residual saturation for three runs were 33.9% in two instances and 30.2% in the other. These results are close to the range observed for larger sizes of sample. Thus, it appears that the normal size of test core should be more than sufficient to give a value of residual saturation properly representative of the core matrix.

Factors Influencing Residual Oil Saturation

Viscosity Ratio

Experimental work on the effect of viscosity ratio was conducted on seven consolidated sandstone samples with brine permeabilities in the range of 68 to 633 md. Seven oils, listed in Table 1.1, were used as the nonwetting phase. Viscosities ranged from 0.38 to 168 cp. A summary of core properties and displacement results is given in Table 1.2. Endpoint waterflood residual oil saturations varied from 27 to 37% PV for these samples. Displacements with a low viscosity oil (heptane, 0.38 cp) gave relatively low initial oil saturations and correspondingly low waterflood residual oil saturations. However, the ratios of residual to initial oil saturation for these displacements were close to those observed for displacements with oils of much higher viscosity. While the relationship between S_{oi} and S_{or}^* is not necessarily linear, the ratio of these two saturations is fairly constant, ranging from 0.5 to 0.58 for the cores used in obtaining the results presented in Table 1.2. A similar range (0.53 to 0.58) is given by end-point residuals reported by Felsenthal and Yuster for a consolidated sandstone.[1,3] In addition to showing that the effect of viscosity on residual oil saturation is likely to be quite minor, the results in Table 1.2 show the importance of establishing a properly representative connate water saturation and distribution as a first step in laboratory determination of waterflood residual oil saturations. The close reproducibility of results for a given core sample indicates that further work would probably yield definitive relationships between initial and residual oil saturations. Possible effects of oil viscosity on these relationships might also be detected.

Core Lithology - Vugular Carbonates

Residual oil saturations were measured for several limestones supplied by Sun Exploration and Production Co. The cores were from Ward "D" No. 2, Breckenridge Field, Stephens County, Texas. Since the majority of the cores were vuggy, some samples were epoxied with Devcon baking compound (liquid type, 9:1 ratio of epoxy to hardener by volume) prior to testing. Samples had air

permeabilities ranging from 29 to 680 md and porosities from 14 to 20% PV. Core properties and flooding data are given in Table 1.3. For the five samples tested, waterflood residuals ranged from 20 to 34% PV, with initial oil saturations ranging from 33 to 58% PV. Microscopic displacement efficiencies (defined as $S_{oi} - S_{or}^*/S_{oi}$) ranged from 0.24 to 0.52, as compared with 0.42 to 0.50 obtained for the sandstones. One distinct difference between the vugular carbonates and the sandstones was that residual oil saturations showed sensitivity to flooding rate, in some cases for capillary numbers of about 10^{-7}. Thus, careful attention should always be paid to the effects of flow rate, and the effect of say a five to ten fold increase in flooding rate on residual oil should be measured for cores for which rate sensitivity might be suspected. Further discussion of the effect of rate on residual oil is presented under discussion of capillary number relationships (Task 2).

Overburden Pressure

Core floods have been run on sandstone and carbonate samples in which waterflood residual oils were established at low overburden pressure. The overburden pressure was then increased from 500 to 5000 psi. Results are given in Table 1.4 for a low permeability carbonate MCA3 (brine permeability of 0.5 md at 500 psi overburden pressure) and for a Berea sandstone EH1 (brine permeability of 176 md at 500 psi overburden). Once residual oil was established, increasing the overburden pressure to 5000 psi did not cause production of additional oil, even though the effective permeability to water at residual oil for the carbonate core MCA3 decreased by as much as 45%.

Displacement tests at various levels of overburden pressure ranging from 500 to 5000 psi were carried out on the Berea sandstone core EH1. The results, presented in Table 1.5, show that neither initial nor residual oil saturations changed significantly with the level of overburden at which they were established.

Wetting Conditions

A 55 gallon drum of Moutray crude oil was obtained from Montfort Drilling Co., Baird, Texas. This oil was known from contact angle studies (see section 1.b.) to produce high contact angles on a smooth glass surface, suggesting that it is likely to have similar effect on rock wettability. A summary of core properties and waterflooding data is presented in Table 1.6 for floods with this oil. The cores had brine permeabilities ranging from 70 to 3300 md. With the exception of cores S6C and S6E, the samples had been soaked in Moutray crude at initial oil saturation, S_{oi}, for more than 2 hours. Following a waterflood at low capillary numbers, the values of residual saturation, S_{or}^*, after flooding with less than 2 1/2 pore volumes were found to range from 24.4 to 34.4% PV. The mean value was 28.6%, S.D. 3.1%. Initial oil saturations, S_{oi}, varied from 57.6 to 71.8% PV. The residual oil saturations were about 5% of pore volume lower than those observed for flooding under water-wet conditions at favorable viscosity ratios, for which the mean value of S_{or}^* was 33.7% with S.D. of 2.3%. However, since initial water saturations were generally lower for the treated cores, the fractions of initial oil recovered were significantly greater than the

recoveries obtained under water-wet conditions. Microscopic displacement efficiencies [the ratio of recovered oil to that initially in place, $(S_{oi} - S_{or}^*)/S_{oi}$] for the water-wet cores were typically in the range 0.42 to 0.48 with a mean value of 0.46; for the treated cores, the values ranged from 0.50 to 0.62 with a mean of 0.56 and standard deviation of 0.04. The average increase in microscopic displacement efficiency of about 25% for the altered cores could well be significant. Recovery of the type reported by Salathiel[1.6] that occurs with prolonged flooding was not detected. A modified apparatus which will permit more direct observation of breakthrough curves and possible slow rates of oil production with continued flooding is now being constructed. Further work should be carried out on other types of core material to test the possible generality of these observations.

This behavior could be a contributing factor in the low residual saturations observed by in situ techniques. It also indicates that recovery might be improved in water-wet reservoirs by the relatively simple expedient of injecting crude oil capable of suitable wettability alteration ahead of a waterflood.

1.b. CONTACT ANGLE MEASUREMENTS

INTRODUCTION

In the previous section, the effect on core flooding of a wettability change induced by Moutray crude oil was reported. Futher discussion of wetting effects on trapping and mobilization of residual oil will be included under Task 2. Contact angles between oil, water and solid provide a measure of wettability which has been used to study further wetting changes induced by crude oil. Such measurements were made in screening crude oils and selecting Moutray crude as an agent for wettability alteration.

In a previous report we presented the results of contact angle measurements under carefully controlled conditions.[1.3] These studies concentrated on the influence of brine and the nature of the solid surface on the resulting contact angle. Refined oil and pure hydrocarbon were used as the oil phases. Advancing and receding contact angles for drops of these oils were reported to be generally finite but low. This indicates that most commonly used laboratory systems provide strongly water-wet conditions but not complete spreading.

EXPERIMENTAL

The experimental set-up used to measure contact angles was described in detail in a previous report.[1.3] The method used was the captive bubble technique

similar to that used by Gaudin, et al.[1.7] Briefly, it consisted of a glass cell filled with water (usually redistilled from potassium permanganate) into which is inserted a glass buret containing the oil phase. The contact angle measured was that of a drop expressed from the buret against the bottom of the glass cell. If the size of the oil drop was increased prior to measurement, a water receding angle was measured. As fluid was drawn back into the buret, water advancing angles were recorded. A Gaertner goniometer was used to measure the angles to a precision of 0.5° for a given measurement, although this does not, of course, mean that measurements were reproducible to 0.5°. All measurements were made at ambient temperature and pressure.

Although we are using the familiar terminology of water receding and water advancing to describe the conditions of measurement, we should point out that at least some of these angles are not exactly analogous to those measured by other methods. Receding angles (Fig. 1.1a) are low and fairly reproducible. These are probably not significantly affected by the fact that the bubble of oil is trapped between the glass and the buret, rather than being held by buoyancy like a sessile drop. The behavior observed for advancing angles is a different matter. Here, an irreproducible phenomenon, adhesion of the oil drop to the glass, dominates the results. When the oil drop does not stick, advancing angles are low and not significantly higher than the receding angles. When the oil drop adheres, the three-phase line of contact remains fixed for wide variation in contact angle. The maximum advancing contact angles observed are generally greater than 90° and not highly reproducible. Fig. 1.1b shows a typical series of configurations. The angle observed increases or decreases continuously according to whether the drop size is increased or decreased. The contact line between oil, water and solid is fixed. Eventually a neck forms in the drop and further retraction causes a break in the drop, leaving varying amounts of oil on the glass surface. Capillary instability at the neck (snap-off) limits the advancing angle measured so that it is not necessarily the maximum possible advancing angle. In fact, most of the angles reported here are those for a stable configuration, short of snap-off, between positions 2 and 3 in Fig. 1.1b, so that

$$\theta_R = \theta_R{}^1 < \theta_A{}^1 \leq \theta_A$$

where θ_R and θ_A are limiting contact angles, and $\theta_R{}^1$ and $\theta_A{}^1$ are measured angles. Fig. 1.2 shows the variation of measured ange as drop size is decreased and increased for the same drop at different contact times. These measurements provide useful information about the system behavior at the three-phase contact line, but the quantitative value of much of the data has limitations, partly set by the irreproducibility of the behavior.

The crude oils used in the initial screening tests were samples on hand. No special storage or handling was involved in the crude oil screening. The samples were already available through other PRRC projects and had been on the shelf for varying lengths of time.

Based on the results of this screening, one crude was chosen for further study. Moutray crude, which had given high advancing angles (103 to 116°) in eight tests with 20 minute contact times, seemed a good candidate. A 55 gallon drum of this oil was acquired which was believed to be free of contaminants such

as oilfield additives. Using this sample, we began to investigate which other factors contributed to the variability of observed advancing contact angles.

RESULTS

Contact Angles for Various Crude Oil Samples

Table 1.7 shows some typical results for the screening of dead crude oils. Receding angles are uniformly low, but advancing angles show a wide diversity of behavior. Some samples, like Mule Gulch crude, maintain strong water-wetting, having advancing angles which are not substantially different from the receding angles. Others start with low advancing angles, but then exhibit sticking and show increasing angles as contact time increases, at least for some repetitions of the tests. Morrison crude, for example, gave low advancing angles in eight trials and high (>100°) in three others.

Moutray Crude Oil Contact Angles

One of the oils in Table 1.7, Moutray crude, was selected for more detailed study of the general phenomena described above. In the preliminary work, all eight tests of Moutray had given advancing angles of more than 100° after 20 minutes of contact. Other available samples, stored in different containers, locations and perhaps acquired at different times, showed much less tendency for increases in advancing angles to high values (Table 1.8).

One possible explanation for the erratic results was differences in samples. Gas chromatographic analyses showed some samples had retained more of the light hydrocarbon fraction than others. Other possible differences might have been differences from one sample to the next in exposure to oxygen, storage temperature, or field sampling techniques. The difficulties of evaluating all such differences are clear. Instead, we chose to acquire a large enough sample (55 gallon drum) of a single crude oil, Moutray crude, for further research.

Moutray Crude Oil - Large Sample

Contact angle measurements with the new sample of Moutray crude and of mixtures of Moutray with varying amounts of toluene or isooctane still showed considerable variability in the resulting advancing angles, despite the fact that a single sample was being used. This lack of reproducibility necessitated closer investigation of other variables which might possibly affect the results.

8

A series of measurements with the Moutray-55 sample were made with detailed consideration as to the nature of the duplication, i.e., which involved a single set-up (cell, buret, and fluid samples). Table 1.9 shows results of such duplicate experiments with the apparatus set for a given series of experiments indicated. Similar distinction was made in making measurements with Moutray crude diluted by aromatic and aliphatic oils with results shown in Tables 1.10 and 1.11 respectively.

Discrepancies as high as about 80° were observed from one set-up to another. However, there was an overall improvement in reproducibility; in half the comparisons, differences of less than 15° were observed. This suggests that factors other than the fluid pairs themselves contribute to the variability of the results observed.

Influence of Surface Preparation on Advancing Contact Angles

To study this question further, the cells and burets were given identifying marks (numbers or letters) so that the exact experimental apparatus and its preparation can be specified for each measurement. The cleaning and drying procedure for the cells was an area of concern. In all cases, the cells were soaked for at least 24 hours in Chem-Solv (a biodegradable, high pH glassware cleaner from Mallinkrodt). They were then rinsed in a series of double-distilled water baths. For each set-up, the cells were either filled while still wet or were initially air dried. Conditions are indicated in Table 1.12.

Table 1.12 compares advancing angles for fluid pairs measured in a given cell, using the same burets, the sole difference being whether or not the cell was air dried in between cleaning and filling with distilled water. It was found that the contact angles measured for initially dried cells were consistently higher than those for wet cells (see Table 1.12). It is also of interest to note that wet cells gave the more highly variable results. This is somewhat surprising since the wet cells had less opportunity to become contaminated.

Contact Angles of Moutray on Carbonate Core Surfaces

Interesting preliminary results were also obtained for drops of Moutray in double-distilled water on carbonate core surfaces (Table 1.13). Three tests on the cut surface showed no rise in advancing angle during an hour exposure time. The polished surface behaved quite differently. All five tests showed some increase in advancing angles, though both the initial results and those after one hour varied widely, with high angles developing in 3 out of 5 cases.

9

DISCUSSION AND FURTHER WORK
_____

    A frustrating but dominant feature of the results was the unpredictable wettability changes induced by crude oils. It is worthwhile, however, to review the results in order to help understand the basic phenomena better or at least to find better ways of studying them.

    Some of the variability is, no doubt, due to the lack of precise definition about where and how the water advancing angle is to be measured when the drop size is decreasing. Each operator has been encouraged to be consistent, but guidelines are difficult to provide. The problems of sampling and surface preparation have also been shown to contribute to scatter in the results. A key feature of the behavior is that development of high contact angles is associated with adhesion of the oil drop to the solid surface. Adhesion was less consistently observed for cells which were kept wet, but when it did occur, contact angles were high.

    It is possible that the addition of solvents as well as surface preparation had some influence over the adhesion phenomenon and the magnitude of contact angles obtained subsequent to adhesion. High angles were observed for dilutions of Moutray with toluene (up to 10 parts toluene to 1 part Moutray) and isooctane (1 to 1). Contact angles with isooctane as diluent were, for the limited data obtained, high in all except one case, whereas those with toluene exhibited a variability comparable to that given by the crude oil alone. The solubility of asphaltenes and their adsorption behavior can be expected to be influenced by the nature of the diluent. The effect of isooctane on the asphaltic component of the Moutray crude may explain the more consistent results obtained when isooctane was the diluent.

    A brief investigation of occurrence of adhesion at varying contact times and contact areas for drops of Moutray in the water-filled cell yielded no obvious correlations. Drops were observed to adhere in as little as 5 seconds on occasion while others did not adhere even after much longer exposure times. Some drops gave a symmetrical area of contact while others adhered only to part of the drop-solid area of contact. The latter condition led to unsymmetrical drop shapes as fluids were withdrawn.

    The interaction between crude oil and mineral surfaces has long been ascribed to adsorption of heavy, fairly polar components from the oil.[1,8] Collins and Melrose[1,9] have reported on monolayer adsorption of petroleum asphaltenes onto clays and other reservoir minerals. In the light of the observations and on foregoing experience, another possible approach to investigating changes in wetting caused by crude oils was tested. Crude oil was first used to pretreat the surface and then removed by washing with a solvent. Any resulting wettability alteration was observed by measurement of the contact angles for refined oil and water on the treated surface. A particular advantage of using refined oil is that limiting values of water advancing contact angles can be measured by expanding a drop of water with a clear oil as the surrounding phase.

As a preliminary test of this approach, a glass cell of the same type used in previous experiments was coated with a thin layer of Moutray crude oil which was allowed to remain in the cell overnight to permit adsorption of surface active components from the oil. Washing with toluene, followed by acetone and air drying, removed excess crude oil. The cell was filled with double-distilled water and the buret was filled with refined oil (Soltrol 130). Previous investigation with Soltrol 130 on clean glass showed no tendency of this oil to wet the glass, receding and advancing angles through the water phase being uniformly low (less than 20°). On the treated surface, however, much different contact angle behavior was observed. Water-receding angles were higher (35 to 45°) and the refined oil adhered instantly to the surface. When the oil was withdrawn, high advancing angles (65° and higher in initial tests) were observed.

It was concluded that coating a surface with a layer of some wettability-altering substance from the crude oil which is not readily removed by solvents and which can be tested with pure or well-characterized fluids might offer a way to proceed in the study of wettability alteration by components of crude oil. An in-house (PRRC) project working along these lines is now underway and will be reported on.[1.10]

CONCLUSIONS

a. Core Flooding Experiments

(Conclusions 1-6 are for strongly water-wet systems)

1. Oil saturations established prior to waterflooding by flooding a water-saturated core with oil at high pressure gradient (250 to 700 psi/ft) showed significant end effects, with high water saturations retained at the outlet end of the core. These could be eliminated satisfactorily by reversing the direction of oil flow. Variation in connate water saturation can be achieved by using high pressure gradients in combination with viscous pressure gradients and by extended flooding times.

2. Provided measures were taken to avoid end effects, no significant effect of sample size on residual oil saturation was observed.

3. The amount of oil trapped was strongly dependent on the initial oil saturation. For Berea sandstones, it was observed that the fraction of oil trapped by waterflooding was a fairly constant fraction of the oil in place (0.5 to 0.6). However, results from the literature indicate the microscopic displacement efficiencies can range from 0.1 to 0.83 depending on details of pore structure. In general, attention should be paid to duplicating the connate water saturation found in the reservoir. Otherwise, some form of simple linear correction should be applied to measured waterflood residuals.

11

4. No dependency of residual oil on overburden pressure was observed for confining pressures ranging from 500 to 5000 psi. However, there were significant changes in relative permeability to water at residual oil saturation.

5. Residual oil saturations in consolidated sandstones were independent of flooding rate for capillary numbers ($K_w \Delta P/L \sigma$) up to about 4×10^{-6}. Once residual oil was established, capillary numbers for mobilization of oil were about 2×10^{-5}. Residual oil saturations for some water-wet vugular carbonates were found to be sensitive to flooding rate even at field rates. It is therefore worthwhile, in cases where such behavior is suspected, to determine if any further reduction in oil saturation occurs for say a 10-fold increase in flooding rate.

6. Final residual oil saturations were essentially independent of oil viscosity for viscosities ranging from 2 to 177 cp. There was a tendency for oils of lower viscosity to give initial and residual oil saturations which were slightly lower than those observed for high viscosity oils, but there was little difference in microscopic displacement efficiencies.

7. Change of wetting from strongly water-wet, by means of crude oil, to a condition of intermediate or oil-wetness resulted in lower initial water saturations and, on average, lower residual oil saturations by about 5% of pore volume. Microscopic displacement efficiencies for the altered cores were, on average, about 25% higher than for the water-wet cores. This observation needs to be tested for a wide variety of rock types before general conclusions can be drawn as to the effects on oil recovery of wettability alteration induced by crude oil.

8. Future work on laboratory-determined residual saturations should focus on reservoir core samples where reliable in situ measurements of residual oil saturation have been made. It would be of particular interest to obtain core samples from reservoirs which have unusually low residual saturations, and determine relevant circumstances under which such low residual saturations can be established by laboratory waterflooding.

b. Contact Angle Measurements

9. Some crude oils can change wettability of smooth glass from strongly water-wet toward intermediate to oil-wet conditions.

10. Changes in wettability induced by crude oil are reflected in increases of oil-water-glass contact angles and by large hysteresis between water advancing and water receding contact angles.

11. In wettability measurements such as the captive bubble technique, adhesion of oil to the solid substrate is a critical but not consistently reproducible feature of contact angle development. When adhesion does occur, advancing contact angles are generally high and hysteresis is large. If adhesion does not occur, contact angles are generally low.

12. Pretreatment of the glass surface with crude oil appears to provide a more reliable method of wettability alteration, because it gives adhesion behavior that is far more reproducible. The method permits use of a pure oil phase and use of the captive bubble technique to obtain limiting advancing and receding contact angles with either oil or water as the drop.

REFERENCES

1.1   "Determination of Residual Oil Saturation," Interstate Oil Compact Commission, Oklahoma City, Oklahoma, 1978.

1.2   Carlisle, C.T., Personal Communication, Geochem Research Inc., Houston, TX, 1983.

1.3   Morrow, N.R. and Chatzis, I., "Measurement and Correlation of Conditions for Entrapment and Mobilization of Residual Oil," First Annual Report to the U.S. Department of Energy, Contract No. DE-AS19-80BC10310, September 1982.

1.4   Chatzis, I. and Morrow, N.R., "Correlation of Capillary Number Relationships for Sandstones," SPE 10114, paper presented at the 56th Annual Fall Technical Conference and Exhibition of SPE of AIME, San Antonio, TX, October 5-7, 1981.

1.5   Felsenthal, M. and Yuster, S.T., "A Study of the Effect of Viscosity on Oil Recovery by Waterflooding," Paper No. 163-G, Los Angeles Meeting of the Petroleum Branch of AIME, October 25-26, 1951.

1.6   Salathiel, R.S., "Oil Recovery by Surface Film Drainage in Mixed Wettability Rocks," J. Pet. Tech. (October 1973) 1216-1224.

1.7   Gaudin, A.M., Witt, A.F., and Decker, T.G., "Contact Angle Hysteresis--Principles and Application of Measurement Methods," Trans., AIME 226 (1963) 107.

1.8   Benner, F.C. and Bartell, F.E., "The Effect of Polar Impurities upon Capillary and Surface Phenomena in Petroleum Production," Drill. and Prod. Prac., API (1941).

1.9   Collins, S.H. and Melrose, J.C., "Adsorption of Asphaltenes and Water on Reservoir Rock Minerals," SPE 11800, presented at the International Symposium on Oilfield and Geothermal Chemistry, Denver, CO, June 1-3, 1983.

1.10   Ward, J.S. and Morrow, N.R., "Observations on Wetting Conditions Induced by Crude Oil," to be presented at AOCS Meeting, Dallas, TX, April 1984.

Table 1.1   Physical Properties of Liquid Systems
Used in Displacement Tests (23 $\pm 1^\circ$C)

Liquid	Density (gm/cm^{-3})	Viscosity (cp) (gm/cm^{-3})	Density Difference $(\rho_w - \rho_o)$	Viscosity Ratio (μ_o/μ_w)
2% CaCl$_2$ (Brine)	1.015	0.95	N/A	N/A
Paraffin Oil-3	0.868	168	0.147	177
Paraffin Oil-2	0.864	79.4	0.151	84
Paraffin Oil-1	0.844	24.2	0.171	25
Moutray Crude	0.838	5.23	0.177	5.5
Soltrol 220	0.789	5.35	0.226	5.6
Soltrol 130	0.755	2.05	0.260	2.2
n-Heptane	0.679	0.38	0.336	0.35

Table 1.2   Displacements of Oils of Different Viscosities by 2% $CaCl_2$ Brine

Sandstone[+] Sample No.	Oil Phase	K_a (md)	K_w (md)	μ_o (cp)	$\frac{\mu_o}{\mu_w}$	K_{rw} at S^*_{or}	S_{oi} (% PV)	S^*_{or} (% PV)	$\frac{S^*_{or}}{S_{oi}}$	$\frac{S_{oi}-S^*_{or}}{S_{oi}}$
S6F[++]	Paraffin Oil-2	1011	633	79.4	84	0.156	64.4	33.9	0.526	0.474
S6G-1[++]	Paraffin Oil-1	955	583	24.2	25	0.121	64.3	36.2	0.563	0.437
S6G-2			-	24.2	25	0.132	66.4	36.5	0.550	0.450
S6G-1R[+++]	Paraffin Oil-2		528	79.4	84	0.074	61.4	33.7	0.549	0.451
S6G-2R	Paraffin Oil-3		487	168	177	0.070	60.0	33.5	0.558	0.442
S6G-2R1			-	168	177	0.070	62.9	33.1	0.526	0.474
S6G-3R	N-Heptane		326	0.38	0.35	0.202	55.0	27.4	0.498	0.502
S6G-3R1			-	0.38	0.35	0.223	54.6	27.2	0.498	0.502
S6K-1		1054	527	0.38	0.35	0.200	52.2	27.8	0.533	0.467
S6K-2			-	0.38	0.35	0.201	52.0	27.3	0.525	0.475
BF-1[++]	Soltrol 130	434	143	2.05	2.2	0.156	49.0	27.9	0.569	0.431
BF-2			-	2.05	2.2	0.131	58.0	32.4	0.559	0.441
HB-1		188	76	2.05	2.2	0.101	61.0	34.4	0.564	0.436
HB-1R			68	2.05	2.2	0.093	60.9	35.5	0.583	0.417
Torpedo 1N		564	239	2.05	2.2	0.209	66.5	34.1	0.513	0.487

[+] All cores were Berea sandstone except that identified as Torpedo

[++] Cores fired at 800°C for 2 hours

[+++] Symbol R indicates core cleaned with IPA

Table 1.3   Summary of Core Properties and Duplicate Waterflooding
Data (Soltrol 130/2% Brine) for Caddo Limestone

Core Sample	Length+ (cm)	Porosity (%)	K_a (md)	K_w (md)	S_{oi} (% PV)	S_{or}^* (% PV)	$\dfrac{S_{or}^*}{S_{oi}}$	$\dfrac{S_{oi} - S_{or}^*}{S_{oi}}$
					53.0	34.0	0.642	0.358
A	4.69	19.6	72.0	37.5	58.6	28.0	0.478	0.522
					55.0	31.7	0.576	0.424
					48.0	28.8	0.600	0.400
B	6.04	17.4	29.0	9.0	42.0	26.9	0.640	0.360
					52.0	29.8	0.573	0.427
					55.5	28.0	0.505	0.495
C	3.10	14.0	75.2	29.5	52.0	27.6	0.531	0.469
					52.0	29.8	0.573	0.427
D	4.90	16.5	680	273	32.3	20.0	0.619	0.381
					34.0	22.0	0.647	0.353
					34.4	22.6	0.657	0.343
E	4.90	17.2	635	250	34.4	23.4	0.680	0.320
					33.5	25.0	0.746	0.254
					33.5	25.4	0.758	0.242

+ All cores were 3.8 cm diameter

Table 1.4   Effect of Change in Overburden Pressure on an
Established Residual Oil Saturation (S_{or}^{*}).
Core EH1, ΔP = 5 psi; Core MCA3, ΔP = 100 psi

Core	Overburden Pressure (psi)	Saturations at Conditions (% PV)		Effective Permeability to Brine at S_{or}^{*} (md)
		S_{oi}	S_{or}^{*}	
MCA3	500	58.6	39.0 (MB)	0.092
	1400	–	39.0 (VB)	0.071
	2600	–	39.0 (VB)	0.065
	4000	–	39.0 (VB)	0.065
	5000	–	39.0 (MB)	0.065
	2400	–	39.0 (VB)	0.064
	1400	–	39.0 (VB)	0.088
	500	–	39.0 (MB)	0.121
EH1	500	71.4	49.1 (MB)	17.9
	1500	–	49.1 (VB)	17.0
	2500	–	49.1 (VB)	16.1
	3500	–	49.1 (VB)	15.2
	4500	–	49.9 (MB)	15.5

Core Properties:

EH1:   Berea Sandstone, L = 6.92 cm, D = 3.81 cm, ϕ = 20.6%, K_a = 672 md, K_w = 176 md.

MCA3: Carbonate, L = 3.41 cm, D = 1.82 cm, ϕ = 6.7%, K_a = 2.2 md, K_w = 0.506 rd

MB = Mass Balance, VB = Volumetric Balance

Table 1.5   Effect of Overburden Pressure on Initial
and Residual Oil Saturation on Core EH1
(see Table 1.4 for properties) Waterflooded
at 10 psi

Overburden Pressure	Saturations[+] (% PV)		Effective Permeability to Brine (md)
(psi)	S_{oi}	S^*_{or}	
500	67.4	47.0	19.3
1500	69.6	44.9	31.2
2500	69.6	44.0	28.0
3500	70.0	44.9	27.7
5000	69.1	43.7	29.7

[+] All saturations from mass balance

Sample No.	Length (cm)	K_a (md)	K_w (md)	Porosity (%)	S_{oi} (% PV)	S^*_{or} (% PV)	$\dfrac{S^*_{or}}{S_{oi}}$	$\dfrac{S_{oi} - S^*_{or}}{S_{oi}}$
FS7[+]	6.48	4824	3277	23.3	58.3	25.7	0.441	0.559
FS5[+]	6.65	2526	1410	21.3	68.8	34.3	0.500	0.500
FS3[+]	6.64	1805	1181	20.3	57.6	24.4	0.424	0.576
B5	6.81	638	381	20.2	63.8	29.6	0.464	0.536
B2	5.80	283	126	19.5	68.2	30.4	0.446	0.554
C1-V[++]	7.15	117	71	19.3	62.0	29.4	0.474	0.526
S6C[+]-SCT	6.43	1175	743	23.9	71.8	28.3	0.394	0.606
S6E[+]-SCT	6.07	863	826	23.5	70.6	26.6	0.377	0.623

[+] Fired sandstone cores (at 800°C for 2 hours)

[++] Carbonate (Baker Dolomite)

SCT = Short Contact Time (<20 minutes) with crude oil

All cores were Berea (3.80 cm) except C1-V

Table 1.7   Survey of Contact Angles and Adhesive
Properties of Dead Crude Oil

Crude Oil Sample	Contact Time (min)	Number of Tests	Advancing Contact Angle (degrees) (External Water Phase)
Coyote Queen	40	1	~80
Grayburg	20	3	~135
Mancos Shale	20	6	~123
	20	4	~22
Morrison	20	3	~107
	10-40	8	~22
Moutray	20	8	~110
Mule Gulch	20	5	~20[*]

* No adhesion

Table 1.8   Distribution of Contact Angles Obtained
             in Preliminary Measurements with Moutray
             Crude Oil

Sample Code[*]	Contact Time (min)	Number of Tests	Advancing Contact Angle Range (degrees)
1	20	8	103-116
1	8	1	143
2	27	1	17
4	242	1	131
4	268	1	28.5
4	1049	1	24
2 (aerated)	300+	3	23-29
3	340	1	15
2	40	1	91
2	40	1	25
2	40	4	102-111
2	40	3	18-20
2	40	2	77-83
2	40	2	131-142
5	40	2	133-147
5	120+	2	20-21
5	120+	5	74-108

[*]Sample code numbers indicate samples taken at various times and
stored under somewhat different conditions (type of container,
temperature and length of storage, etc.)

Table 1.9   Duplicate Measurements of Contact Angles – Moutray-55[*] vs. Distilled Water on Smooth Glass

Drop Fluid	Experiment Set Up No.	Contact Time (min) (after new drop position)	Advancing Angles (degrees) External Water Phase								
			1	2	3	4	5	6	7	8	9
			(positions on surface)								
Moutray-55	1	0	54	52							
		10	60	65							
		30	56	68							
		60	73	68							
		120	81.5	74.5							
	2	0	34	20							
		10	48	40							
		30	60	60.5							
		60	67.5	83							
		120	100	97							
	3	0	18	17							
		10	21.5	18							
		30	21	20							
		60	23	19							
		120	22	22							
	4	0	44	12	21	20	45	26	27.5	47	34
		5	60.5	14	21	22	50	31	24.5	40.5	43
		10		17	18	40	52	30.5	27	40.5	36.5
		30				42	62		29	54	30
		60					80	69.5		80	41
		120					54	58			

[*] Moutray-55:   crude oil from single 55-gallon sample

Table 1.10 Duplicate Contact Angle Measurements for Mixtures of Moutray-55 and Toluene in Proportions Indicated vs. Distilled Water on Smooth Glass

Drop Fluid	Experiment Set Up No.	Contact Time (min)	Advancing Angles (degrees) 1 2 3 (positions on surface)		
Moutray:Toluene 1:1	1	0	55	16	
		10	64	16	
		30	78	17	
		60	79	39	
		120		57	
Moutray:Toluene 1:1	2	0	57	64	
		10	69	69	
		30	79	68.5	
		60	81.5	71.5	
		120	82.5	72.5	
Moutray:Toluene 1:2	3	0	61	51	
		10	76	63	
		30	85.5	76	
		60	104	79	
		120	127	103	
Moutray:Toluene 1:5	4	0	30	54.5	
		10	26	65	
		30	42	75	
		60	24	86	
		120	47	110	
Moutray:Toluene 1:5	5	0	20	20	
		10	21	28	
		30	23	38	
		60	21.5	45.5	
		120	23	69	
Moutray:Toluene 1:10	6	0	18	22.5	
		10	18	22	
		20	18	21	
Moutray:Toluene 1:10	7	0	22	18	17
		10	25	18	17
		30	22	17	30
		40	22	17	29
Moutray:Toluene 1:10	8	0	26	21	
		10	40.5	38	
		30	41.5	44	
		60	41	54	
		120	41	82	
Moutray:Toluene 1:10	9	0	83	90	
		10	112	128	
		30	133	130	
		60	135	130	

Table 1.11   Duplicate Contact Angles – Moutray and
Isooctane vs. Distilled Water on Smooth Glass

Drop Fluid	Experiment Set Up No.	Contact Time (min)	Advancing Angles (degrees) 1 (positions on surface)	2
Moutray:Isooctane 1:1	1	0	23	22
		10	25	22
		20	88	74
		60		106
	2	0	87	101
		10		148
		30	145	147.5
		60	145	145
		120	145	147
	3	0	76.5	90
		10		127
		30	137	142
		60	137.5	143
		120	137.5	143
	4	0	91	22
		10	99	61
		30	126	81
		60	130	89
	5	0	18	21
		10	18	87
		30	20	103
		60	20	102

Table 1.12   Influence of Initial Cell Condition
on Advancing Contact Angles

Fluids	Experiment Set Up No.	Contact Time (min)	Advancing Angles (degrees) 1	2
			(positions on surface)	
Moutray:Toluene 1:10 and Double-Distilled Water	1-wet	0	26	21
		10	40.5	38
		30	41.5	44
		60	41	54
	1-dry	0	83	90
		10	113	128
		30	133	130
		60	135	130
Moutray:Isooctane 1:1 and Double-Distilled Water	2-wet	0	91	22
		10	99	61
		30	126	81
		60	130	89
	2-dry	0	78	
		10	112	
		30	132	
		60	137	
	3-wet	0	18	21
		10	18	87
		30	20	103
		60	20	102
	3-dry	0	89	
		10	126	
		30	142	
		60	148	

Table 1.13   Contact Angles on Carbonate Core Surfaces
for Moutray and Double-Distilled Water

Surface Description	Contact Time (min)	Advancing Contact Angles (degrees)				
		1	2	3	4	5
		(positions on surface)				
Cut Surface	0	23	26	19		
	10	29	24	20		
	30	30	29	19		
	60	28	28	20		
Polished Surface	0	108	141.5	127	32	31
	10	130	162	132	32	30
	30	141	166	144	30	44
	60	154	169	145	47	45
	120	158	171	147		
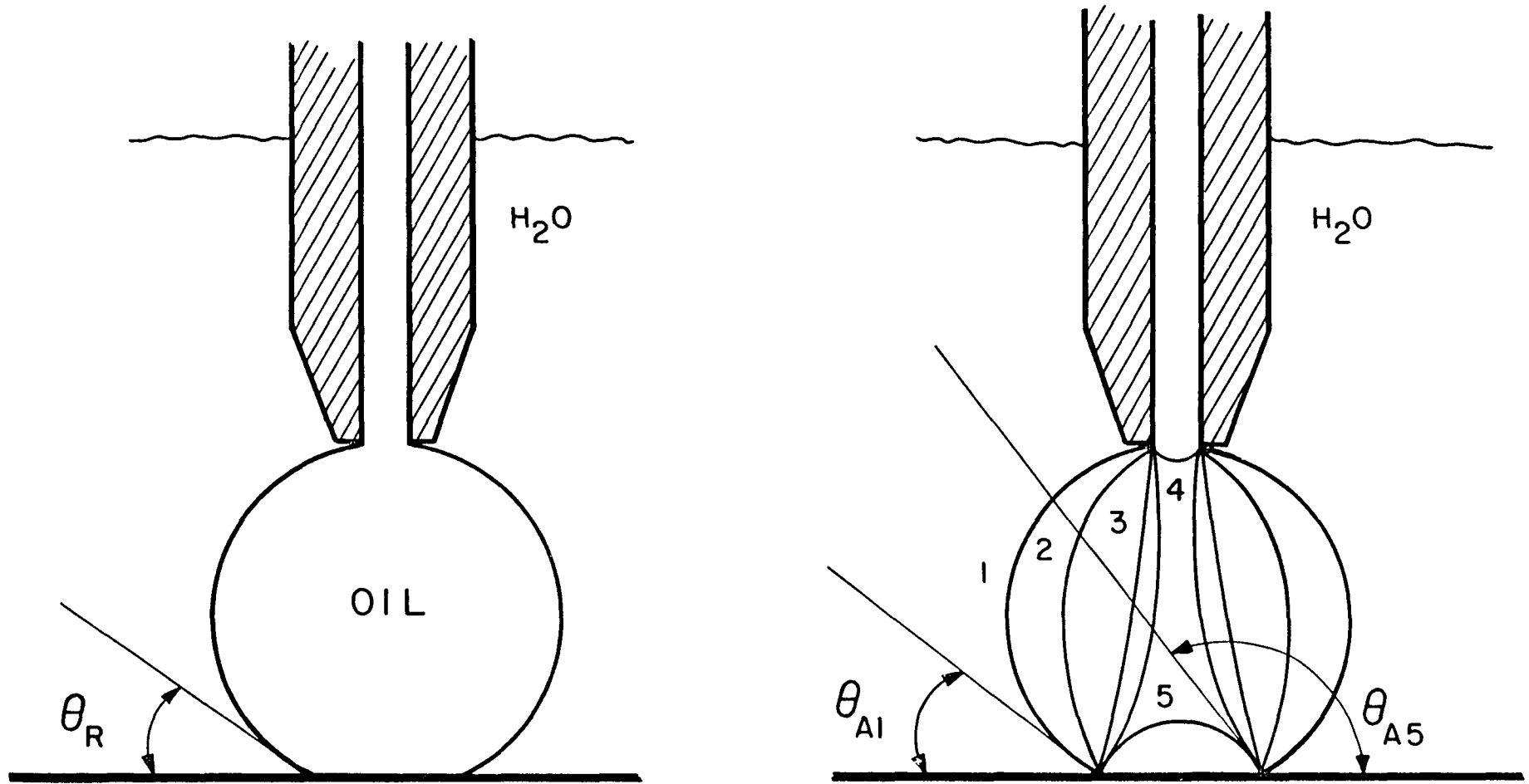
(a) Water receding as crude oil drop contacts glass surface.

(b) Water advancing as crude oil drop is retracted in several stages for a drop which sticks to the glass.

Fig. I.I. Captive drop technique for measurement of contact angles.
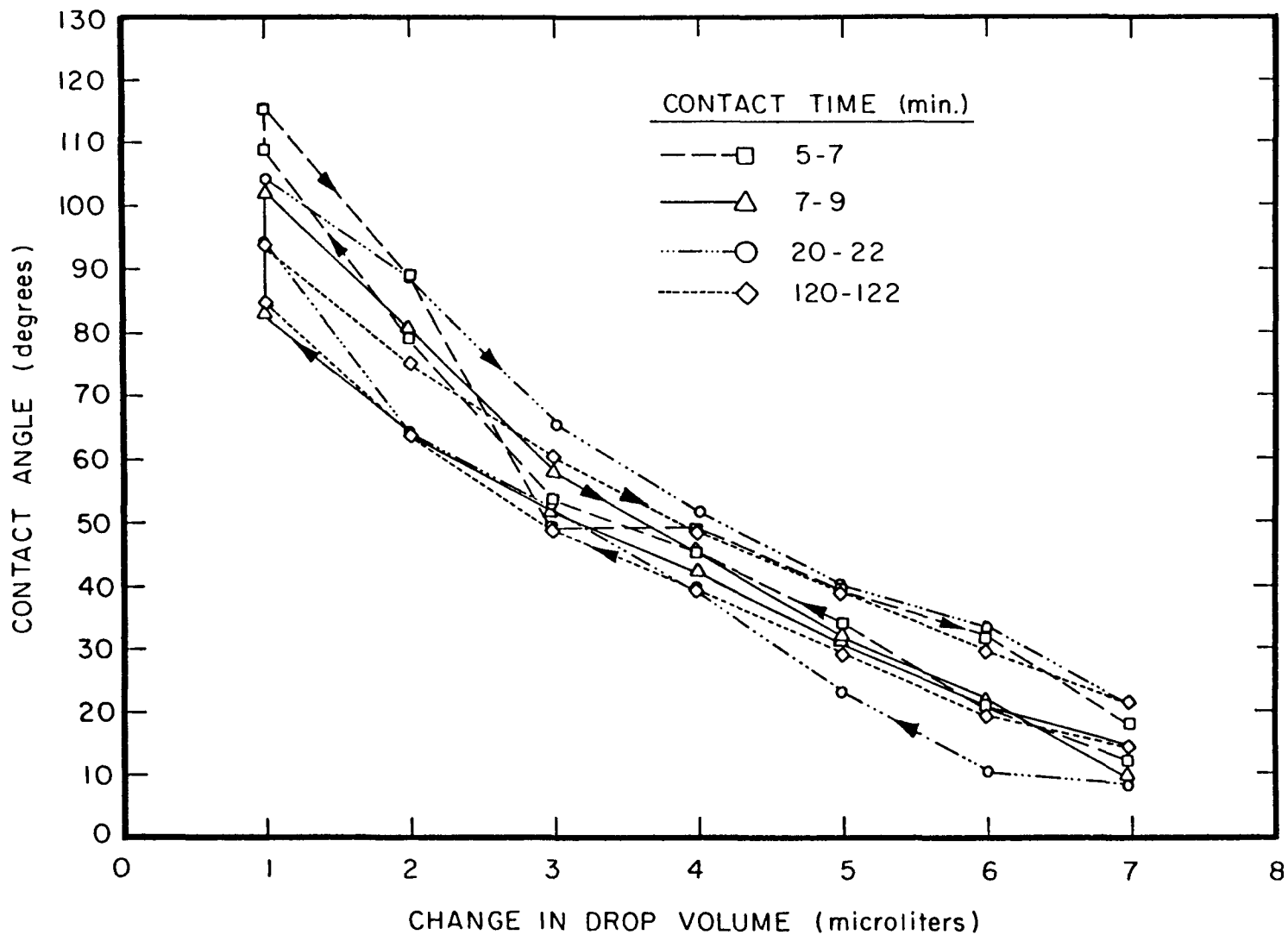
Fig. I.2. Typical variation in contact angle which accompanies change in volume of captive drop. (Volume measured to ± 0.5 $\mu \ell$. Scan time was about two minutes.)

TASK 2. EFFECT OF HIGH PRESSURE GRADIENTS ON RESIDUAL OIL SATURATIONS

BACKGROUND

For tertiary recovery prospects that are under serious condition, residual oil saturations are now being determined by in situ methods. These include pressure coring, new and improved logging techniques, and tracer tests. No single measurement is widely accepted, and each has its own particular advantages and disadvantages. The need for accurate measurements of residual oil is so acute that it is now common practice to use a suite of costly measurements to obtain the best estimate of residual oil saturation.

Except for the tracer method, the more favored methods of measuring residual oil use pressure cores and/or specialized logging techniques that involve the relatively small portion of the reservoir close to the wellbore. Both the pressure cores and the wellbore region will have been subjected to abnormally high pressure gradients as compared to the rest of the formation. The pressure gradients may be high enough to cause significant flushing of the oil from the cores or from the region close to the wellbore as compared with the formation as a whole.

Corrections for the effects of high flow rate to in situ measurements of residual oil require knowledge of capillary number relationships (relationships between the ratio of viscous to capillary forces and reduction in residual saturation) and relative permeabilities at reduced residual saturation. The extent of near wellbore flushing is a function of formation characteristics, interfacial tension, overbalance pressure (the pressure between the mud outside the drill bit and the pressure of the formation fluid), and distance from the wellbore. In formations where waterflood residual oil is to be determined, the overbalance pressure has been shown to be a key variable with respect to oil flushing.

Studies of trapping and mobilization reported previously have included capillary number relationships for a wide variety of water-wet sandstones and sucrosic carbonates. Relationships between capillary number and reduction in residual oil for sandstone cores (most of the tested cores had been stabilized by firing at 800°C) all lay within a fairly consistent range of capillary number.[2.1] A plot of capillary number ($K_w \Delta P/L\sigma$) versus residual oil ratio for the sandstone correlation is shown in Fig. 2.1.

In this work, study of capillary relationships has been extended to include carbonate core samples and effects of wettability change. Implications of these results with respect to flushing of residual oil at the wellbore are included. Also reported are results of a study of changes in electrical resistivity which accompany reductions in residual oil saturation.

2.a. CAPILLARY NUMBER RELATIONSHIPS

Baker Dolomite

Capillary number measurements were made on a Baker dolomite core which had an air permeability of 154 md and a porosity of 22.2%. The low permeability of the sample set limitations on the reduction in residual oil by flowing pressure gradients up to 810 psi/ft. However, for this sucrosic dolomite, it was found that the critical capillary number for displacement[2.2] corresponded closely with values observed for a wide range of sandstones (see Fig. 2.1).

Caddo Carbonates

An extensive set of capillary number measurements was made on a series of five Caddo carbonate samples. Properties of the tested cores are listed in Table 1.3. Results including duplicate runs are shown in Fig. 2.1. Capillary numbers for displacement of residual oil were about one to two orders of magnitude less than for sandstones. In one case (sample 6), residual oil saturation was sensitive to flooding rate even for capillary numbers as low as 10^{-7} which corresponds to less than normal field flooding rates. Thus, it appears that the lowering of interfacial tension needed for enhanced recovery from such formations is much less than would be needed for sandstones or sucrosic carbonates. The problem of wellbore flushing mentioned previously will, of course, be more serious for the Caddo type of formation. Corrections for wellbore flushing effects are discussed in detail later in this section.

Relative Permeability

Results for permeability to water at residual and reduced residual oil saturations for the Caddo carbonates are shown in Fig. 2.2. Also included is the "S curve" which is representative of results obtained for a wide range of sandstones.[2.3] Results were reproducible for a given core and fell reasonably close to the correlation obtained for sandstones. From inspection of pore casts and thin sections, the carbonates were seen to contain vugs and large-scale, sheet-like pores originating from the dissolution of shells. Nevertheless, relative permeability to water at reduced residual oil, as with sandstones, was mainly dependent on the amount of retained oil.

Mobilization of Continuous vs. Discontinuous Oil

In studies on sandstones it was found that for a given capillary number, higher recoveries were obtained when the oil was initially continuous as compared with flooding the core to normal waterflood residual before increasing the flow rate to that same capillary number. Comparable tests were carried out on the Caddo carbonate sample E. It was found that there was no significant difference in recovery between the results for initially continuous and initially discontinuous oil (see Fig. 2.3). Assuming the additional recovery that resulted from increased capillary number was due to mobilization of oil from vugular regions, it appeared that overall connectivity of the oil phase had no significant effect on oil displacement from the vugs.

Effect of Wettability on Capillary Number Relationships

At present, there is very little information available on the effect of wettability change on capillary number relationships for consolidated rocks. Use of crude oils which are known to be capable of inducing wettability alteration was discussed under Task 1. In experiments with Berea sandstone for which Moutray crude was used as the oil phase, it was found that capillary numbers for displacement of residual oil were increased by a factor of about five (see Fig. 2.4) indicating that the wettability of the sandstone had been changed. Corresponding changes in relative permeabilities with reduction in residual oil exhibited some interesting and reasonably consistent general features. Well defined residual saturations were established well within passage of two pore volumes of water through the core. Relative permeabilities to water at residual oil saturation were generally lower than those observed for equivalent tests in water-wet sandstones. This added mobility control may have contributed to the observed increase in microscopic displacement efficiency. However, once mobilization is attempted by increase in capillary number there is dramatic increase in water relative permeability for only slight reduction in the amount of residual oil saturation (see Fig. 2.5). A possible explanation of this behavior is that some of the trapped oil is retained as pore blocking lamellae which might involve only a small volume of oil. Removal of the lamellae by increased flow rate could result in unblocking of the larger pore spaces to give marked increase in water permeability. Tests for possible end effects showed them to be fairly minor.

Moutray crude was also used in capillary number experiments on a Caddo limestone. Preliminary data showed that with crude oil rather than Soltrol as the oleic phase, the critical capillary number for displacement increased by a factor of about three (Fig. 2.6). Once residual oil saturation had been reduced by one-fifth, results for the Moutray crude and refined oil were not significantly different. Thus, the change induced by the crude oil, which was probably mainly related to wettability, was qualitatively the same as, but had less effect, than was observed for the sandstone (cf. Figs. 2.1 and 2.6).

2.b. RESIDUAL OIL FLUSHING AT WELLBORE

We will now consider the significance of the foregoing capillary number relationships to the problem of flushing in the vicinity of the wellbore. In a previously reported investigation of flushing effects in water-wet sandstones,[2.4] it was concluded that the practice of limiting overbalance pressures to less than 200 psi was generally conservative and that flushing effects even at higher overbalance pressures would not be very severe and would require only minor corrections.

Nonwater-Wet Sandstones

Capillary numbers for displacement of residual oil were increased by a factor of about five for nonwater-wet sandstones. This was true for both the displacement of Moutray crude oil and for displacements of Soltrol in sandstones with wettability altered from strong water-wetness by film deposition from Moutray crude in the presence of connate water. The amount of flushing of residual oil would therefore be correspondingly less severe for the sandstones with wettability altered by crude oil. This is likely related to the large contact angle hysteresis observed for these oils which will aid retention of the oil. Thus, if the wettability alteration induced by the Moutray crude oil is reasonably characteristic of nonwater-wet reservoir systems, then it is concluded that wettability alteration will reduce the severity of flushing.

Carbonates

The limited results obtained to date for carbonates indicate that capillary number relationships can be highly dependent on rock structure and slightly dependent on wettability. Since, for the sucrosic Baker dolomite, capillary number displacement curves fell close to results typical of sandstones, flushing effects will be similar to those estimated for water-wet sandstones.[2.4] For the Caddo carbonates, residual oil can be mobilized at capillary numbers of 10 to 100 times lower than those for sandstones. Under these circumstances, flushing could be severe even if overbalance pressures are held at the recommended level of 200 psi.

Calculations of flushing effects have been carried out for reductions in capillary number given by linear scaling of a correlation obtained for water-wet sandstones. Relationships for capillary number curves shifted by factors of 0.01, 0.02, 0.1 and 10 are shown in Fig. 2.7. A method described previously[2.4] of determining pressure gradients around the wellbore for various reductions in residual oil saturation at the wellbore face was used to obtain the results shown in Fig. 2.8. For integration of the pressure gradient over a selected distance (2000 feet was taken as being reasonably typical), relationships between relative

32

wellbore face saturations can be determined as a function of overbalance pressure (Fig. 2.9). For the most permeable core (982 md), over 25% of the oil could be flushed from the face region. Relationships between relative face saturation and overbalance pressure are presented in Fig. 2.10 for capillary number relationships scaled by 0.01, 0.02 and 0.1 relative to results typical of water-wet sandstones. This range is representative of the capillary number relationships observed for the Caddo limestone. In all cases, it is seen that significant flushing will occur at overbalance pressures less than 200 psi and that flushing could be severe for cores where the capillary number is reduced by a factor of 50 to 100. Hence, when making in situ measurements of residual oil by logging or pressure coring techniques, particularly in carbonate reservoirs, it is well worthwhile carrying out laboratory measurements of capillary number curves to check the likelihood of flushing. Where needed, estimates can be made of the amount of flushing that has occurred and its effect on logging tool response or the amount of oil measured in a pressure core.

2.c. ELECTRICAL RESISTIVITIES AT REDUCED RESIDUAL OIL SATURATIONS

In enhanced recovery, where residual oil saturations are reduced below their normal waterflood value, S_{or}^*, ability to obtain information about the magnitude and distributions of reduced oil saturation, S_{or}, from resistivity measurements would be of value in a variety of reservoir and laboratory situations. A laboratory investigation has therefore been made of relationships between electrical resistivity and S_{or}, with S_{or} being achieved by various methods.

Relationships relating resistivity to water saturation are generally presented as empirical correlations,[2.5,2.6] the best known being the Archie equation.[2.7] The resistivity will clearly depend on the microscopic distribution of the aqueous phase, which will in turn depend both on how a given saturation was achieved, and on system wettability.[2.8] Reported resistivity vs. saturation relationships for high water saturations ($S_w > 1 - S_{or}^*$) generally have been determined under drainage conditions, since the range of water saturations for normal imbibition does not extend beyond $S_w = 1 - S_{or}^*$. At this stage in water-wet systems, at least, the oil phase is distributed as disconnected blobs, and in systems with wettabilities described variously as mixed, intermediate or oil-wet, response to further waterflooding demonstrates that the oil is only poorly connected.[2.9] Reduction in oil saturation can be achieved by an increase in capillary number of the flowing fluid. It is expected that the distribution of oil at S_{or}^* and at saturations resulting from high capillary number flow will be very much different from that given by drainage of water starting at 100% water saturation. Since empirical resistivity relationships are based on measurements made under the latter conditions, these will not necessarily apply to oil saturations attained by high capillary number flow. A laboratory investigation has therefore been made of relationships between electrical resistivity and S_{or}, with S_{or} being achieved by high capillary number flow at both high and low interfacial tension.

Empirical Correlation of Resistivities

An important parameter which underlies the interpretation of core resistivity measurements is the formation resistivity factor, F_R

$$F_R = \frac{R_o}{R_w} \qquad (2.1)$$

where R_o is the resistivity of porous medium saturated with brine and R_w is the resistivity of the brine. The resistivity ratio, I, is employed to characterize rocks partially saturated with water and oil:

$$I = \frac{R_t}{R_o} \qquad (2.2)$$

where R_t is the resistivity of the rock at partial water saturation S_w. Consideration of available data led Archie to propose the relationship

$$I = S_w^{-n} \qquad (2.3)$$

where n is the saturation exponent. A modified form of this equation is

$$I = C \, S_w^{-n} \qquad (2.4)$$

which recognizes that C is not necessarily equal to unity.

EXPERIMENTAL

Cores

Eight unfired cores of Berea sandstone were used in this study. Core properties are summarized in Table 2.1. After each run, the cores were flushed with isopropyl alcohol (IPA) and dried. Brines were prepared from reagent grade $CaCl_2$, and resistivity was determined by means of a dip cell equipped with platinum electrodes.

The surfactants, Alfonic 610-50 (Conoco), EOR-200 (Ethyl Corporation), and Petrostep-465 (Stepan Chemicals) in combination with EOR-200, were selected for their compatibility with the brine.

Core resistivities were measured with a Core Laboratories Resistivity Test Model CEF.

Flooding Procedure

In all experiments, 2% $CaCl_2$ brine was the aqueous phase along with various surfactant formulations as indicated. Soltrol 130 was the oil phase. Cores were first completely saturated with brine, and the resistance, R_o, was measured. Each core was subsequently flooded with oil at high pressure gradient to establish a high initial oil saturation. Standard procedure included reversal of flow direction during the oil flood to reduce end effects. Resistance at S_{oi} was determined. Past this point, three different procedures were employed:

1. High interfacial tension flood - The core was flooded with brine, increasing flow rates (capillary numbers) in a stepwise fashion as described by Chatzis and Morrow.[2.1] Flooding rates were kept below those which cause obvious core damage, as indicated by production of a fine suspension of solids.

2. Low interfacial tension flood - Oil was first displaced with 1 PV of surfactant solution and then waterflooded as in 1. In general, lower oil saturations could be obtained because high capillary numbers could be obtained at comparatively low rates of flow.

3. Two-stage flood - The core was first waterflooded to low residual oil saturation using a high pressure gradient (approximately 240 psi/ft). Subsequently, residual oil was further reduced by surfactant flooding followed by waterflooding at pressure gradients sufficient for further oil production.

At the end of each flooding step, the core was weighed to determine the residual oil saturation and its resistance was measured.

RESULTS

S_{or} by High Tension Waterflood

Twenty-three high tension capillary number displacement runs were made in the eight cores. While trends were obvious and individual cores often gave well defined relationships of the expected form, reproducibility could vary from being very good with results showing consistent trends, to highly erratic, with small reduction in oil saturation sometimes causing large increases in resistivity. However, inspection of previous results from which empirical correlations were developed indicated that those of this work showed about the same consistency.[2.7,2.10]

Values of resistivity index are plotted against water saturation in Fig. 2.11. The relationships between I and S_w were analyzed by linear regression using the log-log form of equation (2.4):

$$\log I = \log C - n \log S_w \qquad\qquad (2.4a)$$

Regressions were performed on the results obtained for each core for all data except the points measured at highest oil saturation (produced by drainage). The value of the constant C is close to unity for most cores. The saturation exponents showed considerable variation but were all low compared with typical reported values of the Archie exponent. The regression line for all data shown in Fig. 2.11 corresponds to the equation:

$$I = 1.06 \, S_w^{-1.02} \qquad\qquad (2.5)$$

The correlation coefficient r was −0.84. C and n in equation (2.5) are in fair agreement with the mean values for individual cores shown in Table 2.2. The constant C is quite close to unity, and the omission of this constant in equation (2.4) thus appears to be justified for these results. The saturation exponent n is also close to unity.

The saturation exponent calculated for the saturation range $S_{wi} < S_w < 1 - S_{or}^*$, for which only the end points are available in the present work, gave an average value of n of 1.86. This is consistent with values of close to 2 found by other authors[2.7],[2.10] for strongly water-wet systems. For residual and reduced residual oil saturations ($S_w > 1 - S_{or}^*$) studied here, much lower values are obtained.

Effect of Surfactants on Resistivity

Surfactants were selected for their compatibility with 2% $CaCl_2$ brine. Of the three surfactants employed, Alfonic 610-50 and EOR-200 were completely compatible with the brine, while the Petrostep-465/EOR-200/Pentanol-1 mixture formed some precipitate. This mixed surfactant has been reported by Bansal and Shah[2.11] to be fairly stable in the presence of divalent ions. The surfactant systems used are listed in Table 2.3 together with the corresponding interfacial tensions measured against Soltrol 130. All three surfactant systems reduce interfacial tension by roughly two orders of magnitude.

Core numbers 3, 4 and 5 were used with the surfactant experiments. The results are plotted in Figs. 2.12 through 2.16. C and n in equation (2.4a) and the corresponding correlation coefficient were determined for each combination of core and surfactant. The results are summarized in Tables 2.4, 2.5 and 2.6 for Alfonic 610-50, EOR-200 and Petrostep mixture runs, respectively. Table 2.7 lists average values of C, n and R for all three cores with each surfactant, and with no surfactant.

For the surfactant floods differences among values C and n were greater than for the high tension results. This is especially evident in the cases where more concentrated surfactant is employed (3% Alfonic 610-50 and Petrostep mixture). For Alfonic 610-50 there was significant increase in both C and n over values obtained in the absence of surfactants, but correlation coefficients were poorer. Otherwise, results for reduction of residual oil saturation with the aid of

surfactants gave values of n which were low and comparable with those given by the high interfacial tension systems.

DISCUSSION

The resistivity of a porous medium completely saturated with a conductive phase, as expressed by the formation factor, reflects the structure of the porous medium. If all of the bulk volume of the conductive phase were able to make its maximum contribution to conductivity, the formation resistivity factor would be simply equal to the reciprocal value of porosity. This is obviously not true for a porous medium. As shown in Table 2.1, the value of F_R is always about 2 to 4 times higher than $1/\phi$.

The amount of current passing through a given electrolyte depends on cross-sectional area. In porous rock, the system may be viewed as pore bodies linked together by pore throats which have a smaller diameter. The aspect ratio (i.e., the ratio of pore body diameter to pore throat diameter), or a statistical distribution thereof, will have a dominant effect on both electrical and hydraulic conductivity. In a porous rock having a high aspect ratio, much of the electrolyte present will not contribute effectively to the conduction of electricity, and this in turn will result in a high formation resistivity factor. Similar reasoning can be applied to a porous medium in which a part of the conductive phase has been replaced with a non-conductive phase such as oil or gas.

The traditional interpretation of conductivity vs. water saturation data presupposes that the data fit a power curve. It should be noted, however, that the saturation exponent n is a convenient empirical parameter without fundamental significance. At residual and reduced residual oil saturations, the value of n for a given system will depend on the configuration of the trapped oil in the porous structure and on how this configuration changes with reduction in oil saturation.

The configurations assumed by residual oil will be strongly dependent on wettability. The wettability conditions which arise for the various surfactants listed in Table 2.3 and their effect on residual oil structure are uncertain. An observation of possible relevance to electrical conductivity behavior is the marked increase in hydraulic conductivity (relative permeability to water) at residual and slightly reduced residual oil shown in Fig. 2.5 for displacement of Moutray crude oil. Removal of pore blocking lamellae of oil with increase in capillary number was suggested as a possible explanation.

The initial presence of pore blocking lamellae of oil could also explain the comparatively high initial resistivities generally observed for the 3% Alfonic 610-50 (see Fig. 2.13) and in one instance for the 1% Alfonic surfactant (see linked data points in Fig. 2.12). These systems are also characterized by a comparatively large increase in conductivity with decrease in oil saturation.

However, in no instance did the resistivity at a given saturation fall significantly below average values observed for results given by high interfacial tension floods or other surfactant systems.

For the high interfacial tension systems, there is no reason to believe these are other than strongly water-wet. Chatzis, Morrow and Lim[2,12] have concluded from investigation of oil blob structures in consolidated media, such as the Berea sandstone used in the present work, that most of the residual oil is in the form of singlets (blobs which occupy a single pore body) which form by a snap-off mechanism as a result of high aspect ratio. At 100% water saturation, a relatively high formation resistivity factor is expected for systems of high aspect ratio. Thus, if oil is contained by the system in the form of singlet blobs residing in pore bodies, resistivity will be relatively insensitive to fractional oil saturation. This is consistent with the observed low value of the saturation exponent observed for reduced residual oil saturations. When $n = 1$, resistivity index is simply equal to the reciprocal of fractional water saturation. Thus, it appears that when oil is in disconnected form and is distributed as blobs with relatively few throat pores occupied by oil, the decrease in conductivity is approximately proportional to the diminution of the volume of the conductive phase.

The practical implications of saturation exponents being significantly lower than those usually reported are obvious. For a given value of resistivity index determined by measurement, a range of S_{or} estimates is obtained depending on the value of saturation exponent used. Applying a typical Archie exponent ($n = 2$) to the resistivity index data determined in the present work would result in underestimating the residual oil saturation by an amount corresponding to some 10 to 20% of pore space. In addition, the observed scatter in relationship between resistivity index and S_{or} indicates that electrical measurements do not generally provide a reliable method of determining residual oil saturations either in the field or under laboratory conditions.

CONCLUSIONS

1. Capillary number relationships for a sucrosic Baker dolomite correlated quite closely with results obtained for a variety of sandstones.

2. Capillary numbers for mobilization of residual oil from samples of vugular limestone were one to two orders of magnitude less than those for sandstone. Required interfacial tension lowering for tertiary recovery will be correspondingly less. No significant differences between capillary numbers for initially continuous and initially discontinuous oil were observed.

3. Relative permeabilities to water at reduced residual oil saturation, as with sandstones, were mainly dependent on the amount of retained oil.

4. Wettability change induced by crude oil on sandstones caused capillary

numbers for oil recovery to be increased by a factor of five over those for water-wet sandstones. The induced wettability change resulted in water permeabilities at residual oil saturation which were unexpectedly lower than values observed for water-wet systems but showed marked increase for only small decrease in oil saturation.

5. The low capillary numbers needed for oil recovery in vugular carbonates indicate that in situ determinations of residual oil involving cores or near-wellbore logging measurements could be severely affected by flushing.

6. Correlation of resistivity index with water saturation at below-normal-waterflood residual oil saturations achieved both with and without the aid of surfactants yields saturation exponent values which are generally higher than, but fairly close to, unity. This reflects the fact that at this stage, most of the pore throats are occupied by water, and pore bodies filled by oil greatly outnumber pore throats filled by oil.

7. Although introduction of surfactants sometimes results in greater scatter of data, the saturation exponents for conductivity at reduced residual oil were also close to unity.

8. Problems in reproducibility of results for high tension systems probably arise because of rock damage caused by high flow rates. In low tension systems, even though flow rates for oil recovery are greatly reduced, results are sometimes scattered, possibly because of the effects of surfactants on system wettability and displacement mechanism.

9. Application of values of Archie exponent, n, obtained from saturations established by drainage will generally lead to underestimates of reduced residual saturations.

10. Trends of change in electrical resistivity with reduced residual oil saturation were generally clear even though reproducibility of data was sometimes erratic. In application of resistivity measurements to estimation of reduced residual oil saturations, as with conventional resistivity measurements, caution must be exercised. Results may sometimes provide indication of the wetting condition induced by the surfactants.

REFERENCES

2.1 Chatzis, I., and Morrow, N.R., "Correlation of Capillary Number Relationships for Sandstones," SPE 10114, paper presented at the 56th Annual Fall Technical Conference and Exhibition of SPE of AIME, San Antonio, TX, October 5-7, 1981.

2.2 Taber, J.J., "Dynamic and Static Forces Required to Remove a Discontinuous Oil Phase from Porous Media Containing Oil and Water," Soc. Pet. Eng. J. (March 1969) 3-12.

2.3   Morrow, N.R., Chatzis, I., and Lim, H.T., "Relative Permeabilities at Reduced Residual Saturations," presented at the 34th Annual Technical Meeting of the Petroleum Society of CIM, Banff, Canada, May 10-13, 1983.

2.4   Morrow, N.R., Chatzis, I., Siegel, D., and Taber, J.J., "Corrections to In Situ Measurements of Residual Oil for Flushing at the Wellbore," presented at the International Energy Agency Workshop, Calgary, Canada, September 1982.

2.5   Wyman, R.E., "How Should We Measure Residual Oil Saturation", Bull. Can. Petr. Geol. 25, No. 2 (1977) 233-270.

2.6   "Determination of Residual Oil Saturation," Interstate Oil Compact Commission, Oklahoma City, Oklahoma, 1978.

2.7   Archie, G.E., "The Electrical Resistivity Log as an Aid in Determining Some Reservoir Characteristics," Trans., AIME (1942) 54-61.

2.8   Sweeney, S.A., and Jennings, H.Y., Jr., "Effect of Wettability on the Electrical Resistivity of Carbonate Rock from a Petroleum Reservoir," J. Phys. Chem. 64 (1960) 551-553.

2.9   Salathiel, R.S., "Oil Recovery by Surface Film Drainage in Mixed Wettability Rocks," J. Pet. Tech. (October 1973) 1216-1224.

2.10 Swanson, B.F., "Rationalizing the Influence of Crude Wetting on Reservoir Fluid Flow with Electrical Resistivity Behavior," J. Pet. Tech. (August 1980) 1459-1464.

2.11 Bansal, V.K. and Shah, D.O., "The Effect of Divalent Cations (Ca^{++} and Mg^{++}) on the Optimal Salinity and Salt Tolerance of Petroleum Sulfonate and Ethoxylated Sulfonate Mixtures in Relation to Improved Oil Recovery," J. Amer. Oil Chem. Soc. 55 (1978) 367-370.

2.12 Chatzis, I., Morrow, N.R., and Lim, H.T., "Magnitude and Detailed Structure of Residual Oil Saturation," Soc. Pet. Eng. J. (April 1983) 311-326.

Table 2.1   Core Characteristics

Core	Length (cm)	Area (cm^2)	Porosity (fraction)	Permeability to air (md)	Formation resistivity factor
1	6.93	11.34	0.1897	121	22.31
2	6.97	11.34	0.1763	160	15.78
3	6.52	11.34	0.2026	243	14.88
4	6.18	11.34	0.1926	140	16.04
5	6.96	11.34	0.1796	342	15.42
6	5.83	11.34	0.2236	244	10.71
D	5.85	11.34	0.2182	707	12.33
E	6.80	11.34	0.1939	815	11.01

Table 2.2   Summary of Linear Regression
             Analysis for High Tension
             Displacements*

	Highest Oil Saturation Points Excluded		
Core	C	n	R
1	1.0433	0.6348	−0.8138
2	1.0187	1.0764	−0.9899
3	1.0046	1.3693	−0.9601
4	0.9991	1.3479	−0.9833
5	1.0720	0.9767	−0.9008
6	1.0289	1.0506	−0.9170
D	0.9663	1.4375	−0.9301
E	0.9692	1.4561	−0.8500
Mean	1.0127	1.1687	−0.9181

* Three runs were performed for each core,
  except No. 2 (2 runs only)

Table 2.3 Summary of Surfactant Systems

Surfactant	Type	Manufacturer	Concen-tration (%)	Interfacial tension[*] (mN/m)
Alfonic 610-50	Ethoxylated linear alcohols; non-ionic	Conoco Chemicals	1 3	0.15 0.52
EOR-200	Ethoxylated Sulfonate; anionic	Ethyl Corporation	1	0.91
Petrostep-465 EOR-200 Pentanol-1	Petroleum sulfonate; anionic	Stepan Chemicals	3 2 2	0.92

* Against Soltrol-130 as the oil phase

Table 2.4   Summary of Results with
             Alfonic 610-50 as Surfactant

Core	Alfonic 610-50, 1%		
	C	n	R
3	1.2928	1.0714	-0.6246
4	1.0998	1.0084	-0.8868
5	1.0053	1.2415	-0.9848

	Alfonic 610-50, 3%		
	C	n	R
3	1.1169	1.6916	-0.6941
4	1.1311	2.3349	-0.7399
5	1.3599	1.6415	-0.7471

Table 2.5   Summary of Results with
             EOR-200 as Surfactant

Core	EOR-200, 1%		
	C	n	R
3	1.1102	1.0903	-0.8540
4	1.0304	1.1069	-0.9576
5	1.0755	1.1551	-0.9394

Table 2.6   Summary of Results with
             Petrostep-465 - EOR-200
             Mixture as Surfactant

	Petrostep-465 + EOR-200		
Core	C	n	R
3	1.0188	1.6487	-0.9723
4	1.0195	1.3249	-0.9357
5	0.9895	1.4249	-0.9819

Table 2.7   Average Results for
             Surfactant Floods

	Parameter		
Surfactant	C	n	R
1% Alfonic 610-50	1.1326	1.1071	-0.8320
3% Alfonic 610-50	1.2026	1.8893	-0.7270
1% EOR-200	1.0720	1.1174	-0
Petrostep Mixture	1.0093	1.4662	-0.9633
No Surfactant	1.0252	1.2313*	-0.9480

* Average for Cores 3, 4 and 5
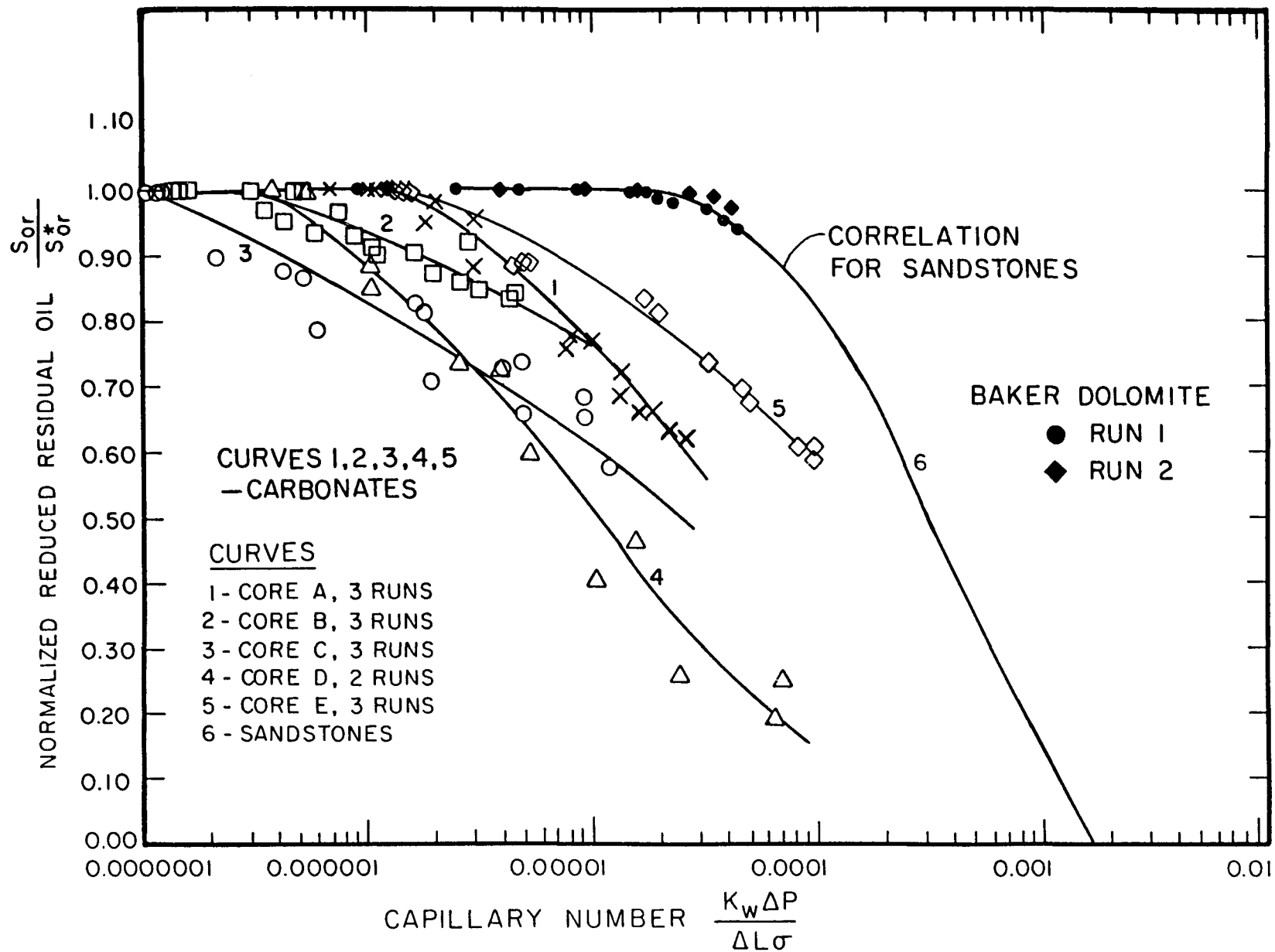
Fig. 2.1. Capillary number relationships for Caddo carbonates compared with correlation for sandstones and results for Baker Dolomite.

- Y-axis: NORMALIZED REDUCED RESIDUAL OIL $\frac{S_{or}}{S_{or}^{*}}$, scale from 0.00 to 1.10
- X-axis: CAPILLARY NUMBER $\frac{K_w \Delta P}{\Delta L \sigma}$, scale from 0.0000001 to 0.01

CORRELATION FOR SANDSTONES

CURVES 1,2,3,4,5 — CARBONATES

CURVES
1 - CORE A, 3 RUNS
2 - CORE B, 3 RUNS
3 - CORE C, 3 RUNS
4 - CORE D, 2 RUNS
5 - CORE E, 3 RUNS
6 - SANDSTONES

BAKER DOLOMITE
● RUN 1
◆ RUN 2
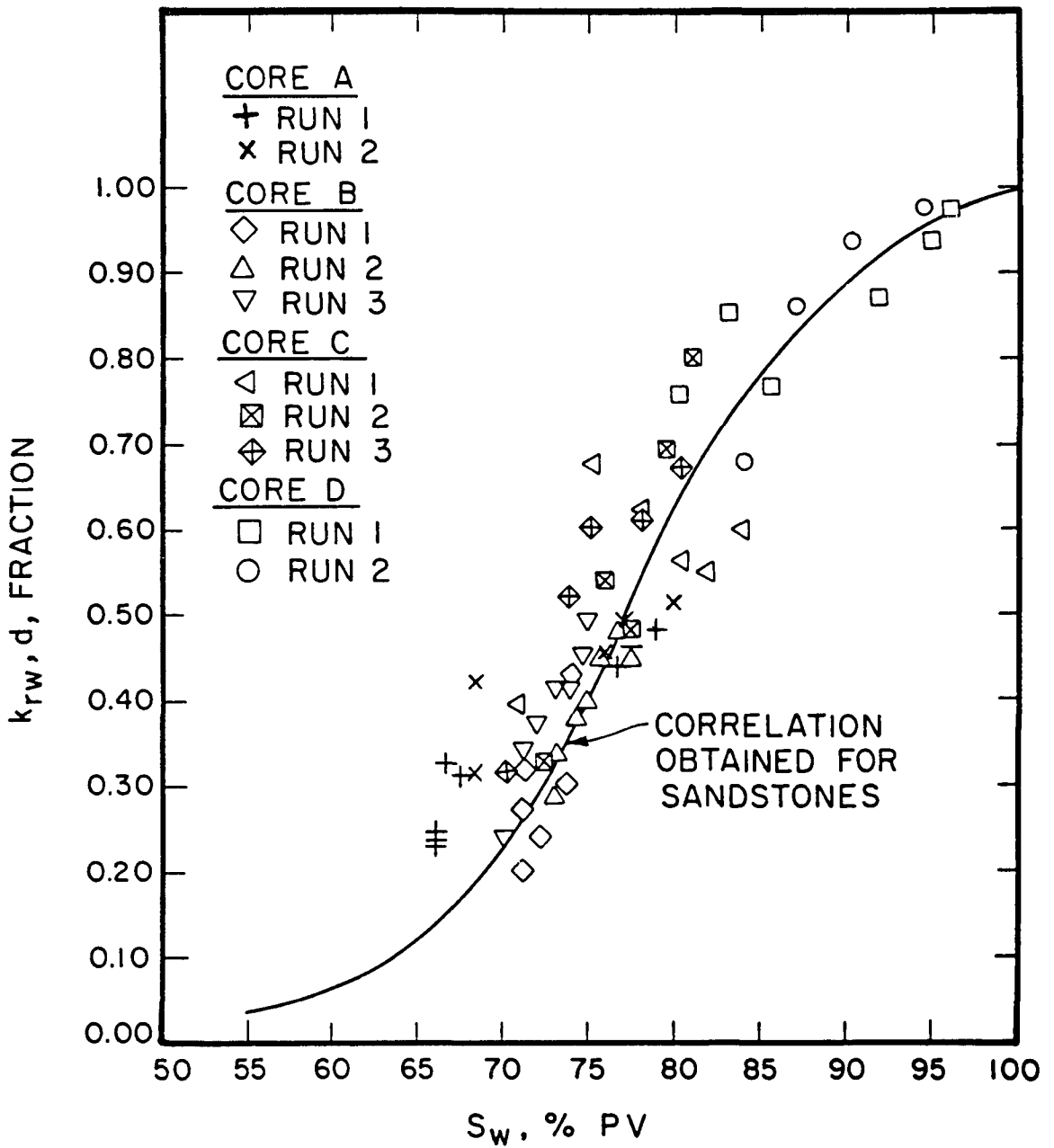
Fig. 2.2. Relative permeability at reduced residual saturation for Caddo carbonates.
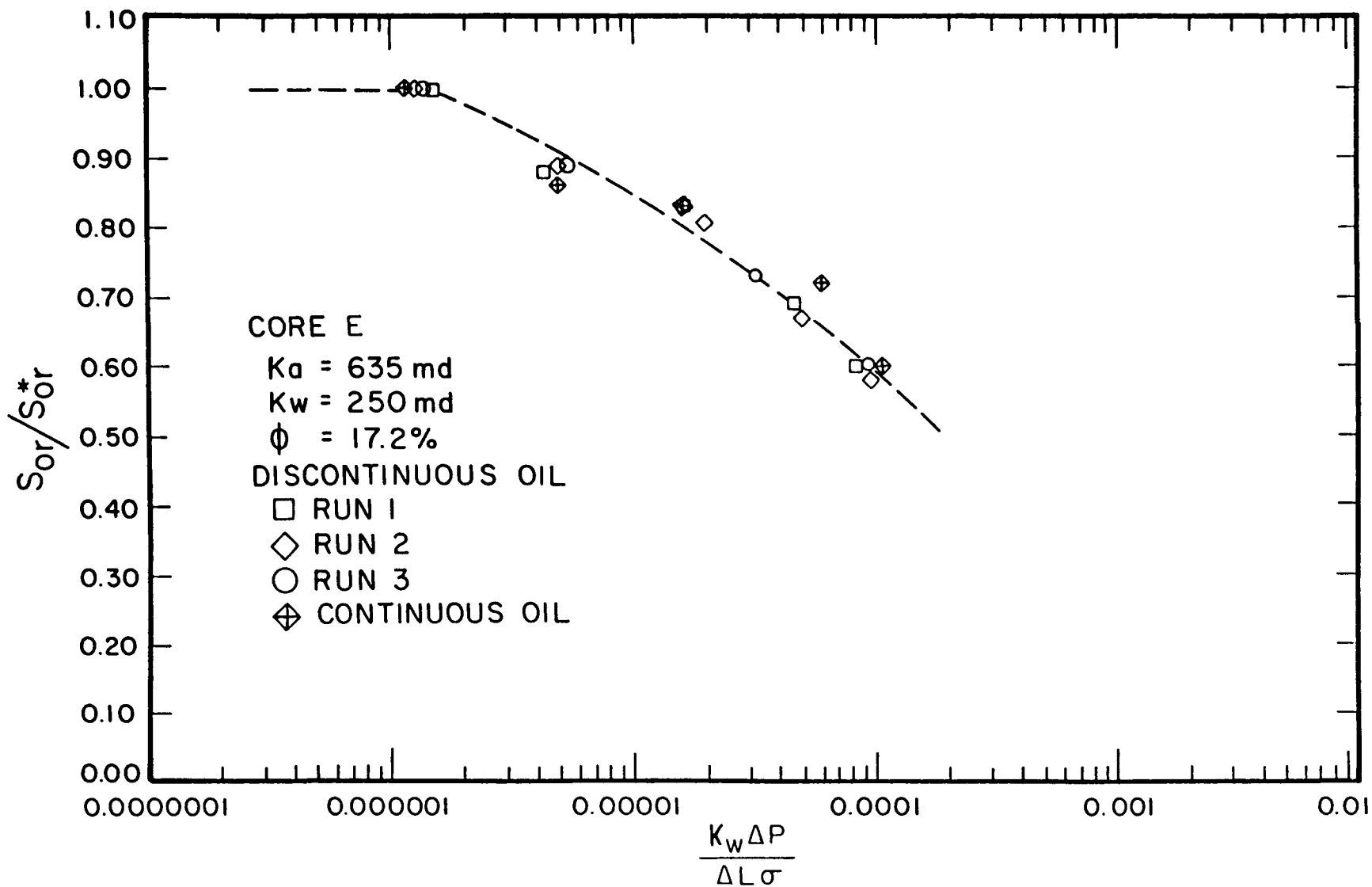
Fig. 2.3. Capillary number relationships for Caddo carbonates for initially continuous and initially discontinuous oil.
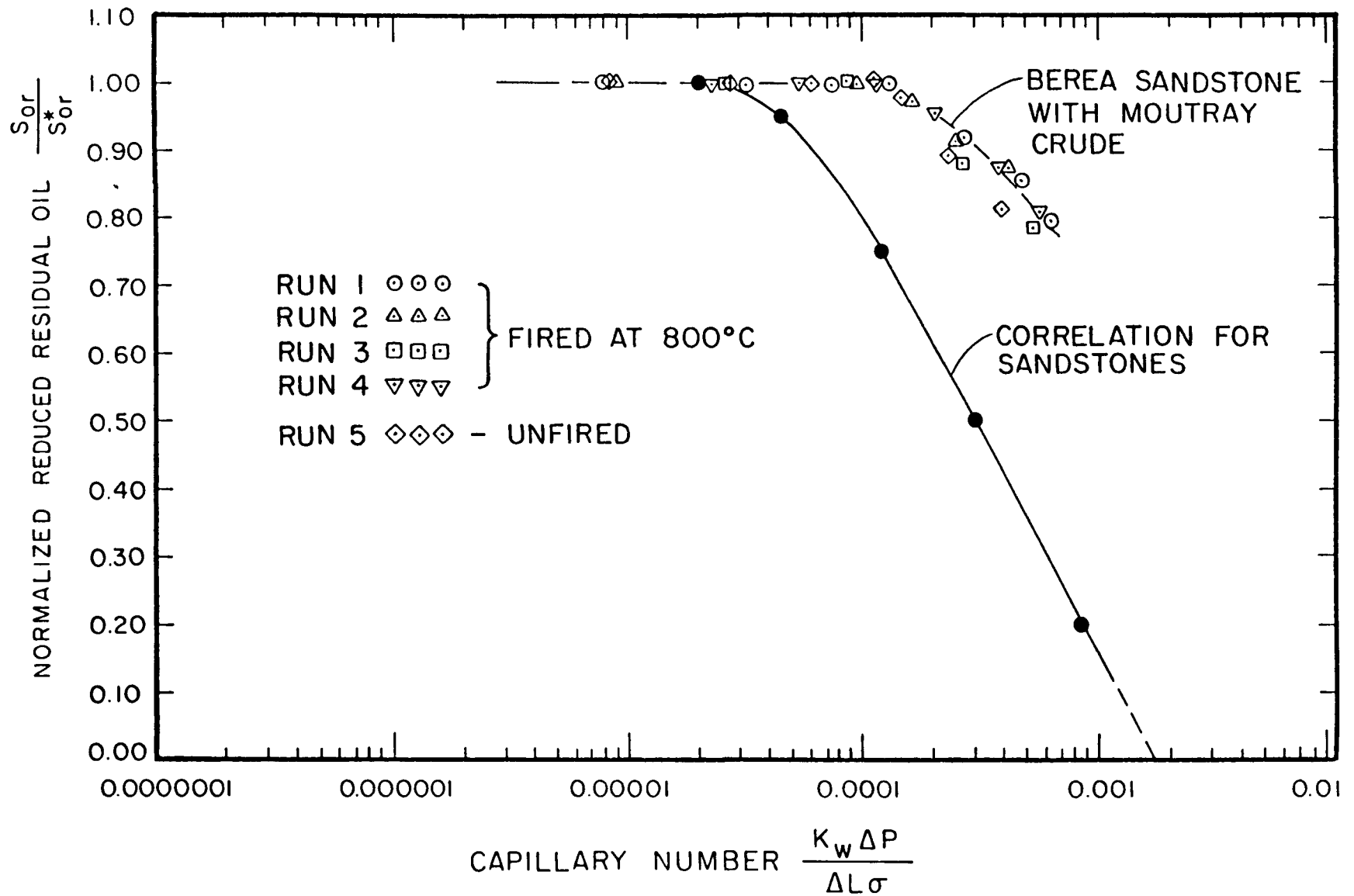
Fig. 2.4. Increase in capillary numbers for oil recovery caused by use of a crude oil which induces change in wettability.
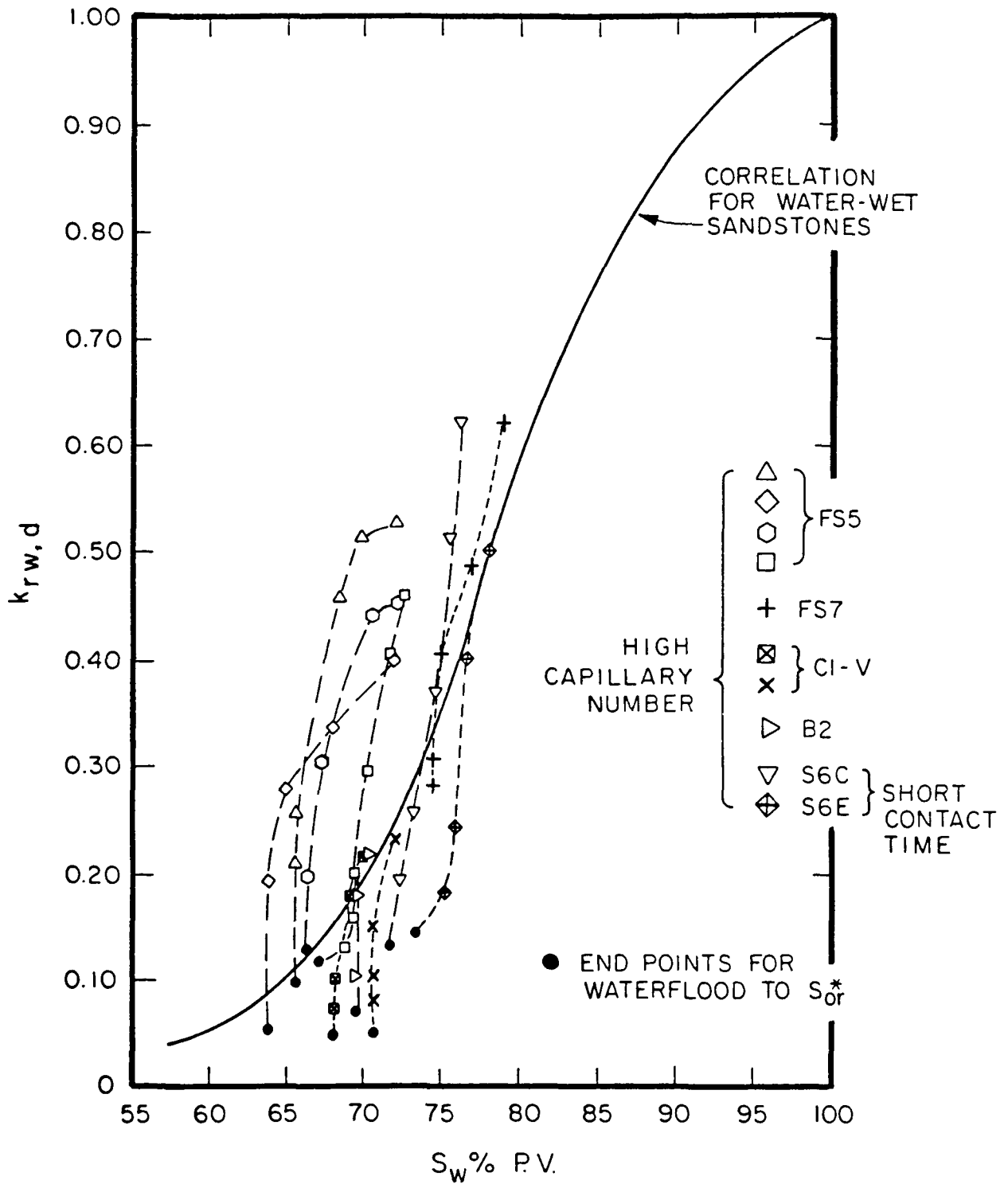
Fig. 2.5. Relative permeabilities at reduced residual saturations for Berea sandstone and Moutray crude oil. ($k_{rw,d}$ values at S_{or}^* are low but increase markedly with only small decrease in oil saturation.)
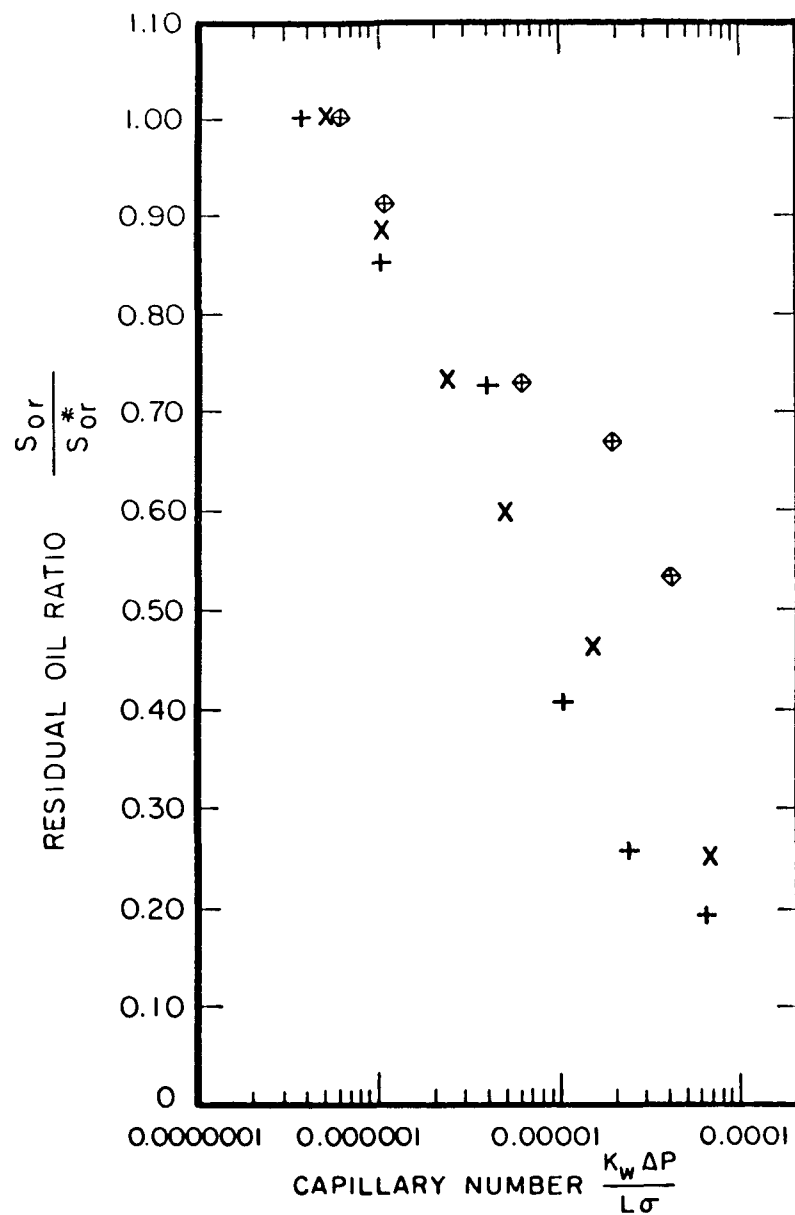
(a) CADDO LIMESTONE CORE D (See Table 1.3)   (b) CADDO LIMESTONE CORE C (See Table 1.3)
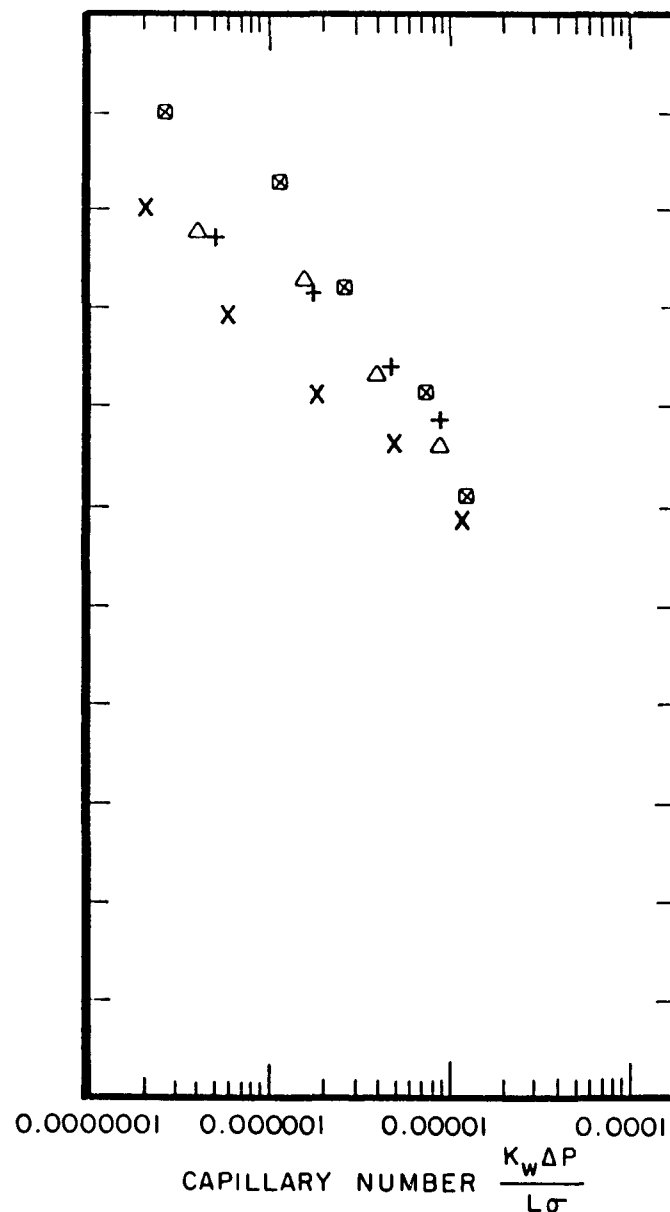
Fig. 2.6. Comparison of capillary number relationships for water-wet and Moutray-crude-induced wettability conditions. (x, +, Δ - Soltrol ; $\boxtimes$, $\oplus$ - Moutrav)
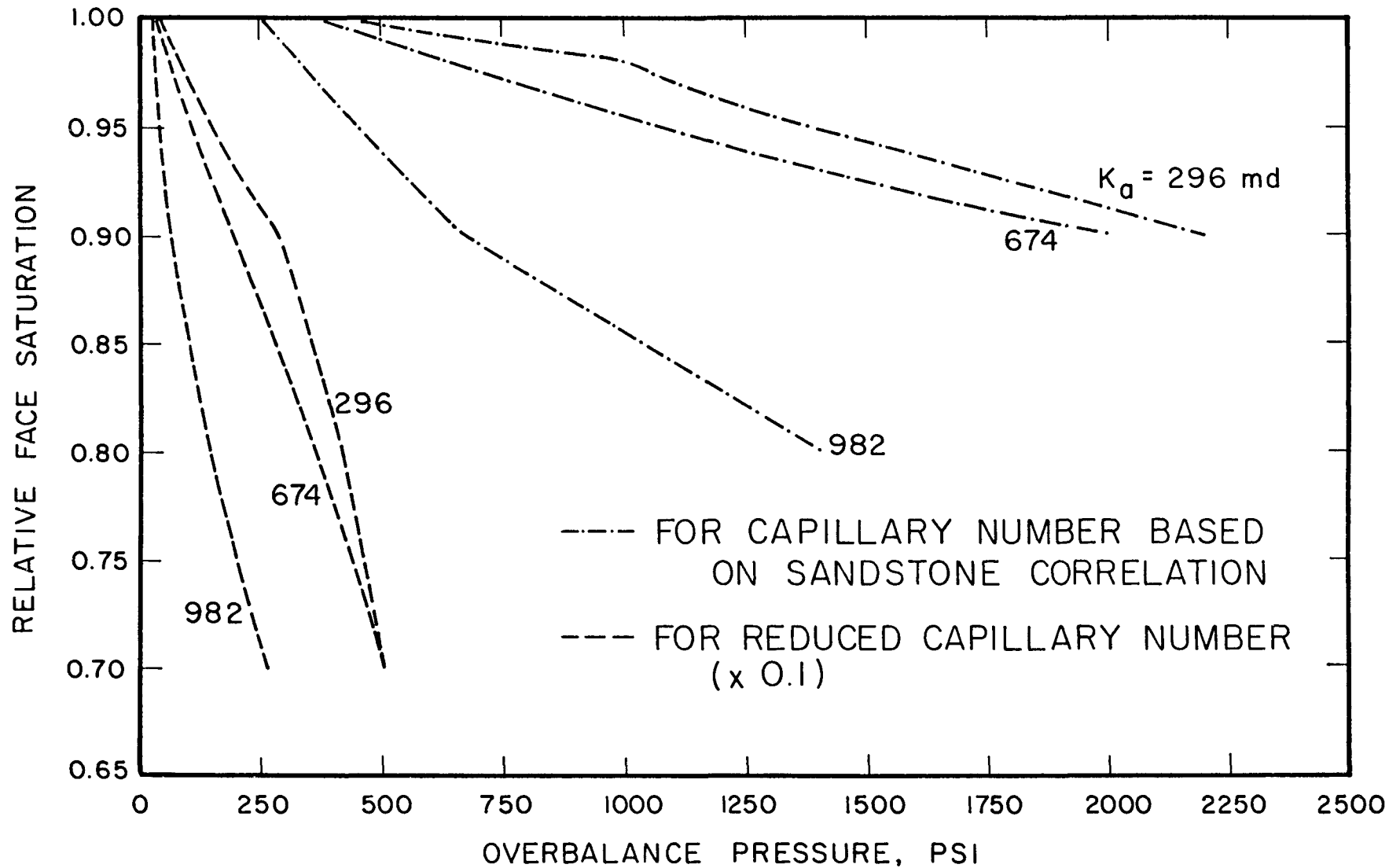
Fig. 2.9. Pressure based on (a) experimental capillary number relationships for three core samples (b) reduced values.
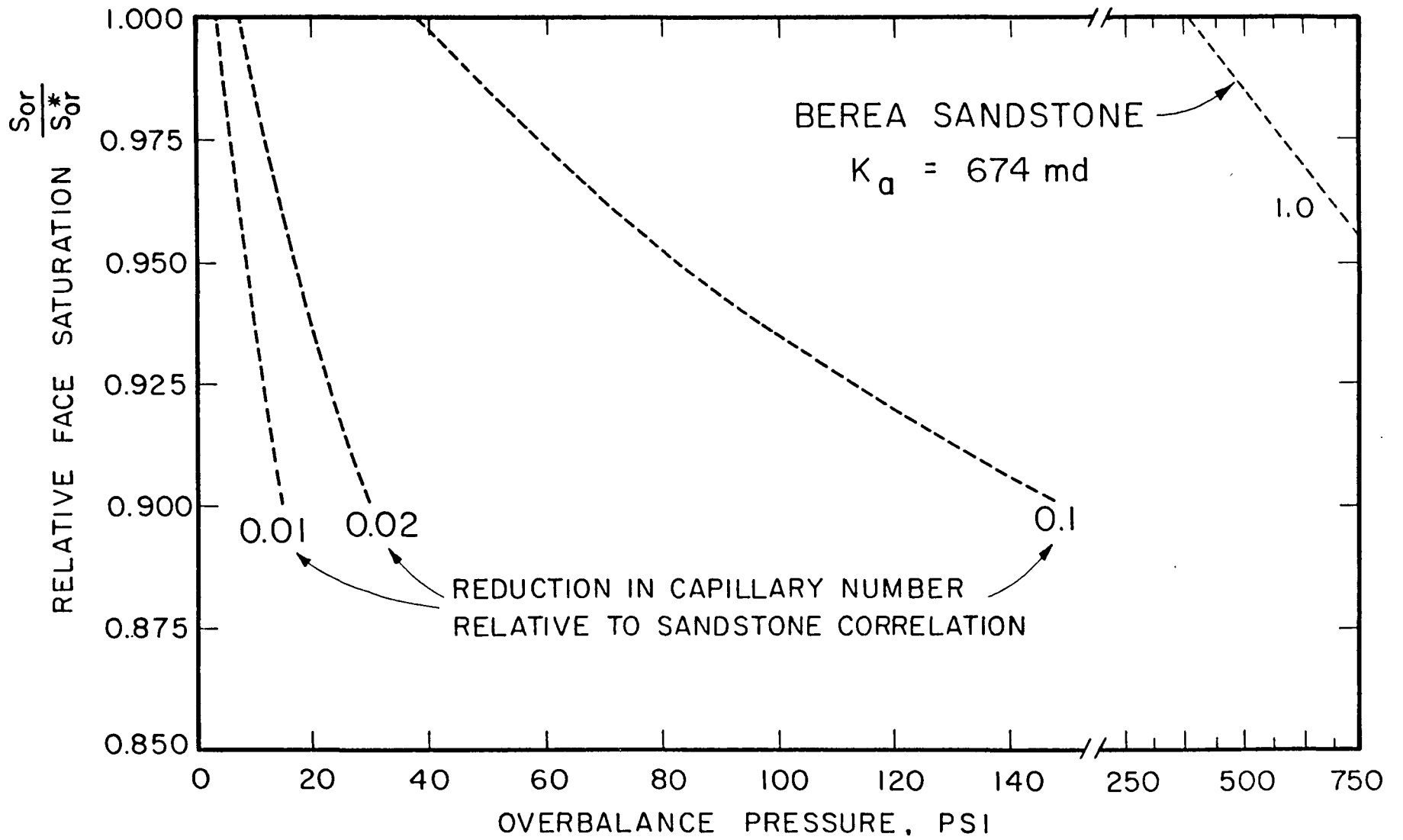
Fig. 2.10. Oil saturation at face of wellbore vs. overbalance pressure.
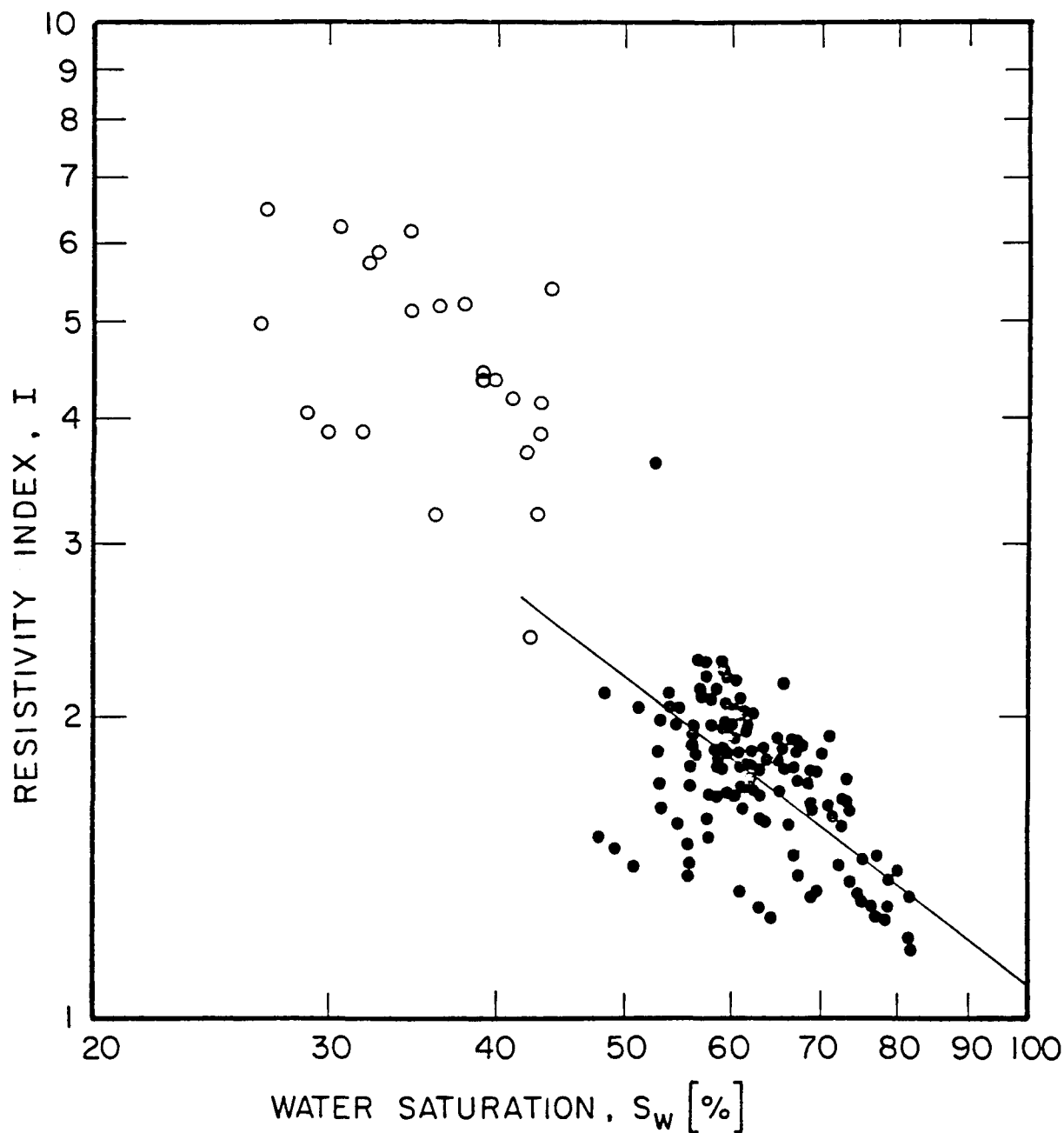
Fig. 2.11.   Resistivity index vs. water saturation for high
tension capillary number experiments. (23 runs)

●--- Residual and reduced residual oil saturations
($1-S_W$) obtained by waterflooding. ($\sim$ 7 data
points for each run)

○--- Initial water saturations obtained by oil
flooding. (1 data point for each run)
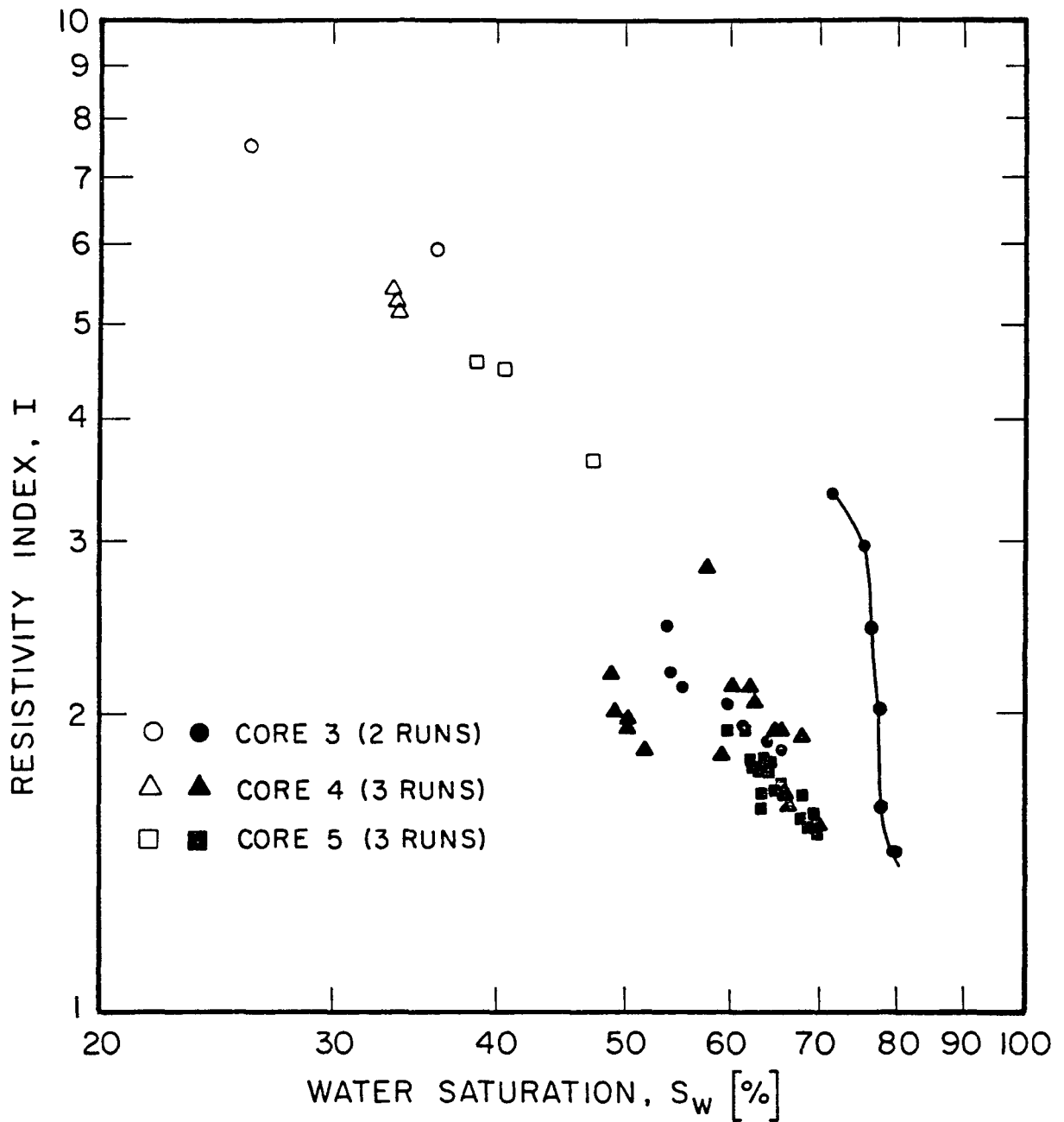
Fig. 2.12. Resistivity index vs. water saturation for 1%
Alfonic 610-50. The run indicated by connected
data points provides example of low initial
saturation and marked decrease in resistivity
with saturation more typical of results obtained
for 3% Alfonic 610-50. (See Fig. 2.13)

(Open symbols designate points obtained by oil flooding.)
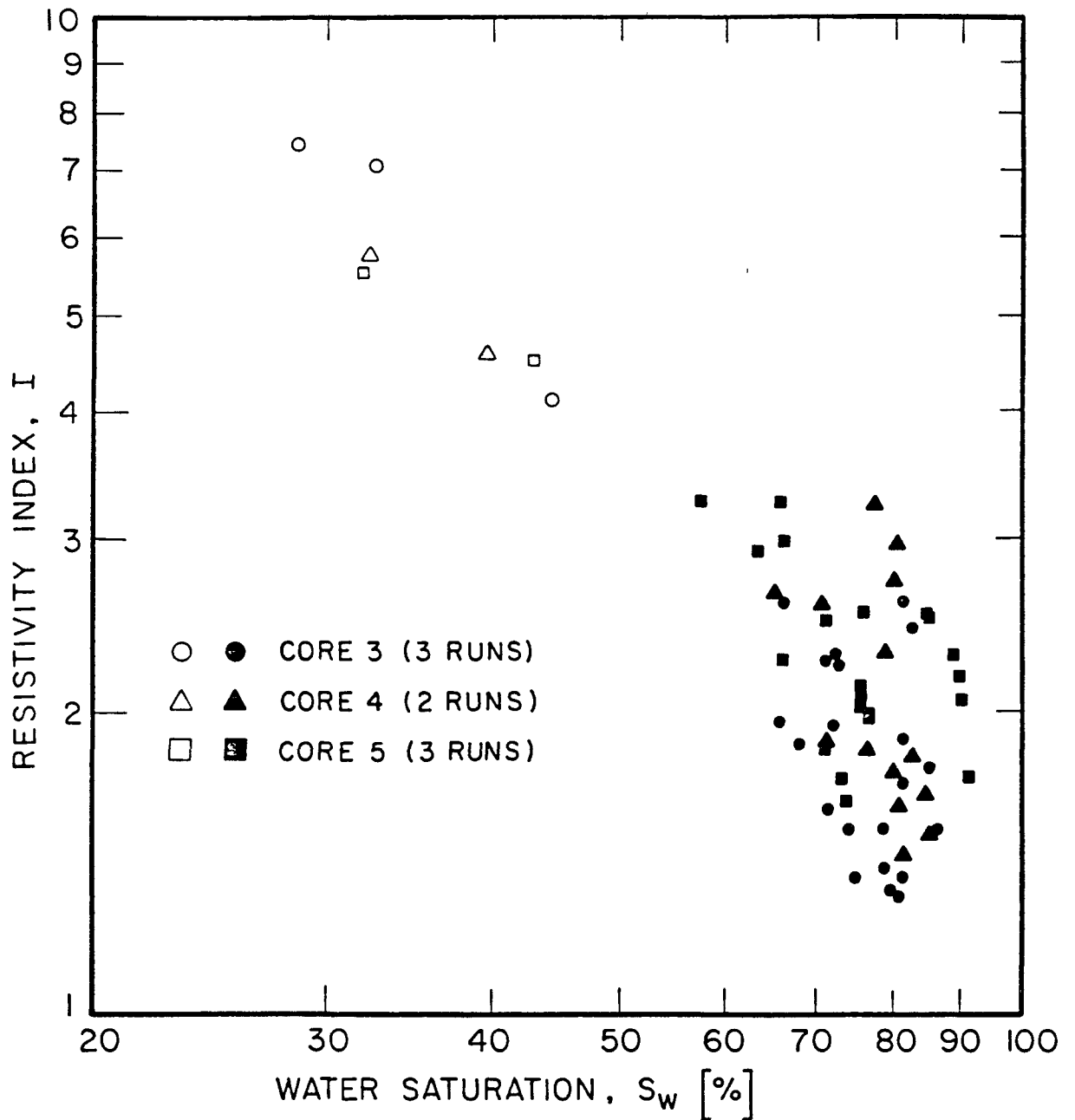
Fig. 2.13. Resistivity index vs. water saturation for 3%
Alfonic 610-50. In general, each run gave
marked decrease in resistivity with decrease
in reduced residual oil.

(Open symbols designate points obtained by oil flooding.)

58
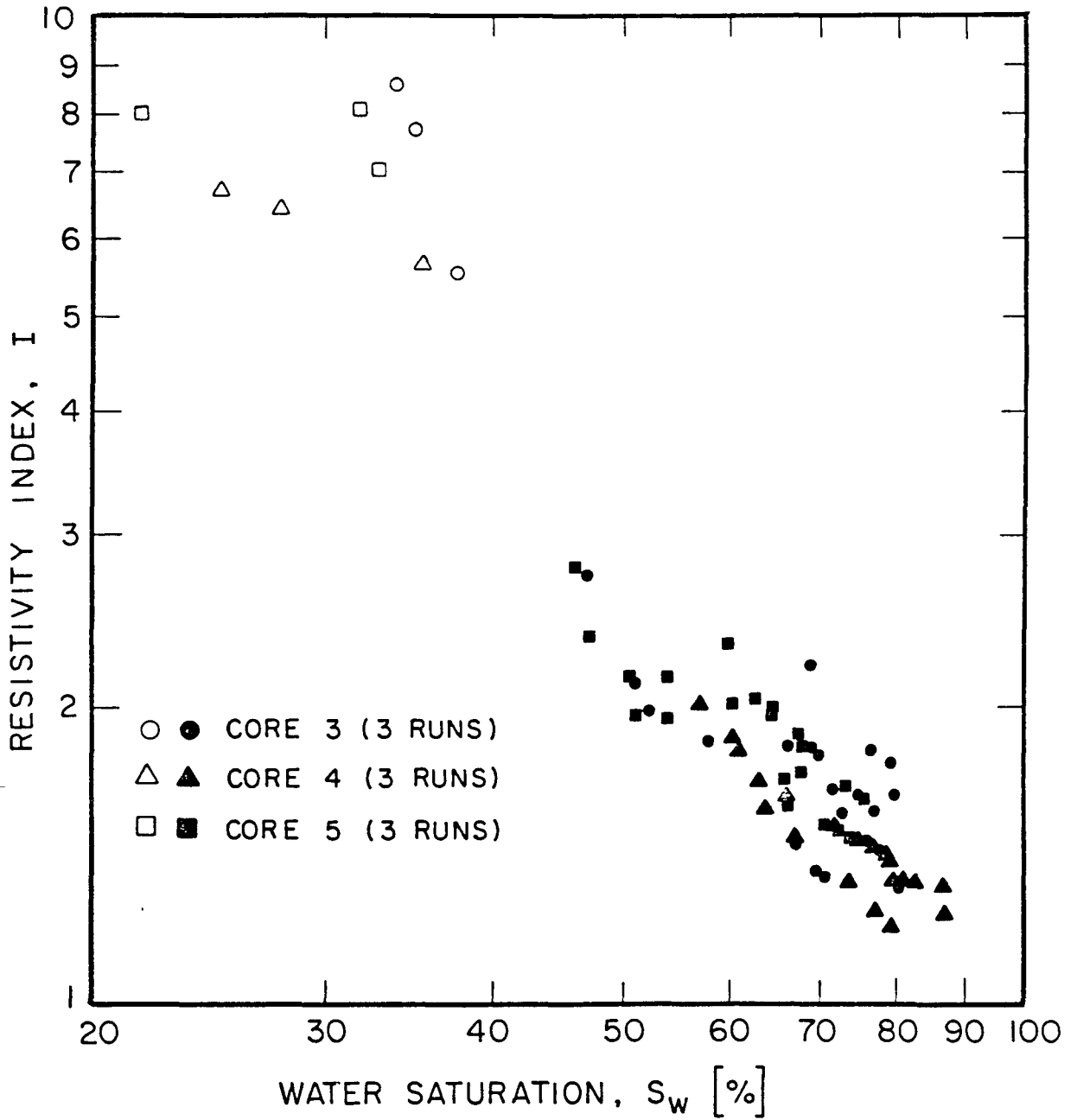
Fig. 2.14. Resistivity index vs. water saturation for 1%
EOR-200.

(Open symbols designate points obtained by oil flooding)
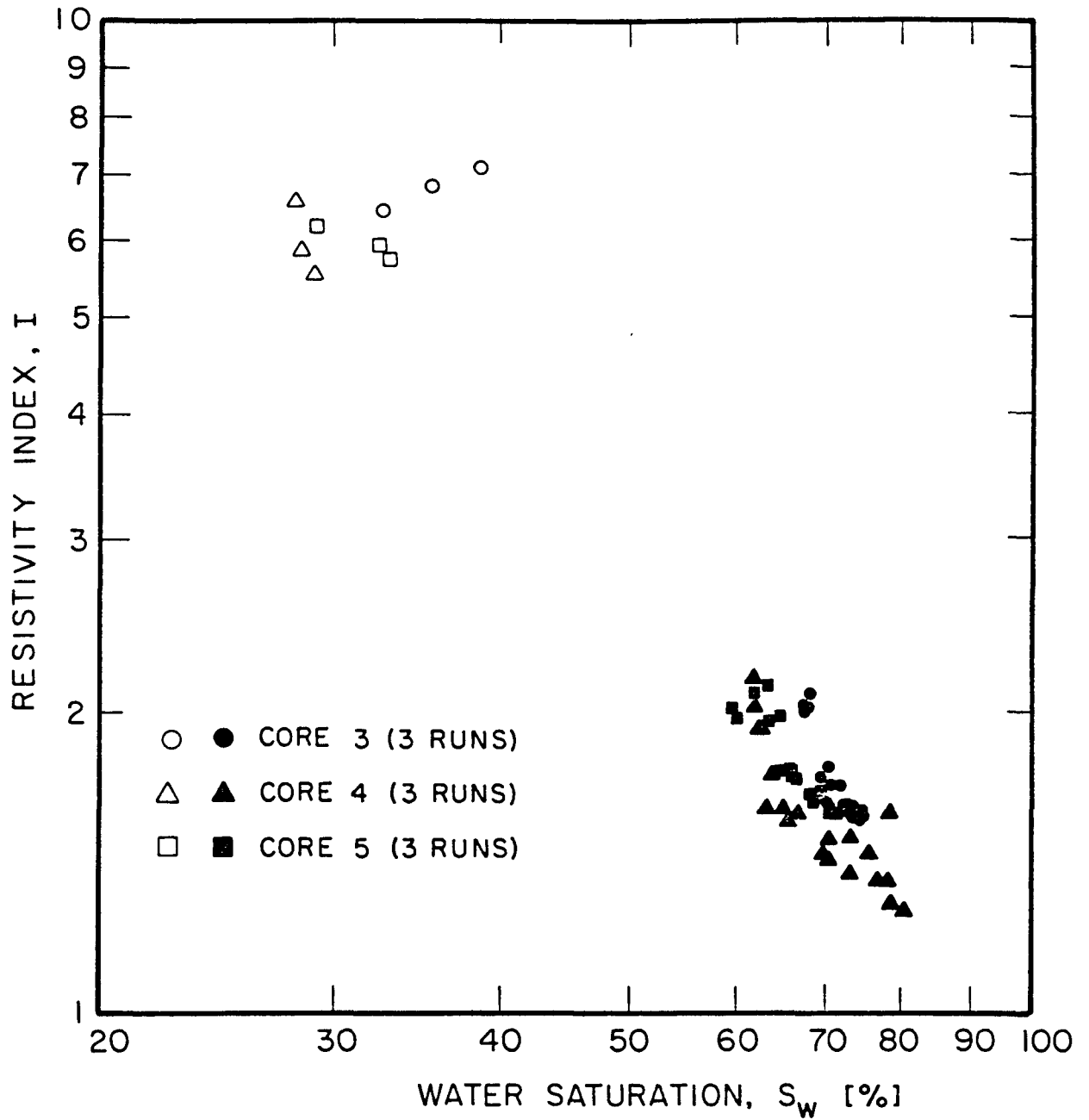
Fig. 2.15. Resistivity index vs. water saturation for the surfactant mixture. (3% Petrostep-465 + 2% EOR-200 + 2% Pentanol-1)

(Open symbols designate points obtained by oil flooding)
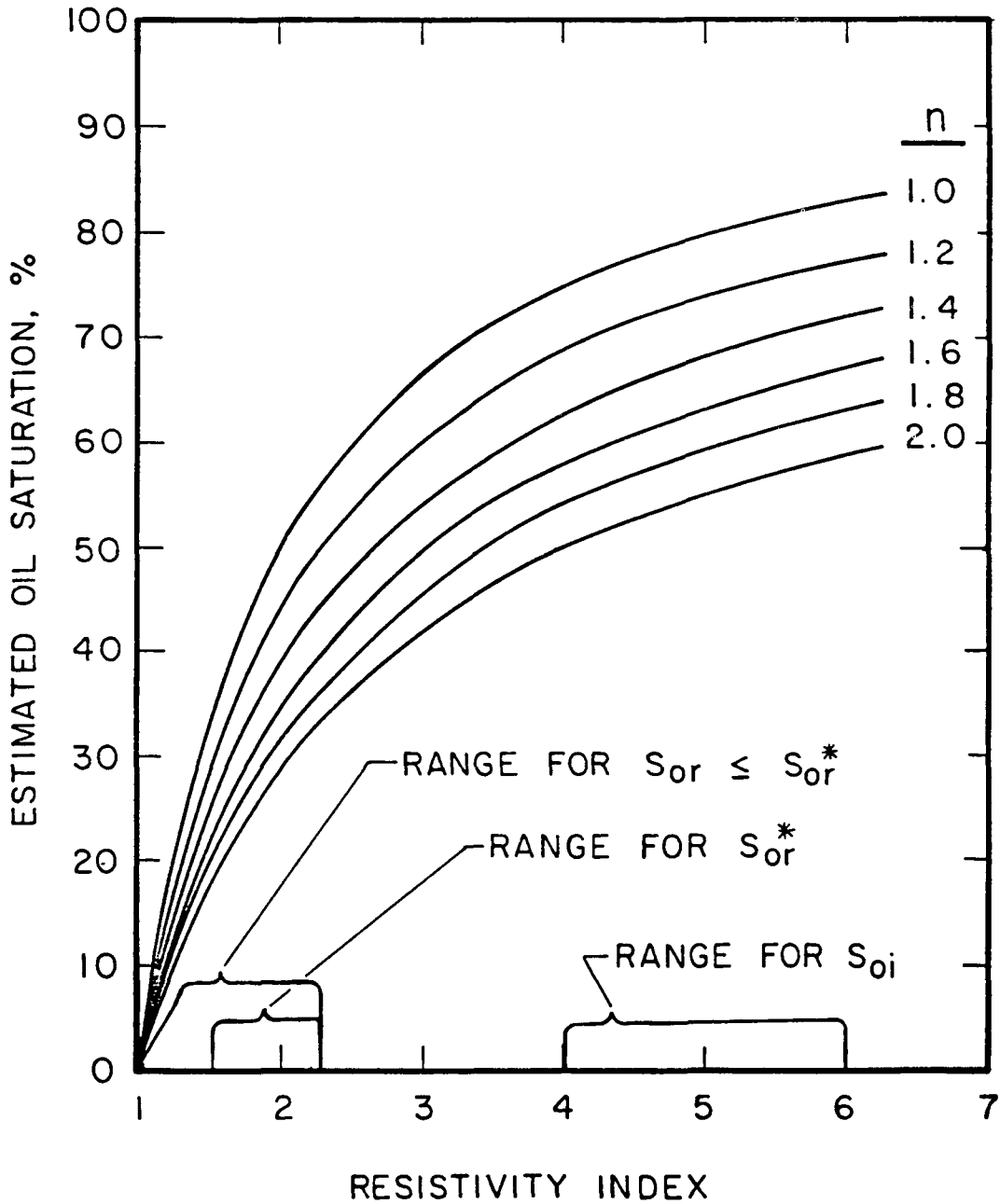
Fig. 2.16. Relationship between estimated oil saturation and resistivity index with saturation exponent as a parameter. Approximate oil saturation ranges corresponding to S_{oi}, and S_{or}^{*} and $S_{or} < S_{or}^{*}$ are shown.

TASK 3. MECHANISMS OF MOBILIZATION AND ENTRAPMENT OF RESIDUAL OIL

BACKGROUND

The objective of Task 3 was to identify mechanisms by which oil can become trapped and how it can be mobilized. Results are presented under three distinct topics:

(a) Magnitude and Detailed Structure of Residual Oil Saturation.

(b) Effect of Interfacial Tension on Stability of Displacement Fronts.

(c) Effect of Pore Shape on Displacement Curvatures.

Work under 3.a. concerns the mechanisms by which oil can become trapped and the factors which govern the magnitude of residual oil saturations. Work reported under 3.b. deals with changes in stability of displacement fronts that can occur when interfacial tensions are reduced to very low values. The effects of pore shape and wettability on mobilization of blobs and on displacement curvatures has been investigated using a combination of theory and experiment. This work is described briefly under section 3.c., along with reference to more detailed accounts which have either been published or are available in manuscript form.

3.a. MAGNITUDE AND DETAILED STRUCTURE OF RESIDUAL OIL SATURATIONS

An extensive study of trapping mechanisms was made for various types of porous media. This work has been reported in detail.[3.1] Conclusions of this study are given at the end of this section of the report along with other conclusions reached under Task 3.

3.b. EFFECT OF INTERFACIAL TENSION ON THE STABILITY OF DISPLACEMENT FRONTS

INTRODUCTION

Flow visualization experiments for immiscible fluid-fluid displacements in porous media have been carried out, with particular attention given to fluid pairs possessing low interfacial tension. For this purpose, special artificial

porous media consisting of 30-40 mesh fused glass beads were prepared, the thickness of these cells being about 5 bead diameters. Displacement patterns were observed and recorded using transmitted light. Instabilities due to viscous fingering, gravity effects and heterogeneities present in the cell can be readily observed and were recorded on videotape.

EXPERIMENTAL MATERIALS AND METHODS

Preparation of Flow Cells

Mirror glass and 30 to 40 mesh glass shot were used to construct the cells. The mirror glass is first cut to desired size to provide top and bottom plates and glass strips which were used as spacers between the plates. Then the copper and silver backing was removed with 50% HNO_3. The glass plates were washed, dried, and glued together temporarily to form a cell frame, open at one end, as shown in Fig. 3.1.

Glass shot was first treated with 50% HNO_3 to remove organic impurities and then washed with water and dried. The cell frame was carefully filled with the dry beads and then the last edge piece was inserted and glued to the frame. The assembled cell was subsequently fused in a muffle furnace. The glue used in assembly burned off during this process. Preliminary experiments have shown that the temperature must be at least 650°C in order to sinter the beads. After annealing, and cooling, the cell was sealed by applying epoxy resin along the edges and joints. Outlet and inlet holes were drilled, and the cells were washed with acetone and dried under vacuum before use.

Materials

Petrostep-420 (Stepan Chemical Company), Marasperse C-21 (American Can Company), butanol-1 (Baker Analyzed Reagent) and sodium chloride (Baker Analyzed Reagent) were employed for the formulation of most of the surfactant solutions and brines used in this work. Stock solutions of the individual components in distilled water were first prepared, and a given pair of these were mixed together to give the desired concentration. A constant order of mixing was maintained. In several experiments, Witco TRS10-80 was used as the principal surfactant. Approximately 0.01% of sodium azide was added to all surfactant solutions to prevent bacterial growth.

The organic liquids (oils) used in this work include isooctane, Soltrol 130 and two grades of paraffin oil (specified as having Saybolt viscosities of 80 to 90 and 180 to 190 at 100°F). Special organic liquids were also prepared by mixing isooctane with paraffin oil and carbon tetrachloride in order to obtain

liquids of desired density and viscosity. Details of liquid compositions and properties are given along with the results.

Oil and aqueous phases were prepared by a procedure described previously.[3.2] In brief, this was as follows: oil-surfactant solution pairs were equilibrated for one week before measuring interfacial tension. In most cases a small opaque region formed between the two main phases. The upper phase (oil) was separated and the lower phase and opaque region were mixed. The dispersion so formed was stable for up to about a month.

Measurement of Physical Properties

Low interfacial tensions were measured using a spinning drop tensiometer. Tensions greater than 2 mN/m were determined using a Rosano tensiometer.

Most density measurements were performed using an Anton Parr digital densitometer. Some surfactant solutions tended to leave a deposit in the densitometer tube; in such cases, the gravity bottle method was employed instead. A Cannon-Fenske viscometer was used to determine viscosities.

Displacement Experiments

The flow cell was filled with the liquid to be displaced (normally oil) under vacuum. The inlet port was connected to an ISCO 28150, Model 314 metering pump charged with the displacing phase prior to a displacement test. Various combinations of dyes were used to aid in videorecording the displacement fronts.

RESULTS AND DISCUSSION

Displacement of Isooctane (100% Initial Saturation) with Surfactant Solutions

The aim of this part of the study was to investigate the effect of interfacial tension and coalescence rate on the displacement of oil by aqueous surfactant solutions. The importance of droplet coalescence for efficient oil recovery has been recognized only recently. Without coalescence, isolated oil droplets or ganglia mobilized by the surfactant flood may undergo breakup and reentrapment.

The overall coalescence process includes all those steps leading up to a direct contact of the constituent droplets. All coalescence processes are

characterized by the formation of a protective layer between the droplets. Coalescence, if it occurs at all, must be preceded by two steps: 1) the drainage of the intervening film to such a thickness that it becomes unstable, and 2) rupture of this film. The rate of coalescence is often expressed in its reciprocal form, t_cF, where t_c is the time required for the rupture of the film and F is the coalescence force.

The fluid pairs selected for this work had been previously studied by Son, Neale and Hornof,[3.2,3.3] and their interfacial tensions and coalescence rates have been determined. Isooctane was selected as the oil phase despite its very low viscosity (0.4 cp.) In water-wet media at least, one would expect stable displacements because of the favorable viscosity ratio (assuming an aqueous phase viscosity of 1.0 cp or more). However, preliminary experiments showed that these systems may, in fact, exhibit considerable instabilities at low interfacial tensions which correspond to high coalescence rates.

Table 3.1 lists the composition of the surfactant solutions used for the displacement of isooctane from sintered glass bead packs. Interfacial tensions were close to previously observed values for the two series of solutions (A,B).

A summary of test conditions is included in Table 3.1. Illustrations, prepared from tracings of fronts at intermediate stages of displacement, are shown in Figs. 3.2 through 3.14.

Set A (Figs. 3.2 through 3.5) were the first experiments in this study. For these, no particular attention was paid to how long the oil phase was present in the cell before the flooding was initiated. System C1A (IFT = 1.28 mN/m) shows a very stable displacement; systems C2A (IFT = 0.84), C3A (IFT = 0.35) and C4A (IFT = 0.06) show an increasing degree of instability. It is interesting to note, however, that the amount of oil recovered at breakthrough is greater for C4A than for C3A. This is also evident in Set B. This apparent anomaly is explained by increased mobilization of initially bypassed oil blobs and regions of bypassed oil and their rapid coalescence in the presence of the C4 surfactant, which exhibits very low interfacial tension against the oil phase. The rapid coalescence of moving oil blobs to form an oil bank behind the advancing surfactant front was in evidence both in C4A and in C4B.

Because the systems had distinctly favorable viscosity ratios, the instabilities observed with C3A, C4A, and to some extent with C2A were rather unexpected. Although the observed instabilities were clearly associated with low interfacial tension values, the possibility that they were caused by some experimental condition other than interfacial tension and coalescence rate must be considered. Perhaps the most important factor which can affect displacements of this type is wettability. While the glass bead models have been shown by preliminary experiments to be strongly water-wet, introduction of the dyed oil phase and of the surfactant solution could affect the wetting behavior of the glass bead surface.

Contact angles on a smooth glass surface (the bottom of large UV cells) for systems C1A through C4A were therefore determined. The advancing angles (measured through the water phase) are shown in Table 3.2. It is seen that the initial contact angles are strongly water-wet in all four cases. They all

increase with time, although this increase is more rapid with C2A and C4A (see Table 3.2). It is thus possible that intermediate wettability conditions may have prevailed in the flow cells for the C2A and C4A systems.

In Set B, contact angles for isooctane against water were included. None of the blue dye and only 0.05% of Oil Red O dye were added. The values of advancing contact angles measured for these systems are shown in Table 3.3. In this case, all the contact angles remain in the water-wet range, although some variation with time is still present. Moreover, it would appear from the results shown in the extreme right column in Table 3.3 that the red dye has little to do with the wettability change. Thus, it is tentatively concluded that the presence of surfactant and/or cosurfactant probably accounts for the increase in contact angles observed for the CA and CB systems. Interaction of surfactant with the dye is also a possibility, of course.

Because of the changes in contact angles with time, set B displacement experiments were conducted at two different oil residence times: 5 minutes (Figs. 3.6 through 3.9) and 45 minutes (Figs. 3.10 through 3.13). Although the displacement patterns are not entirely identical for the 5 and 45 minute experiments, the trend of increasing instability with decreasing interfacial tension is clearly visible in both and is in agreement with the results of Set A experiments. The oil recovery data shown in Table 3.1 is also qualitatively similar for all three sets of experiments. It is concluded that the effects observed are primarily related to the variation in interfacial tension.

Sources of Instability in Low Tension Flooding

The displacement pattern observed in the blank experiment CO (Fig. 3.14), in which 1% NaCl brine was used to displace isooctane, is essentially identical with the behavior of systems C1A, C1B-5 and C1B-45 in that a stable displacement front is formed. It is evident that in order for instabilities to occur, it is necessary to reduce the interfacial tension to about 1 mN/m.

In a high tension displacement in which the wetting phase is displacing the nonwetting phase, any perturbation occurring at the interface between the two phases will be blunted by capillary forces. A rapidly advancing "finger" which is initiated, for example, by a heterogeneity in the pore structure, will not be allowed to develop fully because the liquid in it will be drawn by capillary forces into adjacent pores, thus damping the perturbations and creating a stable interface. When capillary forces are diminished by reducing the interfacial tension (or by using a nonwetting liquid as the displacing phase, as will be shown later), this damping effect will be reduced and instabilities will have a chance to develop.

Another important feature of the low-tension displacements is gravity separation. While the high interfacial tension systems C1 and CO showed sharp interfaces (see Figs. 3.2, 3.6, 3.10 and 3.14) with little or no overlapping of the phases, at lower interfacial tension, even though the depth of beads was only ten layers, the interfaces became fuzzy or almost invisible. In regions of

66

partial saturation, it appeared that isooctane was floating on the more dense aqueous phase.

Vertical stability of two fluids in a porous medium depends on the value of the corresponding Bond number. This dimensionless quantity compares capillary forces with the force of gravity acting over a microscopic length.

$$N_{B(K)} = \Delta\rho gK/\sigma \qquad (3.1)$$

where $\Delta\rho$ = density difference
K = permeability
σ = interfacial tensions

For bead packs, Morrow and Songkran[3.4] define Bond number as:

$$N_{B(R^2)} = \Delta\rho gR^2/\sigma \qquad (3.2)$$

where R is the sphere radius. The permeability-based Bond number is related to the radius-based Bond number through the relation:

$$N_{B(K)} = 0.00317 \ [N_{B(R^2)}] \qquad (3.3)$$

In vertical displacements, it was found that for $N_{B(R^2)} > 0.35$ no trapping of the nonwetting phase occurred. On the other hand at $N_{B(R^2)} < 0.0067$, the gravity force has no effect on trapping. In terms of $N_{B(K)}$, according to equation (3), these limiting values correspond to 1.11×10^{-3} and 2.11×10^{-5}, respectively.

The values of Bond number calculated for the present systems are listed in Table 3.1. Comparing these with the limiting values shown above, it would appear that the systems C0, C1B, and perhaps to some extent C1A and C2B, should not suffer underride, and this is borne out by the experiments. In contrast, system C4A which had a high Bond number was characterized by fuzzy interfaces and phase layering. All the other systems are situated well between the two limiting values of $N_{B(K)}$, and their displacement tests show various degrees of instability and superposition of phases.

Displacement in Porous Media Initially Containing Both Oil and Water

Model studies of both secondary displacement of oil at connate water saturation, and tertiary displacement of oil at normal waterflood residual oil saturation (S_{or}^*) present additional problems. In particular, dilution of the injected surfactant solution with the water (brine) will give rise to concentration gradients which in turn may produce interfacial tension gradients involving a change of several orders of magnitude. Since the phases are not in equilibrium, mass transfer effects may become important. Also, such displacements are difficult to visualize in the models since the phases are intermingled, and it is often not possible to see clearly where flow and/or displacement and mobilization occurs.

To date, two displacement experiments in which connate water was present have been performed using systems C1A and C4A. To carry out these tests, the cell was first filled with 1% NaCl brine. Three pore volumes of oil (isooctane equilibrated with solution C1A or C4A) were then injected at a high rate. This was followed by flooding with the corresponding surfactant solutions.

In system C1A, the surfactant fingered rapidly through the cell. The low tension system C4A, however, gave mobilization of oil blobs and formation of an oil bank in front of the advancing surfactant.

Displacements with Fluids Having Matched Density and Viscosity

The results discussed in the previous section have indicated that even in the thin layered micromodel media, buoyancy forces may be important in inducing instability during the displacement of isooctane with surfactant solutions. Thus, it was of interest to investigate what would happen if such buoyancy effects were eliminated by matching the density of the fluid to be displaced with that of the displacing fluid. The viscosities of the two fluids were also closely matched. This made it possible to carry out the displacement of the nonwetting phase with the wetting phase and vice-versa, at constant viscosity ratio.

Formulation of Fluid Pairs

Using the density and viscosity of the aqueous phase as a basis, organic solutions (oils) were formulated by mixing together three components: isooctane, carbon tetrachloride, and paraffin oil. The properties of these substances are summarized in Table 3.4. This procedure takes advantage of the high density of CCl_4 to adjust the density of the oil phase, and of the high viscosity of paraffin oil to adjust the viscosity, in order to match the density and viscosity of the aqueous phase.

Although the density of such a mixture of nonpolar components can be predicted with reasonable accuracy, the viscosity dependence is more complex. Consequently, a trial and error method was employed. The resulting composition is shown in Table 3.5. Its density and viscosity are compared with the corresponding properties of the aqueous phase, and both density and viscosity are very well matched (within ±1%). Due to other effects such as evaporation of the volatile component (isooctane), variations in salinity and the addition of a surfactant and/or cosurfactant, the fluctuation of density and viscosity in the fluids used for displacement experiments might be somewhat greater (3%).

The techniques employed for measuring interfacial tension necessitate a certain density difference between the two fluids. As a consequence, the interfacial tension of matching-density, organic-aqueous pairs cannot be measured directly. To circumvent this difficulty, organic solutions were prepared in

68

which the proportion of CCl_4 was somewhat lower in order to create a density difference between the two phases (about 0.05 g/cm^3). As shown in Table 3.6, the amount of CCl_4 added had a relatively small effect on interfacial tension.

Formulation of Aqueous Phase for Low Interfacial Tension

Aqueous phases complementary to the organic solution shown in Table 3.5 were formulated to provide a range of interfacial tensions extending to very low values. The lack of density difference once again made it impossible to equilibrate the two phases in the normal fashion as they tended to disperse in each other, making their quantitative separation impossible. Therefore, a method similar to that employed for measuring interfacial tension was used. The aqueous phase was equilibrated with an organic solution containing less CCl_4 to provide a sufficient density difference. The pairs were equilibrated for one week, and then separated. Their interfacial tensions were determined and subsequently the complementary amounts of CCl_4 were added to adjust the concentration to that shown in Table 3.5.

The compositions of the aqueous phases are shown in Table 3.7. The same table also lists interfacial tensions against the organic phase. It was difficult to obtain reproducible contact angle values because of the very small density differences between the phases. The data obtained are listed in Table 3.8. With the exception of the system M3, most contact angles seem to be in the water-wet region. The ultra-low IFT system M2-B seems to exhibit a maximum contact angle after 4 to 15 minutes; there also seems to be a maximum in the case of M3. It would appear that, in general, ultralow interfacial tension goes hand in hand with higher advancing contact angles. Also, under low tension conditions, it becomes very difficult to obtain reproducible contact angle values. When an oil droplet is first ejected from the pipette and touches the surface which has been in contact with the aqueous phase, the corresponding (receding) contact angles are, in general, strongly water-wet. When the droplet is then retracted, the corresponding (advancing) contact angle may vary from water-wet to intermediate wettability.

The system M2-B is very close to optimal salinity.[3.2] Reed and Healy[3.5] observed the value of contact angle at optimal salinity to be approximately 68°. For system M2-B, the mean value of advancing contact angle calculated from Table 3.8 is about 63°, which is consistent with the work cited above.

In those experiments where the aqueous phase is displaced by injecting the oil phase, water is retreating from the pores and therefore receding contact angles are of importance. The measured values of receding contact angles are shown in Table 3.8. The corresponding advancing angles are also shown and are significantly higher for all four systems. Once again, the angles are higher for systems with low interfacial tension (i.e., M2-B and M3); and the reproducibility of measured values for these systems is obviously very poor.

Displacement Experiments

Cell Initially Saturated with Oil Phase

Displacement experiments have been carried out using systems M1, M2, M2-B, M3 and M4. These systems provided about four orders of magnitude variation of interfacial tension. Preliminary experiments gave an indication that these displacements were quite different from the C series. Thus, the removal of buoyancy forces caused significant change in behavior. There was no visible underflow (or overflow) at the advancing front of the displacing solution, nor was there any vertical separation as would be indicated by a superposition of the two phases. The behavior described above was characteristic of all experiments in the M series, regardless of whether water was displacing oil or vice-versa and no matter how unstable a displacement appeared to be. Each experiment was performed at least twice as a check that observed trends were reproducible.

The results of experiments in which aqueous phase displaces oil phase are summarized in Table 3.9. Typical displacement patterns obtained with the five systems are shown in Figs. 3.15 through 3.19. It is seen that although there are some differences in the displacement behavior of these five systems, these are not substantial. Interpretation of the oil recovery data listed in Table 3.9 must be regarded with extra caution, as the amount of oil recovered depends a great deal on how the displacement begins. Thus a test in which a smooth displacement front forms in the downstream half of the cell area may yield less oil than a test showing a ragged interface throughout, simply because of areas bypassed by the displacing solution at the start. After breakthrough, low interfacial tension displacements tend to yield more additional oil since the oil left behind after the initial sweep is more readily mobilized. The initial development of the displacement front depends very much on the presence of heterogeneities in the porous medium. Thus, a repetition of an experiment usually gives a very similar displacement pattern (e.g., a formation of two broad tongues along the sides of the cell which later fuse into one solid front).

The effect of interfacial tension is not readily discernible in these displacements. The system M2-B, which had the lowest interfacial tension, gave rather stable displacements comparable to, or even more stable than those with high tension systems (M1, M2). The instability observed with the system M3 (and probably also M4) is most likely due to the high advancing contact angles, which reduce or eliminate completely the damping effect of capillary imbibition. It is apparent that in the absence of density difference, there is no longer a marked effect of interfacial tension on the stability of the displacement front.

Cell Initially Saturated with Water Phase

In the second set of experiments, the cell was initially saturated with the aqueous phase and subsequently flooded with oil phase. The results are summarized in Table 3.10. Once again, it should be noted that the percentages of water recovered shown in Table 3.10 are only approximate values. Determination of the breakthrough point was quite difficult in most of these experiments, resulting in a high degree of uncertainty in the measurements of recovery. The

70

injected oil tended to flow along the edges of the cell, and the breakthrough was not always clearly visible. Nevertheless, there was a trend of more aqueous solution being recovered prior to breakthrough in the low-tension displacements.

In a qualitative sense, it is evident that the stability of the displacement front increases dramatically with decreasing interfacial tension. The high tension floods (M1) show a very ragged interface (Fig. 3.20). Long capillary fingers advance a considerable distance (up to 10 bead diameters or even more) ahead of the advancing oil front. These branch out and reconnect extensively, thereby enclosing and leaving behind regions of trapped aqueous phase. Even when the flow rate was increased 25 times (to 200 cm^3/hr), patches of trapped water were retained.

The system with intermediate interfacial tension (M2: σ = 1.2 mN/m) also shows a ragged interface, but the capillary fingers are shorter, and little aqueous fluid is left behind (Fig. 3.21). There is still considerable flow along the edges of the cell, but the displacement front advances steadily even after breakthrough.

The stabilization effect of low interfacial tension becomes clearly evident in systems M2-B, M3 and M4 (Figs. 3.22, 3.23 and 3.24, respectively). In the case of M2-B, the injected oil advances as a growing semicircle around the inlet. The capillary fingers are very short, not exceeding 1 to 2 bead diameters. The displacement is stable, with much less advance of fluid along the permeable edges. As a consequence, recovery of the aqueous fluid is high.

The M2-B displacement pattern is more or less repeated with the other low tension systems, M3 and M4, although they both appear to give a less uniform interface than M2-B. In particular, the M4 displacement starts in a ragged fashion, resulting in a larger amount of trapped aqueous phase. It should be noted that these experiments in which the aqueous phase is displaced by the oil phase show a remarkable reproducibility. In the high tension experiments, the flow pattern is determined by the heterogeneities of the porous medium. Any effect of such heterogeneities, on the other hand, is almost completely masked when the interfacial tension is lowered sufficiently.

3.c. EFFECT OF PORE SHAPE ON DISPLACEMENT CURVATURES

A series of four papers on the relationship between pore shape and displacement curvatures has been prepared. Some of these papers are published; the others are available in manuscript form as indicated below. Topics dealt with in these papers are presented here in brief summary. The status of work on a fifth topic, the combined effect of contact angle and pore geometry for pores of nonuniform cross section is also reported.

Effect of Contact Angle on the Meniscus between Two Equal Contacting Rods and a Plate[3.6]

Initial work was concerned with menisci in the space between two rods and a plate. Experiments were performed using capillary rise and bubble movement to test theoretical values for both perfectly wetted systems and for systems which gave reproducible advancing and receding contact angles. Results were in excellent agreement with a theoretical approach to calculating displacement curvatures proposed by Princen for capillary rise in systems of rods.[3.7-3.9] During the course of this work, it was concluded that the theory could be generalized and subjected to more rigorous experimental tests.

Meniscus Curvatures in Capillaries of Uniform Cross Section[3.10]

Menisci in capillaries of uniform cross section can be broadly classed according to whether wedge-like structures exist, such as in the case of triangular section tubes, or do not exist, as for example in circular section tubes. In tubes which form wedge menisci, the liquid in the wedge adopts a form so that a section through the liquid surface is the arc of a circle. The volume of liquid per unit length of the wedge is constant along the tube. A non-wedging meniscus, however, is locally bounded by its tube and has a curvature inversely proportional to the hydraulic radius of the tube. Mayer and Stowe[3.11] proposed an approximate method of determining displacement curvatures in sphere packs, later applied independently by Princen[3.7-3.9] to estimate capillary rise in spaces between parallel rods. This method, which incorporates the presence of wedges, is shown to be exact for determining displacement curvatures in systems of constant curvature. Experimental confirmation of the theoretical predictions was obtained to within 1 1/2% from measurements of capillary rise of a perfectly wetting liquid in tubes formed either by a rod and a square corner (see Fig. 3.25 for configuration) or by two rods and a plate. Results are presented in Fig. 3.26. The conditions of pore geometry and contact angle which give rise to wedge menisci are discussed in general terms and illustrated by examples which include menisci in a tube of polygonal section (see Fig. 3.27).[3.10] Example results for polygons of 3, 4 and an infinite number of sides are presented in Fig. 3.28.

Coexistence of Menisci and the Influence of Neighboring Pores on Capillary Displacement Curvatures in Sphere Packings[3.12]

Even with the simplifying assumption that the porous media is formed from packings of equal spheres, solutions for the configurations at which a meniscus penetrates are very difficult to obtain. In general, calculation of the displacement of a wetting phase from porous media involves boundary conditions that are set in part by neighboring pores. In the past, various approximations to the meniscus curvature have been used to obtain estimates of this maximum curvature, the most widely applied being the Haines approximation which takes the

meniscus to be a portion of the spherical surface which just fits into the pore.[3.13] Present work has been concerned with drawing together and comparing presently available analyses. Examples drawn from the literature[3.11,3.13-3.15] are presented in Fig. 3.29. These have then been extended with particular emphasis being placed on the influence of boundary conditions provided by neighboring pores on the values of maximum curvature developed in a given pore.

A key result of this investigation was establishing a link between curvatures for pores formed by rods and those formed by spheres. For rods, displacement curvatures can be calculated exactly, whereas the mathematics of calculating displacement curvatures in sphere packings is close to intractable. However, experimental results for spheres were in reasonable agreement with theoretical results for rods. Calculations for rods were therefore extended to a wider range of configurations including both asymmetric and symmetric pore shapes with defined boundary conditions determined by mirror-image neighbors.

Comparison of a complete range of computed results (which strictly apply to rods) with the Haines insphere approximation shows that, to a first approximation, the theory gives dimensionless curvatures (normalized with respect to sphere radius) which are about 1.5 lower than the Haines values, and in good agreement with available experimental results.

Consideration of the effects of neighboring pores on displacement curvatures indicated that the assumption of mirror-image neighbors was generally appropriate. If the change in boundary conditions caused by drainage of one pore affects its neighbor, the result may be either simultaneous drainage of both pores, or if the neighboring pore remains filled, its drainage curvature will be reduced because the mirror-image neighbor boundary condition no longer applies. Both of these mechanisms will tend to cause pore sizes estimated from capillary pressure relationships to be narrower than those given by the geometrical structure of the packing.

Capillary Displacement Curvatures for a Spreading Liquid in Pore Throats Formed by Spheres[3.16]

The main feature of this work is an experimental investigation of displacement curvatures for pores formed by spheres. Pore throats were formed from four ball bearings in rhomboidal arrays with the half angle of the rhombus varying from 30 to 45°. The pore-throat configurations thus ranged from three spheres in a triangular arrangement to four spheres in a square arrangement. The maximum meniscus curvature at which a penetrating meniscus became unstable and passed through such arrangements was measured using a modified capillary rise technique. Results were compared with theoretical values of meniscus curvature given by comparable arrangements of rods and were found to be in good agreement (see Fig. 3.30).

In view of the difference in geometry provided by pores formed by rods and spheres, the close agreement in displacement curvatures for the two types of systems was somewhat surprising. It may be connected with the fact that

somewhere between the almost spherical bottom of the meniscus and each partial pendular ring held at a sphere contact, the meniscus passes through a point of inflection. At the inflection, one principal radius of curvature is infinite, and the other will be close to the arc of a circle. The curvature of the arc is equal to the surface curvature. This section is analogous to wedge menisci in tubes of constant cross section, where one of the radii of curvature is infinite; this is an underlying requirement of the theoretical analysis. Furthermore, this point of inflection likely occurs near the plane of the maximum constriction in the pores and so, in some ways, the constant curvature meniscus formed between spheres is basically similar to that between rods. Experimental investigation was also carried out on the effect of change from uniform to nonuniform cross-sectional pores by systematic substitution of rods by spheres. Curvatures were generally increased by the introduction of a rod and that substitution of one or two rods (in pore throats originally formed from four spheres) makes the pore behavior close to that observed for pores formed from only rods.

The Effect of Contact Angle Capillary Displacement Curvatures in Pore Throats Formed by Spheres

The theoretical treatment described previously was proposed by Mayer and Stowe[3.11] as a method of predicting the effect of contact angle on capillary displacement curvatures in pores given by sphere packings. Computed results given by this approach are presented in Fig. 3.31. This application, which is now sometimes applied to mercury porosimetry results, suffers the weakness that such pores have nonuniform cross section. For finite contact angles the effect of pore geometry could be particularly serious. Purcell used a simple doughnut shaped pore to demonstrate how pore geometry and contact angle can interact to determine displacement curvatures (Fig. 3.32).[3.17] In an attempt to improve on the Mayer and Stowe theory, by making some allowance for change in cross section, the results of the doughnut model were superimposed on the values computed by Mayer and Stowe (Fig. 3.33). Results for specific pore shapes formed by spheres are reported by Melrose.[3.18] The net effect of contact angle on displacement curvatures, shown in Fig. 3.33, corresponds to an increase in curvatures over those predicted by Mayer and Stowe. However, preliminary experimental results show contact angle (receding angles for Class II surface roughness[3.19] were assumed) to have even less effect on displacement curvatures than that predicted by the modified theory (Fig. 3.34). Work on this aspect of the effects of pore shape on displacement curvatures will continue.

CONCLUSIONS

a. Magnitude and Detailed Structure of Residual Oil Saturations

1. Displacement tests in random packings of equal spheres and in two-component packings show residual oil to be independent of absolute pore size (and permeability) per se.

2. Heterogeneous, two-component bead packs can be constructed that lead to either increased or decreased residual oil saturation according to packing structure.

3. Two main mechanisms of trapping are distinguished: bypassing and snap-off. Examples of the variety of hierarchic displacements and residual oil configurations that can arise because of detailed pore structure have been illustrated using pore doublet models.

4. Large pores, clusters of large pores, and vugs surrounded by smaller pores will retain oil mainly through bypassing; the trapping mechanism could also involve snap-off.

5. If aspect ratios exceed critical values for snap-off, oil is trapped in individual pores as singlet blobs, and for micromodels, it is clear that most of the recovered oil comes from the pore throats. At high aspect ratio, the trapping mechanism is essentially independent of coordination number.

6. Blob size distribution is affected by pore size distribution, but is affected more by the manner in which pores are distributed with respect to each other.

7. Oil blobs measured for Berea sandstone ranged in length from 1 to 10 pore bodies with more than half the residual volume probably being held as singlets. This implies that pores in Berea rock have generally high aspect ratio, and macroscopic heterogeneities involving large pores are not likely to extend over more than about eight grain diameters.

8. The tendency for increased trapping with decrease in porosity is believed to be related to the decrease in volume of oil associated with pore throats. The effect of coordination number on residual oil saturation when trapping occurs mainly by snap-off is probably minor, except that oil recovery from pore throat regions will tend to increase as the number of throats per pore body increases.

9. Decrease in oil recovery with decrease in porosity is likely related to accompanying increase in aspect ratio, which causes the volume of throat pore regions, from which recovery is efficient, to decrease relative to the total PV.

b. Effect of Interfacial Tension on Stability of Displacement Fronts

10. Instability of displacement fronts was observed in low tension displacements at favorable mobility ratios in an artificial porous media of only 10 particle layers thickness. Ratios of gravity to capillary force (the Bond Number) at which the segregation occurred were consistent with previously determined conditions for gravity segregation of phases at the microscopic level. Fingering and trapping phenomena given by low tension systems can be eliminated by matching fluid densities.

c. Effect of Pore Shape on Displacement Curvatures

11. Experimental results for the effect of wettability on blob mobilization are consistent with theoretical predictions provided contact angle hysteresis is taken into account.

12. Menisci in capillaries of uniform cross section can be broadly classed according to whether wedge-like liquid structures exist, such as is the case in triangular tubes, or do not exist, as happens in circular section tubes. If wedges do not exist, curvatures are given by hydraulic radii. If they do exist, curvatures can be computed precisely provided they are taken into account.

13. In general, meniscus curvatures of a given pore are affected by boundary conditions that are set in part by neighboring pores.

14. Computations of curvatures for pores formed by rods were in close agreement with experimental measurements of displacement curvatures for pores formed by spheres for systems of zero contact angle.

15. Further work is needed to explain the disparity between theory and experimental values of displacement curvatures for systems of finite contact.

REFERENCES

3.1 Chatzis, I., Morrow, N.R., and Lim, H.T., "Magnitude and Detailed Structure of Residual Oil Saturation," Soc. Pet. Eng. J. (April 1983) 311-326.

3.2 Son, J.E., Neale, G.H., and Hornof, V., "Interfacial Tension and Phase Behavior Characteristics of Petroleum Sulfonate/Lignosulfonate Mixtures," Can. J. Chem. Eng. 60 (1982) 684.

3.3 Son, J.E., Neale, G.H., and Hornof, V., "Effects of Petroleum Sulfonate-Lignosulfonate Surfactant Mixtures on the Coalescence Behavior of Oil Droplets," J. Can. Pet. Tech. (July-August 1982) 42.

3.4   Morrow, N.R., and Songkran, B., "Effect of Viscous and Buoyancy Forces on Nonwetting Phase Trapping in Porous Media," in Surface Phenomena in Enhanced Oil Recovery, D. O. Shah, Ed., Plenum Press (1981) 387-412.

3.5   Reed, R.L. and Healy, R.N., "Contact Angles for Equilibrated Microemulsion Systems," SPE 8262, presented at the 54th Annual Fall Technical Conference and Exhibition of SPE of AIME, Las Vegas, NV, September 23-26, 1979.

3.6   Mason, G., Nguyen, M.D., and Morrow, N.R., "Effect of Contact Angle on the Meniscus between Two Equal Contacting Rods and a Plate," J. Coll. Inter. Sci. 95 (October 1983) 494-501.

3.7   Princen, H.M., "Capillary Phenomena in Assemblies of Parallel Cylinders. I. Capillary Rise between Two Cylinders," J. Coll. Inter. Sci. 30 (May 1969) 69-75.

3.8   Princen, H.M., "Capillary Phenomena in Assemblies of Parallel Cylinders. II. Capillary Rise in Systems with More than Two Cylinders," J. Coll. Inter. Sci. 30 (July 1969) 359-371.

3.9   Princen, H.M., "Capillary Phenomena in Assemblies of Parallel Cylinders. III. Liquid Columns between Horizontal Parallel Cylinders," J. Coll. Inter. Sci. 34 (October 1970) 171-184.

3.10 Mason, G. and Morrow, N.R., "Meniscus Curvatures in Capillaries of Uniform Cross Section," Trans., Faraday Soc., In Press.

3.11 Mayer, R.P. and Stowe, R.A., "Mercury Porosimetry--Breakthrough Pressure for Penetration between Packed Spheres," J. Coll. Inter. Sci. 20 (October 1965) 893-911.

3.12 Mason, G. and Morrow, N.R., "Coexistence of Menisci and the Influence of Neighboring Pores on Capillary Displacement Curvatures in Sphere Packings," Submitted Manuscript.

3.13 Haines, W.B., "Studies in the Physical Properties of Soil. V. The Hysteresis Effect in Capillary Properties, and the Modes of Moisture Distribution Associated Therewith," J. Agric. Sci. 20 (1930) 97-116.

3.14 Hackett, F.E. and Strettan, J.S., "The Capillary Pull of an Ideal Soil," J. Agric. Sci. 18 (1928) 671-681.

3.15 Hwang, S.T., "The Gauss Equation in Capillarity," Preprints, 48th National Colloid Symposium, Div. of Coll. and Surface Chem., Amer. Chem. Soc. (1974) 54-59.

3.16 Mason, G. and Morrow, N.R., "Capillary Displacement Curvatures for a Spreading Liquid in Pore Throats Formed by Spheres," Submitted Manuscript.

3.17 Purcell, W.R., "Interpretation of Capillary Pressure Data," Technical Note 60, Trans., AIME 189 (1950) 369-371.

3.18 Melrose, J.C., "Wettability as Related to Capillary Action in Porous Media," Soc. Pet. Eng. J. (September 1965) 259-270.

3.19 Morrow, N.R., "The Effects of Surface Roughness on Contact Angle with Special Reference to Petroleum Recovery," J. Can. Pet. Tech. 14 (1975) 42.

Table 3.1 Displacement Experiments - Sets A and B

Surfactant Composition:
Petrostep-420, 0.2%
Butanol-1, 0.2%
NaCl, 1.0%
Marasperse C-21, variable

Set A Model:
MG-35-5
K_w = 25.9d (2.55 x 10^{-7} cm^2)
Model pore volume: 3.33 cm^3
Flow rate: 8 cm^3/hr
Frontal velocity: 4.39 m/day

Set B Model:
MG-35-9
K_w = 14.0d (1.38 x 10^{-7} cm^2)
Model pore volume: 3.55 cm^3
Flow rate: 8 cm^3/hr
Frontal velocity: 4.94 m/day

System	Marasperse C-21 (%)	Interfacial tension* (mN/m)	Interfacial tension** (mN/m)	Reciprocal coalescence rate** (mN·s)	Capillary number $\dfrac{v \cdot \mu}{\gamma}$	Bond number $\dfrac{\Delta\rho g K_w}{\gamma}$	Oil residence Time (min)	Oil recovered at BT (% OOIP)
CO***	--	24.24	--	--	--	--	--	--
C1A	0.00	1.28	2.00	6 x 10^{-2}	9.15 x 10^{-6}	6.15 x 10^{-5}	--	84
C2A	0.04	0.84	0.60	1 x 10^{-2}	1.40 x 10^{-5}	9.52 x 10^{-5}	--	69
C3A	0.08	0.35	0.09	2 x 10^{-3}	3.72 x 10^{-5}	2.31 x 10^{-4}	--	39
C4A	0.12	0.06	0.02	8 x 10^{-4}	2.23 x 10^{-4}	1.37 x 10^{-3}	--	68
C1B-5 C1B-45	0.00	2.08	2.00	6 x 10^{-2}	5.03 x 10^{-6}	2.50 x 10^{-5}	5 45	70.4 70.4
C2B-5 C2B-45	0.04	1.33	0.60	1 x 10^{-2}	7.91 x 10^{-6}	3.90 x 10^{-5}	5 45	81.7 64.8
C3B-5 C3B-45	0.08	0.57	0.09	2 x 10^{-3}	2.04 x 10^{-5}	9.06 x 10^{-5}	5 45	62.0 47.9
C4B-5 C4B-45	0.12	0.08	0.02	8 x 10^{-4}	1.49 x 10^{-4}	6.62 x 10^{-4}	5 45	67.6 56.3

*Determined in the laboratory
**Estimated from reference 2
***1% NaCl brine with no surfactants or cosurfactants added

79

Table 3.2   Effect of Oil-Glass Contact Time
            on Advancing Contact Angle (Set A)

Surface: smooth glass

Oil: isooctane dyed with a mixture
       of Oil Blue N and Oil Red O
       (Sigma Chemical Company)

Time (min)	Advancing contact angle, θ (degrees)			
	C1A	C2A	C3A	C4A
0	18	18	20	28
2	18	39	21	33
4	19	47	21	51
6	33	58	23	58
8	34	67	23	63
10	36	73	24	67
15	37	80	26	87
20	36	86	27	95
25	38	91	26	96
30	41	98	28	94
35	39	103	27	96
40	39	102	27	96

Table 3.3   Effect of Oil-Glass Contact Time
             on Advancing Contact Angle (Set B)

Surface: smooth glass

Oil: isooctane dyed with Oil Red O
        (Sigma Chemical Company)

Time (min)	Advancing contact angle, θ (degrees)				
	C1B	C2B	C3B	C4B	isooctane C3 dyed red vs. distilled water
0	65	13	41	38	16
2	--	16	15	51	14
4	--	16	26	50	17
5	--	--	42	--	--
6	--	16	39	38	--
7	63	--	--	--	11
8	--	12	44	33	--
9	--	--	--	--	--
10	--	16	55	33	11
15	--	--	53	60	--
20	61	11	63	57	--
25	--	15	67	61	--
30	--	14	--	69	17
35	--	12	--	63	--
40	--	--	--	47	--
45	--	15	49	71	17
>50	60	--	36	--	--

Table 3.4   Physical Properties of the Components of Organic Solutions

Component	Density (g/cm^3)		Viscosity ($mPa \cdot s$)	
	Literature	Laboratory	Literature	Laboratory
Isooctane	$0.6919^{20°/4°}$	$0.688^{25°}$	$0.479^{20°}$	$0.471^{25°}$
Carbon Tetrachloride	$1.594^{20°/4°}$	--	$0.969^{20°}$	--
Paraffin Oil	--	$0.8643^{25°}$	--	$79-80^{25°}$

Table 3.5   Composition and Properties of Solution A and NaCl Brine

Component	Composition		Density*	Viscosity*
	% (by vol.)	% (by wt.)	(g/cm^3)	($mPa \cdot s$)
Isooctane	50	33.6		
Carbon Tetrachloride	34	52.9	1.0171	0.9292
Paraffin Oil	16	13.5		
2.5% NaCl in Water			1.0138	0.9130

*At 25 ±1°C

82

Table 3.6   Effect of the Composition of Organic
Phase on Interfacial Tension Against
2.5% NaCl Brine

Volume of Component (cm^3)			$\Delta\rho$ (g/cm^3)	σ (mN/m)
Isooctane	CCl$_4$	Paraffin Oil		
25	15	8	0.0197	17.0[*]
25	13	8	0.0455	18.8
25	10	8	0.0854	15.4

[*]This system presented some difficulty because of the small
density difference.

Table 3.7   Characterization of Aqueous Phases

Designation	Composition	Interfacial Tension (mN/m)
M1	2.5% NaCl	17.0*
M2	0.5% NaCl; 0.1% Petrostep-420: 0.1% Butanol-1	1.2
M2-B	2.5% NaCl; 0.1% Petrostep-420; 0.1% Butanol-1	0.002
M3	2.5% NaCl; 0.2% Petrostep-420; 0.2% Butanol-1; 0.06% Marasperse C-21	0.029
M4	1.0% NaCl; 0.2% Petrostep-420; 0.2% Butanol-1	0.040
M5	2.5% NaCl; 0.2% Witco 10-80	0.291
M6	2.5% NaCl; 0.2% Witco 10-80; Marasperse C-21	0.283

* Measured against the organic solution A shown in Table 3.5

Table 3.8 Effect of Time on Advancing and Receding Contact
Angles for Systems M1, M2, M2-B and M3

Surface: smooth glass

Time (min)	System							
	M1		M2		M2-B		M3	
	adv.	rec.	adv.	rec.	adv.	rec.*	adv.	rec.*
0	30	14	36	15	70	41,12	73	13,23
2	--	--	44	29	42	--,24	82	--,25
3	--	--	44	26	--	--,--	98	42,--
4	42	--	47	31	85	36,--	105	--,72
5	--	--	43	25	--	--,26	--	--,--
6	36	18	--	--	--	--,--	92	68,63
8	37	--	44	26	88	--,24	98	67,61
10	37	15	49	29	86	50,38	112	87,55
15	41	16	46	26	88	48,22	111	--,83
20	37	--	40	12	52	43,--	109	87,--
25	31	18	35	23	56	40,22	122	73,93
30	32	20	37	30	53	--,27	118	67,--
35	--	--	38	28	--	--,--	120	82,--
40	--	--	40	28	34	40,67	93	74,--
50	49	--	55	25	40	28,--	--	--,--

* Duplicate measurements

Table 3.9   Displacements with Solutions having Matching Density
and Viscosity: Aqueous Solution Displacing Oil

System	Run No.	Model	Flow rate cm³/hr	IFT mN/m	Oil rec'd. at BT % OOIP**	Displacement Characteristics*
M1	3	MG-35-8	8	17	64	S after ragged start
M1	4	MG-35-8	8	17	50	One broad finger otherwise S
M1	5	MG-35-8	8	17	72	Two broad fingers later forming S front
M1	17	MG-35-9	10.4	17	59	S after ragged start
M1	18	MG-35-9	11.7	17	59	Similar to #17
M1	1	MG-35-8	8	17	--	Similar to #17
M2	2	MG-35-8	8	1.2	82	Some fingering at start; later becomes S
M2	6	MG-35-8	8	1.2	82	Very similar to #2
M2	19	MG-35-9	7.5	1.2	56	S after ragged start
M2	10	MG-35-9	10.9	1.2	93	Fingering at start then S
M2-B	21	MG-35-9	14.6	0.002	76	Much fingering at start becoming VS later on
M2-B	22	MG-35-9	14.3	0.002	70	Similar to #21
M3	23	MG-35-9	15.0	0.029	70	Ragged front throughout; from FS to U
M3	24	MG-35-9	16.7	0.029	52	Similar to #23
M3	13	MG-35-9	10.5	0.029	75	FS to U
M3	14	MG-35-9	11.8	0.029	63	FS to U
M4	15	MG-35-9	10.7	0.040	48	FS to U
M4	16	MG-35-9	10.9	0.040	66	FS to U

* VS = Very Stable; S = Stable; FS = Fairly Stable; U = Unstable

** Of Oil In Place

Table 3.10 Displacements with Solutions having Matching Density
and Viscosity: Oil Displacing Aqueous Solution

System	Run No.	Model	Flow rate cm^3/hr	IFT mN/m	H$_2$O rec'd. at BT % OOIP**	Displacement Characteristics*
M1	7	MG-35-8	8	17	23	Very ragged throughout; U
M1	9	MG-35-8	8	17	36	A little more stable than #7; FS to U
M1	29	MG-35-9	9.7	17	<10	Very ragged; U
M1	30	MG-35-9	--	17	19	Similar to #7 and #29; U
M2	10	MG-35-8	8	1.2	39	More stable than M1, but still ragged; FS
M2	11	MG-35-8	8	1.2	40	Similar to #10, FS
M2	25	MG-35-9	17.6	1.2	25	Similar to #10, FS
M2	26	MG-35-9	9.9	1.2	31	Similar to #10, FS
M2-B	27	MG-35-9	9.7	0.002	>50	Very stable front; VS
M2-B	28	MG-35-9	10.2	0.002	>50	#27 and #28 were almost identical; VS
M3	31	MG-35-9	10.6	0.029	>50	S to VS
M3	32	MG-35-9	10.1	0.029	>50	S to VS
M4	33	MG-35-9	10.1	0.040	>50	FS to S
M4	34	MG-35-9	10.1	0.040	>50	FS to S

* VS = Very Stable; S = Stable; FS = Fairly Stable; U = Unstable

** Original Oil In Place

KEY TO DISPLACEMENT DIAGRAMS

Medium saturated with phase originally in place

Medium saturated with displacing phase

Medium partially saturated with both phases

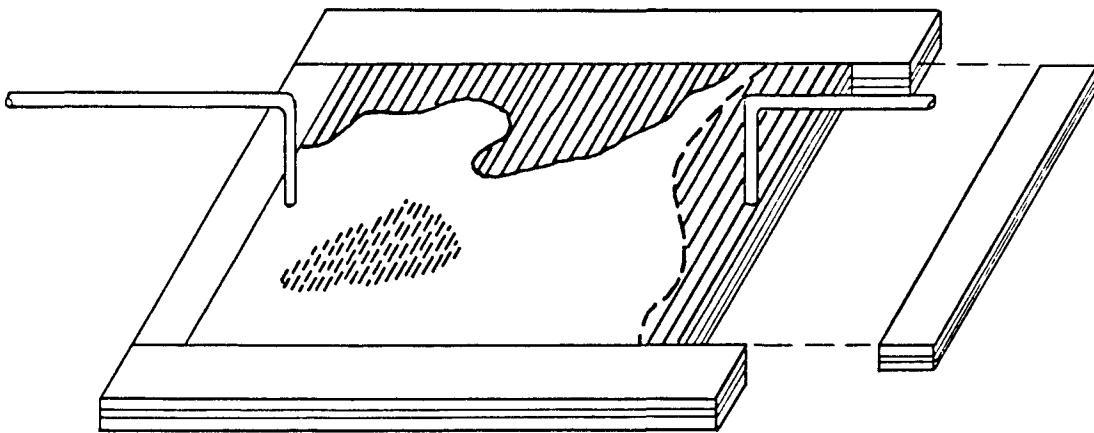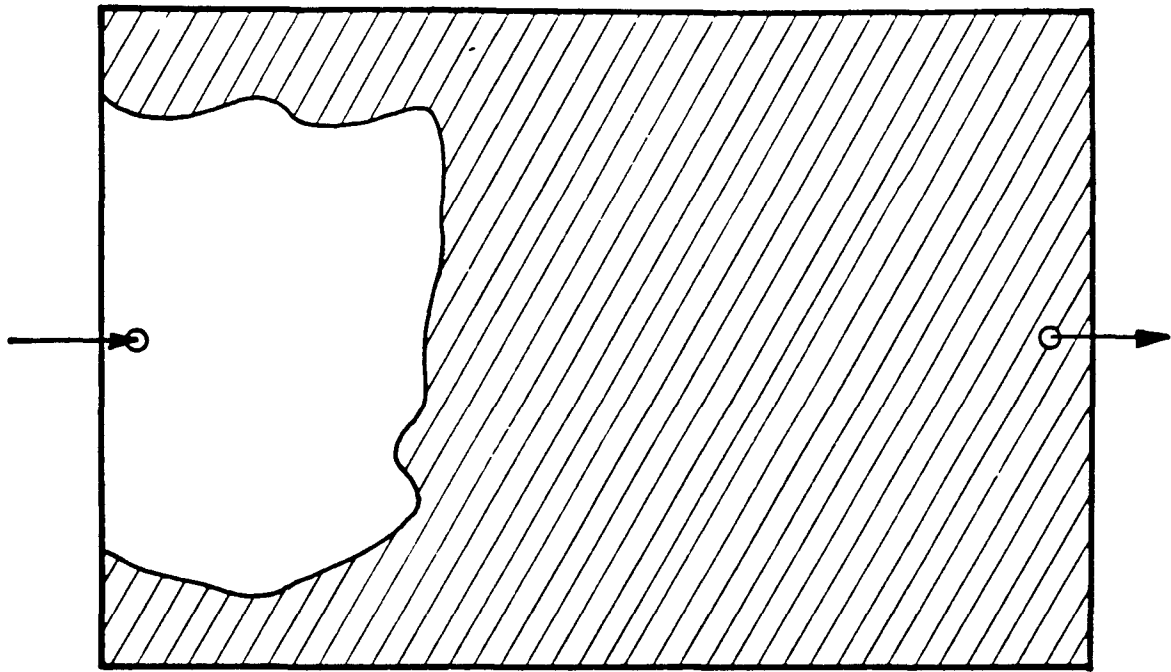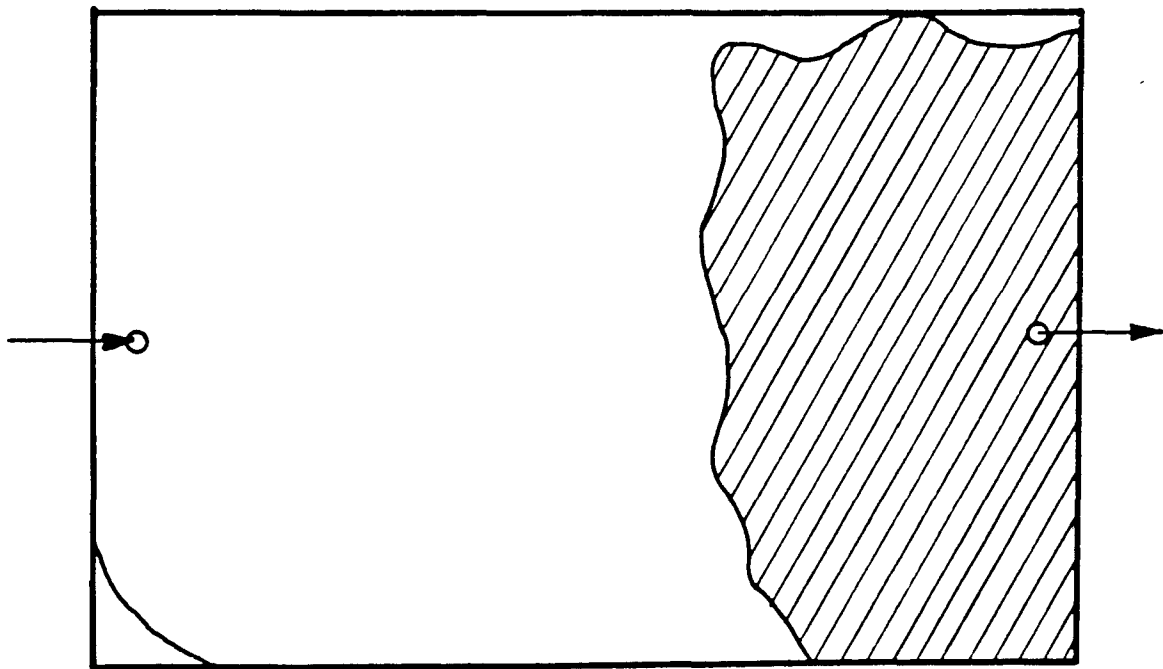Sharp interface

Fuzzy interface

Fig. 3.1. Schematic diagram of flow cells and key for displacement front profiles at two stages of displacement presented in Figs. 3.2 through 3.24.
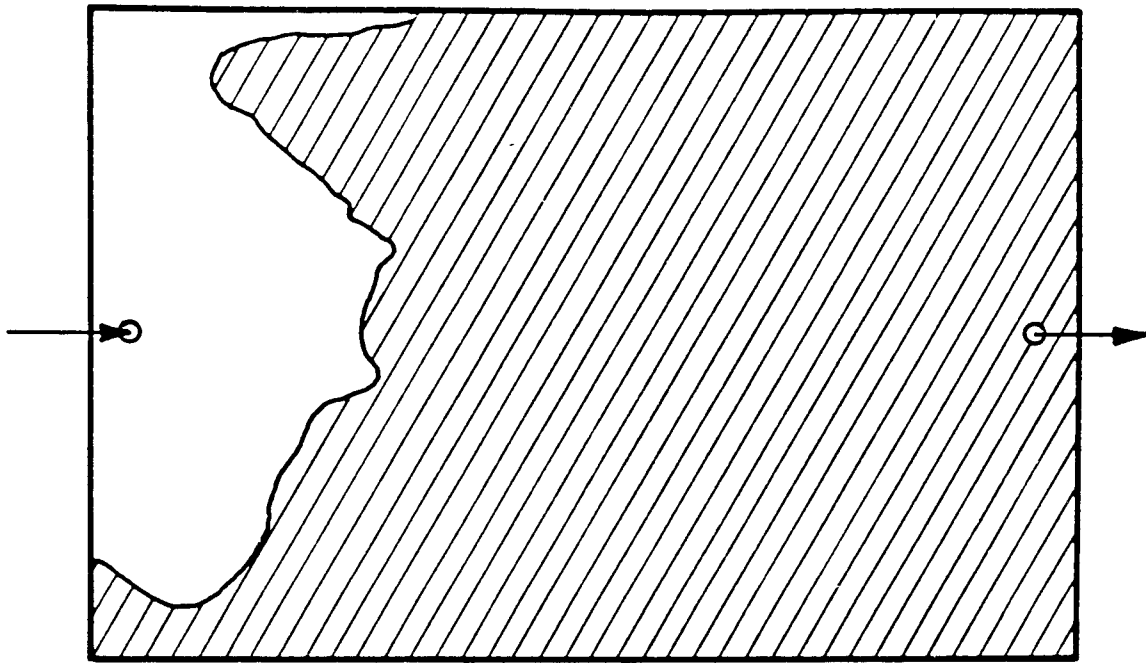
(a)

(b)

SYSTEM : CIA   IFT = 1.28 mN/m

Fig. 3.2. Displacement front profiles. (See Fig. 3.1 for key)
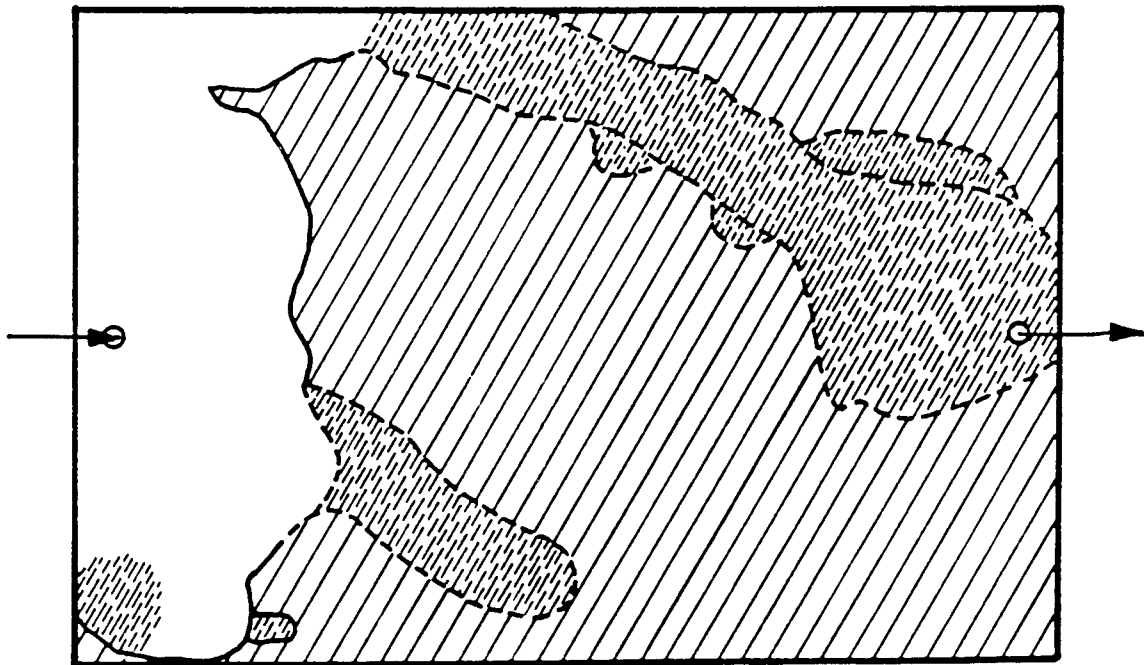
89

(a)

(b)

SYSTEM: C2A   IFT = 0.84 mN/m

Fig. 3.3. Displacement front profiles. (See Fig. 3.1 for key)

(a)

(b)

SYSTEM : C3A   IFT = 0.35 mN/m

Fig. 3.4. Displacement front profiles. (See Fig. 3.1 for key)
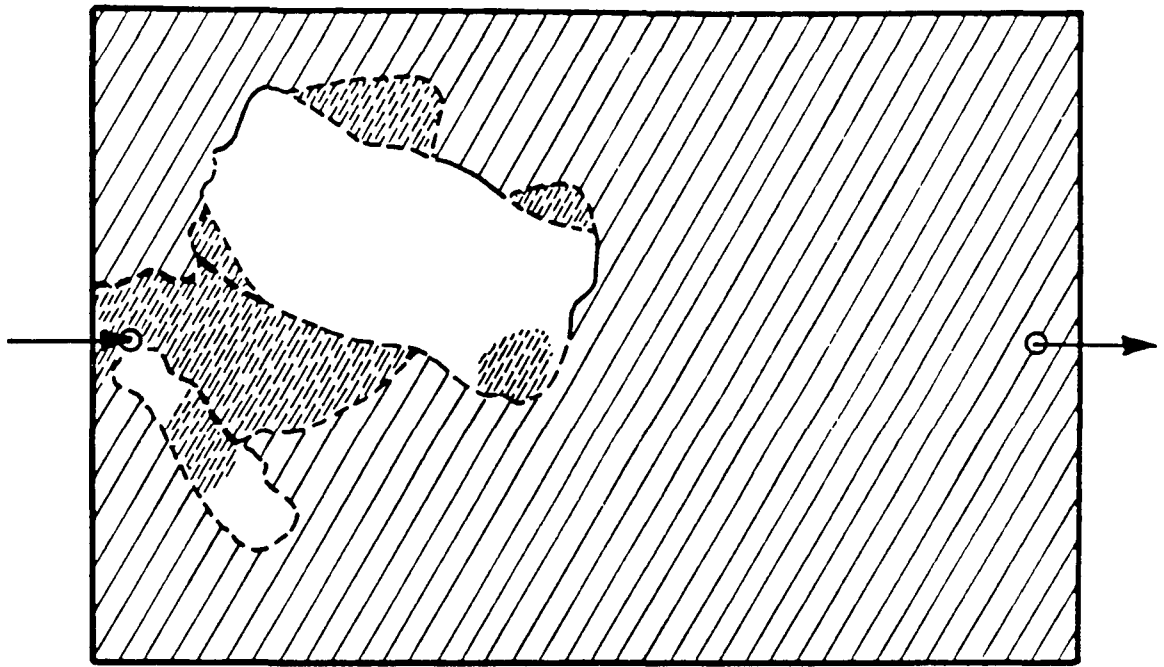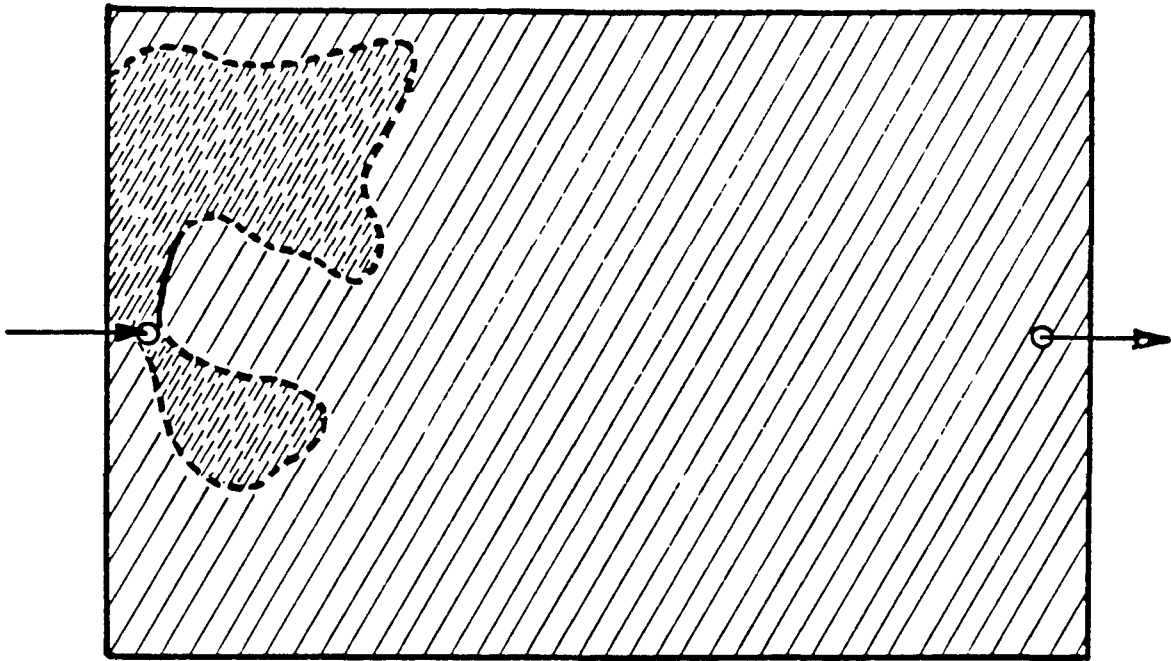
(a)

(b)

SYSTEM : C4A   IFT = 0.06 mN/m

Fig. 3.5. Displacement front profiles. (See Fig. 3.1 for key)
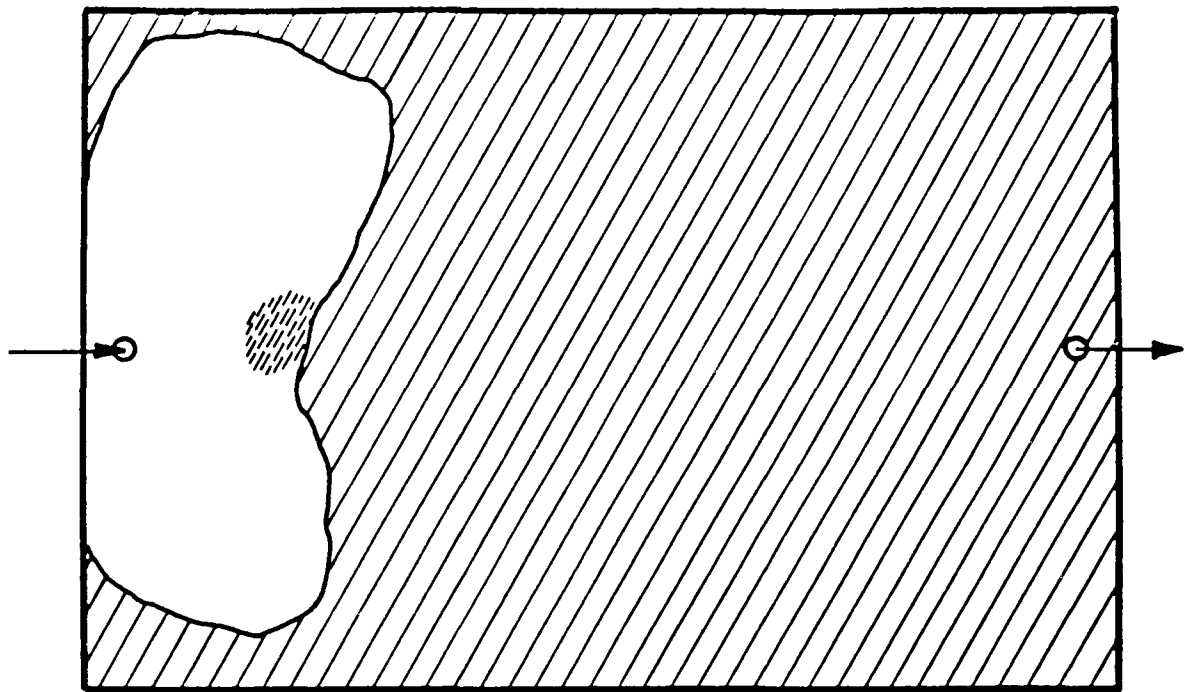
(a)
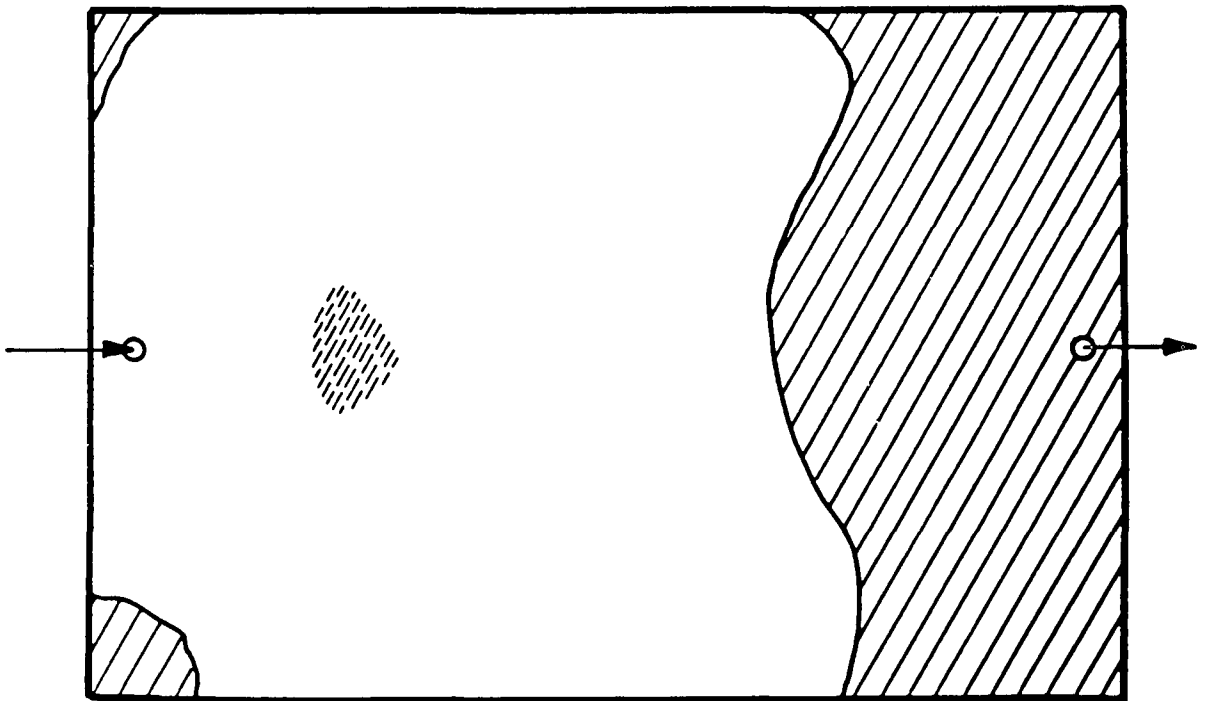
(b)

SYSTEM : CIB-5   IFT = 2.08 mN/m
RESIDENCE TIME: 5 min.

Fig. 3.6. Displacement front profiles. (See Fig. 3.1 for key)
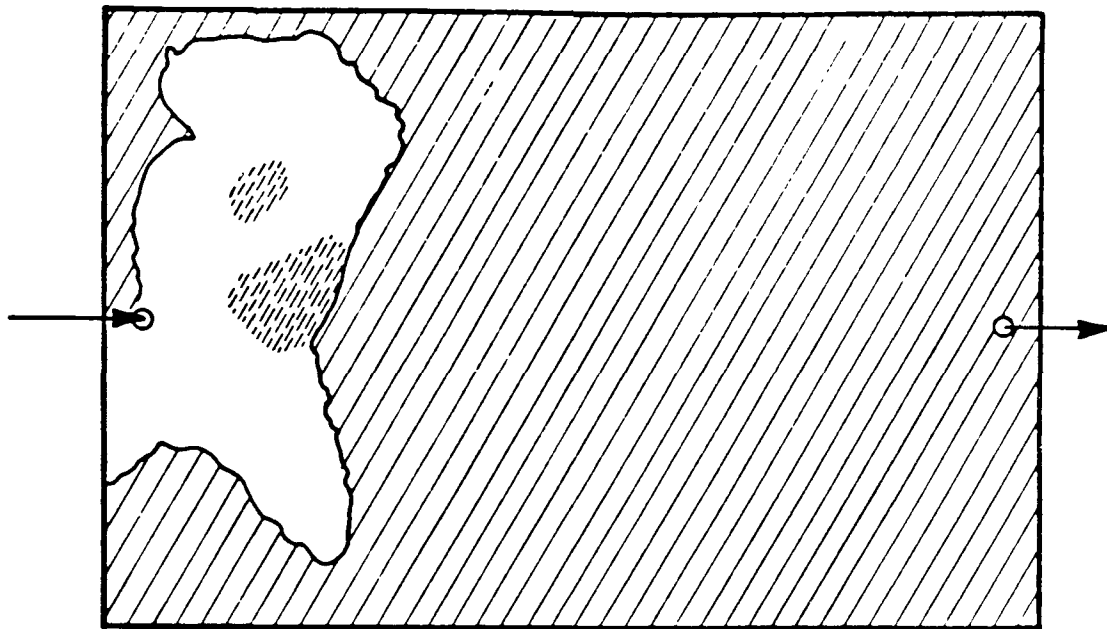
(a)
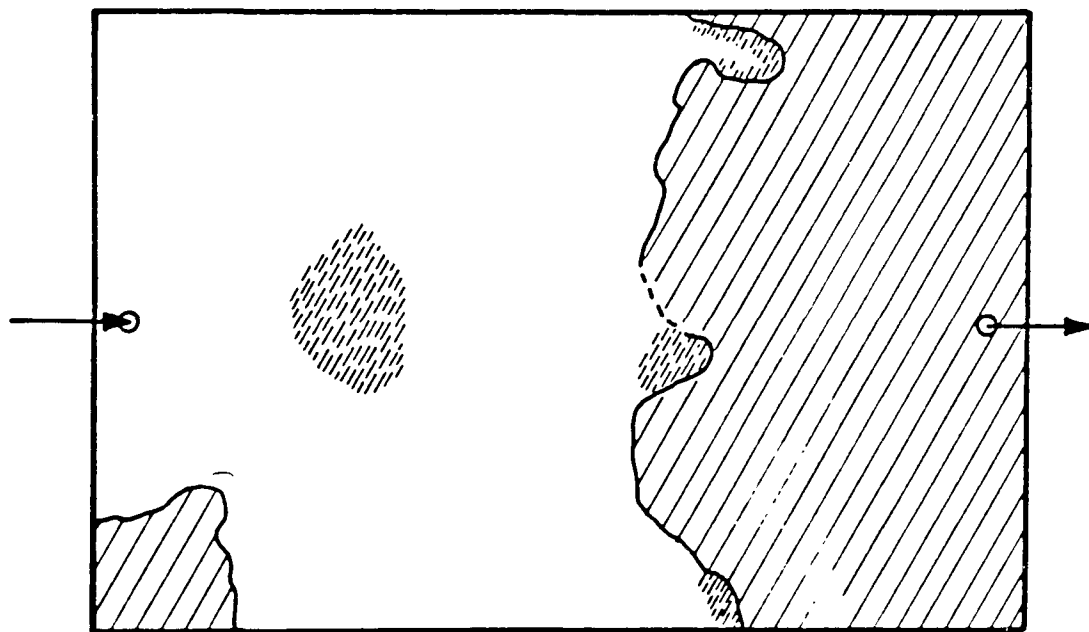
(b)

SYSTEM : C2B-5   IFT = 1.33 mN/m
RESIDENCE TIME : 5 min.

Fig. 3.7. Displacement front profiles. (See Fig. 3.1 for key)
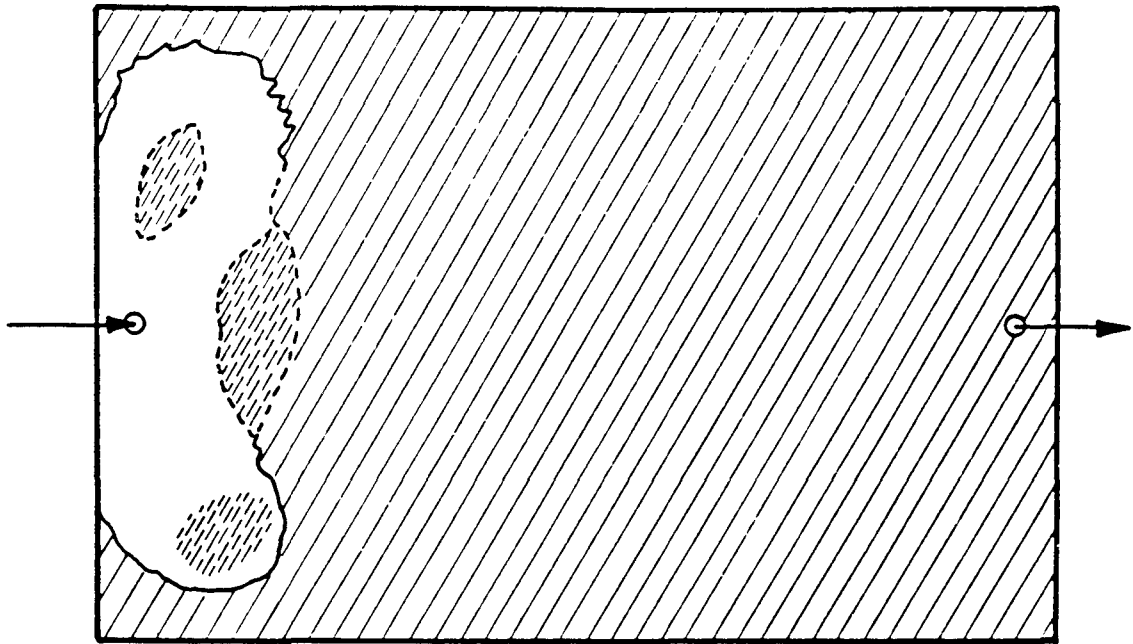
(a)
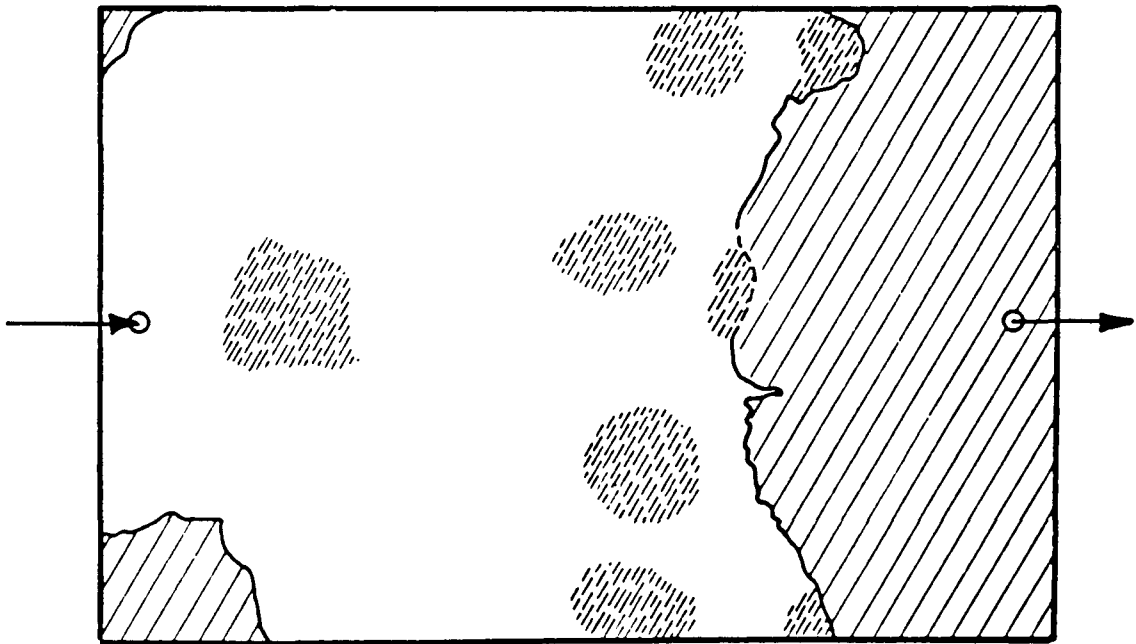
(b)

SYSTEM: C3B-5 IFT = 0.57 mN/m
RESIDENCE TIME: 5 min.

Fig. 3.8. Displacement front profiles. (See Fig. 3.1 for key)
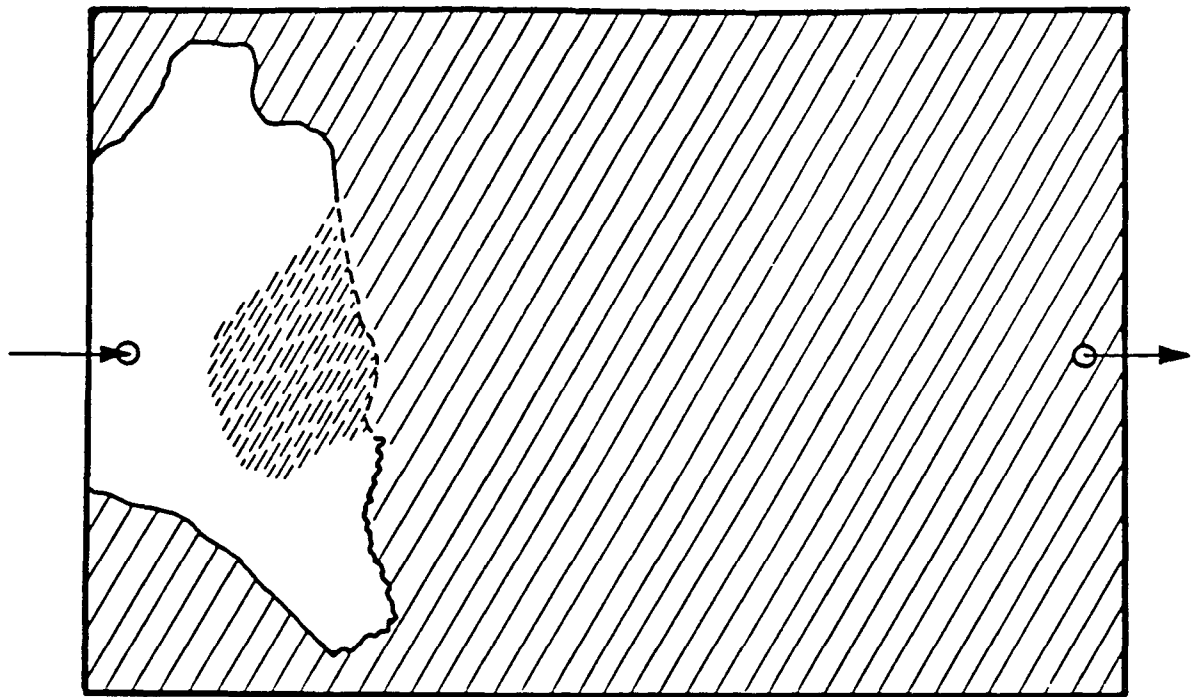
(a)
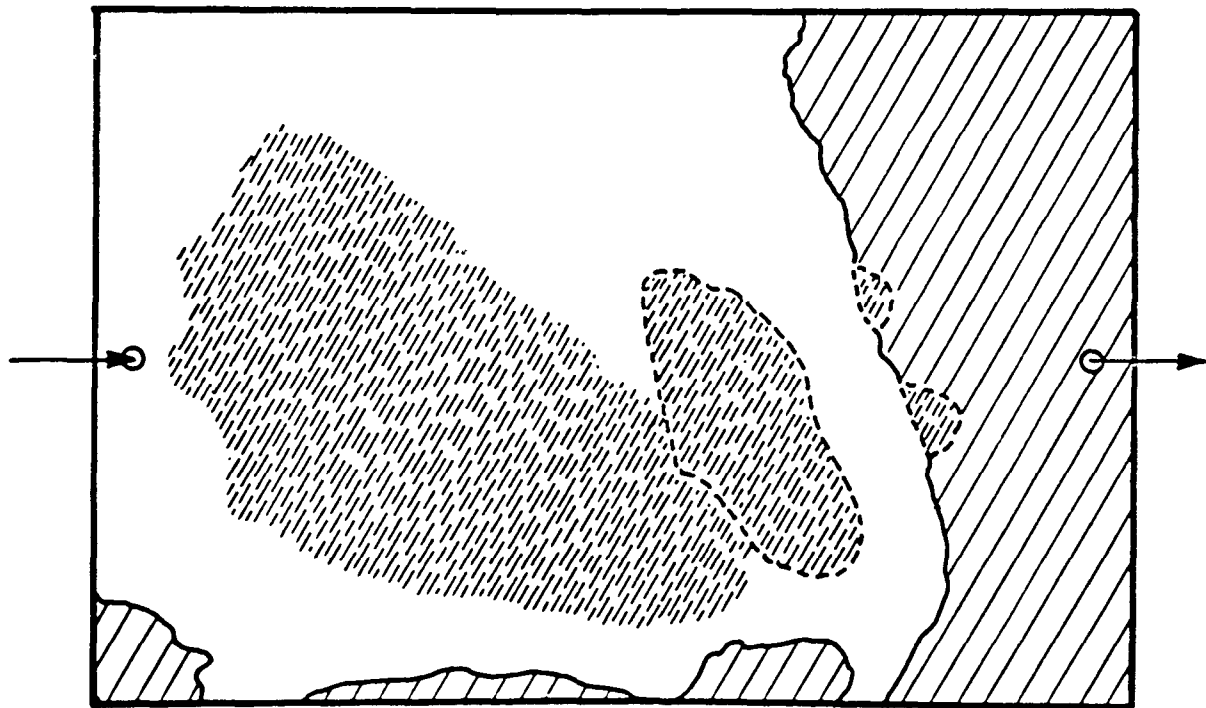
(b)

SYSTEM: C4B   IFT = 0.08 mN/m
RESIDENCE TIME: 5 min.

Fig. 3.9. Displacement front profiles. (Interfacial
           tension = 0.08 mN/m) (See Fig. 3.1 for key)
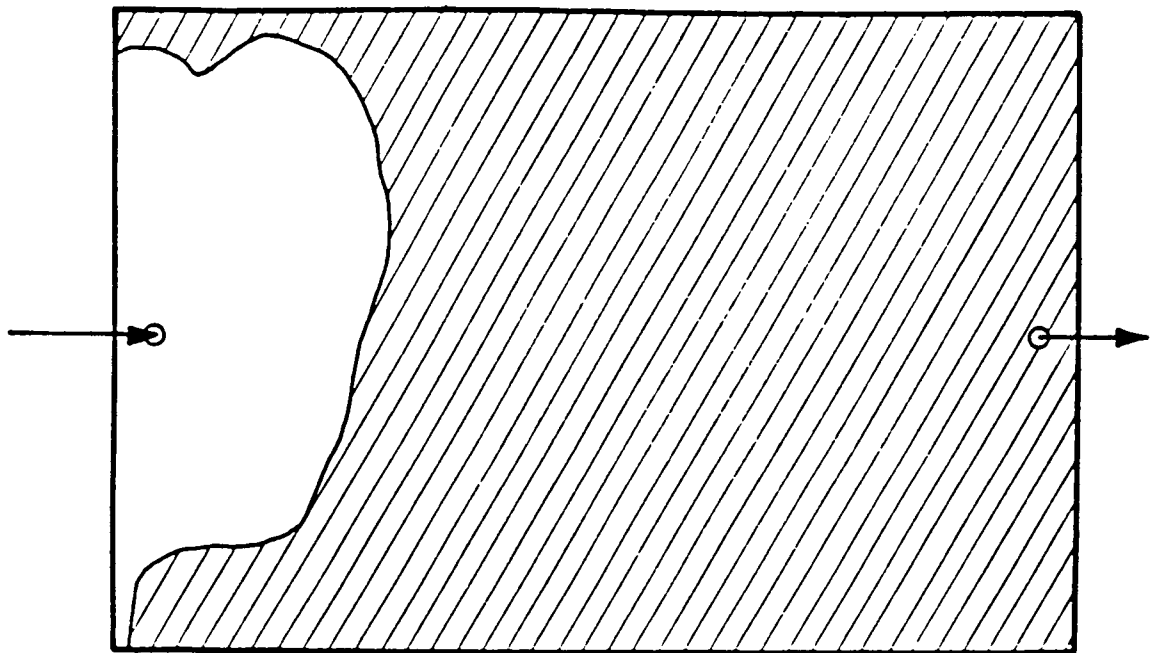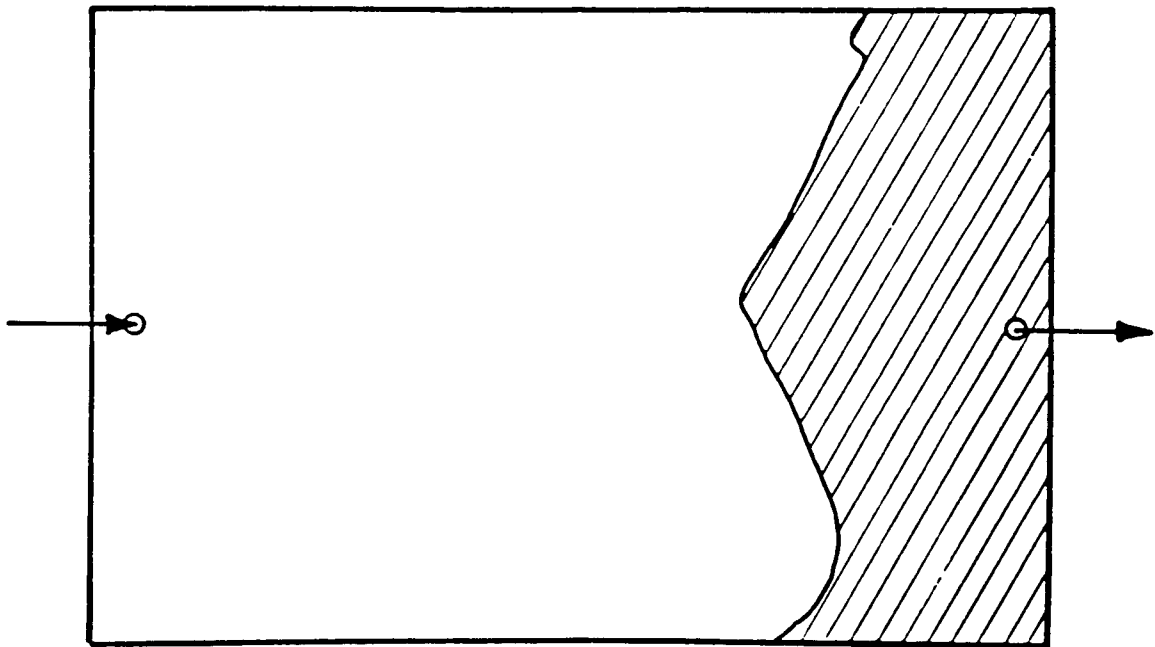
SYSTEM : CIB-45 IFT = 2.08 mN/m

RESIDENCE TIME : 45 min.

Fig. 3.10. Displacement front profiles. (See Fig. 3.1 for key)
(Interfacial tension = 2.08 mN/m)
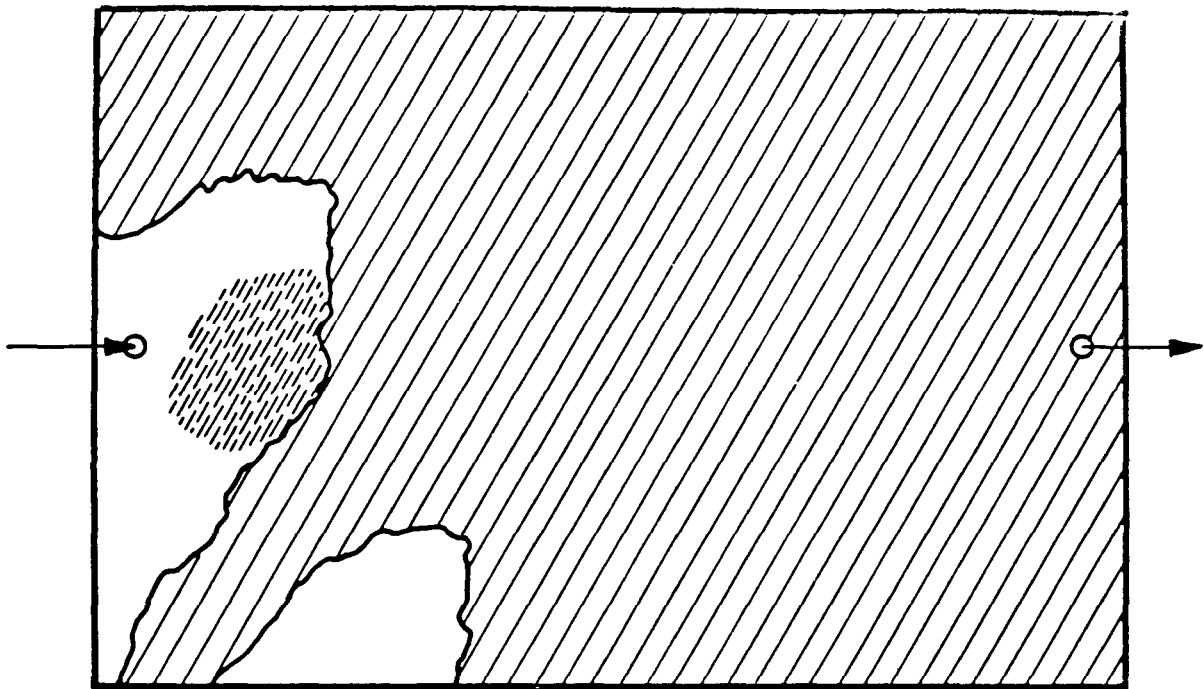
(a)
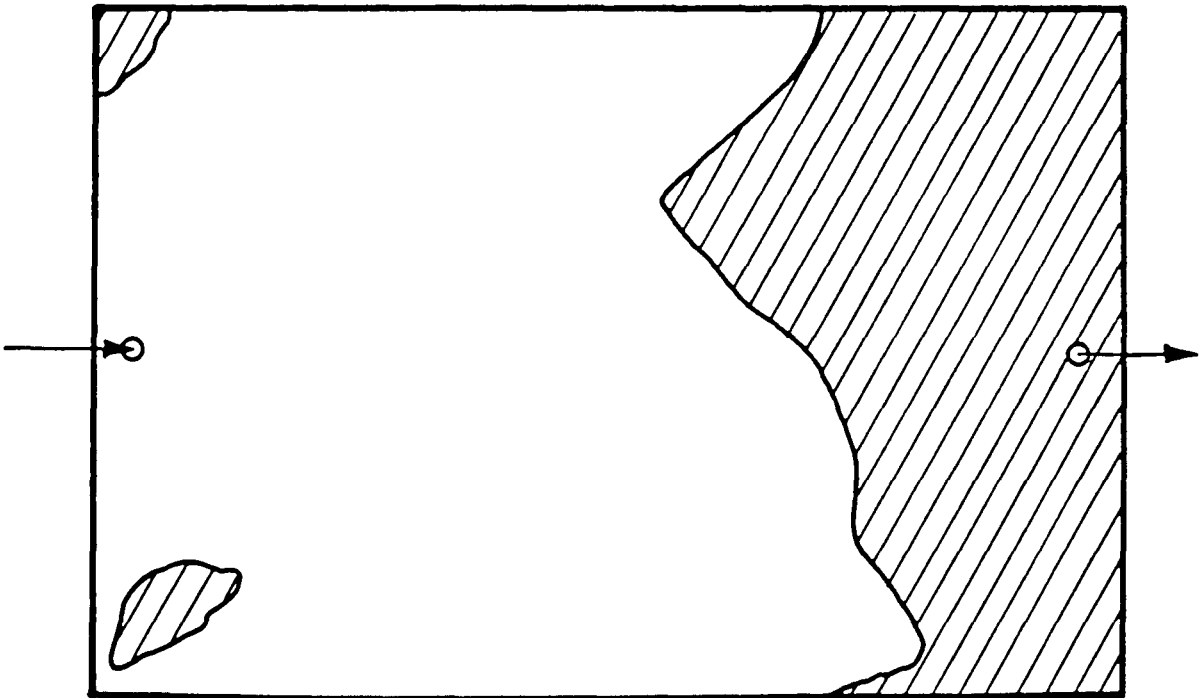
(b)

SYSTEM : C2B   IFT = 1.33 mN/m

RESIDENCE TIME : 45 min.

Fig. 3.11. Displacement front profiles. (See Fig. 3.1 for key)

(a)
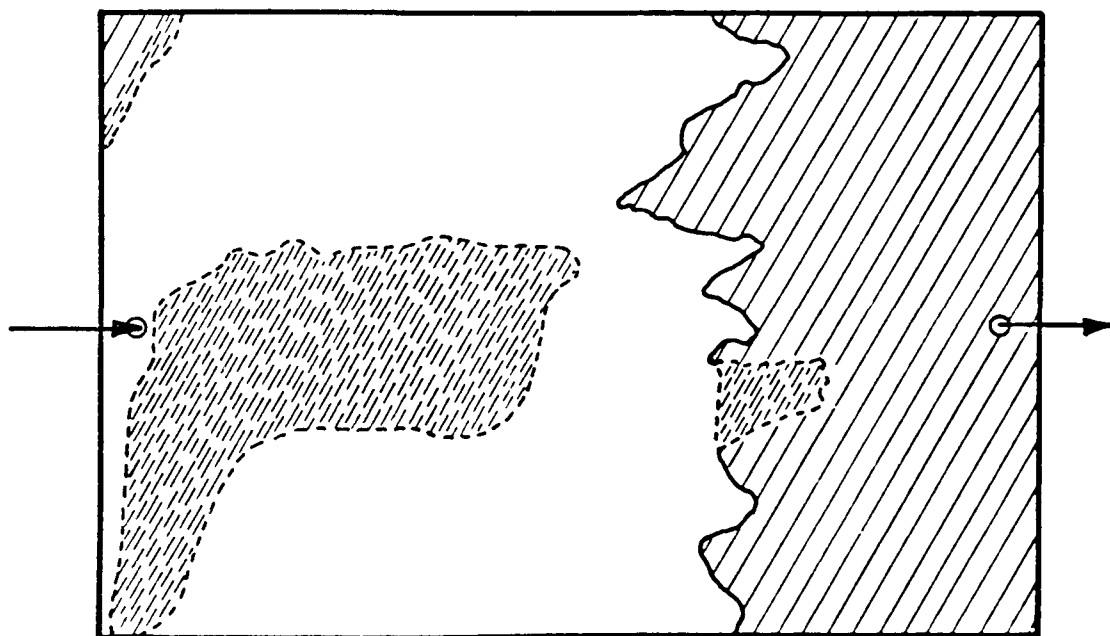
(b)

SYSTEM : C3B-45 IFT = 0.57 mN/m
RESIDENCE TIME : 45 min.

Fig. 3.12. Displacement front profiles. (See Fig. 3.1 for key)

(a)
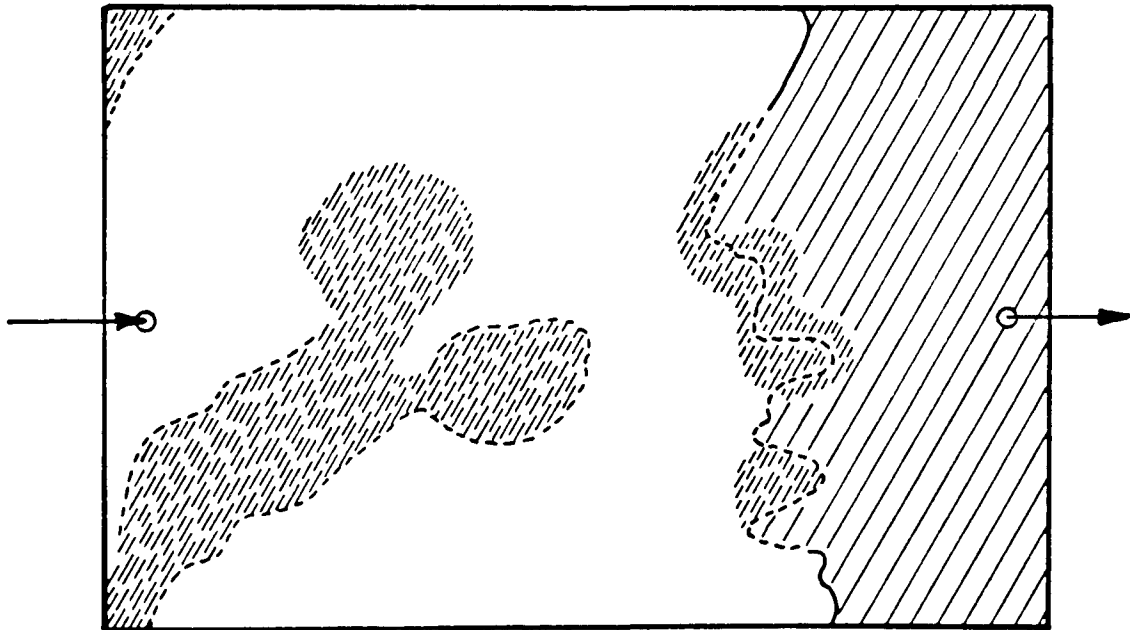
(b)

SYSTEM: C4B-45 IFT = 0.08 mN/m
RESIDENCE TIME : 45 min.

Fig. 3.13. Displacement front profiles. (See Fig. 3.1 for key)
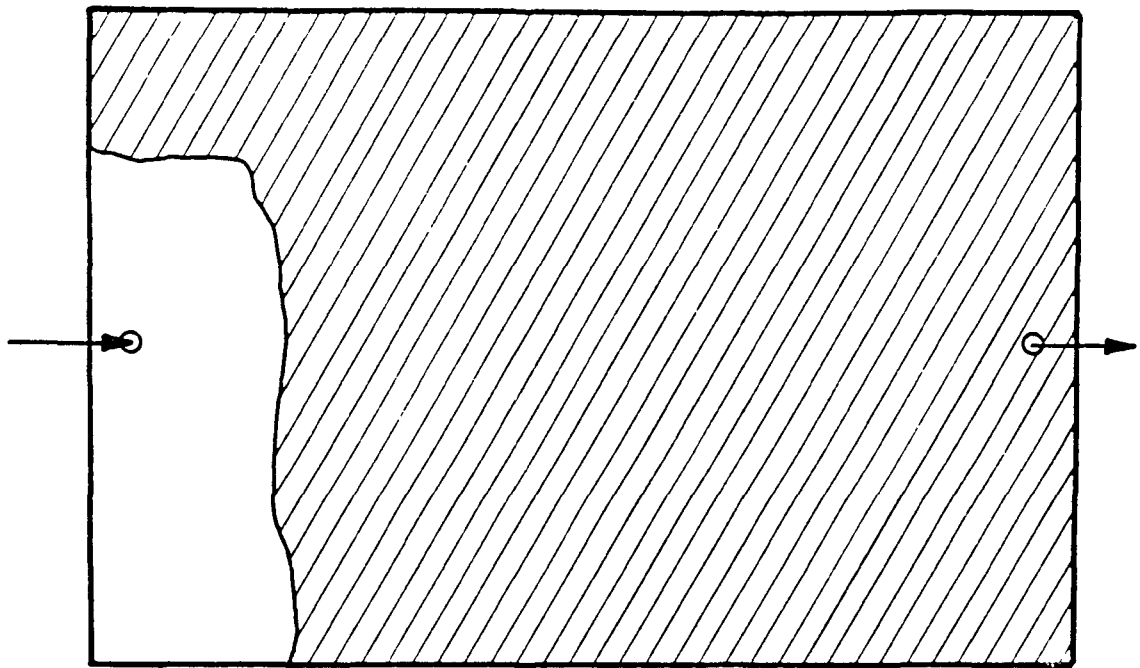
(a)
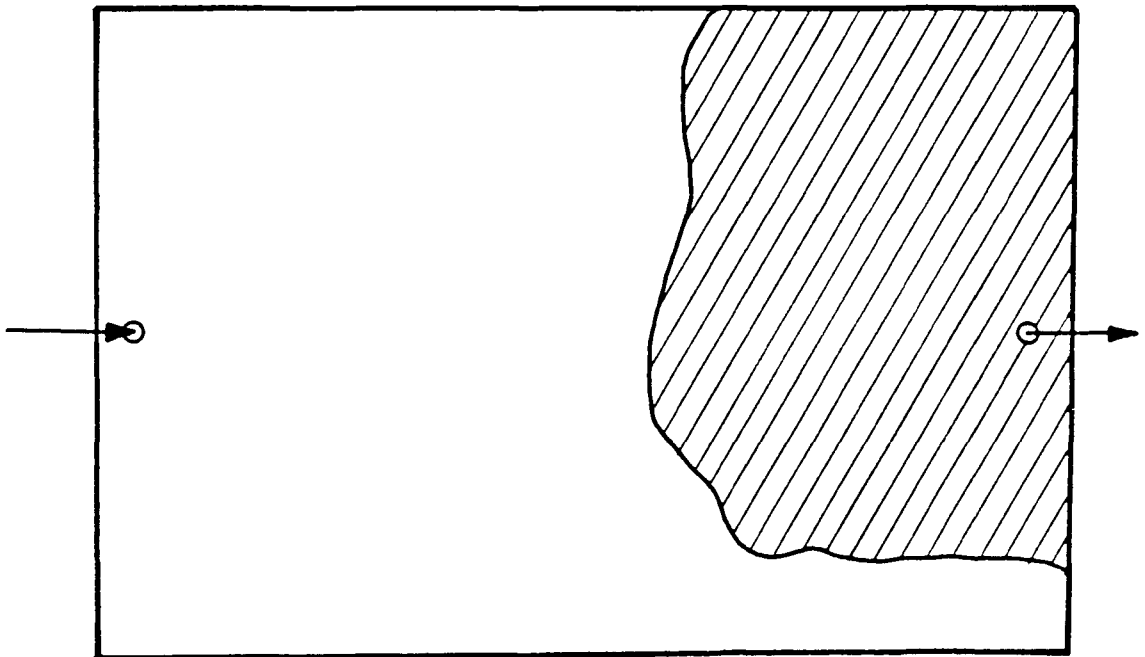
(b)

SYSTEM: CO   IFT = 24 mN/m

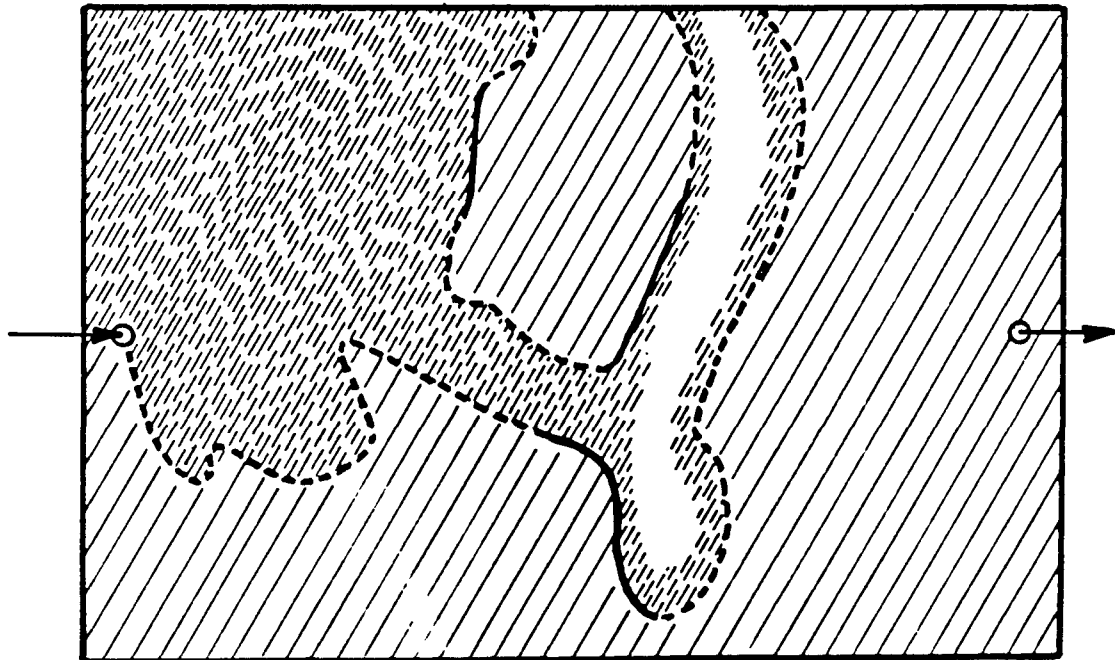Fig. 3.14. Displacement front profiles. (See Fig. 3.1 for key)

(a)

(b)
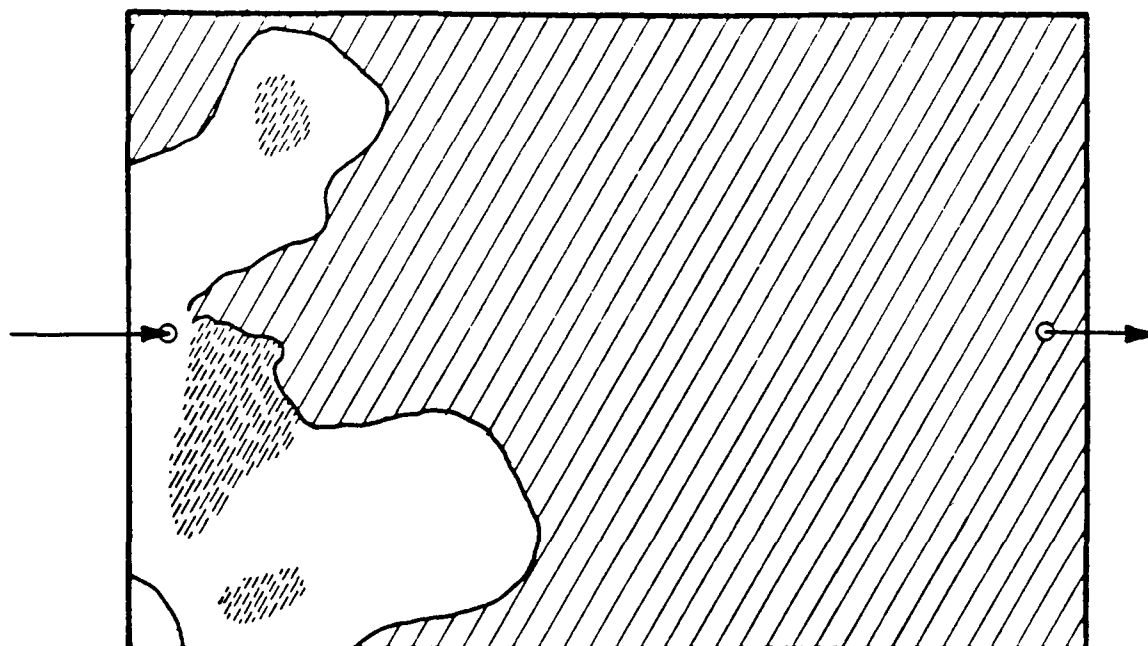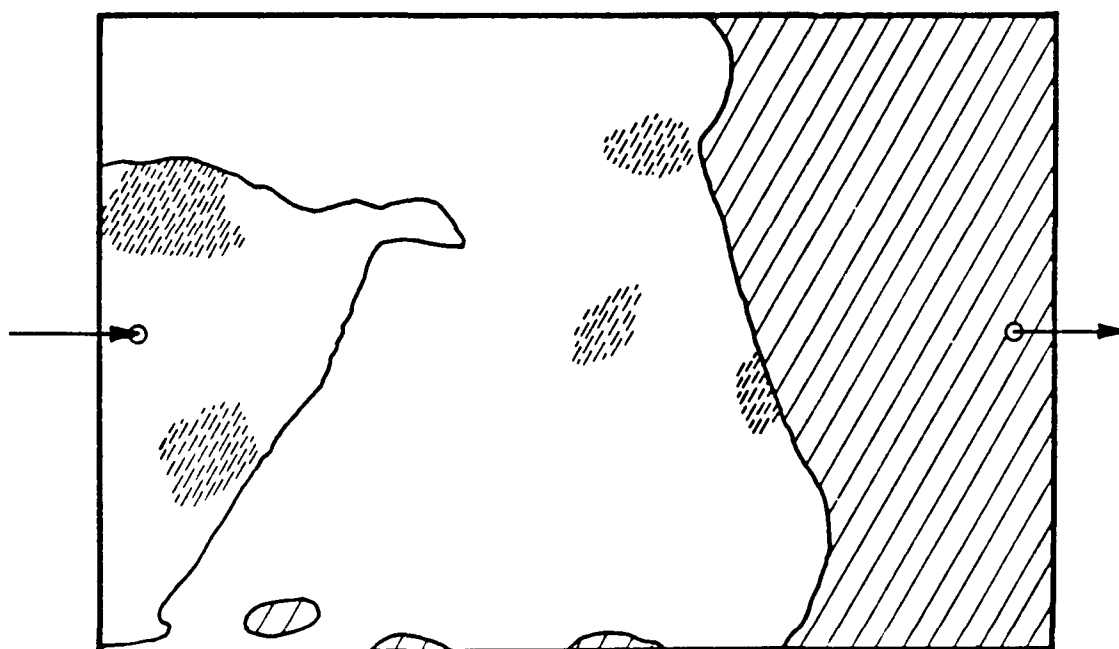
SYSTEM: MI   IFT = 17 mN/m
MODE: WATER DISPLACING OIL

Fig. 3.15. Displacement front profiles. (See Fig. 3.1 for key)

(a)

(b)
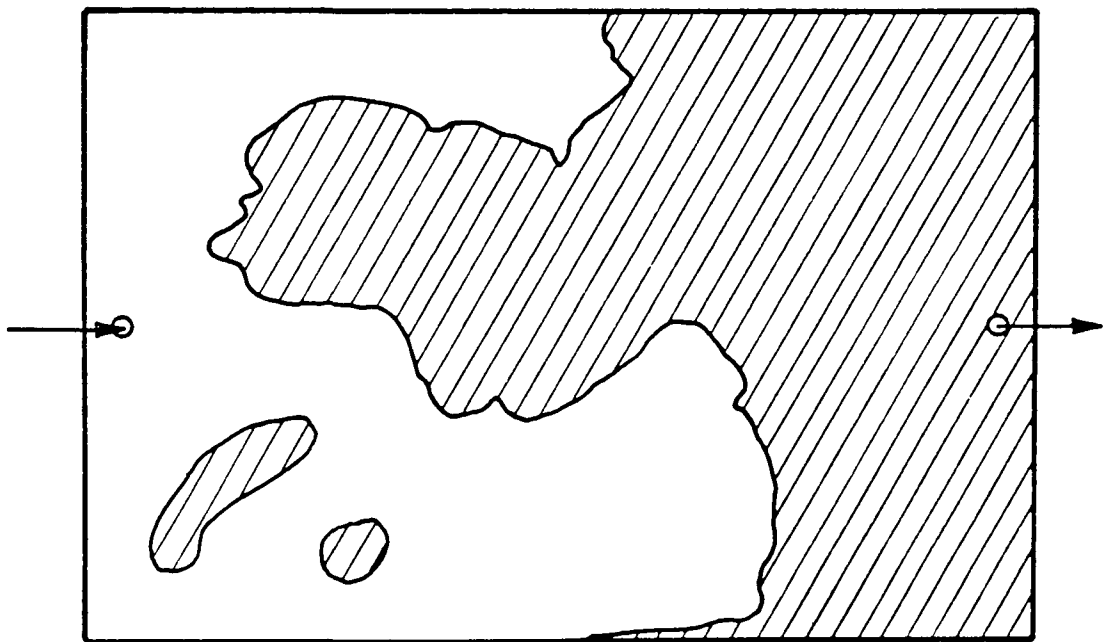
SYSTEM: M2   IFT = 1.2 mN/m

MODE: WATER DISPLACING OIL

Fig. 3.16. Displacement front profiles. (See Fig. 3.1 for key)

103

(a)

(b)
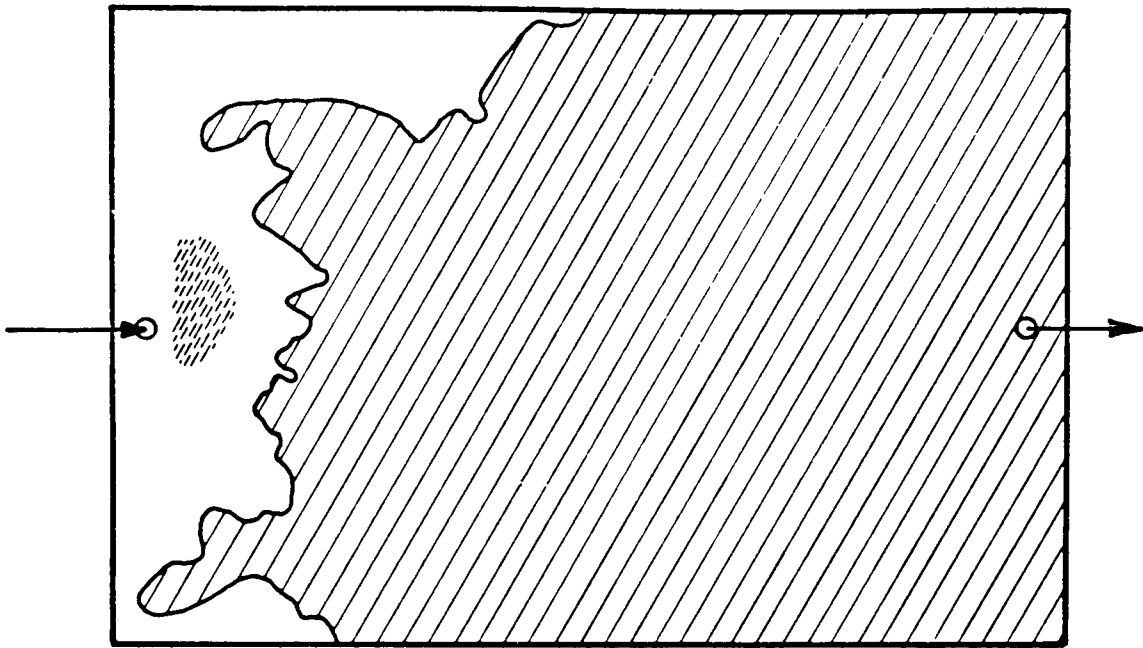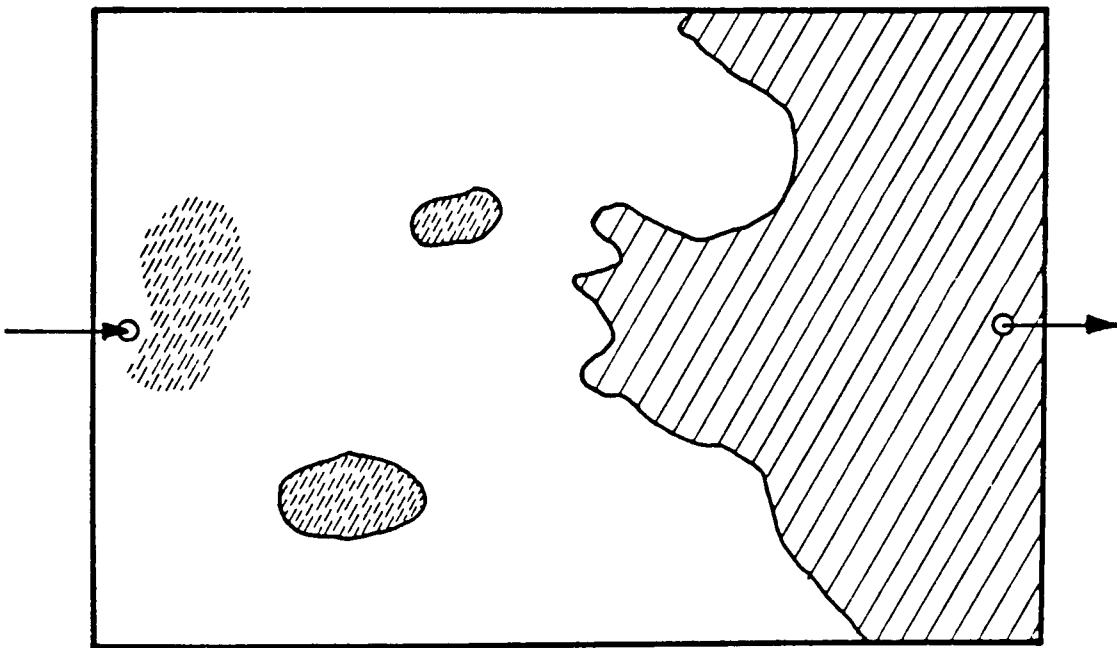
SYSTEM: M2-B   IFT: 0.002 mN/m
MODE: WATER DISPLACING OIL

Fig. 3.17. Displacement front profiles. (See Fig. 3.1 for key)
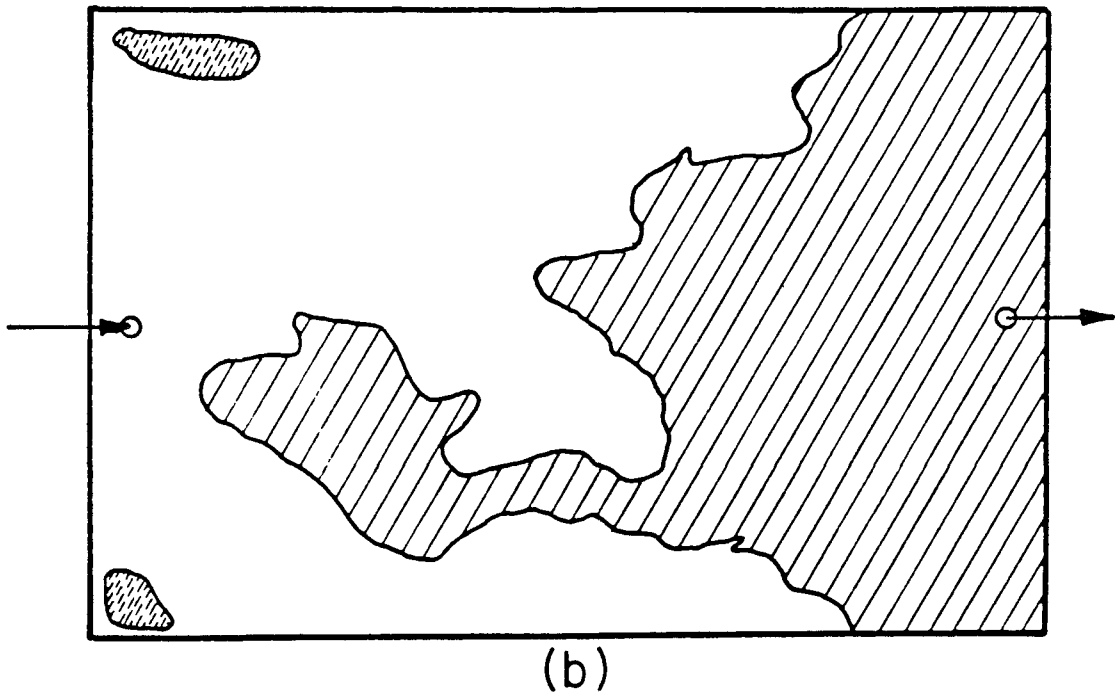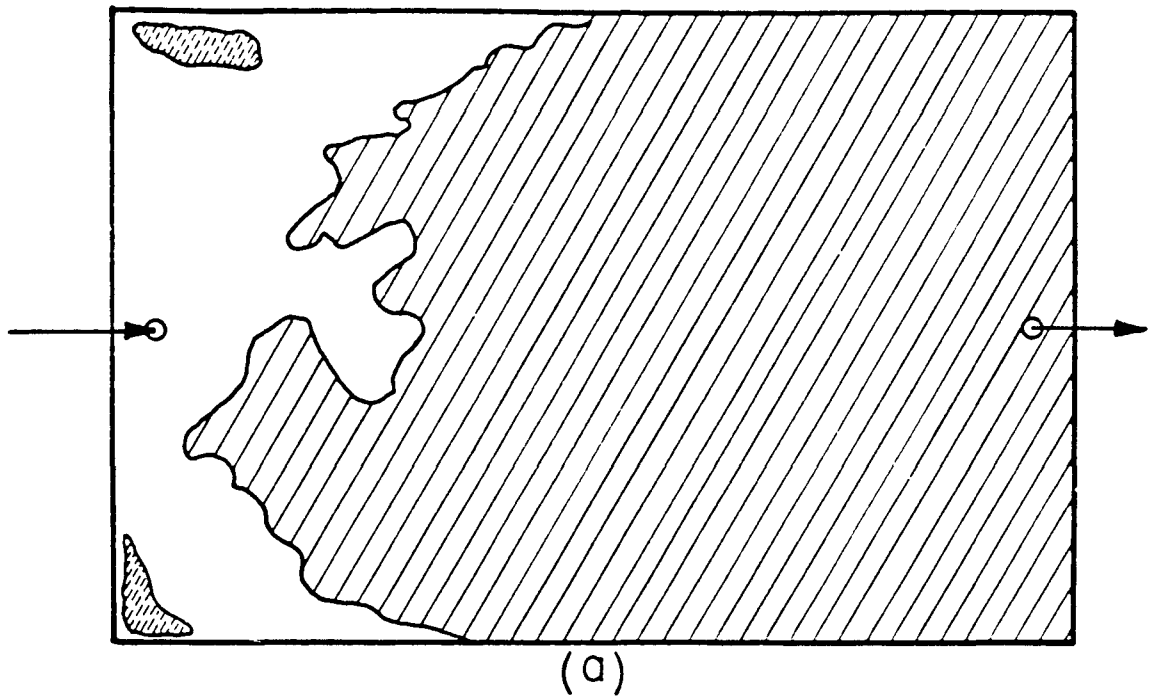
SYSTEM: M3   IFT: 0.029 mN/m

MODE: WATER DISPLACING OIL

Fig. 3.18. Displacement front profiles. (See Fig. 3.1 for key)

(a)

(b)
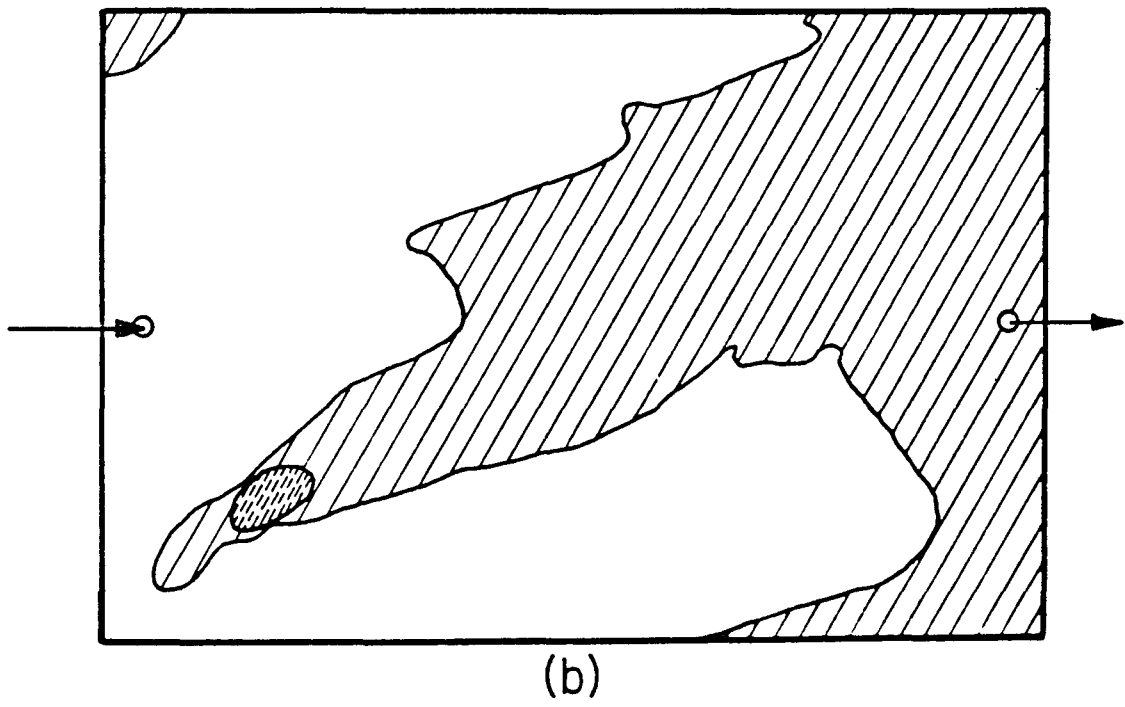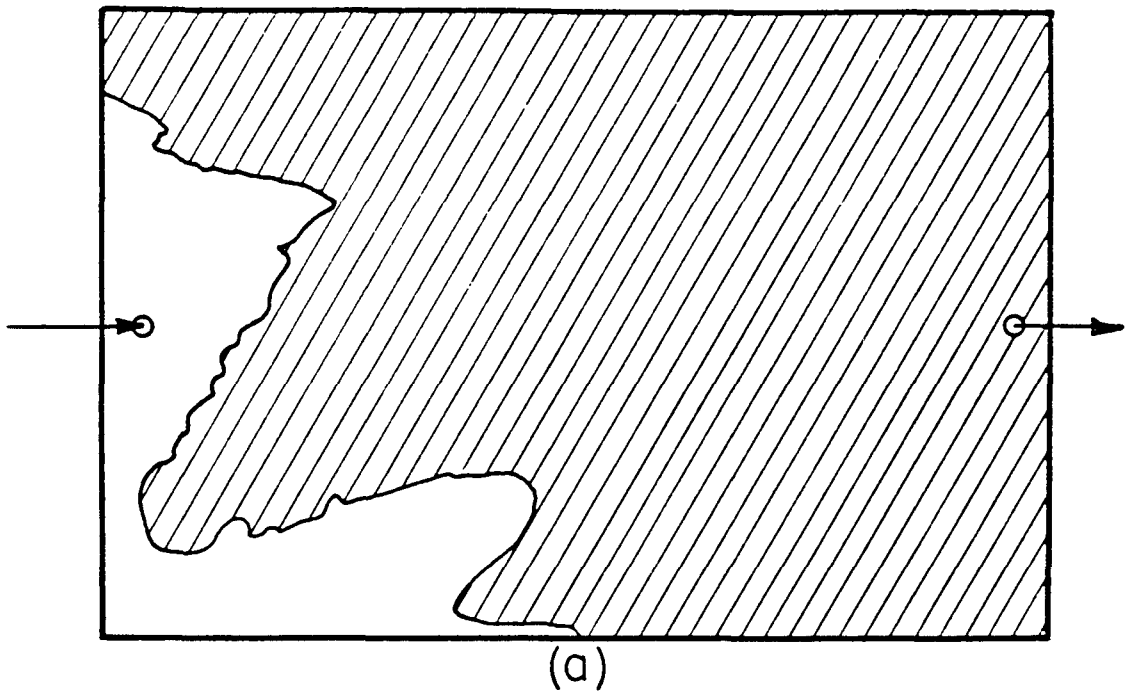
SYSTEM: M4   IFT = 0.040 mN/m

MODE: WATER DISPLACING OIL

Fig. 3.19. Displacement front profiles. (See Fig. 3.1 for key)

(a)

(b)
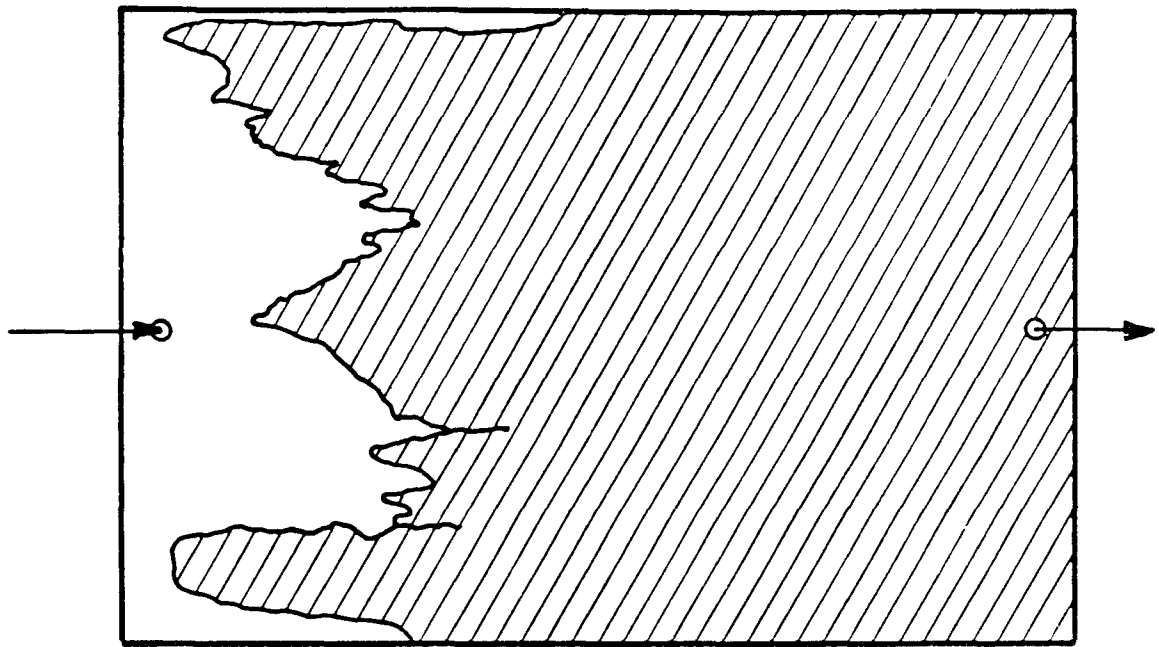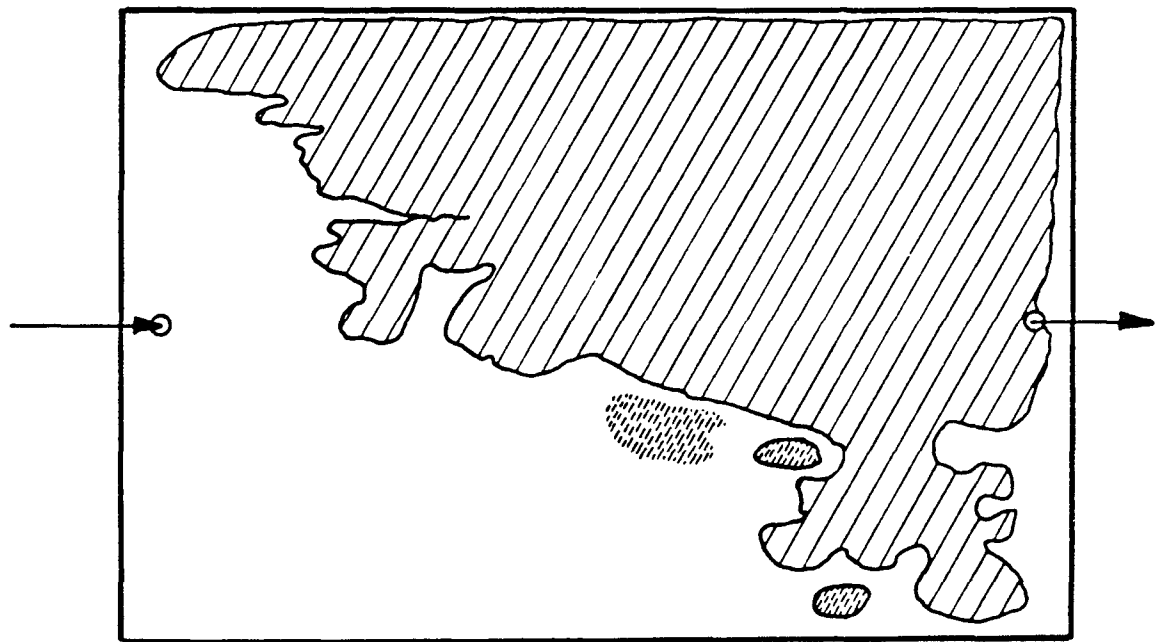
SYSTEM: MI   IFT = 17 mN/m

MODE: OIL DISPLACING WATER

Fig. 3.20. Displacement front profiles. (See Fig. 3.1 for key)

(a)

(b)
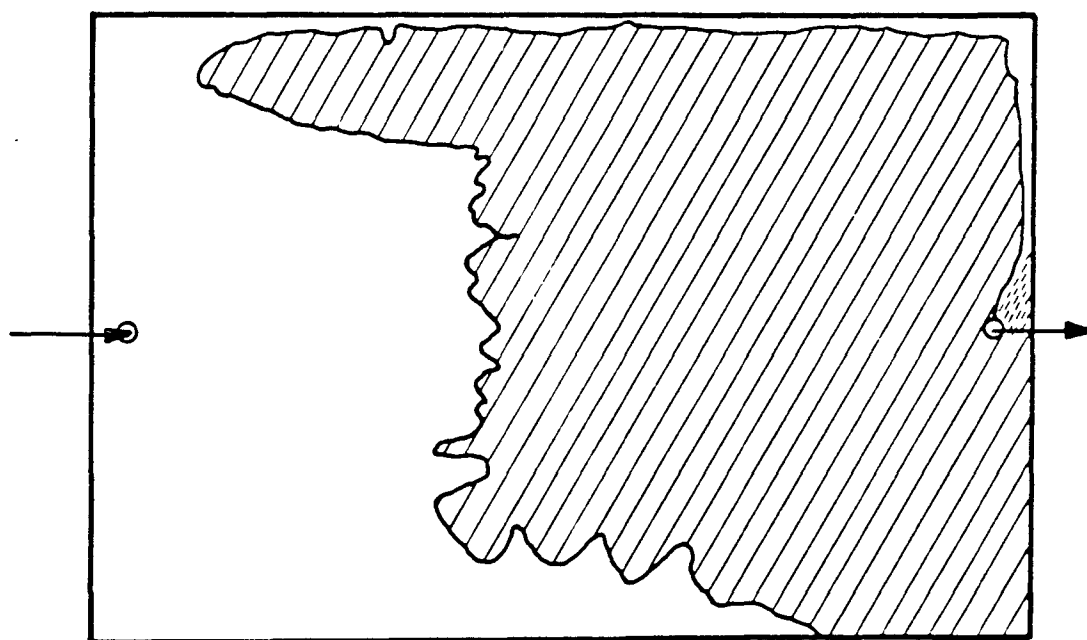
SYSTEM: M2   IFT = 1.2 mN/m
MODE: OIL DISPLACING WATER

Fig. 3.21. Displacement front profiles. (See Fig. 3.1 for key)

(a)

(b)
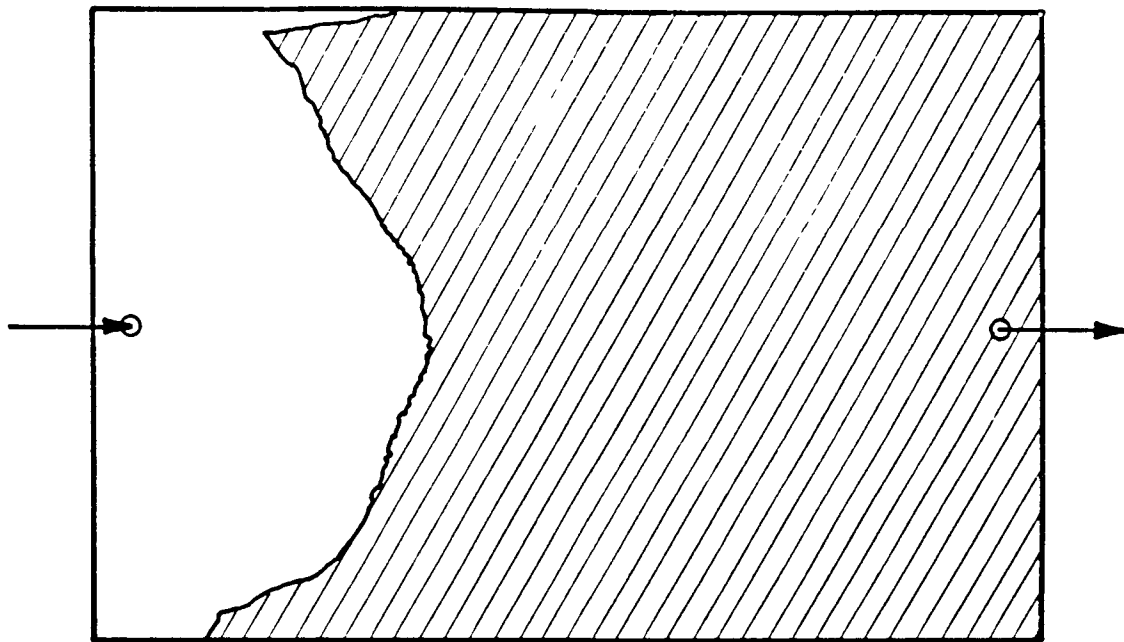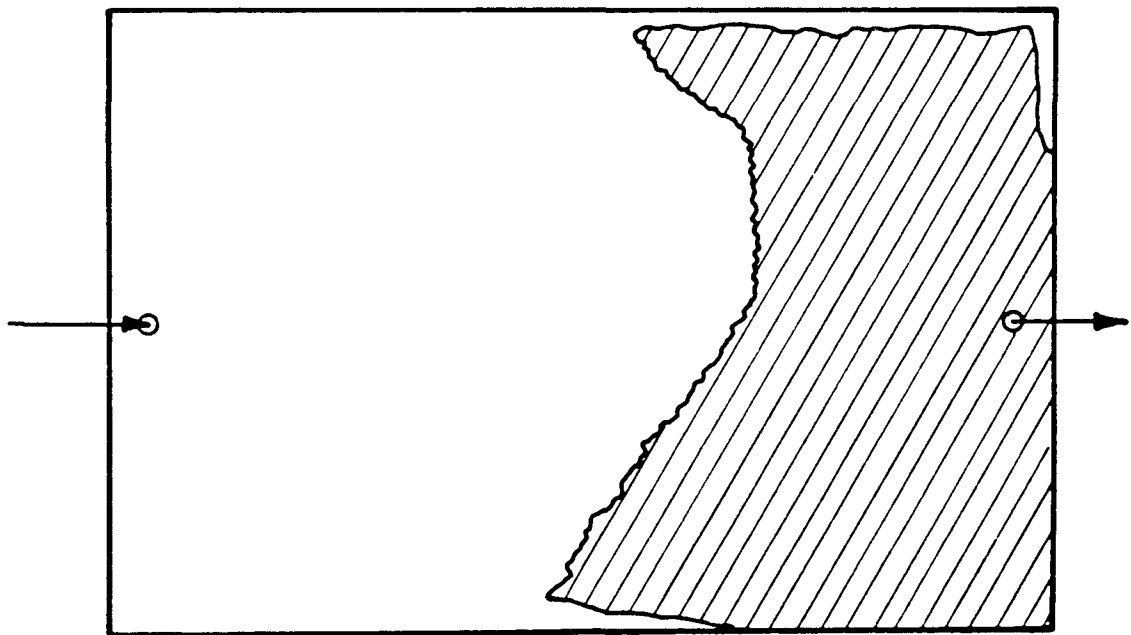
SYSTEM: M2-B   IFT= 0.002 mN/m

MODE: OIL DISPLACING WATER

Fig. 3.22. Displacement front profiles. (See Fig. 3.1 for key)
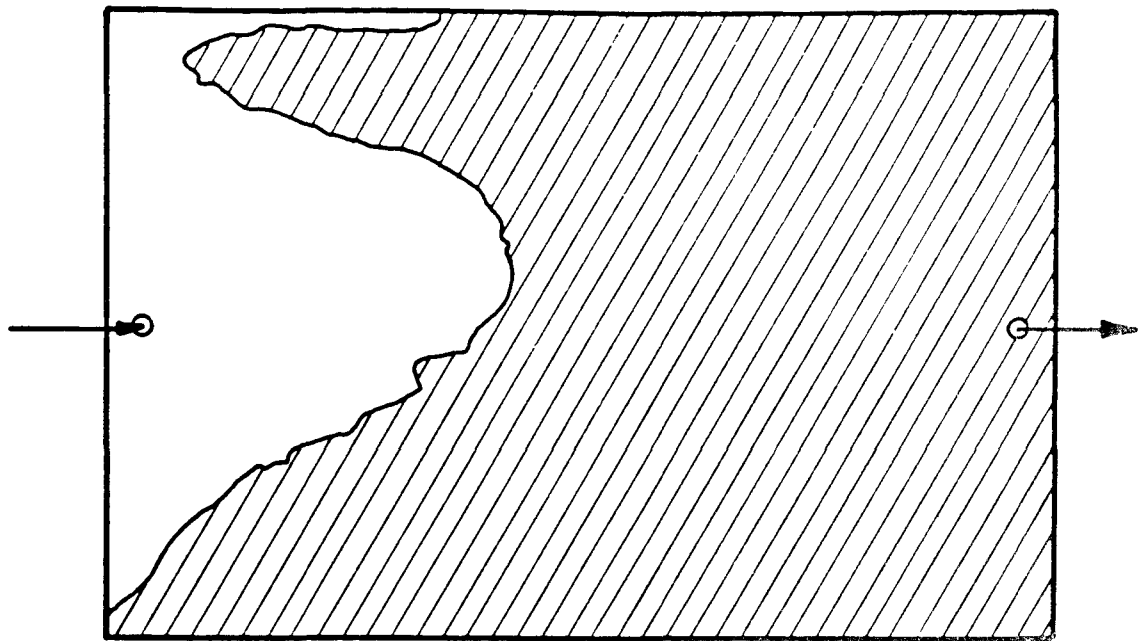
(a)
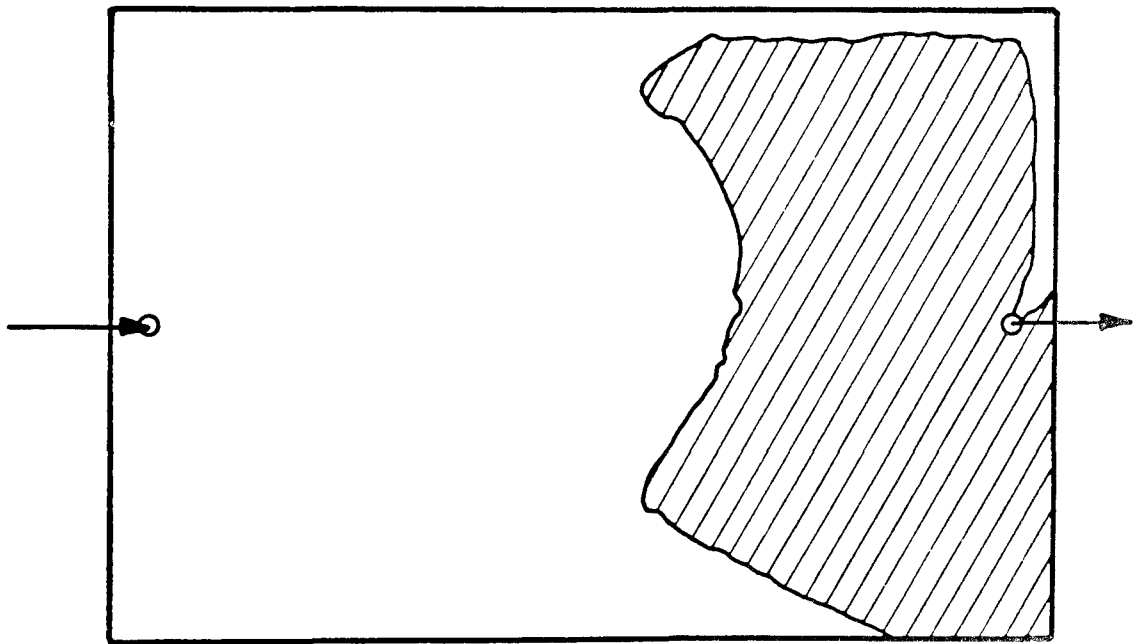
(b)

SYSTEM: M3   IFT = 0.029 mN/m

MODE: OIL DISPLACING WATER

Fig. 3.23. Displacement front profiles. (See Fig. 3.1 for key)

(a)

(b)
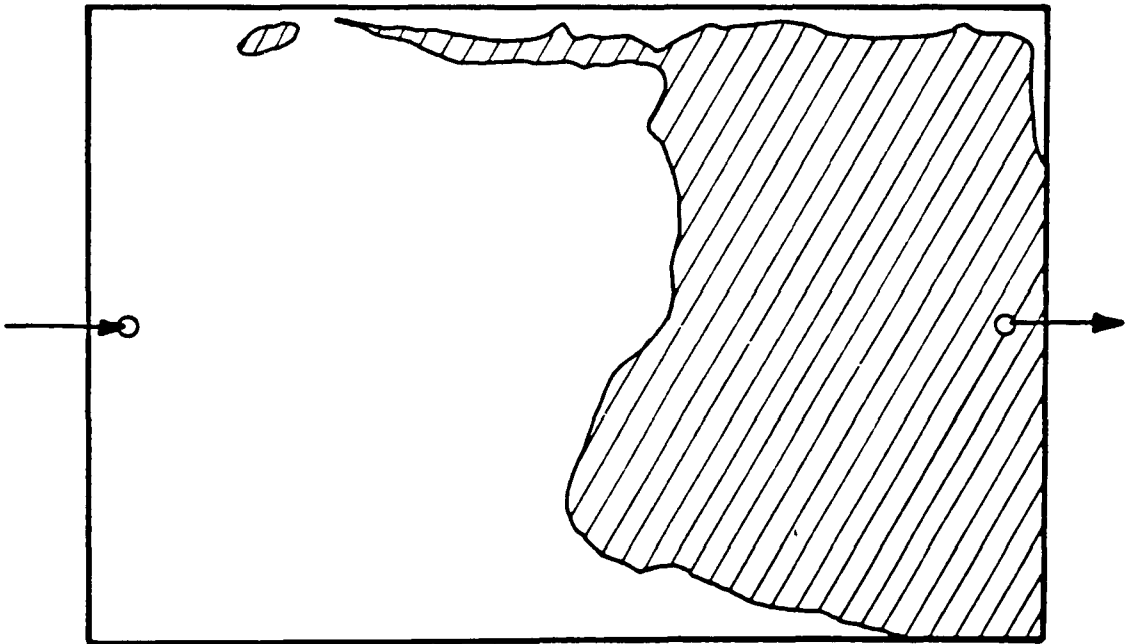
SYSTEM: M4   IFT = 0.040 mN/m

MODE: OIL DISPLACING WATER

Fig. 3.24. Displacement front profiles. (See Fig. 3.1 for key)
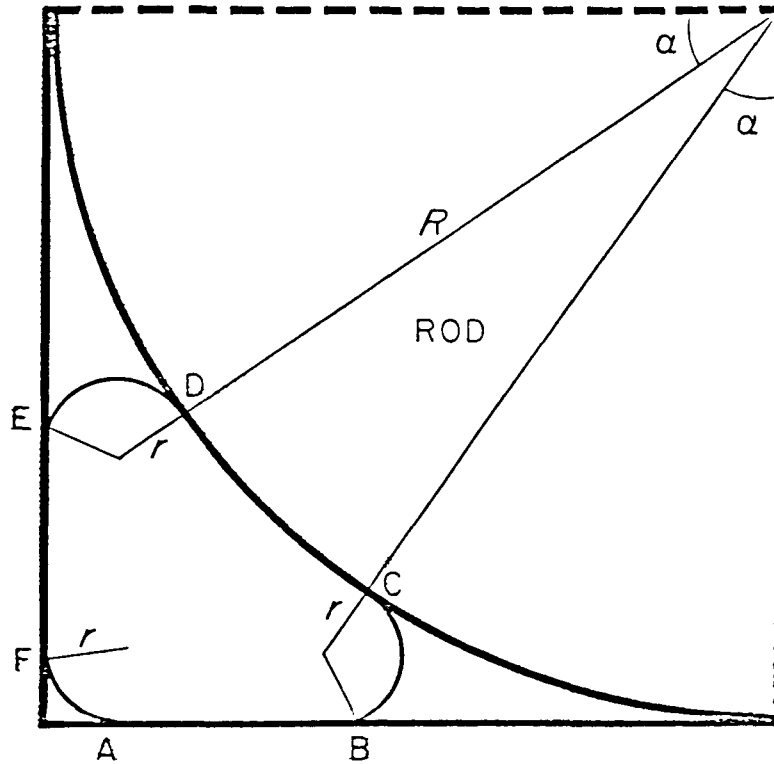
Fig. 3.25. Cross section of the rod-in-corner space and section through the three wedge menisci. The sections through these wedge menisci are arcs of circles of the same radius, r.
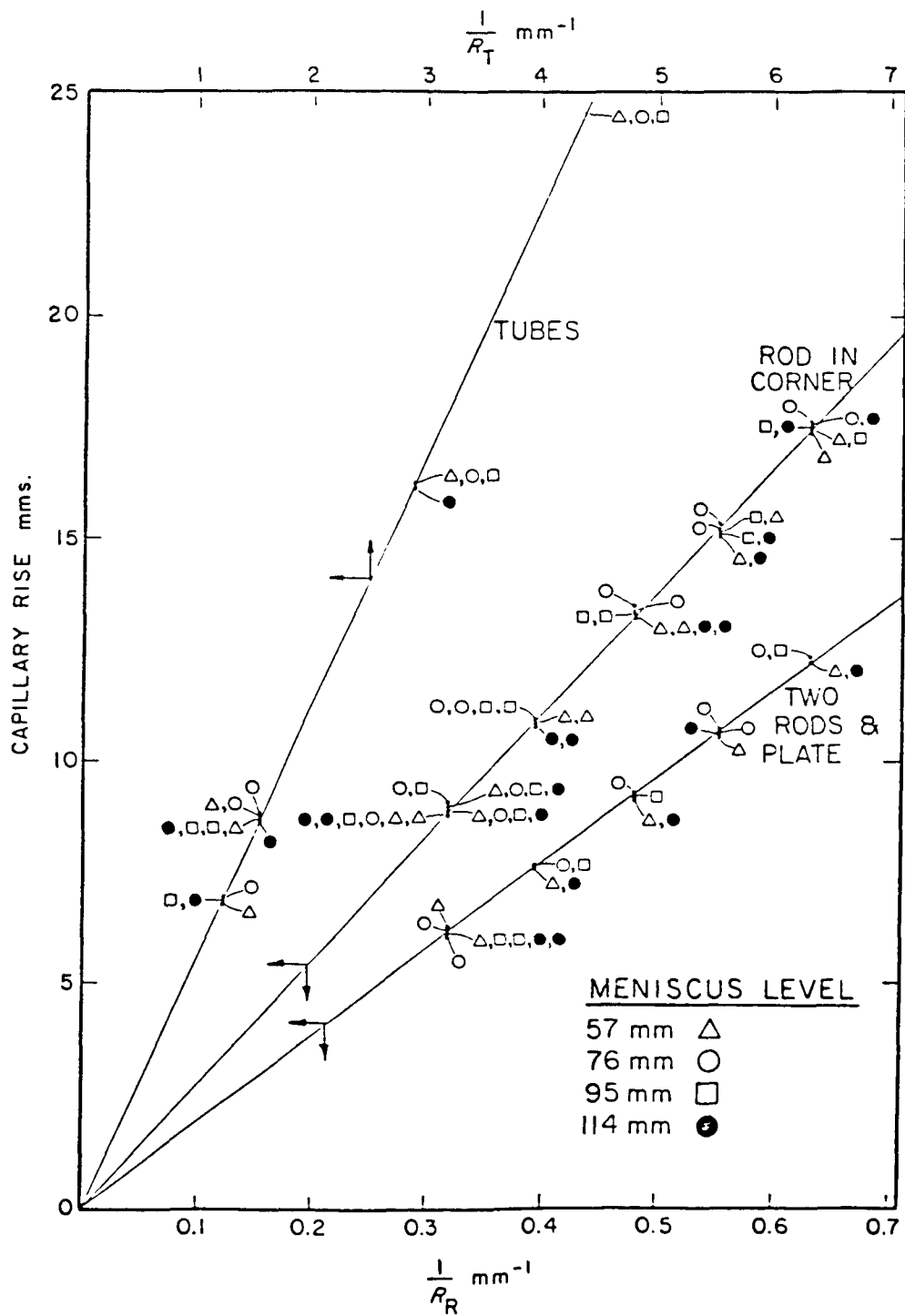
Fig. 3.26. Graph of the heights of capillary rise against $1/R_T$ for capillary tubes, $1/R_R$ for rod-in-corner and rod and plate menisci.

113
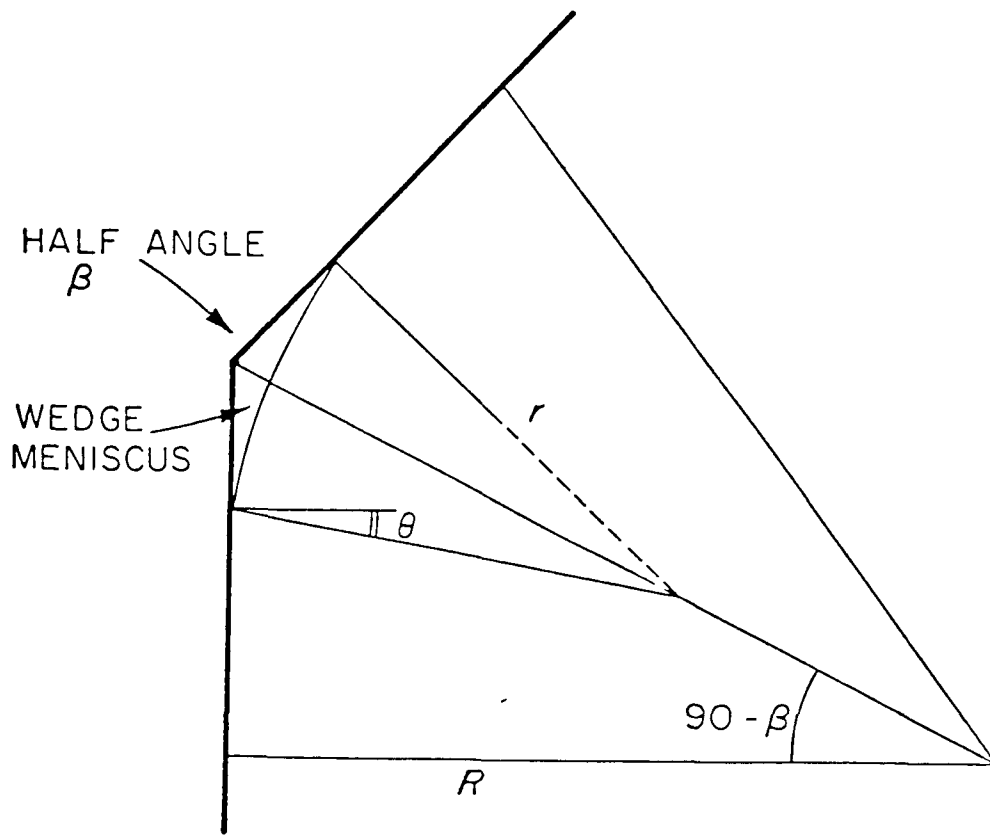
Fig. 3.27. Diagram of a corner of a polygonal section tube. Depending on the contact angle, θ, a wedge meniscus may exist in the corners.
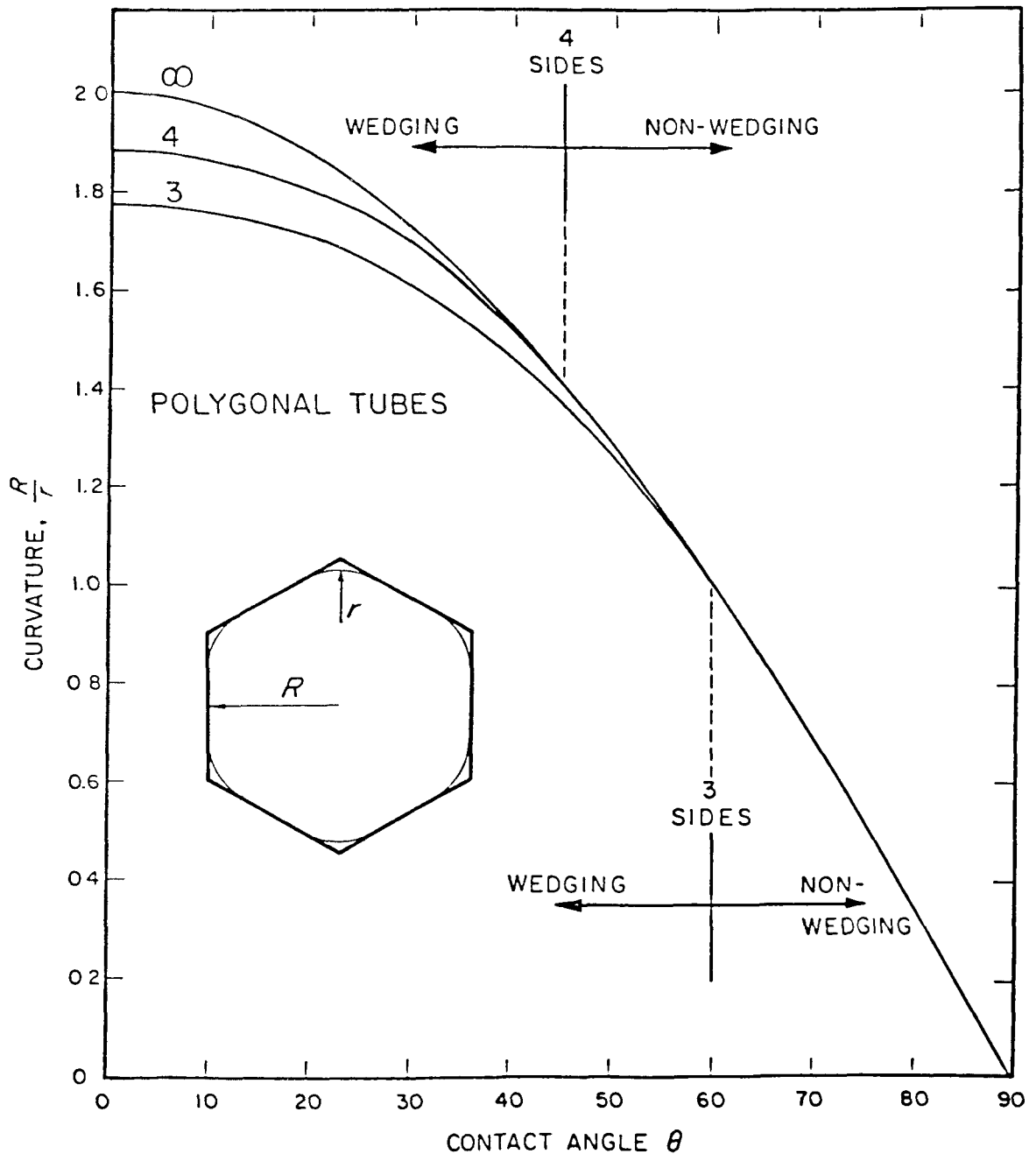
Fig. 3.28. Plot of the curvature of the meniscus in regular polygon tube normalized relative to the radius of the insphere as a function of contact angle. (The tube having an infinite number of sides is simply a cylinder.)
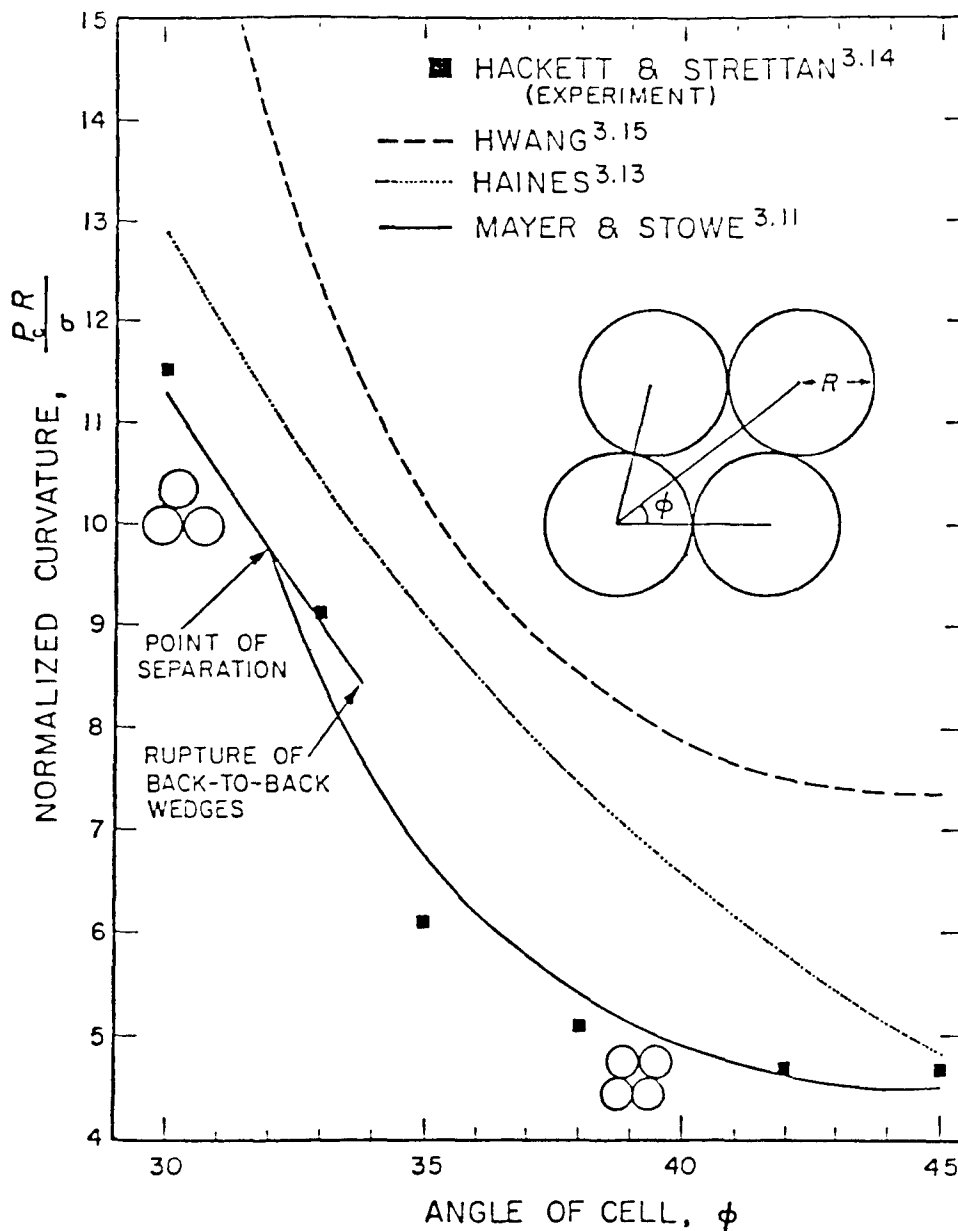
Fig. 3.29. Comparison of the experimental results of Hackett and Strettan[3.14] with various theoretical approximations. The model pore consists of four contacting spheres with cell angle varying such that the pore varies from triangular to square. The Haines approximation[3.13] assumes the meniscus is spherical. Hwang[3.15] obtained curvatures which are inversely proportional to the hydraulic radius. The Mayer and Stowe analysis[3.11] is actually for rods and not spheres as claimed.
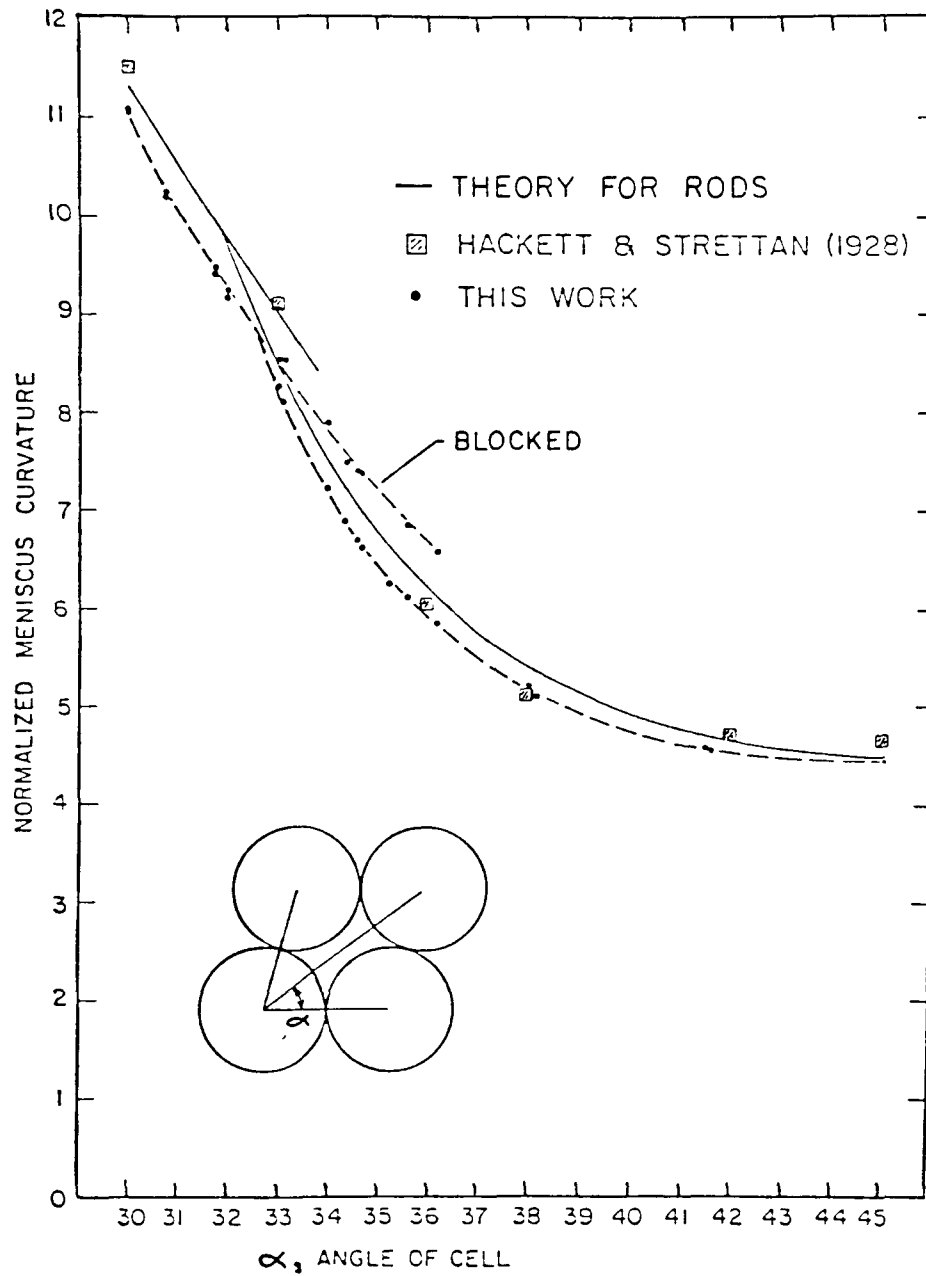
Fig. 3.30. Results of meniscus curvature vs. cell angle. Dual values over a limited range depend on whether the pore was partially blocked or not. Also shown are the results for spheres of Hackett and Strettan[3.14].
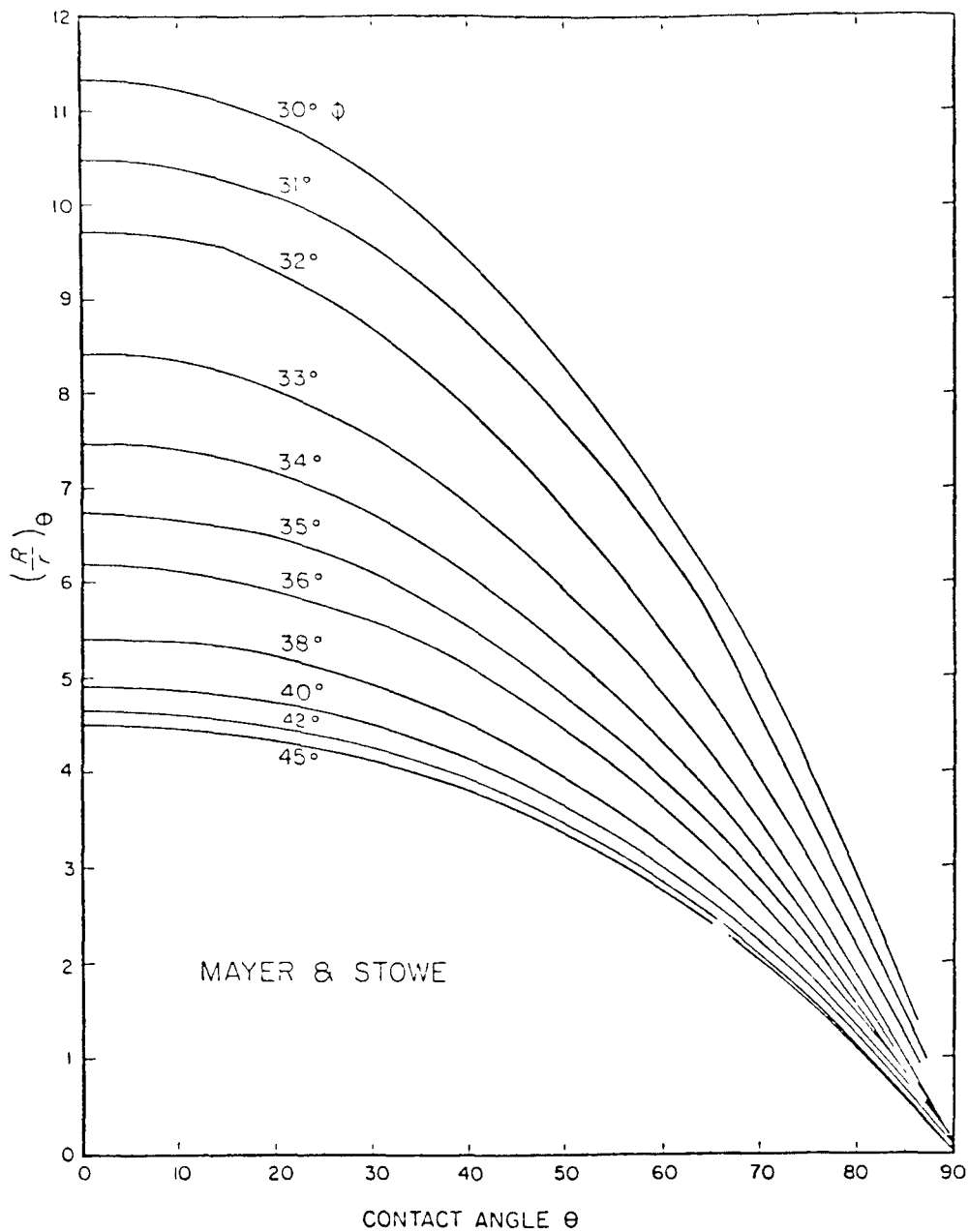
Fig. 3.31. Values of normalized curvature calculated by Mayer and Stowe. Note the quite rapid drop of curvature as the contact angle is increased. This is particularly obvious for the smaller cell angles.

118
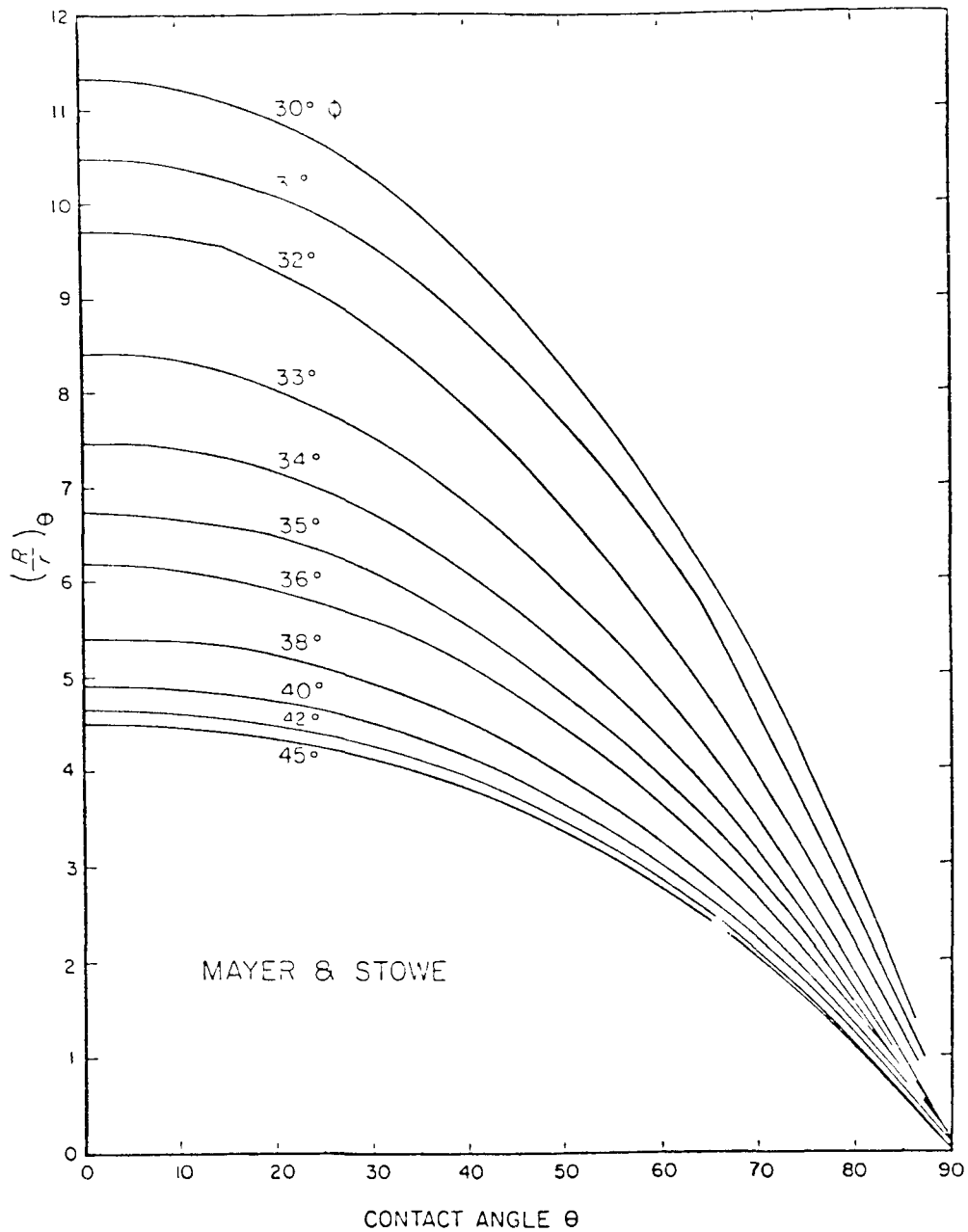
Fig. 3.31. Values of normalized curvature calculated by Mayer and Stowe. Note the quite rapid drop of curvature as the contact angle is increased. This is particularly obvious for the smaller cell angles.
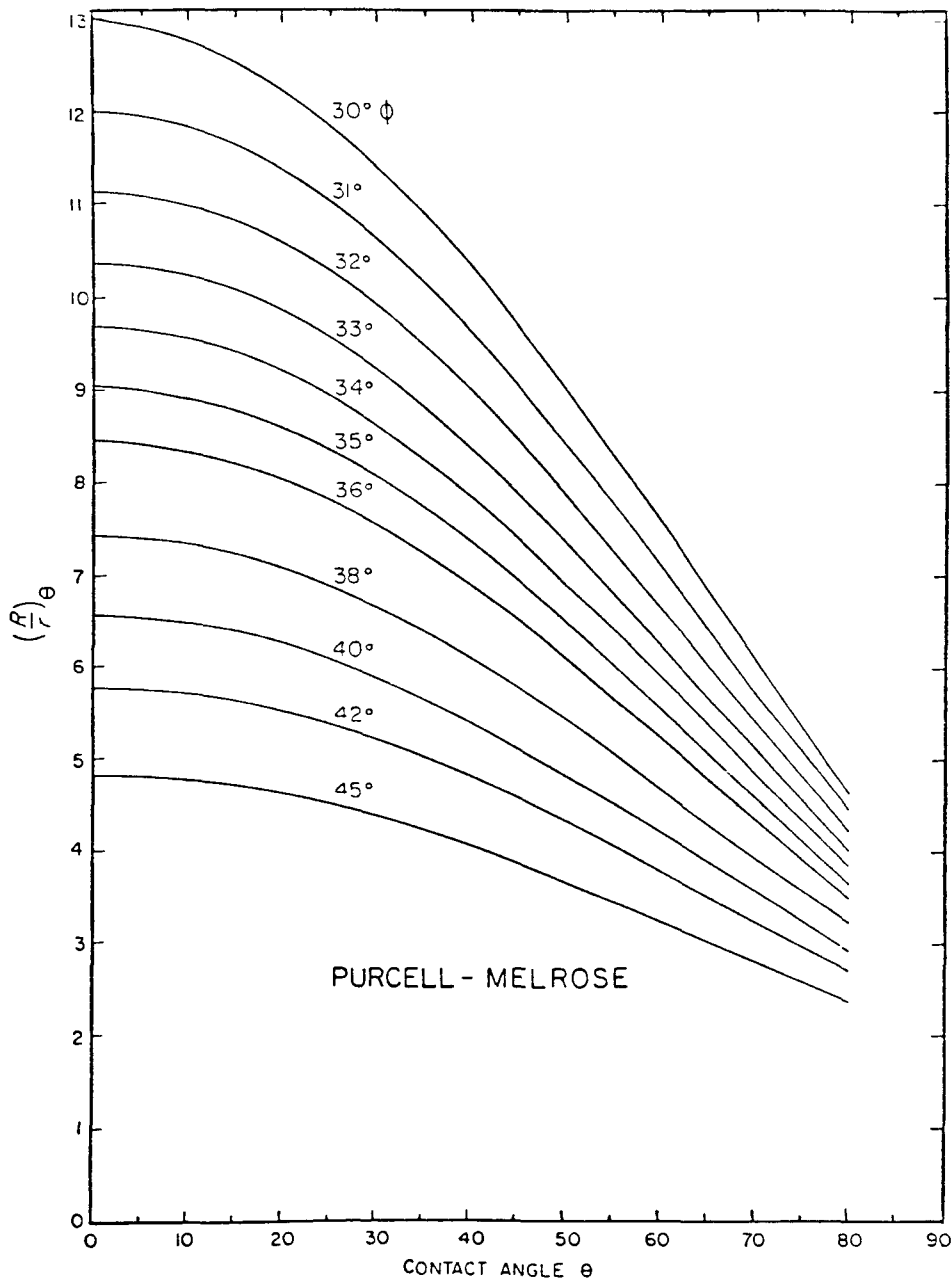
Fig. 3.32. Values of the maximum meniscus curvature calculated from the insphere approximation following the method of Purcell[3.17] and Melrose[3.18]. This analysis approximates the meniscus curvature to a sphere but does incorporate the fact that the maximum meniscus curvature occurs away from the plane of centers.
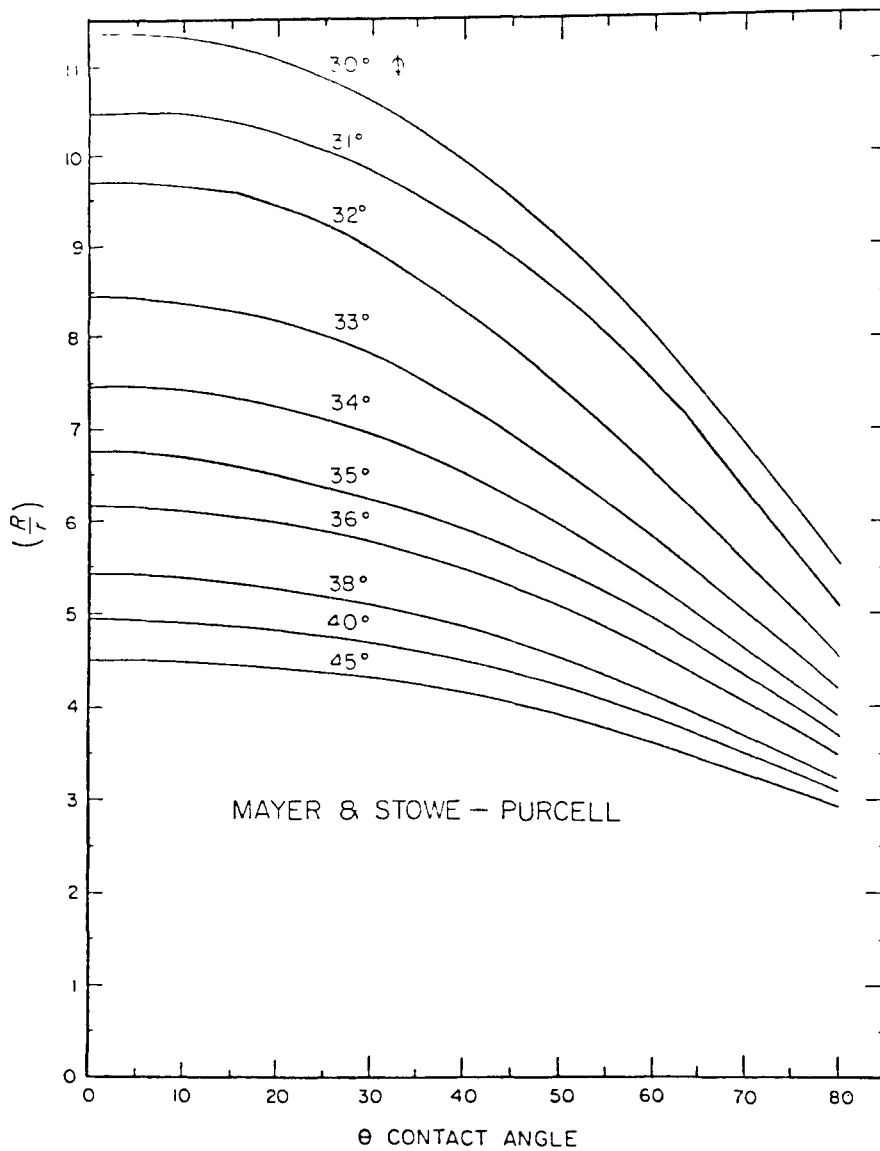
Fig. 3. 33. Maximum meniscus curves calculated for rods to give the curvature in the constriction of the pore, calculating an equivalent toroid, and then displacing the now spherical meniscus to the position of maximum curvature using the Purcell method[3.17]. Note that these curves fall less rapidly than either the Mayer and Stowe or Purcell-Melrose values alone. (cf. Figs. 3.31 and 3.32)
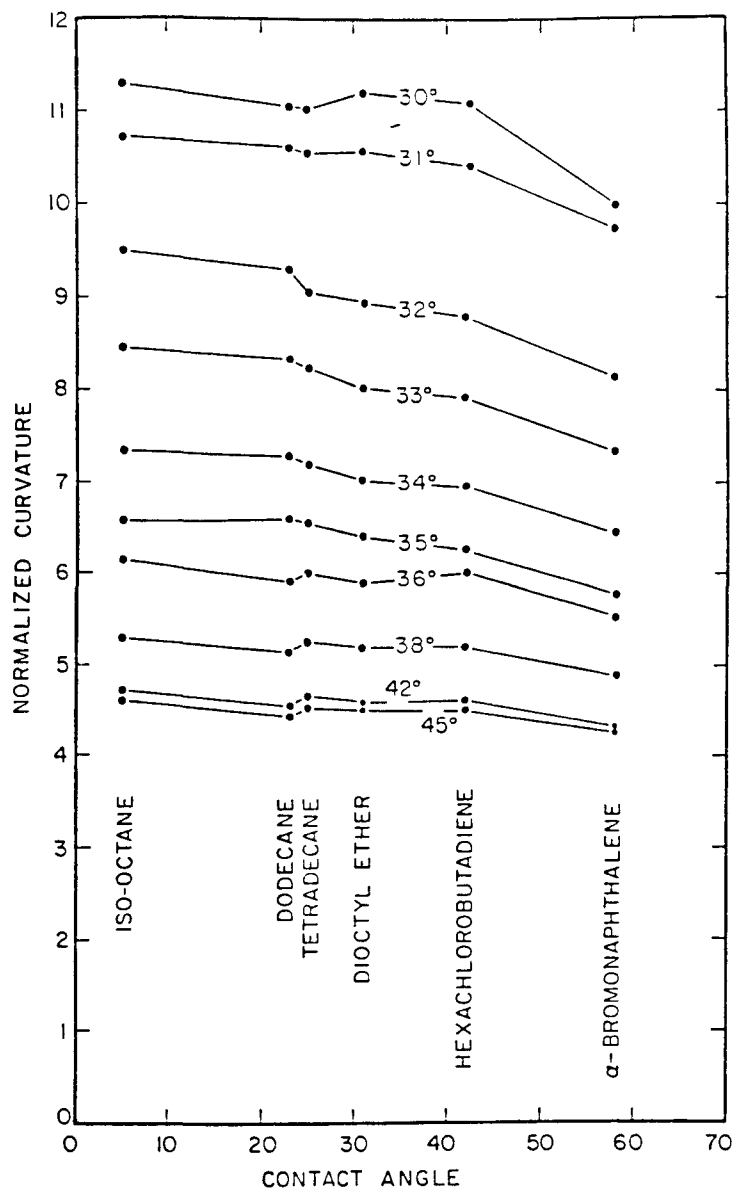
Fig. 3.34. The meniscus displacement curvature vs. receding contact angle as determined by experiments with model pores. The contact angle was varied by using polytetrafluoroethylene spheres and liquids of known contact angle. These values fall even more slowly than any of the theoretical predictions. (See Figs. 3.31 through 3.33.)

TASK 4. RESIDUAL OIL STRUCTURE

4.a. ANALYSIS OF BLOB-SIZE DISTRIBUTIONS BY COULTER COUNTER

BACKGROUND

The microstructure of residual oil following a waterflood spans a wide spectrum of shapes and sizes within the reservoir pore space. Investigation of blob-size distributions as a function of capillary number, therefore, involves the determination of size statistics of populations of highly anisotropic particles over a broad size range. In these studies,[4.1,4.4] polymerized styrene particles represent the oil droplets trapped in various sandstone cores under prevailing waterflood conditions.

The method of image analysis was initially attempted[4.1,4.2] to obtain frequency distributions based on feature perimeter (P) and feature projected area (A), using two-dimensional scans of photomicrographs of blob populations numbering between 1,500 and 2,500. This work was performed with the aid of a Quantimet Image Analyzer by an independent laboratory. Because of the large number (nineteen) of samples to be analyzed and the excessive length of time required to conduct a single analysis, it was decided to pursue an alternative method of size analysis using the Coulter Counter. Besides the convenience of in-house operation and rapid analysis, the latter method offered the additional advantage of three-dimensional, volume-based characterization of particle size compared to strictly two-dimensional feature characterization by the method of image analysis. It is, of course, still possible that results may be somewhat sensitive to the presence of highly anisotropic particles because of orientation effects.

The following is a detailed description of the Coulter instrument, principle of operation, and procedures used in carrying out the size analysis on the various blob samples. The blob samples under investigation (Table 4.15) also contained minor amounts of insoluble mineral residues and precipitates arising from incomplete dissolution or leaching of the rock matrix during the recovery of blobs from the core sample. Except in the case of a few blob samples (viz, Berea-2, Berea-6, Berea-9 and Berea-10), the contamination by particulate debris was minor and was not likely to affect the final results significantly. Results of the size distribution data and a discussion of the results are presented in section 4.b.

122

EXPERIMENTAL PROCEDURES

Equipment Description

A model TA II L Coulter Counter (Coulter Electronics, Hialeah, Florida) equipped with a population accessory and a special stand was used to perform size distribution analysis. In principle, this analyzer can simultaneously count and size particles, regardless of shape, on the basis of three-dimensional sensing of particle volume. The particles are suspended in an inert electrolyte medium which conducts electricity between two electrodes placed on either side of an aperture. The change in electrical current between the electrodes is monitored during sampling as an individual particle passes through the aperture and displaces an equal volume of electrolyte. The electronics of the counter rapidly translate each instantaneous change in current to a particle being counted and the amount of change to the particle volume. The particle size is calculated as the diameter (D_{bv}) of a sphere of equal volume and assigned an appropriate channel. As the particles of the dispersion enter the aperture during sampling, their presence is indicated as fleeting electrical pulses on a built-in oscilloscope screen. A separate oscilloscope displays the volume- or number-size distribution during analysis. Provision exists for either direct numeric readouts or transfer of results to an x-y plotter or to a printer supplied as an integral component of the population accessory.

Selection of Aperture Tube

According to the Coulter Counter operation manual,[4.3] the diameter (D_{bv}) range of particles that can be effectively sized corresponds to from ~2% to 40% of the chosen aperture diameter. That is, a single aperture is suitable for analyzing a population in which the largest and smallest particles may differ in size (expressed as D_{bv}) by a factor of up to 20, or equivalently in volume by a factor of up to $(20)^3 = 8,000$.

Two key factors must be noted regarding the selection of a proper aperture for a given particle population. In the event that the sample contains many particles smaller than the lower sizeable limit (i.e., $D_{bv} < 20$ μ with the 1000 μ aperture), coincident passage of two or more such particles through the aperture may be falsely registered as that of a single particle of larger size and thus may introduce error in the analysis. The coincidence error will then be confined to the lower channels and affects the population distribution more than the volume distribution. A different situation arises even if relatively few large particles are present that exceed the upper sizeable limit (i.e., $D_{bv} > 406$ μ for the 1000 μ aperture tube). In this case, considerable error may be manifested in the volume distribution results because the last channel gives only a minimum size of 406 μ with an upper limit being set by the aperture size.

For a population composed of a broad spectrum of particle sizes that cannot

be satisfactorily sized with the use of a single aperture, it becomes necessary to apply multi-aperture analysis. Such was the case for certain blob samples obtained under low capillary number displacement conditions. For these samples, a two-aperture analysis was carried out.

Analysis Using a 1000 µ Aperture Tube

The operating manual for the machine provides some leads, but very few details, on the use of large apertures and associated problems. We found that use of very large apertures necessitated improvisation and modifications at various phases of the sampling procedure.

The procedure for analysis with the 1000 µ aperture was varied in two aspects from the normally recommended operation. Firstly, the control cable from the sample stand was disconnected from the main console to permit direct control of the electronic counter. Secondly, two steps were undertaken with the aim of reducing extremely high flow rates through the aperture that could conceivably cause cavitation while sampling. Glycerin was added to enhance the viscosity of an electrolyte formed from brine (NaCl) and isopropanol. The choice of the electrolyte was primarily dictated by considerations that the liquid be a good dispersion medium for the polystyrene particles without promoting agglomeration, provide an almost neutrally buoyant environment for the particles and be chemically inert. In addition, a reduced vacuum was applied on the downstream side of the aperture to provide an adjustable pressure head of 1.5" to 2" Hg instead of the standard 6.5" Hg head. Prior to analysis, the suspending medium was subjected to filtration (5 µ Millipore filter) and deaeration, using a combination of a vacuum pump and an ultrasonic bath.

Channel Calibration and Analysis

The instrument was calibrated first for channel size using well-characterized, monodisperse latex microspheres of uniform diameter (91.2 µ) supplied by Coulter Electronics, Inc. The calibration was checked at weekly intervals during the course of analysis. A motor-driven stirrer was used to aid uniform dispersion of particles in the sample container. Occasionally, when acute electrical noise interfered with the low background counts expected of the electrolyte, a pneumatically operated stirrer was used instead. The count rates during sampling were always maintained below 100 particles per second to minimize coincidence error.

In all, fifteen channels were in active use, beginning with channel 2, which corresponds to an equivalent-volume sphere diameter (D_{bv}) lying between 16 µ and 20.2 µ. The channels, excepting the last, are arranged in order of increasing volume in a geometric progression, with a common ratio of 2. In terms of size, the two edges of an active channel differ by a factor of $(2)^{1/3} = 1.26$. The last (sixteenth) channel is essentially open-ended with respect to sizing in that it

brackets all particles whose D_{bv} are larger than 406 µ but less than the aperture size of 1000 µ.

Mode of Analysis

A choice of three operational modes is available by which sampling can be done with respect to either a preset total count, a preset channel count or a preset sampling time. After experimenting with all three options in the preliminary stages, it was decided to perform the entire analysis in the preset time mode. This provided the most convenient check on count rates and the extent of coincidence error. Table 4.1 provides a summary of the operating conditions during analyses.

RESULTS AND DISCUSSION OF 1000   APERTURE ANALYSIS

A given blob sample was subjected to Coulter size analysis several times (a minimum of three runs) to test for reproducibility. Fig. 4.1 illustrates the differential volume distributions obtained on sample Berea-6 in four passes, of which pass 1 corresponds to the original suspension in a 1250 ml container. As a means of conserving the blobs that had passed through the aperture, the effluent sample was collected in a clean vacuum trap flask and returned to the sample container for repeat analysis. These results are represented by passes 2, 3 and 4. No blobs were registered in channel 16. This showed that no blobs of sizes, $D_{bv} > 406$ µ, are present in sample Berea-6, and therefore, two-aperture analysis is not necessary for this sample. The data demonstrate close reproducibility of the experimental method.

As a further check on the results, a different pool of blobs was selected out of the original blob sample Berea-6 and analyzed on the Coulter Counter. Again, closely reproducible data were obtained for a series of runs on the new sample. In Fig. 4.2, the averaged results of volume-size disribution are shown for the two different blob populations of sample Berea-6. Good agreement is evident, implying that the sample size and sampling procedures adopted for analysis are satisfactory. Additional results on other blob samples are given in Figs. 4.3 through 4.14. In no case did the volume contribution by particles in channel 16 exceed 2% of the total sample volume. The population distributions of these samples are shown in Tables 4.2 through 4.7. It is quite probable that the true number-based size distribution, $f_n(D_{bv})$, will significantly differ from that obtained in the analysis due to the presence of smaller blobs (5 µ to 16 µ size) that lie outside the effective sizing range of the 1000 µ aperture. The coincidence error attributable to these particles will mostly be limited to the lower channels and so will have a relatively minor impact on the volume distribution results.

A conservative estimate of the amount of sample used up in analysis per run may be made as follows. Taking the density of polystyrene to be ~1.05 gm/cc, the total volume of blobs recovered after polymerization and leaching of rock matrix was 2.71 and 0.73 cm^3 respectively for samples Berea-1 and Berea-BF. For illustration purposes, the volume-averaged blob diameter ($\bar{D}_{bv,n}$) or the number frequency distribution has been used with values of ~150 μ for Berea-1 and ~800 for Berea-BF samples. Thus, a typical experimental run in which ~30,000 may be sampled comprises, at most, 1.1~2.0% of the initial blob population.

Need for Two-Aperture Analysis

The use of a 1000 μ aperture was adequate to yield frequency and volume histograms for a majority of blob samples (e.g., Berea-6, Berea-14, Berea-1?, etc.) trapped under high capillary number (order of $10^{-4} \sim 10^{-3}$) conditions. However, samples resulting from low capillary number displacements generally contained a wider distribution of blob sizes, larger blobs, highly complex features and projected end-to-end lengths exceeding 1000 λ blob samples, even if able to pass through the 1000 aperture, would not effectively sized because the relative volume contribution of particles in the last channel (406 μ < D_{bv} < 1000 μ) often exceeded the limit (1 ~ 2% of total sample volume) considered acceptable for differential volume distribution data. Another difficulty experienced during the analysis was blockage of the 1000 aperture caused by large particles. Even only temporary presence at the mouth of the orifice could cause spuriously large pulses to be recorded in the blob count; these pulses caused inaccurate output.

It was therefore necessary to apply a two-aperture size analysis to these blob samples, using a 2000 μ aperture for the original blob population and a 300 μ aperture for a sample which was prescreened so that plugging of the aperture during sampling was eliminated. The results of both analyses were then weighted appropriately to arrive at a final volume distribution.

Analysis Using a 2000 μ Aperture Tube

The calibration of channel size was first performed using standard microspheres of polystyrene-divinylbenzene of uniform diameter (271 μ). On the basis of volume-based sphere diameter, the effective range of sizing covered 40.3 μ to 1024 μ. Under operating conditions (1.5 ~ 1.75" Hg), cavitation, which was a serious problem at usual pressures, did not occur during analysis. Some important considerations which prompted modifications in the sampling procedure will be addressed now. In order to keep the maximum coincidence error below 5%, the particle count rates during sampling had to be less than 30 per second. The high flow rates of the suspension through the aperture, together with the low particle count rates, severely restricted the total number of particles which could be sized in a single pass through the 2000 μ aperture. However, accurate statistical features of the distributions cannot be calculated unless the sampled volume is sufficiently large and is fully representative of the whole.

In an attempt to obtain meaningful results, a new sampling procedure was followed in which the differential volume distribution for the blob sample was automatically updated for a sequence of passes through the aperture by switching on the "Inhibit Reset" feature on the main unit. This made possible accumulation of a reasonably large particle count (10,000 to 12,000) of the same suspension by recycling the effluent for continued analysis. A cumulative series of at least four passes constituted a run. A minimum of two such runs was made on the same blob sample, and the results averaged to give a volume distribution reported as the result of one experimental run. Often, after sampling, a second switch ("Scope Special") was activated to amplify the existing low output signals (by a factor of 5 at most) to a level which permitted automatic normalization of the volume distribution data.

In all cases, the background counts (for the electrolyte) prior to sampling were generally negligible in relation to the total number of particles sampled. The concentration of the particulate system in the sample container was altered, as desired, by the addition of pure electrolyte or blobs.

Two-Aperture Analysis

After completion of size analysis using the larger aperture, the sample suspension was filtered through a U.S. standard 50 mesh screen (nominal sieve opening of 300 μ), and the underflow was analyzed using a 1000 μ aperture, as previously described. The resulting differential volume distribution of the filtered blob sample was then combined with the differential volume distribution for the original sample (2000 μ analysis) to obtain an overall normalized distribution of the blob sample in the size range of 16 to 1024 μ. The calculation procedure, which involves superposition of results for overlapping channels, is illustrated in the operating manual[4.3] of the counter. Ability to achieve proper overlapping may, to some degree, be influenced by the bias inherited by the blob sample during preparation for 1000 μ analysis. This occurs as a result of screening highly anisotropic large blobs through a uniform mesh sieve.

RESULTS AND DISCUSSION OF TWO-APERTURE ANALYSIS

Results of two-aperture analysis on a blob sample for a displacement in a Berea sandstone at a capillary number ($K_w\mu/L\sigma$) of 1.14 x 10^{-5} are shown in Fig. 4.15. To examine the effects of sample size and sampling method on blob-size statistics, different samples were selected out of the original blob population and were analyzed by the Coulter instrument. For blobs obtained from the sandstone core Berea-2, runs 124 and 131 correspond to separate analyses of the same blob sample, whereas run 147 was performed on an entirely new sample. Compared to similar results achievable with the 1000 μ aperture, reproducibility

127

of volume distribution data is more difficult to demonstrate in this case for two reasons. The first is due to the inherent sensitivity of the volume distribution to the presence of the largest blobs. Even if these are small in number (perhaps only two or three) they can still be a significant part of the total sample volume. Secondly, the probability that two or more blobs pass coincidently through the very large aperture of 2000 μ is increased. In particular, the small particles (say D_{bv} of 40 μ and less) are present in very large numbers and therefore have a high probability of being involved in coincidence errors. However, the effect on volume distribution data due to these blobs is expected to be small. Taking into account these potential uncertainties in the size analyses, the agreement between the three runs appears satisfactory.

In addition to coincidence error resulting from the presence of smaller blobs, and possible bias in the screened sample used in 1000 μ analysis, another factor needs to be considered in the evaluation of the two-aperture analysis. While sizing with a 2000 μ aperture, the presence of a relatively few blobs of large size in the sample suspension can cause significant distortions in the differential volume distribution data at the high end. This scatter is generally limited to two or three of the higher channels. The combined volume contribution by blobs in these channels usually lies within ~15% of the cumulative volume distribution, $P_v[D_b < D_{bv}]$. Results of two-aperture analysis on other blob samples are provided in tabular form in Tables 4.8 through 4.14. The final blob-volume distribution, $f_v(D_{bv})$, appearing in the last column has been calculated from the averaged results for the filtered sample and for the original sample.

4.b. CHANGES IN RESIDUAL OIL STRUCTURE WITH OIL RECOVERY

BACKGROUND

Although considerable attention has been paid to the obviously important subject of residual oil structure, the amount of experimentally determined, quantitative information on blob structure and the statistics of blob populations is very limited. To obtain such information, techniques for preparing statistically representative blob samples and measurement of their size distributions were developed, as described in section 4.a.

EXPERIMENTAL WORK

Preparation of Residual Oil Blobs

Experimental techniques for preparation and recovery of solidified oil blobs were described in detail previously.[4.4] Core flooding procedures employed in the study of the structure of residual oil as a function of capillary number (e.g., the ratio of viscous to capillary forces) were as follows:

1) The core properties -- porosity, ϕ, air permeability, K_a, and brine permeability, K_w, -- were first determined using standard core analysis procedures.

2) The core sample was saturated with 2% $CaCl_2$ brine. Then a high initial oil saturation, S_{oi}, was established by flooding the sample with styrene monomer at pressure gradients ($\Delta P/L$) of about 150 kPa/cm. About 15 to 20 pore volumes (PV) of styrene were passed through the sample. This included flow in both directions in order to reduce saturation gradients caused by capillary end effects.

3) Normal waterflood residual oil saturation, S_{or}^*, was established by waterflooding the sample at S_{oi} at a capillary number, $K_w \Delta P/L\sigma$, in the range of 1×10^{-6} to 1×10^{-5}, by passing nearly 1.5 PV of brine through the core. Permeability to brine was measured at S_{or}^*.

4) Reduced residual oil saturation, S_{or}, for a given sample was obtained by first waterflooding to S_{or}^* as described above. Then residual oil was mobilized by flowing 3 to 5 PV of brine at a constant pressure drop across the sample, such that the capillary number, $K_w \Delta P/L\sigma$, exceeded the critical capillary number observed[4.5] for sandstones (2×10^{-5}). The permeability to brine at reduced residual oil conditions was measured after 3.5 PV of brine had passed through the core sample.

By this procedure, a series of cores was prepared in which reduced residual oil saturations were established at selected capillary numbers ranging from 2×10^{-5} to 7×10^{-4}. The procedures for polymerization of the styrene monomer and subsequent recovery of the polystyrene blobs by acid leaching procedures have been described.[4.4]

Structure and Size Distribution

Three kinds of analyses were performed on the solidified oil (polystyrene) blobs recovered from a given core sample: 1) visual examination and measurement of blobs or of micrographs of blobs carried out with the aid of optical and scanning-electron microscopes; 2) image analysis of photomicrographs of a

representative number of oil blobs to give population distributions based on projected blob perimeter and projected blob area respectively;[4.2] and 3) size analysis of residual oil blobs by the Coulter Counter method.

Visual examination of blobs provided a qualitative picture of the pore structures where oil was trapped, and also information about the typical capillary structures of residual oil encountered. Scanning electron photomicrographs of typical oil blobs from a given sample provided structural details including absolute sizes. Indications of the wetting conditions were also obtained since blobs formed under water-wet conditions have typically rotund nodes and smooth surfaces.

In the present study, analyses by the image analyzer and the Coulter Counter methods were aimed at quantitative evaluation of the effect of capillary number on blob-size distributions.

EXPERIMENTAL RESULTS AND DISCUSSION

Displacement Behavior

Solidified blobs of residual oil were obtained under the flow conditions listed in Table 4.15. Data on the amount of trapped styrene in a given core sample and the subsequent recovery of residual oil as solidified polystyrene blobs are also given, the latter being the quoted residual oil saturation (S_{or}) in column 6. The next column lists S_{or} estimates based on k_{rw} measurements and a previously developed[4.12] correlation of k_{rw} versus S_w for sandstones.

The capillary number values (based on an interfacial tension value of 29.7 dynes/cm for a system of 2% $CaCl_2$ brine and aged styrene containing benzoyl peroxide) in these experiments varied from 8.2×10^{-7} to 6.9×10^{-4}. The range of residual oil saturations varied from 38.0% to 11.0% depending upon the capillary number.

Microscopic Inspection

Each batch of solidified oil blobs was inspected routinely by microscope to further confirm from their contours that the residual styrene had been trapped and polymerized under water-wet conditions. Blobs of various shapes and sizes were observed for all N_{ca} conditions. It is convenient to classify shapes of blobs as singlet, doublet and branched. Singlet blobs occupy one pore body and have sizes that are consistent with the range of pore-body sizes as revealed by pore casts. For Berea sandstone, practically all of the volume contributed by singlet blobs found at low capillary number conditions fall in the size range of 30 μ to 200 μ which corresponds to the pore-body sizes observed in pore casts of Berea sandstone.[4.2] Blobs involving two pore bodies connected by a liquid bridge

are classified as doublets. Blobs of this shape commonly range from 100 μ to 400 μ in length. Examples of singlet and doublet blobs are shown in Fig. 4.2 of reference 4.1. Blobs involving three or more pore bodies are broadly described as branched, with possible ring and linear structures included. They typically range from about 150 μ to 1000 μ in length and are more frequent at low capillary number conditions (see Fig. 4.1 of reference 4.1). These were from Berea sandstone sample, Berea-8. For this sample the lengths ranged from about 400 to 1000 μ, and often involved more than about 15 pore bodies.

An indication of the ratio of pore body to pore throat size -- the aspect ratio -- can be obtained from measurements of blob dimensions. The capillary structures of all branched blobs at all N_{ca} have narrow constrictions which vary in diameter from 10 μ to 30 μ and link pore-body sized nodes which vary from about 30 μ to 200 μ in diameter. The average length of pore constrictions appears to be about twice the average pore-throat diameter. From examination of a relatively large collection of photomicrographs of blobs, the ratio of pore-body size to pore-throat size of branched blobs was found to range from 1.5 to as high as 10, with most frequent values of this aspect ratio falling between 2.5 and 4.0.

Even though Berea sandstone usually retains a high residual oil saturation of about 35%, the majority of the number population of oil blobs trapped in Berea sandstone occur as singlet and doublet structures. This form of residual oil structure was demonstrated previously[4.2] for micromodels having high aspect ratio and is considered to be characteristic of pore networks having high aspect ratio.

Blobs of residual oil, trapped at low capillary number in the Boise sandstone sample, were similar in appearance to those for the Berea samples (e.g., Berea-1, Berea-2), the only difference being the absolute size of blobs. The change in absolute sizes was consistent with the Boise sandstone having higher permeability and relatively larger pore-body and pore-throat sizes than the Berea sandstone.

Inspection by microscope of oil blobs corresponding to reduced residual saturations in Berea sandstone samples (e.g., Berea samples 6, 15, E-F, and DO4) showed that there was an increase in the number of relatively small blobs in relation to the number of large blobs. Nevertheless, a significant proportion of branched blobs still remained after mobilization at high capillary number. The fact that not all of the relatively large blobs of oil are mobilized at capillary number conditions higher than the critical capillary number for mobilization of large blobs is not surprising. Large oil blobs may not always be exposed to high pressure gradients, because of their orientation or because of blocking of surrounding pathways by singlet and other blobs that cannot be mobilized at the prevailing conditions.

Formation of Sub-Singlet Sized Drops

An interesting observation with respect to blob population after mobilization of part of the residual oil is that many spherical blobs of sizes

131

less than 30 μ are found. These droplets comprise only a small volume fraction (less than 5%) of the remaining reduced residual oil. However, their presence indicates that in the process of mobilization, some of the oil filament constituting oil blobs breaks up into smaller blobs, some of which have sizes smaller than the pore-throat dimensions in the medium. Observations of similar break-up of liquid drops in shear fields have been reported by Rumscheidt and Mason.[4.6] This result indicates that at high capillary number displacements, partial emulsification of residual oil and entrainment of oil droplets may contribute to oil recovery. The phenomenon of oil blobs breaking up and coalescing during mobilization has been given considerable attention.[4.7,4.8] However, the breakup of blobs into sizes much smaller than the pore dimensions has not been considered in previous accounts of modelling blob mechanics.

Experiments in micromodels[4.2] provide direct visual confirmation that at high capillary number, mobilized blobs of oil partially break down into sub-singlet blobs of sizes less than those of the pore throats in the system. As such, in the process of motion, droplets were observed to collect in pore bodies, without coalescing, to give a cluster of sub-singlet blobs which had the appearance and mobilization characteristics similar to normal blobs. This behavior is in some ways analogous to the transport of fine particles through porous media in that accumulation occurs within pore spaces and it also demonstrates the likely importance of coalescence phenomena in recovery mechanisms.

Blob-Size Distributions by Image Analysis

A limited amount of data was obtained with a Quantimet image analyzer. In this method of determining blob-size distribution, samples of blobs from a given core sample are dispersed on a microscope slide which is then scanned with the aid of an image analyzing system. About 2000 blobs from a given sample were analyzed and classified in terms of both projected blob perimeter and projected blob area. The number distribution of projected blob perimeters and projected blob areas can be converted to a number distribution of equivalent blob diameters, D_{bp} and D_{ba}, given by the diameter of a circle, having the same perimeter and area, respectively, as that measured for the blob. Thus, two types of number distribution may be obtained which are based on two-dimensional features of blob shape and size.

Blob samples from Berea cores 1, 2, 6 and 8 have been analyzed using this method. Figs. 4.16a and 4.16b show the number-based, blob-size distributions for Berea-1 given by projected blob perimeters and areas respectively. Note that distributions of the two types of equivalent blob-size diameters are not the same, particularly at large blob sizes. This is to be expected because objects with the same projected perimeter can obviously have different projected areas, and vice versa. Perimeter lengths of branched blobs will obviously yield equivalent blob diameters (D_{bp}) which are higher than those for projected areas (D_{ba}).

An important feature of the blob-size distributions for Berea-1 is that 50%

132

of blob sizes fall in the range of 30 μ to 130 μ. These sizes are consistent with pore sizes measured from SEM micrographs of resin pore casts for a Berea sandstone having properties similar to the Berea-6 sample. Taking into consideration published data on the complete photomicrographic distribution of pore sizes in Berea sandstone,[4.9] measured pore sizes from SEM micrographs of resin pore casts for Berea sandstone, and trapping behavior as seen in transparent micromodels,[4.2] the blob-size distributions in Figs. 4.16 and 4.17 suggest that the pore network in Berea sandstone involves pores of high aspect ratio which causes extensive trapping of oil as singlet blobs by snap-off mechanism.

Fig. 4.17 provides a comparison of perimeter-based, cumulative frequency distributions of blobs collected from samples Berea-1, Berea-6, and Berea-8. Note that there are significant differences between the blob sizes remaining after high-capillary-number mobilization of residual oil (Berea-6) and those given by normal waterflood residual oil conditions (Berea-1 and Berea-8). Qualitatively similar changes in blob-size distribution with capillary number were also observed in mobilization experiments run in transparent micromodels of etched capillary networks on glass plates.[4.2]

Characterization of residual oil blobs by volume, based on the number distributions given in Figs. 4.16 and 4.17, involves somewhat arbitrary assumptions about blob shape. Because blob shape depends strongly on blob size, and because the pore-body sizes as well as the pore-throat sizes do not have a narrow distribution, the approximation of a realistic volume distribution in terms of say, equivalent blob diameter by perimeter, would be difficult to justify.

Volume-Based Analysis of Blob-Size Distributions by Coulter Counter Method

The Coulter Counter technique for measuring particle size distributions appears, as opposed to the image analyzer, to be especially well suited to volumetric analysis of irregularly shaped particles. In this method, the incremental electrical resistance offered by a particle relative to that of the dispersion medium (electrolyte) is measured as the particle passes through an electrical sensing zone. This additional resistance is taken to be directly proportional to the particle volume, regardless of its shape. Particles entering an aperture during sampling are thus sized according to volume. Once satisfactory procedures have been established, this method has the inherent advantages of convenience, rapid data collection and analysis for large sample populations. Experimental details of the technique used to obtain blob-size distributions are given in section 4.a. All of the blob samples appearing in Table 4.15 were analyzed by this method. Results are expressed in terms of an equivalent blob diameter (D_{bv}) which corresponds to the diameter of a hypothetical sphere having the same volume as the actual blob.

The close reproducibility of results is evident in Figs. 4.1, 4.2, 4.3 and 4.18 for repeated analyses run in our laboratory for blobs of Berea-6 and Berea-1 samples. It can be seen that the volume-based, blob-size distribution is very

reproducible (particularly for single aperture analysis with 1000 μ aperture) and that blob populations in excess of 12,000 to 15,000 blobs do not affect the results. The general procedure was to analyze each sample at least three times as a test of reproducibility and then average the results. In addition, different population pools from the original blob sample were selected and analyzed to examine the effect of sampling procedure on results (see Figs. 4.4 through 4.15 of section 4.a.).

Comparison of Coulter Counter and Image Analysis Results

A comparison of the blob-size distribution by the Coulter Counter method with the blob-size distribution obtained by the photomicrographic method is presented in Figs. 4.19a, b and c for sample Berea-6. It is noted from these figures that the two types of analysis are consistent with respect to the range of blob sizes measured and to the bimodal frequency distribution of blob sizes sometimes observed after high capillary number displacement ($N_{ca} \sim 10^{-4}$). The blob number distributions obtained by the two methods, based on D_{bp} and D_{bv}, for sizes less than 40 μ are in good agreement. This is to be expected because most of these blobs are spherical; so their computed size should be independent of the method of analysis. However, there is a significant difference between the two number distributions for characterizing blobs of sizes greater than 40 μ where shapes are generally other than spherical. The cumulative frequency distribution curves based on D_{ba} and D_{bv} tend to lie closer than those corresponding to D_{bp} and D_{bv}, as the blob size increases. This is as it should be, for the area-based equivalent blob diameter (D_{ba}) is a better approximation to the volume-based equivalent diameter (D_{bv}) than the perimeter-based D_{bp} in characterizing large-size blobs of highly irregular geometrical features. Fig. 4.19c also illustrates that 73% of the blob population having sizes less than 80 μ comprise only 17% of the residual saturation of Berea-6, whereas just 7% of the blob population of sizes exceeding 128 μ contribute to as much as 47% of S_{or}.

In making the above comparison, it is emphasized that only a limited amount of data was obtained by the image analysis method and relatively little development work was carried out with respect to procedures used in applying the image analyzer method.

Effect of Capillary Number on Blob-Frequency Distributions

The cumulative number-based size distributions, $P_n[D_b < D_{bv}]$, obtained from the Coulter Counter method generally appear as sharply declining curves on a semi-log plot of number frequency versus blob size (D_{bv}). Blob samples collected from low capillary number displacements exhibited a broad range of equivalent blob sizes, D_{bv} approaching 800 μ and projected blob lengths as large as 1000 to 1600 μ (e.g., Boise, Berea-1, Berea-2, etc.). In a typical sample population, there were relatively fewer blobs of large sizes in contrast to the very large number of smaller blobs.

134

Certain blob samples trapped under high capillary number waterflood conditions (N_{ca} of the order of $> 2 \times 10^{-4}$) displayed bimodal (differential) frequency distributions similar to that of the Berea-6 sample (see Fig. 4.19c). This may be a consequence of the shifts in blob-size distribution as they occur during the course of partial mobilization of residual oil. This experimental result is consistent with the notion that some oil blobs, as they become mobilized and move under the prevailing pressure gradient, may break up into smaller blobs (including sub-singlets) that remain trapped in the medium. The onset of the bimodal population distribution, however, does not appear to be solely controlled by the capillary number, and other factors including aspect ratio and local topology as dictated by the permeability may be influential. Of all the blob samples from sandstone cores, only Berea-6, Berea-14, Berea-D03, Berea-9 and Berea-10 demonstrated distinct bimodal frequency distributions. In this context, it is noteworthy that the last two blob samples obtained in relatively low permeability cores ($K_w \approx 180$ md) showed the bimodal characteristic at intermediate N_{ca} of $\sim 4.5 \times 10^{-5}$ while some other samples, such as Berea-BF, Berea-15, etc., corresponding to much higher N_{ca} floods ($> 4.3 \times 10^{-4}$) did not.

Effect of Capillary Number on Blob-Volume Distributions

The anticipated trend in volume-based blob-size distribution with increased capillary number is illustrated in Fig. 4.20. At increased capillary number conditions, there is a shift towards smaller size blobs. For example, blobs of size $D_{bv} < 200$ μ in the Berea-12 sample make up 66% of the residual oil saturation, while blobs of size $D_{bv} < 200$ μ in samples Berea-14 and Berea-15 make up 87% and 94% of the residual oil saturation respectively at the capillary number conditions indicated in Fig. 4.20. Furthermore, blobs of size $D_{bv} < 80\mu$ make up only 14% of the value of S_{or} in Berea-12, whereas in Berea-15 blobs of size $D_{bv} < 80$ μ make up 38% of the value of S_{or}. Taking into account that the S_{or} values for Berea-12 and Berea-15 were 30.8% and 15.7% respectively, the blob-size distributions show that at increased capillary number conditions, additional small blobs are obtained as a result of breakup of blobs into singlets and sub-singlets during the process of mobilization. This mechanism is consistent with observations of mobilization in micromodels.[4.2] However, it differs from mechanisms of mobilization of residual oil used in the modelling of residual oil saturation as a function of capillary number.[4.10,4.11] The theoretical treatments of oil-blob mechanics during mobilization[4.7,4.8] appear to be qualitatively correct with respect to the mechanism of breakup of blobs.

Fig. 4.21 shows additional results of volume-based size distribution of blobs from Berea cores which had very similar water and air permeabilities (K_w ranged from 294 to 361 md and K_a from 642 to 977 md). To illustrate the concomitant effect of N_{ca} on the amount as well as the microscopic distribution of residual oil, the differential volume distributions are plotted on a relative basis. The areas under the histograms for samples Berea-2, Berea-D04 and Berea-15 are scaled appropriately to represent the prevailing S_{or} in each of the cores. The ordinate scale is chosen so that the histogram for Berea-2 exactly corresponds to the differential volume % of blobs for this sample.

The broad size distribution of Berea-2 ($N_{ca} = 1.14 \times 10^{-5}$) is typical of

residual oil microstructure under low N_{ca} flood conditions. As expected, larger blobs ($D_{bv} > 256 \mu$) contribute significantly more to the residual in sample Berea-2 than in either of the other two samples which were run at higher capillary numbers. Furthermore, a comparison of these histograms suggests redistribution of residual oil in the equivalent blob-diameter range (D_{bv}) of 40 μ to 128 μ. For instance, sample Berea-D04 contains more residual oil in this size range than either Berea-2 or Berea-15. On the other hand, sample Berea-15 contains more trapped oil than Berea-2 in the smaller blob sizes, D_{bv} less than 102 μ, and slightly more residual than Berea-D04 in larger blob sizes, $D_{bv} > 161$ μ. These observations imply that a significant proportion of oil blobs continue to alter their shapes and sizes as N_{ca} is increased beyond the critical value. In other words, branched blobs which are locally mobilized may yet be trapped in a displacement as such or as smaller blobs after breakup. Aspect ratio and local topology may dictate the fate of a locally mobilized oil ganglia, i.e., whether or not it will be recovered, stranded or broken up into smaller blobs due to snap-off or pore blockage mechanisms.

It can be seen from Fig. 4.19c that in blob sample Berea-6, although blobs of size smaller than 40 μ make up about 35% of the blob-number population, their volume contribution to the S_{or} value for this sample is negligible (e.g., about 1% of S_{or}). A similar observation can also be made for sample Berea-D04 (Fig. 4.21). These results suggest that when it comes to population balances in the modelling of blob mechanics and residual oil structure at capillary number conditions above critical values, one may ignore the volume contribution of sub-singlet sizes retained in the medium to the total residual oil saturation at prevailing conditions. However, the occurrence of sub-singlet blobs cannot be ignored in the modelling of relative permeability at reduced residual oil conditions,[4.12] since sub-singlet blobs can block pore throats and thus affect the flow mechanism.

Fig. 4.22 contains differential blob-volume distribution data of several blob samples, as determined by the Coulter Counter technique. It may be noted that blob populations of five samples (not all shown in Fig. 22) corresponding to high N_{ca} in the range of 2.5×10^{-4} to 7×10^{-4} exhibit very similar patterns of volume-based size distributions, the range of D_{bv} being ~20 μ to ~322 μ. The modes for these blob samples lie between 102-128 μ and more than 90% of S_{or} is contributed by blobs having sizes between 32 μ and 256 μ. A possible cause for the apparent inconsistency in the size distribution results for Berea-13 and Berea-6 samples in relation to the effect of N_{ca} may lie with the reduced interfacial tensions occasionally observed with aged styrene.

An interesting observation is that the volume distribution curves for Berea-9 and Berea-10 samples ($N_{ca} \approx 4.5 \times 10^{-5}$) fall in the same pattern as the blob samples obtained at much higher N_{ca}. The narrow size distributions characterizing these blob samples may be related to their low K_w and the associated high aspect ratio.

Statistical features of blob-volume distributions of residual oil are given in Table 4.16 for all the sandstone samples. These results were obtained from the Coulter Counter method of size analysis and were based on the cumulative volume distribution curve, $P_v[D_b > D_{bv}]$ versus log D_{bv}. The median ($D_{bv,m}$) and volume-averaged blob diameter ($\bar{D}_{bv,v}$) shown in Table 4.16 provide gross measures of the mean blob size for each sample population.

CONCLUSIONS

1. The novel application of the Coulter Counter technique to size several samples of anisotropic particle populations in the 20 μ to 800 μ size range was demonstrated.

2. Under the operating conditions, the size of the sample used in analysis was adequate to yield reproducible volume distribution results, typically within ±2% of the mean for each channel in 1000 μ analysis and within ±4% of the mean in two-aperture analysis. The scatter in data was always restricted to a few higher channels; close matching was obtained in the lower channels.

3. During mobilization of residual oil, oil blobs break up into sub-singlet blobs, with a significant fraction of temporarily locally mobilized oil blobs being retained in the porous medium. This leads to narrower blob-size distribution at high capillary number displacement, without much recovery of oil.

4. Although the blob population may change considerably with capillary number, the volume-averaged, blob diameter $(\overline{D}_{bv,v})$ and the median $(D_{bv,m})$ of the volume distributions are not very sensitive to capillary number conditions in the range 1×10^{-4} to 1×10^{-3}.

NOMENCLATURE

$K_w \Delta P/L\sigma$	=	Capillary number corresponding to waterflood
S_{or}	=	Residual nonwetting phase (oil) saturation at the conclusion of waterflood, (% of pore volume)
D_b	=	Blob size (microns)
D_{bv}	=	Equivalent blob-size expressed as the diameter of a sphere having the same volume as the blob, (microns)
D_i, D_{i+1}	=	Lower and upper edges of active channel i, (microns)
ΔV_i	=	Volume fraction (or %) of blobs contained in channel i
Δn_i	=	Number fraction (or %) of blobs contained in channel i
$f_v(D_{bv})$	=	Differential volume distribution of blobs
	=	$[f_{vi}(D_{bv}), i = 1$ to $N] = [\Delta V_i, i = 1$ to $N]$
N	=	Total number of active channels

$f_n(D_{bv})$ = Differential number distribution of blobs

= $[f_{ni}(D_{bv}),\ i = 1\ \text{to}\ N] = [\Delta n_i,\ i = 1\ \text{to}\ N]$

$P_v[D_b > D_{bv}]$ = Cumulative volume fraction (or %) of all blobs of sizes greater than stated size, D_{bv}

$P_n[D_b > D_{bv}]$ = Cumulative number fraction (or %) of all blobs of sizes greater than stated size, D_{bv}

$\bar{D}_{bv,n}$ = Volume-averaged mean blob-size based on the population distribution

$$= \left[\sum_{i=1}^{N} \Delta n_i\ (D_i D_{i+1})^{3/2} \right]^{1/3} \text{, (microns)}$$

$\bar{D}_{bv,v}$ = Volume-averaged mean blob-size based on the volume distribution

$$= \left[\sum_{i=1}^{N} \Delta V_i\ (D_i D_{i+1})^{3/2} \right]^{1/3} \text{, (microns)}$$

REFERENCES

4.1 Morrow, N.R. and Chatzis, I., "Measurement and Correlation of Conditions for Entrapment and Mobilization of Residual Oil," First Annual Report to the Department of Energy under Contract No. DE-AS19-80BC10310, Publication DOE/BC/10310-20 (September 1982).

4.2 Chatzis, I., Morrow, N.R., and Lim, H.T., "Magnitude and Detailed Structure of Residual Oil Saturation," Soc. Pet. Eng. J. (April 1983) 311-326.

4.3 Coulter Counter, Model TA II, Operator's Reference Manual, supplied by Coulter Electronics, Inc., Hialeah, Florida (July 1981).

4.4 Morrow, N.R. and Chatzis, I., "Measurement and Correlation of Conditions for Entrapment and Mobilization of Residual Oil," Final Report to the U.S. Department of Energy, Report No. DOE/BETC/3251-12 (October 1981).

4.5 Chatzis, I. and Morrow, N.R., "Capillary Number Relationships for Sandstones," SPE 10114, presented at 56th Annual Fall Meeting of SPE of AIME, San Antonio, October 5-7, 1981.

4.6 Rumscheidt, F.D. and Mason, S.G., "Particle Motions in Sheared Suspensions: XII Deformation and Burst of Fluid Drops in Shear and Hyperbolic Flow," J. Coll. Inter. Sci. 16 (1964) 238-261.

4.7 Ng, K.M. and Payatakes, A.C., "Stochastic Simulation of the Motion, Breakup

and Stranding of Oil Ganglia in Water-Wet Granular Porous Media During Immiscible Displacement," AIChE J. 26 (1980) 419-429.

4.8   Payatakes, A.C., Ng, K.M. and Flumerfelt, R.W., "Oil Ganglion Dynamics During Immiscible Displacement: Model Formulation," AIChE J. 26 (1980) 430-443.

4.9   Dullien, F.A.L. and Dhawan, G.K., "Characterization of Pore Structure by a Combination of Quantitative Photomicrography and Mercury Porosimetry," J. Coll. Inter. Sci. 47 (1974) 337.

4.10   Larson, R.G., Davis, H.T., and Scriven, L.E., "Displacement of Residual Nonwetting Fluid from Porous Media," Chem. Eng. Sci. 36 (1981) 75-85.

4.11   Larson, R.G., Scriven, L.E., and Davis, H.T., "Percolation Theory of Residual Phases in Porous Media," Nature 268, No. 4 (1977) 409-413.

4.12   Morrow, N.R., Chatzis, I., and Lim, H.T., "Relative Permeabilities at Reduced Residual Saturations," presented at International Energy Agency Workshop, Winfrith, U.K., September 1981.

Table 4.1   Experimental Conditions for Blob-Size Analysis Using the Coulter Counter

Electrolyte (Suspending Medium):   40/40/20 mixture (by volume %) of glycerin, brine
solution (8% by weight of NaCl in water) and
isopropanol. Solution was prefiltered through
a 5 μ Millipore filter and deaerated before use.

Temperature: Room conditions (22~26°C).

		Aperture Tube Used	
		1000 μ	2000 μ
A.	Calibration Particles	Latex Microspheres	Polystyrene-Divinyl-benzene spheres
	Nominal Diameter (manuf. spec.)	91.2 μ	271 μ (S.D. = 4.8 μ)
	Supplier	Coulter Electronics, Hialeah, Florida	Duke Scientific Corp., Palo Alto, California
B.	Active Channels	2 through 16	2 through 16
	Measurable Size Range (D_{bv})	16 to 406 μ	40.3 to 1024 μ
	Manometric Head (inches of Hg)	1.5~2.0	1.5~1.75
	Average Flow Rate through Aperture (ml/sec)	~1.4	~4.0
	Maximum Count Rate for Coincidence Error to be ≤5%	100 particles/sec.	30 particles/sec.
	Typical Sampling Rates	50-90 particles/sec.	12-27 particles/sec.
	Typical Total Counts per Pass	10,000 to 20,000	2,000 to 4,000
	Typical Sampling Times per Pass	200 to 300 sec.	150 to 200 sec.
	Typical Background Counts	<200 particles in 100 sec.	<50 particles in 100 sec.
	Special Features used in Sample Analysis	None	"Inhibit Reset" and "Scope Special" modes

Table 4.2   Differential Population-Size Distributions of Blobs of
Berea-6 (S_{or} = 20.0%) and Berea-7 (S_{or} = 27.9%) Samples

Lower edge of channel i D_{bv} (microns)	Channel number i	BEREA-6 Number frequency % Δn_i			BEREA-7 Number frequency % Δn_i	
		Run 5* (4 passes)	Run 149+ (3 passes)	Run 163* (2 passes)	Run 37* (3 passes)	Run 98+ (4 passes)
12.7	1	-	-	-	-	-
16.0	2	10.33	30.88	8.78	17.11	20.75
20.2	3	7.94	9.61	8.51	15.39	17.50
25.4	4	8.00	9.14	8.28	14.20	15.30
32.0	5	8.30	9.24	9.17	12.55	12.30
40.3	6	11.48	9.83	12.44	11.22	10.12
50.8	7	13.76	8.93	13.47	8.44	7.45
64.0	8	13.29	7.51	12.99	6.22	5.30
80.6	9	11.31	6.37	11.11	4.80	4.09
101.6	10	8.53	4.60	8.32	4.10	3.21
128	11	4.62	2.58	4.50	2.96	2.03
161	12	1.87	0.97	1.81	1.75	1.18
203	13	0.50	0.306	0.51	0.89	0.53
256	14	0.07	0.03	0.11	0.327	0.205
322	15	0.002	0.004	0	0.04	0.035
406	16	0	0	0	0.003	0.001
Total number of blobs sampled =		46,284	49,660	26,094	71,764	82,988

*, + represent different blob samples

141

Table 4.3   Differential Population-Size Distributions of Blobs of
Berea-9 (S_{or} = 27.0%) and Berea-10 (S_{or} = 29.6%) Samples

Lower edge of channel i D_{bv} (microns)	Channel number i	BEREA-9 Number frequency % Δn_i				BEREA-10 Number frequency % Δn_i			
		Run 38* (3 passes)	Run 68* (4 passes)	Run 151+ (3 passes)	Run 160+ (3 passes)	Run 39* (4 passes)	Run 69* (3 passes)	Run 100+ (3 passes)	Run 154x (4 passes)
12.7	1	–	–	–	–	–	–	–	–
16.0	2	8.94	9.67	15.79	8.80	8.25	9.85	10.60	7.51
20.2	3	9.75	10.24	9.94	10.85	9.32	10.85	11.16	9.32
25.4	4	11.44	12.04	10.63	12.36	10.58	12.59	12.50	10.97
32.0	5	12.87	13.18	11.84	13.69	11.90	13.57	13.60	12.42
40.3	6	15.13	14.68	13.54	15.61	14.27	15.29	14.31	14.64
50.8	7	13.95	12.99	12.69	13.77	13.58	13.32	12.45	13.94
64.0	8	10.71	10.62	10.39	10.65	11.99	10.42	10.36	12.13
80.6	9	8.05	7.63	7.45	7.31	8.98	7.20	7.46	9.20
101.6	10	5.18	5.25	4.726	4.28	6.48	4.20	4.74	6.03
128	11	2.77	2.60	2.10	1.96	3.25	1.90	2.00	2.774
161	12	0.97	0.875	0.69	0.58	1.08	0.63	0.63	0.83
203	13	0.22	0.20	0.18	0.13	0.28	0.14	0.166	0.20
256	14	0.02	0.026	0.03	0.01	0.036	0.03	0.022	0.03
322	15	0.002	0	0.002	0	0.004	0.01	0.002	0.005
406	16	0	0	0.002	0.002	0	0	0	0.002
Total number of blobs sampled =		55,343	84,491	44,770	39,442	74,030	70,015	62,105	57,896

*, +, x represent different blob samples

Table 4.4 Differential Population-Size Distributions of Blobs of
Berea-12 (S_{or} = 30.8%) and Berea-14 (21.3%) Samples

Lower edge of channel i D_{bv} (microns)	Channel number i	BEREA-12 Number frequency % Δn_i		BEREA-14 Number frequency % Δn_i		
		Run 165[*] (3 passes)	Run 166[+] (2 passes)	Run 150[*] (4 passes)	Run 159[+] (4 passes)	Run 178[*] (4 passes)
12.7	1	–	–	–	–	–
16.0	2	14.73	12.21	11.78	11.22	12.17
20.2	3	13.07	12.25	12.77	10.96	12.83
25.4	4	12.84	12.37	13.43	10.59	13.47
32.0	5	12.18	12.72	13.24	10.41	13.65
40.3	6	12.72	13.41	13.81	11.26	13.70
50.8	7	10.96	10.94	11.72	10.24	11.45
64.0	8	8.02	8.55	8.76	9.94	8.56
80.6	9	6.08	6.21	6.20	9.80	5.93
101.6	10	4.16	4.97	4.33	8.38	4.41
128	11	2.30	3.04	2.60	4.67	2.43
161	12	1.59	2.03	1.00	1.796	1.02
203	13	0.84	0.86	0.316	0.61	0.31
256	14	0.427	0.39	0.04	0.10	0.06
322	15	0.08	0.05	0.004	0.02	0.003
406	16	0.003	0	0	0.004	0.007
Total number of blobs sampled =		38,407	26,618	50,184	50,599	55,645

[*], [+] represent different blob samples

Table 4.5 Differential Population-Size Distributions of Blobs of
Berea-15 (S_{or} = 15.7%) and Berea-BF (S_{or} = 11.0%) Samples

Lower edge of channel i D_{bv} (microns)	Channel number i	BEREA-15 Number frequency % Δn_i			BEREA-BF Number frequency % Δn_i		
		Run 74* (4 passes)	Run 91+ (5 passes)	Run 155x (3 passes)	Run 72* (4 passes)	Run 75* (3 passes)	Run 90+ (3 passes)
12.7	1	–	–	–	–	–	–
16.0	2	22.84	24.77	14.67	15.82	15.59	15.45
20.2	3	18.57	18.91	14.50	12.89	12.18	12.84
25.4	4	14.79	14.35	14.06	11.67	10.49	10.90
32.0	5	11.81	11.16	14.11	10.27	9.22	9.53
40.3	6	10.20	9.88	14.16	9.99	9.50	9.83
50.8	7	8.13	7.80	11.23	9.60	9.15	9.20
64.0	8	6.27	5.73	8.25	8.73	9.01	9.10
80.6	9	3.93	3.63	4.87	8.63	9.44	9.46
101.6	10	2.19	2.27	2.61	7.62	9.10	8.43
128	11	0.96	0.98	1.07	3.51	4.40	3.87
161	12	0.24	0.39	0.38	1.00	1.48	1.08
203	13	0.06	0.11	0.07	0.23	0.35	0.26
256	14	0.007	0.017	0.02	0.038	0.075	0.046
322	15	0	0.003	0	0.001	0.012	0.004
406	16	0.002	0	0	0.001	0.004	0
Total number of blobs sampled =		91,402	128,940	41,161	75,246	50,930	55,454

*, +, x represent different blob samples

Table 4.6   Differential Population-Size Distributions of Blobs of
Berea-DO3 (S_{or} = 20.1%) and Berea-DO4 (S_{or} = 18.4%) Samples

Lower edge of channel i D_{bv} (microns)	Channel number i	BEREA-DO3 Number frequency % Δn_i		BEREA-DO4 Number frequency % Δn_i	
		Run 152* (4 passes)	Run 162+ (3 passes)	Run 153*	Run 161+ (3 passes)
12.7	1	–	–	–	–
16.0	2	9.35	8.01	11.01	13.50
20.2	3	11.07	9.77	12.12	13.72
25.4	4	12.70	11.58	13.50	13.40
32.0	5	14.13	12.85	14.70	13.69
40.3	6	14.68	14.79	14.95	14.34
50.8	7	13.28	13.64	12.64	11.93
64.0	8	10.44	11.61	9.51	8.77
80.6	9	7.64	8.82	6.13	5.71
101.6	10	4.21	5.48	3.65	3.29
128	11	1.86	2.58	1.335	1.31
161	12	0.51	0.70	0.38	0.28
203	13	0.11	0.16	0.065	0.05
256	14	0.02	0.01	0.01	0.01
322	15	0	0	0	0
406	16	0	0	0	0
Total number of blobs sampled =		60,580	40,507	55,648	43,229

*, + represent different blob samples

Table 4.7   Differential Population-Size Distributions of Blobs of
Carbonate-3 (S_{or} = 47%) and Carbonate-4 (S_{or} = 39%) Samples

Lower edge of channel i D_{bv} (microns)	Channel number i	CARBONATE-3 Number frequency % Δn_i		CARBONATE-4 Number frequency % Δn_i	
		Run 73[*] (5 passes)	Run 156[+] (4 passes)	Run 157[*] (3 passes)	Run 183[+] (3 passes)
12.7	1	–	–	–	–
16.0	2	22.12	15.94	14.96	19.85
20.2	3	18.13	15.21	14.34	16.77
25.4	4	14.97	13.77	13.25	14.84
32.0	5	12.20	12.59	12.60	12.26
40.3	6	10.84	12.51	13.04	11.69
50.8	7	8.225	10.19	10.86	9.20
64.0	8	5.68	7.86	8.51	6.45
80.6	9	3.71	5.56	5.87	4.24
101.6	10	2.34	3.71	3.79	2.72
128	11	1.15	1.69	1.86	1.26
161	12	0.44	0.68	0.68	0.52
203	13	0.145	0.21	0.18	0.17
256	14	0.04	0.07	0.05	0.027
322	15	0.01	0.008	0.01	0.003
406	16	0	0.003	0	0
Total number of blobs sampled =		133,243	62,273	42,509	45,142

[*], [+] represent different blob samples

Table 4.8   Volume Distribution of Blobs of Berea-1 Sample by Two-Aperture Analysis

$$S_{or} = 28.3\%$$

Lower edge of channel D_{bv} (microns)	Channel number (i)		1000 μ Analysis (Filtered - 50 mesh) % ΔV_i		2000 μ Analysis (as is) % ΔV_i							Resultant averaged % ΔV_i
	2000 μ	1000 μ	Run 80	Run 96	Run 104[x]	Run 120[*]	Run 123[+]	Run 133[++]	Run 144[*]	Run 171[+]	Run 172[++]	
12.7		1	–	–								–
16.0		2	0.12	0.29								0.13
20.2		3	0.73	0.83								0.50
25.4		4	1.65	1.76								1.08
32.0	1	5	3.03	3.29	–	–	–	–	–	–	–	2.00
40.3	2	6	6.28	6.72	1.93	1.77	1.69	2.07	2.81	2.52	2.08	4.13
50.8	3	7	9.20	9.69	4.40	3.92	4.60	4.22	5.38	5.70	4.98	6.00
64.0	4	8	11.82	12.95	6.36	5.40	5.74	6.04	7.81	8.06	6.79	7.85
80.6	5	9	13.62	15.03	8.27	7.36	7.58	7.58	9.95	9.56	8.27	9.10
101.6	6	10	14.37	15.28	10.94	10.53	9.94	9.59	12.86	11.42	9.84	9.40·
128	7	11	14.13	13.56	10.29	11.79	8.96	8.54	11.81	9.40	7.97	8.79
161	8	12	11.20	11.83	12.23	14.36	10.54	11.17	10.94	9.24	9.24	9.83
203	9	13	9.67	7.13	8.53	12.77	11.38	10.12	9.72	8.23	8.68	8.79
256	10	14	2.89	0.96	12.46	10.95	14.10	13.62	10.09	9.12	10.95	10.28
322	11	15	0.73	0.23	10.98	9.71	16.25	13.24	11.15	13.05	14.66	11.27
406	12	16	0.56	0.45	10.04	5.82	7.92	9.83	5.01	8.22	11.67	7.40
512	13				3.57	1.16	1.30	3.98	2.47	3.28	4.87	2.61
645	14				0	4.46	0	0	0	2.20	0	0.84
812	15				0	0	0	0	0	0	0	0
1024	16				0	0	0	0	0	0	0	0

x, *, +, ++ represent different blob samples

147

Table 4.9   Volume Distribution of Blobs of Berea-2 Sample by Two-Aperture Analysis

$$S_{or} = 31.1\%$$

Lower edge of channel D_{bv} (microns)	Channel number (i)		1000 μ Analysis (Filtered - 50 mesh) % ΔV_i		2000 μ Analysis (as is) % ΔV_i			Resultant averaged % ΔV_i
	2000 μ	1000 μ	Run 62	Run 94	Run 124*	Run 131*	Run 147+	
12.7		1	-	-				-
16.0		2	0	0				0
20.2		3	0.30	0.33				0.24
25.4		4	0.73	0.82				0.59
32.0	1	5	1.30	1.64	-	-	-	1.12
40.3	2	6	2.71	3.35	1.57	1.53	1.56	2.30
50.8	3	7	3.85	5.10	3.67	3.52	3.65	3.40
64.0	4	8	5.53	6.90	4.61	4.67	5.23	4.72
80.6	5	9	7.69	9.28	5.80	6.20	7.38	6.45
101.6	6	10	13.08	13.54	8.03	8.53	10.84	8.87
128	7	11	19.34	17.95	9.13	9.82	12.58	10.21
161	8	12	22.33	21.00	13.37	14.50	13.12	13.29
203	9	13	17.57	15.65	17.68	17.65	14.38	16.10
256	10	14	5.57	4.37	14.03	14.88	13.85	13.85
322	11	15	0	0.07	10.84	7.59	5.42	7.73
406	12	16	0	0	6.23	7.49	6.41	6.52
512	13				5.04	3.62	2.80	3.71
645	14				0	0	2.78	0.90
812	15				0	0	0	0
1024	16				0	0	0	0

*, + represent different blob samples

148

Table 4.10   Volume Distribution of Blobs of Berea-8 Sample by Two-Aperture Analysis

$$S_{or} = 27.2\%$$

Lower edge of channel D_{bv} (microns)	Channel number (i)		1000 μ Analysis (Filtered - 50 mesh) % ΔV_i			2000 μ Analysis (as is) % ΔV_i				Resultant averaged % ΔV_i
	2000 μ	1000 μ	Run 66	Run 67	Run 93	Run 103[x]	Run 125[*]	Run 139[+]	Run 146[+]	
12.7		1	-	-	-					-
16.0		2	0	0	0					0
20.2		3	0.30	0	0.25					0.15
25.4		4	0.85	0.40	0.81					0.58
32.0	1	5	1.57	0.85	1.58	-	-	-	-	1.10
40.3	2	6	3.47	2.11	3.43	1.98	1.95	2.24	2.80	2.49
50.8	3	7	4.85	3.31	5.08	3.63	4.50	4.49	5.63	3.67
64.0	4	8	5.99	4.75	6.79	5.85	6.59	6.42	8.28	4.85
80.6	5	9	7.59	6.96	8.39	8.08	8.59	8.51	10.26	6.35
101.6	6	10	11.20	11.26	12.81	11.85	13.34	11.54	13.50	9.76
128	7	11	16.69	18.13	17.47	14.98	14.44	12.46	12.49	14.48
161	8	12	19.93	22.78	20.71	17.75	17.73	13.95	13.24	17.56
203	9	13	20.82	21.33	17.47	13.59	14.23	12.83	10.21	13.89
256	10	14	6.48	8.12	5.21	11.30	9.69	10.31	8.79	10.94
322	11	15	0.26	0	0	6.31	4.75	8.13	6.89	7.12
406	12	16	0	0	0	2.30	4.19	1.80	4.87	3.59
512	13					2.38	0	2.68	0	1.38
645	14					0	0	4.64	3.04	2.09
812	15					0	0	0	0	0
1024	16					0	0	0	0	0

x, *, + represent different blob samples

Table 4.11   Volume Distribution of Blobs of Berea-13 Sample by Two-Aperture Analysis

$$S_{or} = 20.1\%$$

Lower edge of channel D_{bv} (microns)	Channel number (i)		1000 μ Analysis (Filtered – 50 mesh) % ΔV_i		2000 μ Analysis (as is) % ΔV_i				Resultant averaged % ΔV_i
	2000 μ	1000 μ	Run 55	Run 77	Run 114[x]	Run 129[*]	Run 135[+]	Run 137[+]	
12.7		1	–	–					–
16.0		2	0.26	0					0.10
20.2		3	0.62	0.39					0.41
25.4		4	0.97	0.69					0.65
32.0	1	5	1.36	1.14	–	–	–	–	0.98
40.3	2	6	2.59	2.28	2.21	2.64	2.08	2.57	1.91
50.8	3	7	4.08	3.86	4.61	5.66	4.78	5.13	3.13
64.0	4	8	6.86	6.88	6.53	8.01	6.38	7.42	5.42
80.6	5	9	10.42	11.04	8.45	10.30	8.50	9.54	8.45
101.6	6	10	14.73	15.74	12.25	14.01	10.82	12.02	12.00
128	7	11	17.36	17.43	13.21	13.09	11.35	11.00	13.69
161	8	12	17.03	16.09	15.32	13.67	11.94	10.80	13.04
203	9	13	13.37	13.96	12.83	12.70	12.60	10.85	12.65
256	10	14	9.38	9.85	10.56	8.74	13.43	13.08	11.83
322	11	15	0.97	0.45	7.07	5.42	8.22	7.46	7.28
406	12	16	0	0.20	4.18	5.76	5.99	6.06	5.68
512	13				2.78	0	3.91	4.07	2.78
645	14				0	0	0	0	0
812	15				0	0	0	0	0
1024	16				0	0	0	0	0

x, *, + represent different blob samples

Table 4.12   Volume Distribution of Blobs of Berea-DO1 Sample by Two-Aperture Analysis

$$S_{or} = 38.0\%$$

Lower edge of channel D_{bv} (microns)	Channel number (i)		1000 μ Analysis (Filtered - 50 mesh) % ΔV_i		2000 μ Analysis (as is) % ΔV_i						Resultant averaged % ΔV_i
	2000 μ	1000 μ	Run 58	Run 99	Run 13*	Run 102*	Run 111*	Run 126+	Run 141x	Run 148+	
12.7		1	-	-							-
16.0		2	0	0							0
20.2		3	0.32	0.30							0.26
25.4		4	0.71	0.74							0.61
32.0	1	5	1.34	1.38	-	-	-	-	-	-	1.13
40.3	2	6	2.77	2.91	1.42	1.96	1.37	1.59	2.61	2.10	2.37
50.8	3	7	4.33	4.83	3.85	4.44	3.86	3.96	5.40	5.18	3.82
64.0	4	8	6.76	7.05	5.70	6.58	5.79	5.80	7.52	7.33	5.76
80.6	5	9	10.50	10.55	8.25	8.74	8.78	8.56	9.69	10.03	8.78
101.6	6	10	15.78	14.98	12.74	12.02	13.10	13.43	11.96	14.03	12.83
128	7	11	21.41	19.13	14.57	12.46	14.14	16.03	11.28	13.69	13.50
161	8	12	20.85	18.38	16.42	14.01	14.97	18.37	13.46	13.87	14.96
203	9	13	12.63	14.63	14.51	13.74	14.45	15.34	14.08	11.76	13.78
256	10	14	2.28	5.12	13.66	10.42	9.70	10.83	10.12	8.42	10.37
322	''	15	0.10	0	6.52	5.91	4.47	4.54	5.59	3.99	5.12
406		16	0.22	0	1.86	4.38	4.57	1.55	6.02	4.51	3.76
512					0.50	0	0	0	2.27	0	0.45
645	14				0	5.34	4.80	0	0	5.09	2.50
812	15				0	0	0	0	0	0	0
1024	16				0	0	0	0	0	0	0

*, +, x represent different blob samples

151

Table 4.13   Volume Distribution of Blobs of Boise Sample by Two-Aperture Analysis

$$S_{or} = 28.1\%$$

Lower edge of channel D_{bv} (microns)	Channel number (i)		1000 μ Analysis (Filtered - 50 mesh) % ΔV_i		2000 μ Analysis (as is) % ΔV_i		Resultant averaged % ΔV_i
	2000 μ	1000 μ	Run 59	Run 81	Run 110*	Run 122+	
12.7		1	-	-			-
16.0		2	0	0			0
20.2		3	0.29	0.35			0.23
25.4		4	0.74	0.83			0.56
32.0	1	5	1.42	1.59	-	-	1.06
40.3	2	6	2.83	3.37	0.83	0.91	2.18
50.8	3	7	3.90	4.92	1.40	2.11	3.10
64.0	4	8	4.96	6.53	2.51	2.93	4.04
80.6	5	9	6.16	8.12	3.94	4.34	5.03
101.6	6	10	9.70	10.78	7.10	6.96	7.20
128	7	11	13.38	14.06	11.00	9.98	9.65
161	8	12	19.08	17.40	16.47	14.51	14.21
203	9	13	20.18	18.36	18.07	17.23	16.19
256	10	14	15.98	12.59	17.03	15.23	14.80
322	11	15	1.38	1.10	11.62	12.47	11.04
406	12	16	0	0	5.37	7.11	5.72
512	13				2.36	4.07	2.95
645	14				2.30	2.15	2.04
812	15				0	0	0
1024	16				0	0	0

*, + represent different blob samples

Table 4.14   Volume Distribution of Blobs of Carbonate-2 Sample by Two-Aperture Analysis

$$S_{or} = 44.0\%$$

Lower edge of channel D_{bv} (microns)	Channel number (i)		1000 μ Analysis (Filtered - 45 mesh) % ΔV_i		2000 μ Analysis (as is) % ΔV_i			Resultant averaged % ΔV_i
	2000 μ	1000 μ	Run 60	Run 182	Run 143[+]	Run 170[+]	Run 174[*]	
12.7		1	-	-				-
16.0		2	0	0.41				0.18
20.2		3	0.36	0.95				0.53
25.4		4	0.91	1.59				1.03
32.0	1	5	1.64	2.60	-	-	-	1.75
40.3	2	6	3.60	5.10	2.64	2.65	3.79	3.59
50.8	3	7	5.53	7.83	5.09	5.60	8.47	5.50
64.0	4	8	8.15	10.87	7.69	8.46	10.05	7.84
80.6	5	9	11.28	13.79	10.42	10.64	10.76	10.33
101.6	6	10	15.64	16.20	14.16	13.54	12.85	13.13
128	7	11	19.65	17.28	14.31	13.71	11.78	12.89
161	8	12	18.81	14.45	13.80	14.42	13.21	13.43
203	9	13	11.65	7.26	10.16	10.48	8.55	9.46
256	10	14	2.32	1.67	8.53	10.33	9.06	9.05
322	11	15	0.46	0	4.16	5.50	7.40	5.53
406	12	16	0	0	5.17	4.67	4.08	4.51
512	13				3.87	0	0	1.25
645	14					0	0	0
812	15					0	0	0
1024	16					0	0	0

+, * represent different blob samples

Table 4.15 Cores and Flow Conditions Used in Experiments on Blob Size Distributions

Core Sample	Sample Properties				Waterflooding Data				Polymerization Data		
	ϕ	K_a	K_w	Pore Volume	S_{or} (%P V)		k_{rw}	$\dfrac{K_w \Delta P}{L\sigma}$	Weight of blobs in sample	Weight of blobs collected after leaching	Re over of blobs
	(%)	(md)	(md)	(cm^3)	(1)	(2)			(g)	(g)	(~)
Berea-1	21 26	884	269	12 40	28 3	31	0 173	$4\ 78 \times 10^{-6}$	3 18	2 85	89 6
Berea-2	21 58	977	312	12 24	31 1	34	0 126	$1\ 14 \times 10^{-5}$	3 45	1 85 †	(53 6)
Berea-6	20 76	1014	507	12 46	–	27	0 296	$2\ 21 \times 10^{-6}$			–
					13 1	20	0 605	$1\ 28 \times 10^{-4}$	1 48	1 75 ++	
Berea-7	20 72	716	276	15 20	–	33	0 135	$3\ 90 \times 10^{-6}$			
					27 9	30	0 178	$2\ 53 \times 10^{-5}$	3 84	3 2	83 3
Berea-8	20 56	696	243	12 25	–	27 2	0 299	$8\ 15 \times 10^{-7}$	–	2 45	–
Berea-9	17 84	248	184	12 20	–	27	0 265	$4\ 82 \times 10^{-5}$	–	1 90 †	–
Berea-10	17 44	240	173	12 26	29 6	28	0 218	$4\ 39 \times 10^{-5}$	3 29	2 10 †	(63 8)
Berea-12	19 36	937	619	11 74	–	30	0 175	$7\ 85 \times 10^{-6}$			
					30 8	28	0 245	$6\ 93 \times 10^{-5}$	3 28	2 61	79 6
Berea-13	20 08	881	518	11 25	–	29	0 193	$2\ 37 \times 10^{-6}$			
					20 1	22	0 492	$1\ 54 \times 10^{-4}$	2 05	2 02	97 6
Berea 14	20 59	840	505	10 81	–	–	–	$2\ 85 \times 10^{-6}$			
					21 3	–	–	$2\ 52 \times 10^{-4}$	2 09	1 90	90 9
Berea-15	21 60	642	361	7 050	–	29	0 217	$4\ 15 \times 10^{-6}$			
					15 7	11	0 920	$4\ 25 \times 10^{-4}$	1 00	0 81	81 0
Berea-BF	18 53	957	790	10 30	–	36	0 085	$2\ 74 \times 10^{-6}$			
					11 0	20	0 611	$6\ 89 \times 10^{-4}$	1 03	0 77	7↔ 8
Berea D01	18 58	142	116	12 05	38 0	35	0 095	$5\ 52 \times 10^{-6}$	4 15	3 56	85 8
Berea-D03	19 63	343	295	7 97	–	40	0 043	$1\ 86 \times 10^{-6}$			
					20 1	17	0 720	$2\ 79 \times 10^{-4}$	1 45	1 08	74 5
Berea D04	20 60	671	294	10 82	–	34	0 111	$1\ 70 \times 10^{-6}$			
					18 4	15	0 781	$3\ 41 \times 10^{-4}$	1 80	1 44	80 0
Boise	25 72	2090	690	19 20	28 1	32	0 139	$1\ 35 \times 10^{-6}$	4 88	3 80	77 9
Carbonate-2	19 22	75	41 1	3 08	–		0 227	$2\ 69 \times 10^{-6}$			
					44*		0 261	$1\ 09 \times 10^{-5}$	1 18	0 56	47 5
Carbonate-3	19 60	75	41 0	1 59	–		0 150	$5\ 15 \times 10^{-6}$			
					47*		0 438	$2\ 06 \times 10^{-5}$	0 69	0 43	62 2
Carbonate-4	19 60	75	38 7	2 06	–		0 153	$2\ 32 \times 10^{-6}$			
					39*		0 410	$3\ 48 \times 10^{-5}$	0 73	0 417	57 1

† only part of the rock sample was leached by HF acid

++ particulates of rock material along with the blobs

* values are for small samples and are approximate

(1) S_{or} determined from gravimetric measurements, with $\rho = 0\ 906$ g/cm^3 for styrene

(2) S_{or} estimated from k_{rw} versus S_w correlation for sandstones in reference 4 12

154

Table 4.16 Summary of Blob-Volume Distribution Results by the Coulter Counter Technique

| Blob Sample | $\dfrac{K_w \Delta P}{L\sigma}$ | K_w (md) | S_{or} (%PV) | *Equivalent Blob-Size D_{bv} (microns) at $P_v(D_b > D_{bv})$ values of | | | | | Mode (microns) | Volume-Averaged Blob Diameter $\bar{D}_{bv,v}$ (microns) |
				1% ($D_{bv,max}$)	10%	50% ($D_{bv,m}$)	90%	99% ($D_{bv,min}$)		
Berea-8	8.15×10^{-7}	243	27.2†	730	362	176	70	30	161 –203	285
Boise	1.35×10^{-6}	690	28.1	720	415	211	76	33.5	203 –256	313
Berea-1	4.78×10^{-6}	269	28.3	620	410	165	55.5	28	322 –406	293
Berea-D01	5.52×10^{-6}	116	38.0	730	345	164	68.5	33.5	161 –203	280
Berea-2	1.14×10^{-5}	312	31.1	620	422	198	71.5	33.5	203 –256	299
Berea-7	2.53×10^{-5}	276	27.9	380	273	156	64.5	28.5	161 –203	199
Berea-10	4.39×10^{-5}	173	29.6	275	185	108	55	29	101.6–128	141
Berea-9	4.82×10^{-5}	184	27.0†	268	185	108	54	28	101.6–128	137
Berea-12	6.93×10^{-5}	619	30.8	380	282	164	67	32.5	161 –203	208
Berea-6	1.28×10^{-4}	507	20.0†	287	205	124	65	35.5	128 –161	153
Berea-13	1.54×10^{-4}	518	20.1	575	385	172	71	30	161 –203	271
Berea-14	2.52×10^{-4}	505	21.3	330	213	125	58.5	29.5	128 –161	162
Berea-D03	2.79×10^{-4}	295	20.1	247	174	103	51.7	28.5	101.6–128	130
Berea-D04	3.41×10^{-4}	294	18.4	252	157	95	47.5	24.5	101.6–128	122
Berea-15	4.25×10^{-4}	361	15.7	298	182	96	43.5	21.5	101.6–128	140
Berea-BF	6.89×10^{-4}	790	11.0	297	194	121	68	34.5	101.6–128	153

* quoted values of D_{bv} at the specified cumulative volume percentiles are based on the $P_v(D_b > D_{bv})$ distribution curve

† estimated from relative permeability versus saturation relationship (reference 4.12)
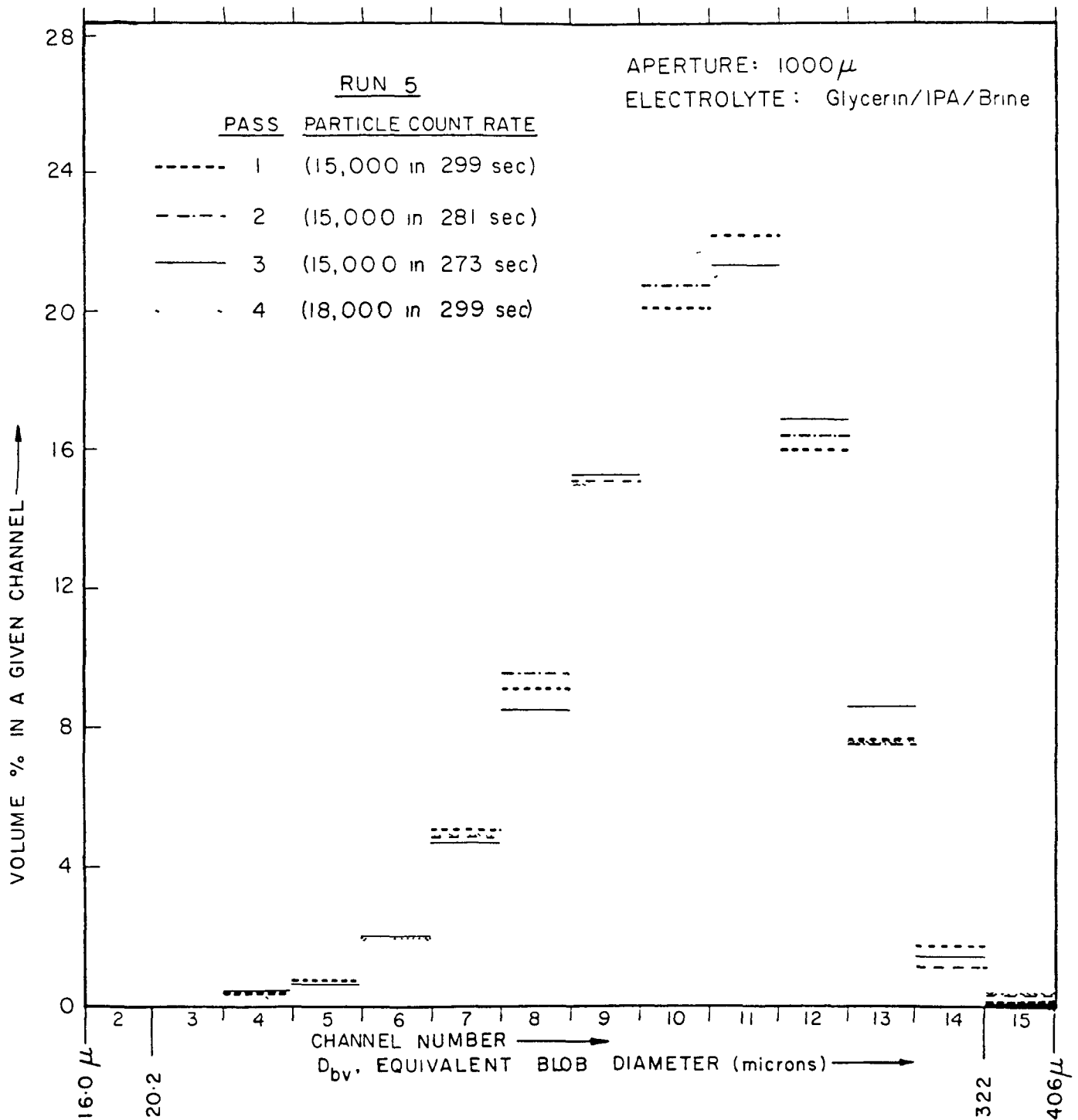
Fig. 4.1. Repeat measurements of blob-volume distribution for a given sample suspension of Berea-6. (Pass number is identified.)
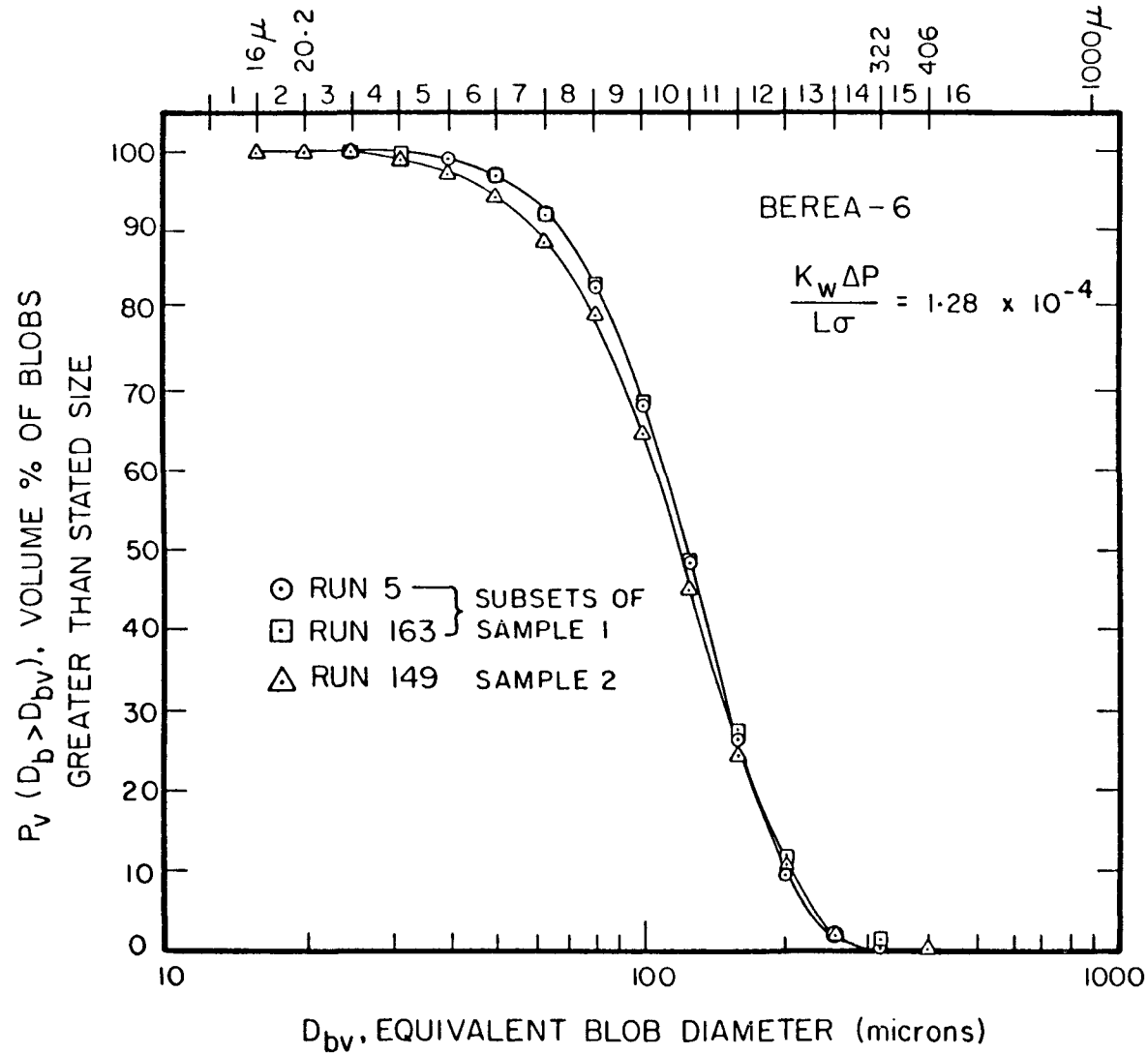
Fig. 4.2. Analysis of blob-size distribution for two independent samples of Berea-6. (Results for each run are obtained from the average of at least three passes of a sample subset.)
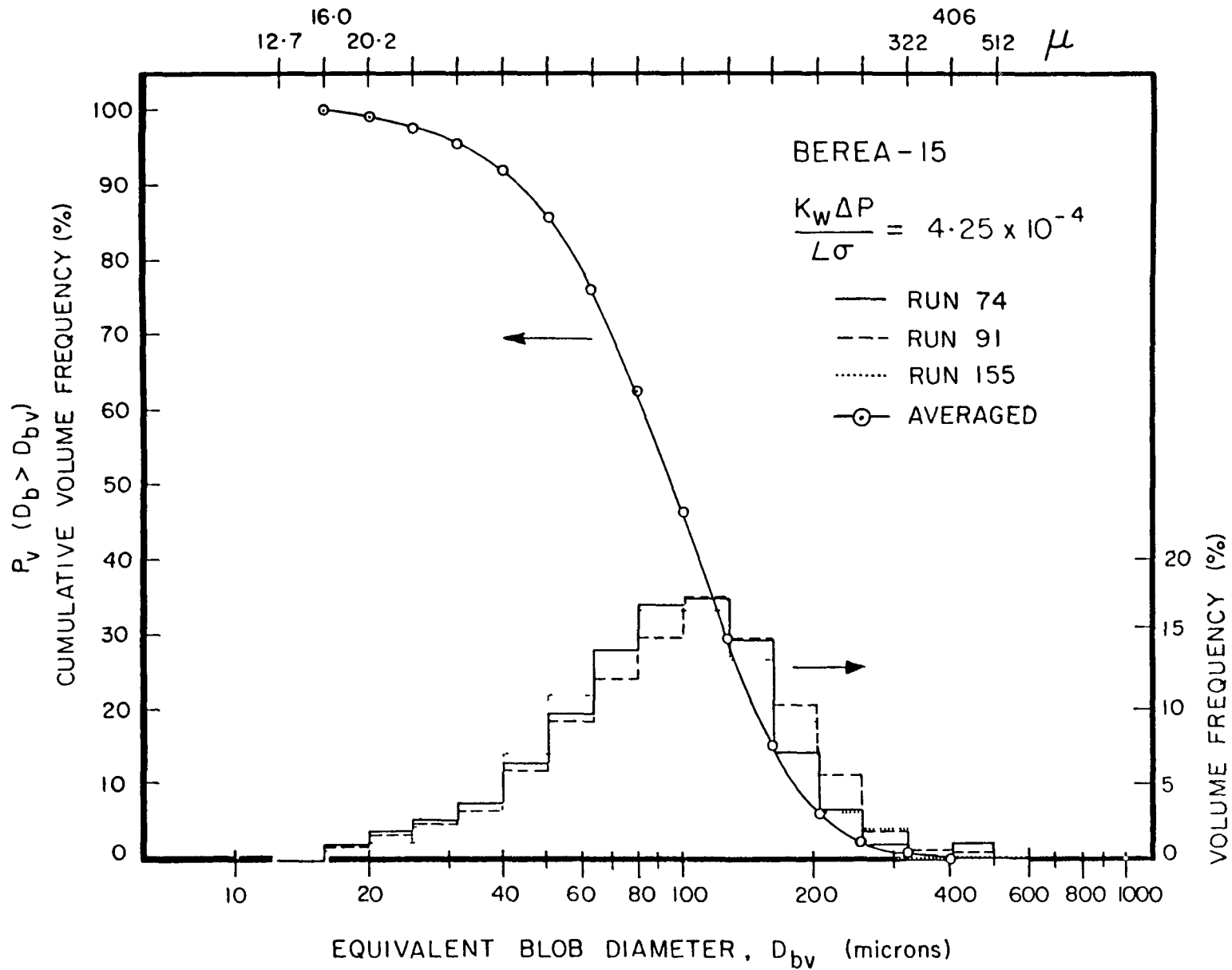
157
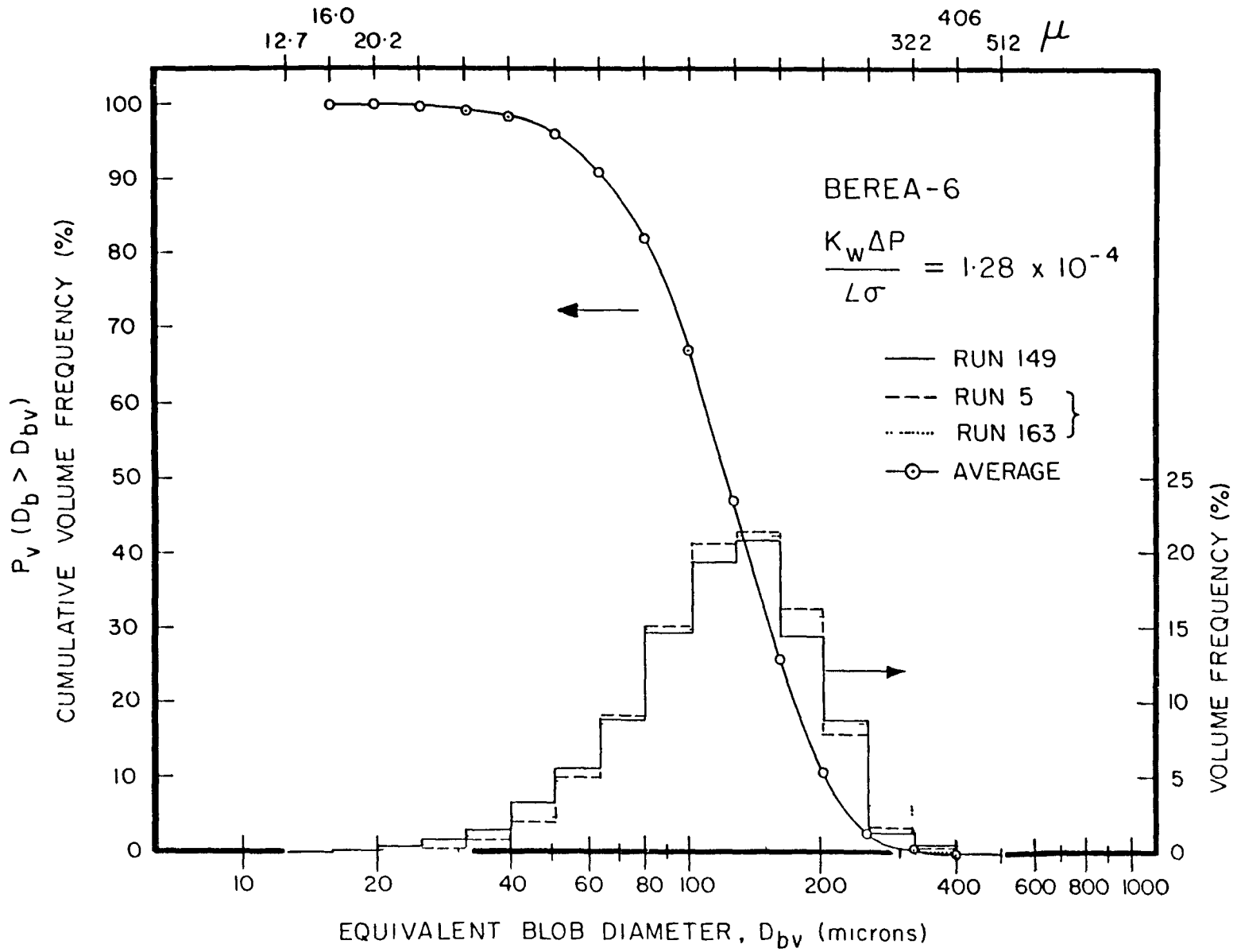
Fig. 4.3. Volume distribution of residual oil blobs of Berea-6 sample.
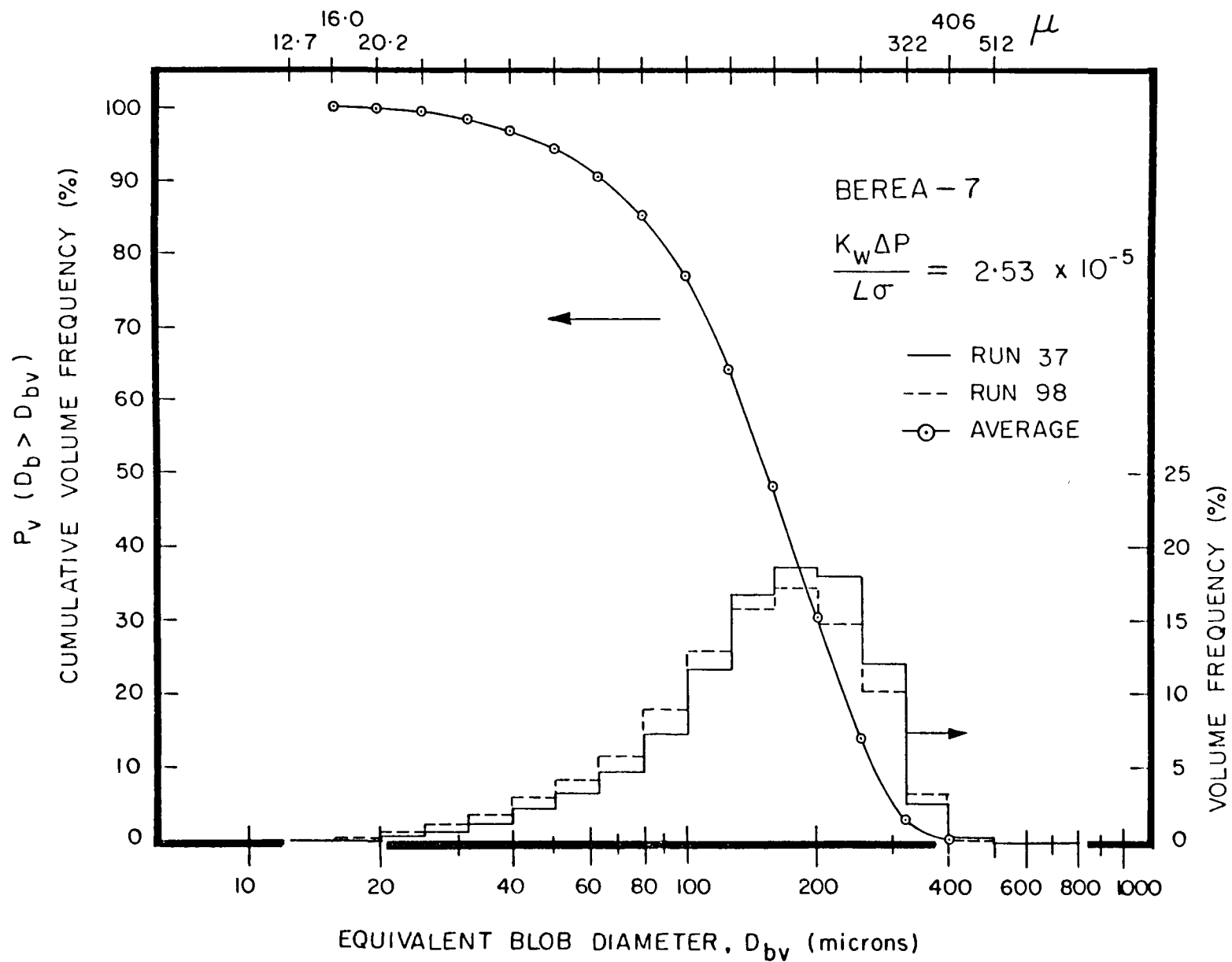
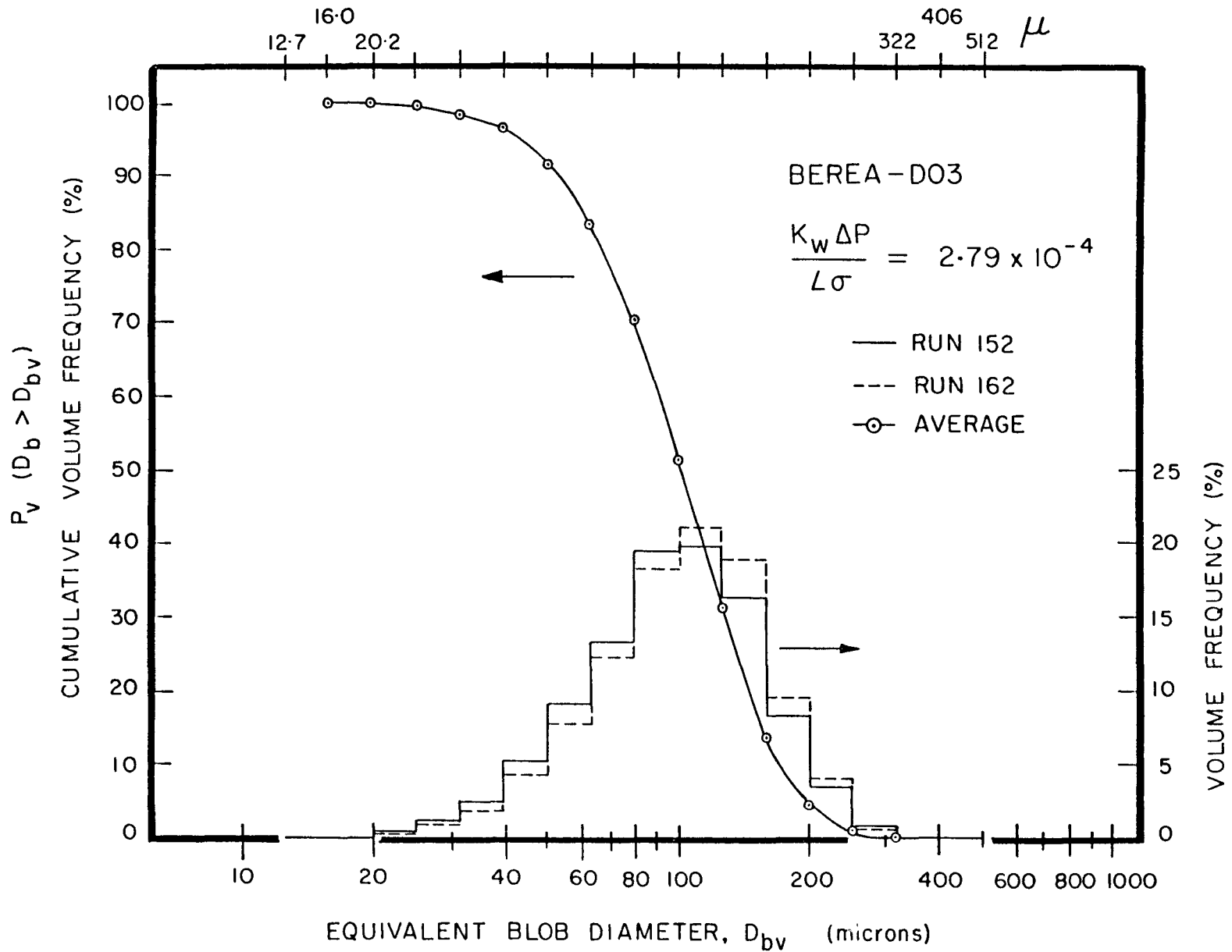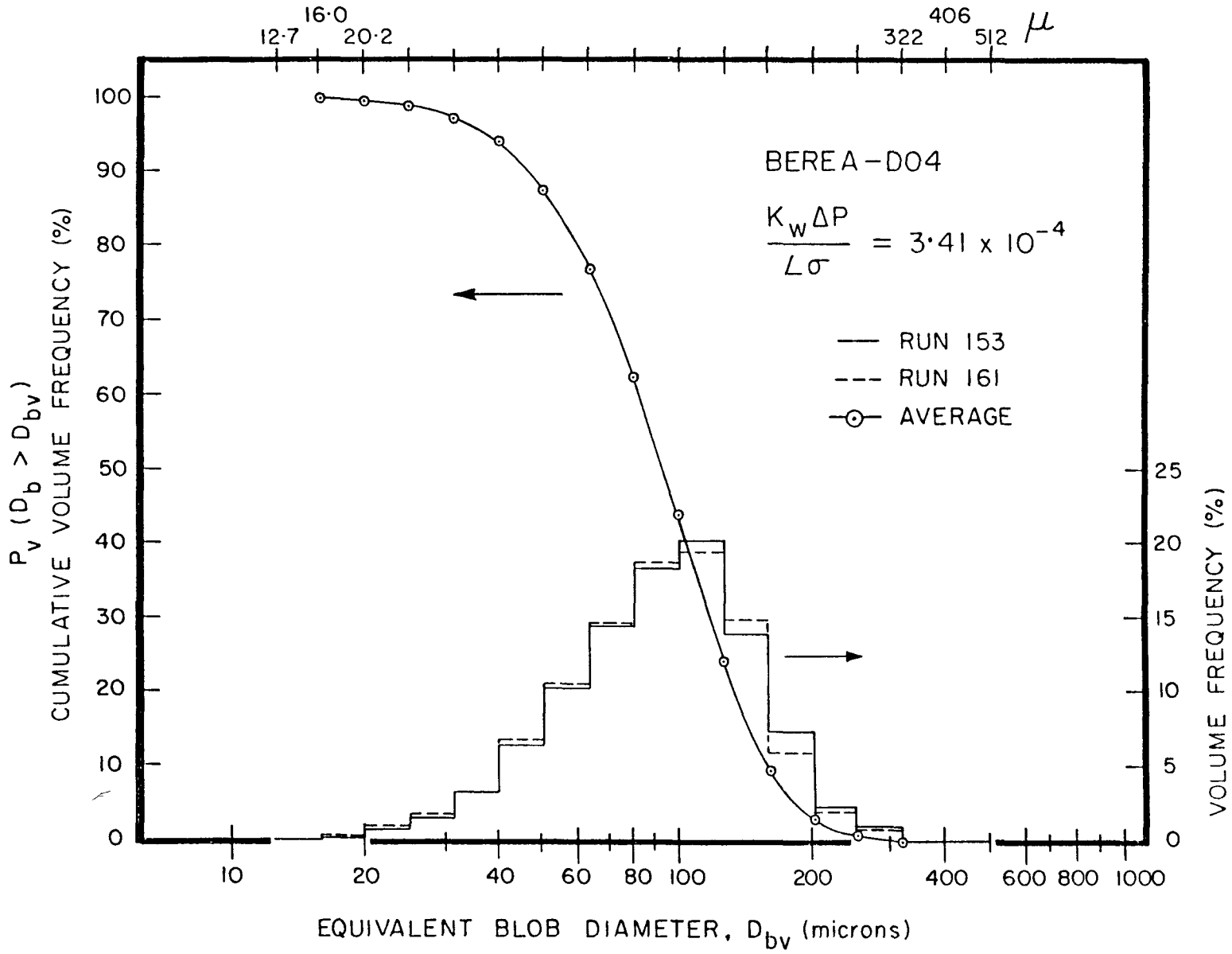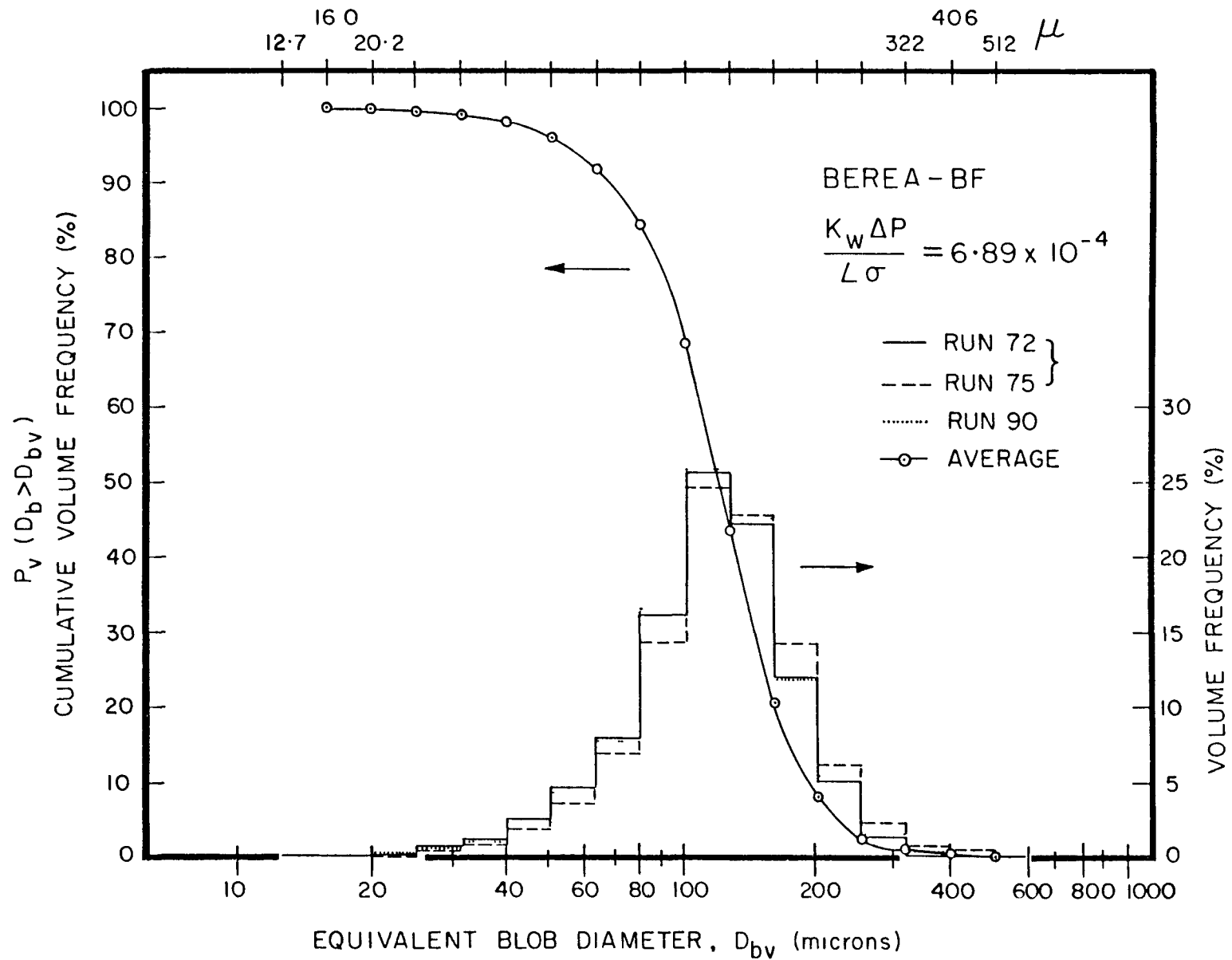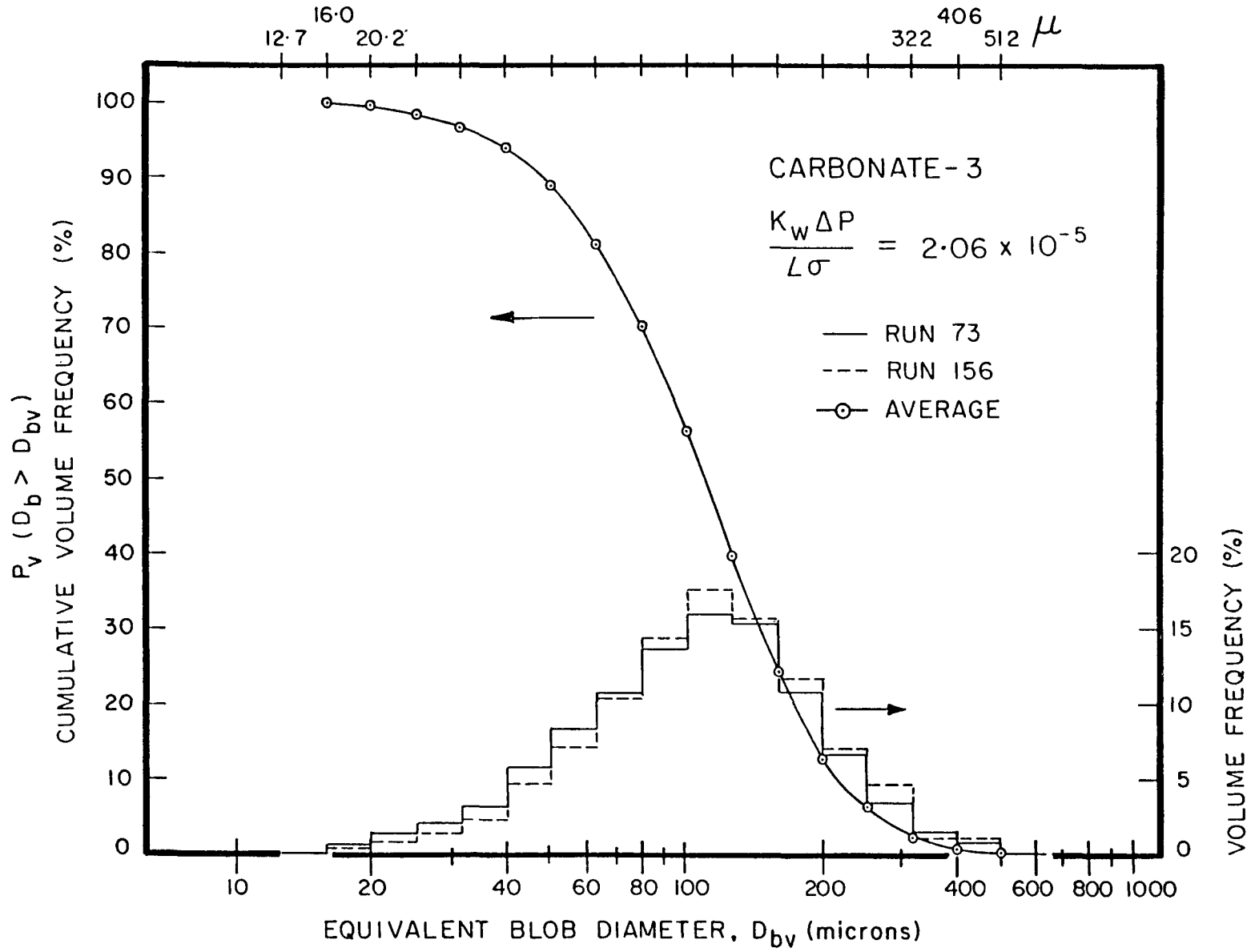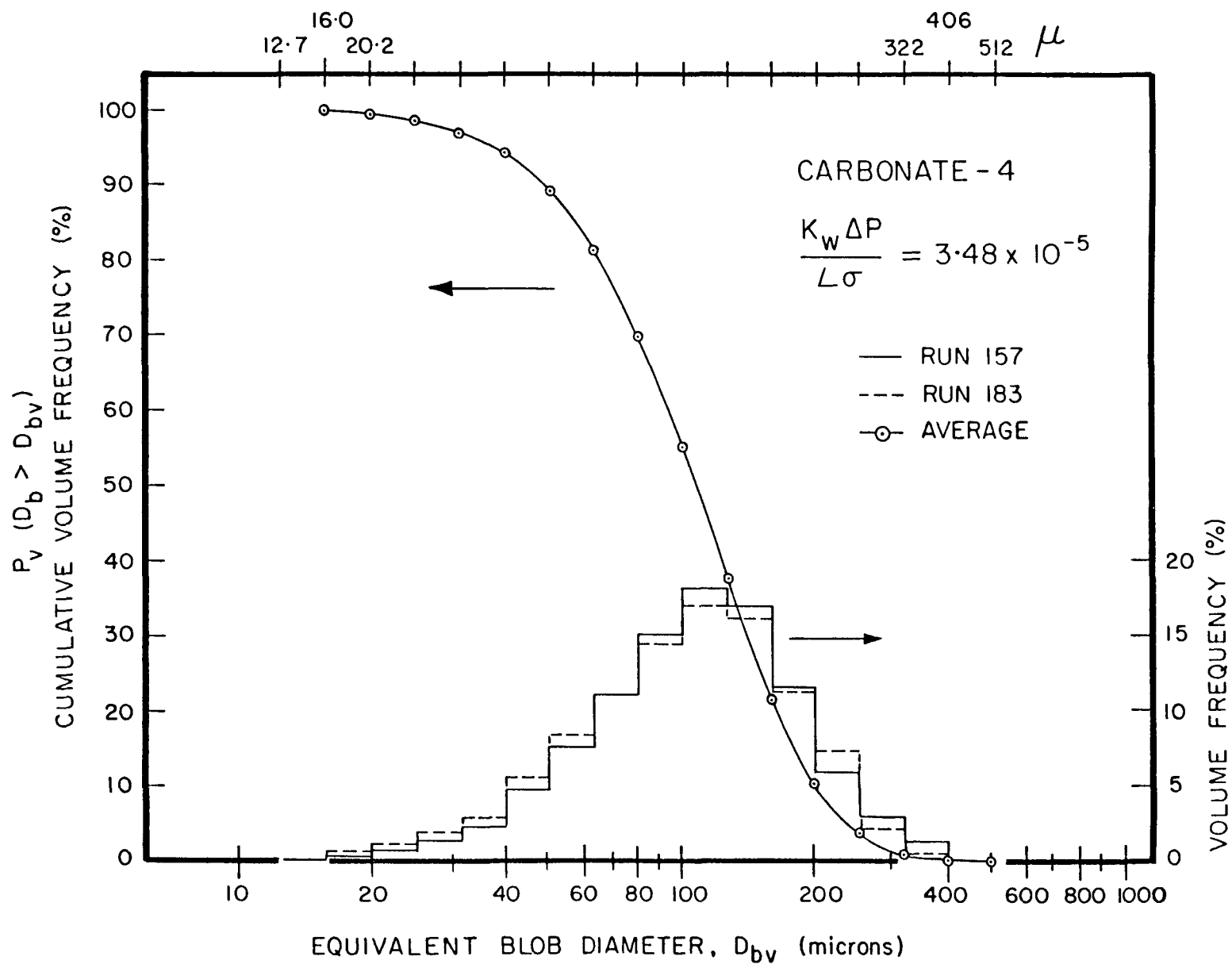Fig. 4.4. Volume distribution of residual oil blobs of Berea-7 sample.
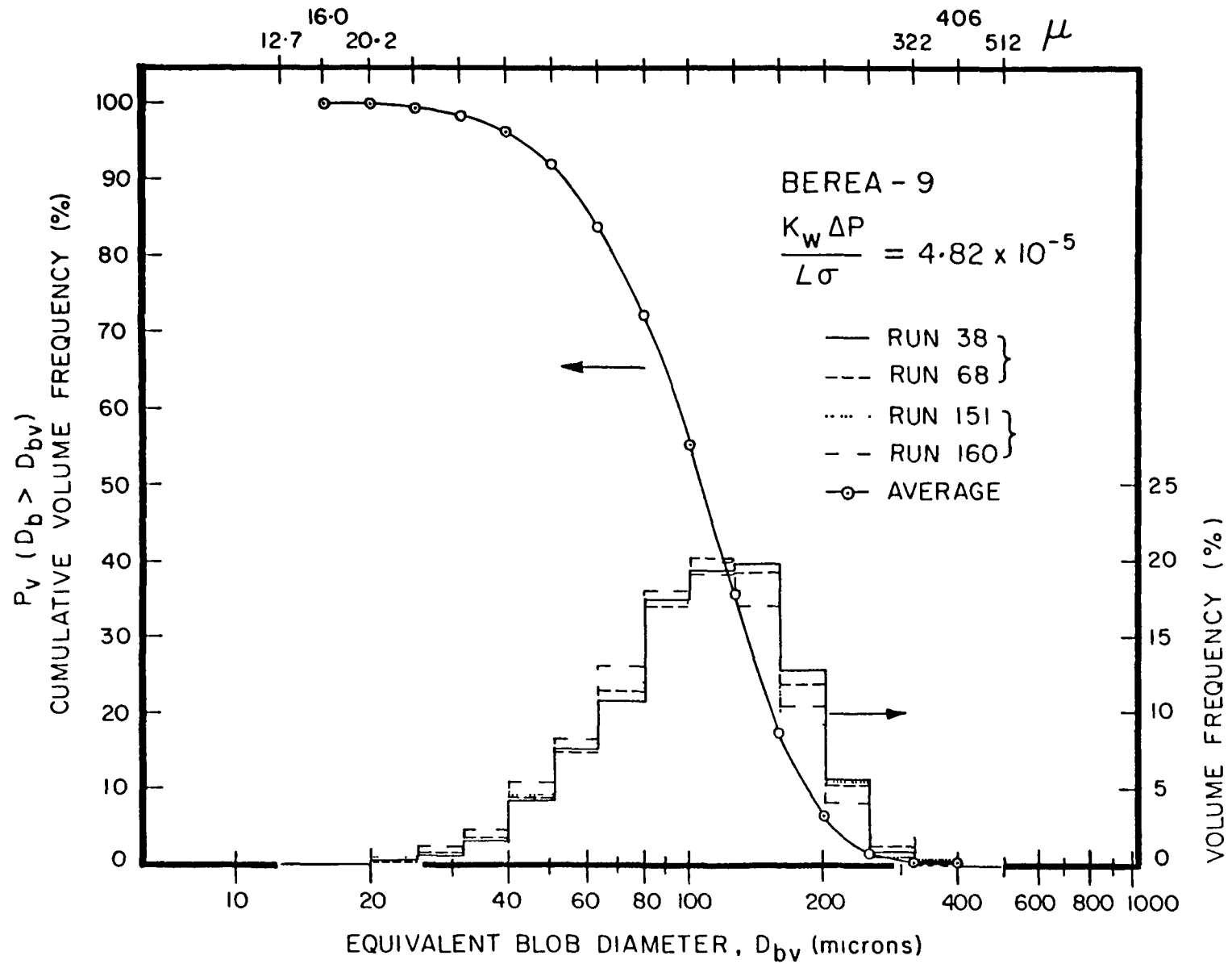
Fig. 4.5. Volume distribution of residual oil blobs of Berea-9 sample.

160
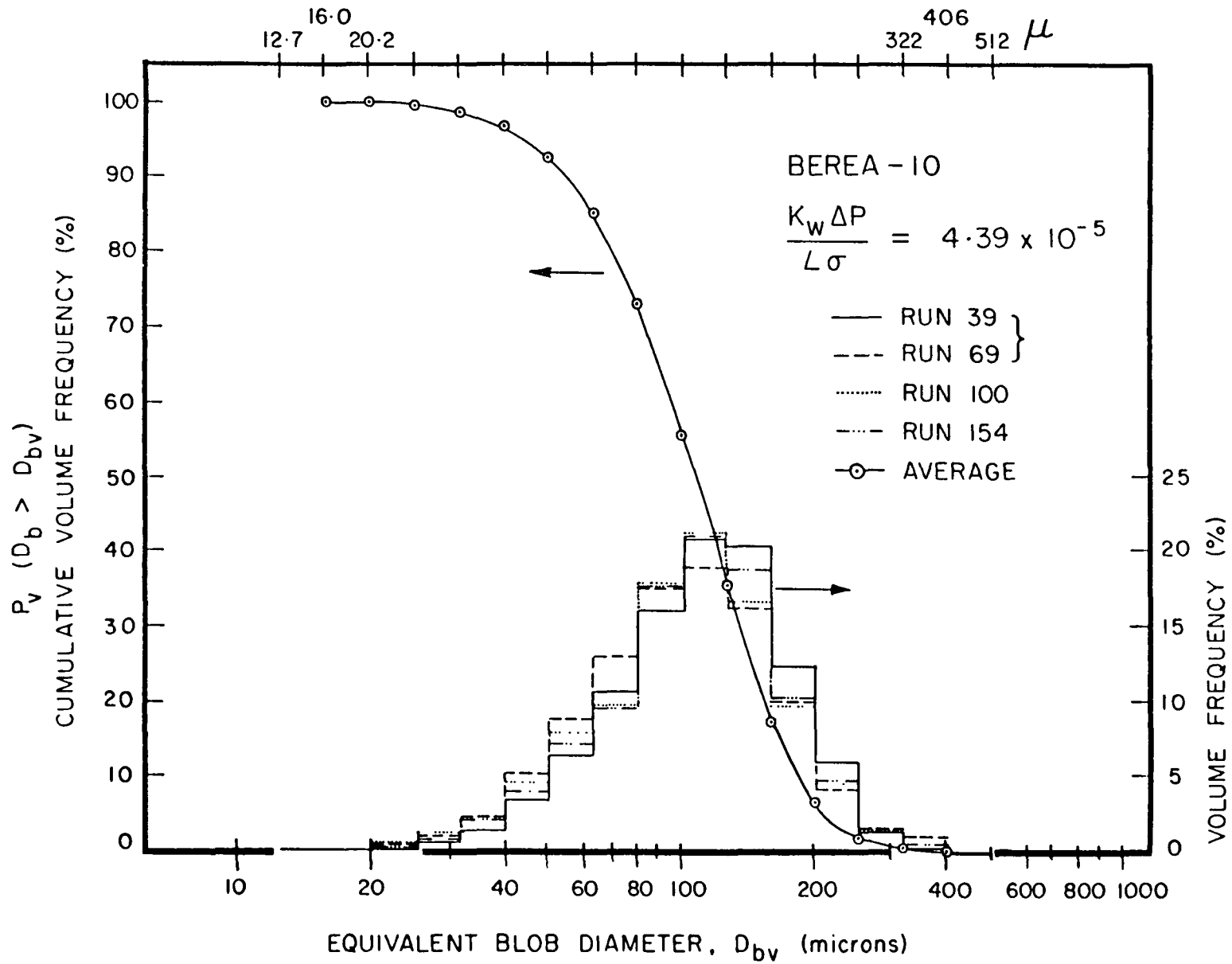
Fig. 4.6. Volume distribution of residual oil blobs of Berea-10 sample.
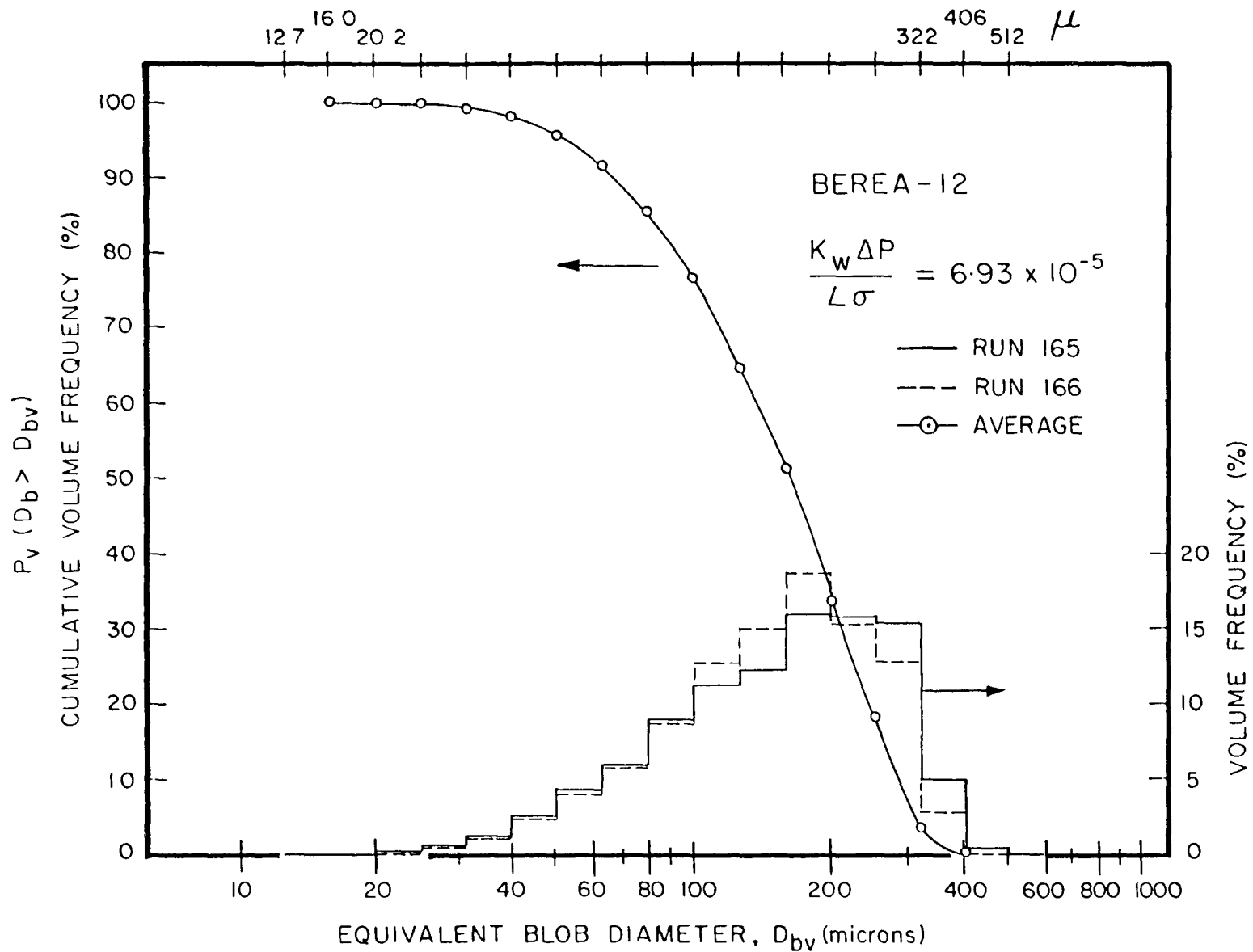
Fig. 4.7. Volume distribution of residual oil blobs of Berea-12 sample.
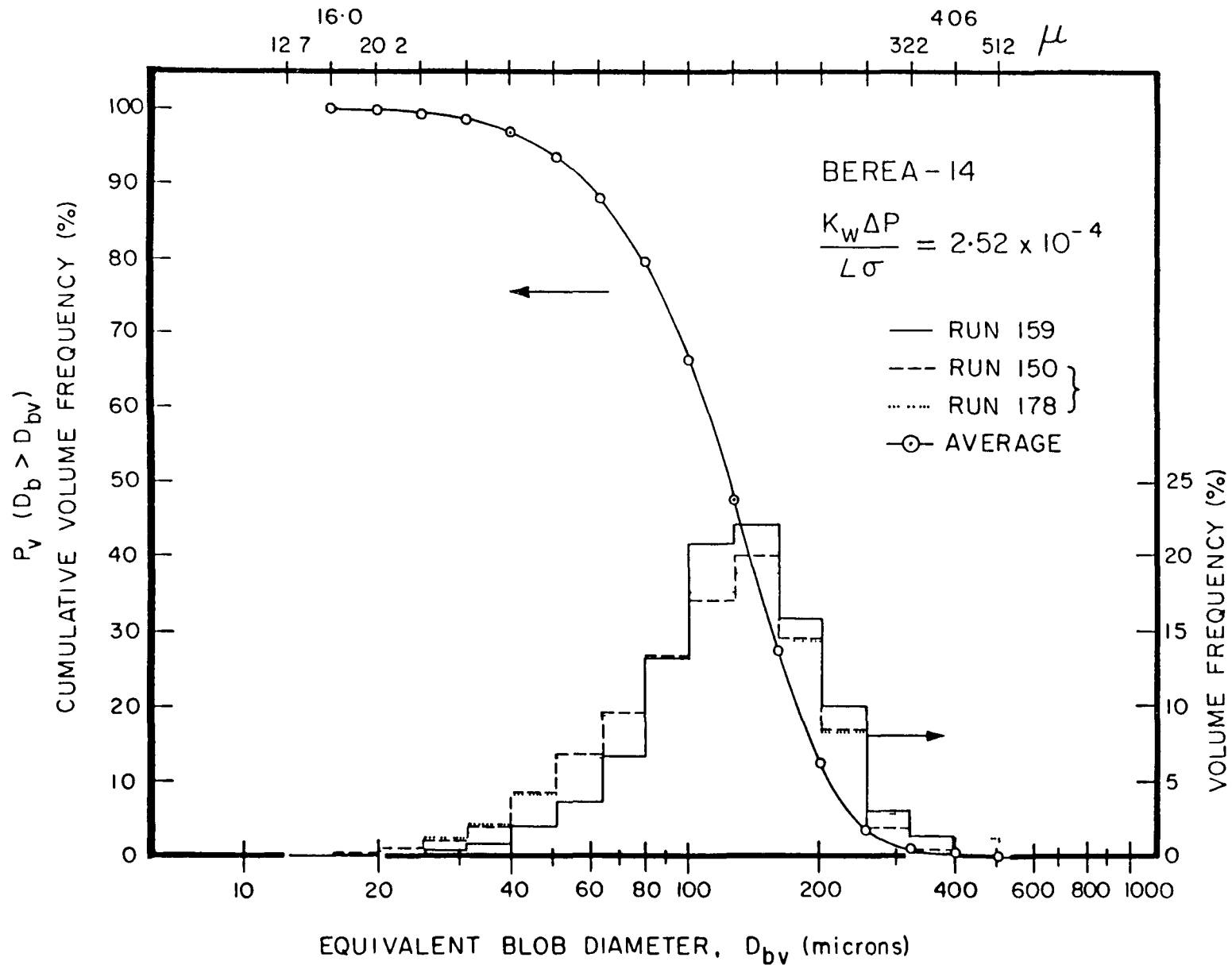
Fig. 4.8. Volume distribution of residual oil blobs of Berea-14 sample.

163

Fig. 4.9. Volume distribution of residual oil blobs of Berea-15 sample.

Fig. 4.10. Volume distribution of residual oil blobs of Berea - DO3 sample.

Fig. 4.11. Volume distribution of residual oil blobs of Berea-DO4 sample.

166

Fig. 4.12. Volume distribution of residual oil blobs of Berea-BF sample.

Fig. 4.13. Volume distribution of residual oil blobs of Carbonate-3 sample.

Fig. 4.14. Volume distribution of residual oil blobs of Carbonate-4 sample.
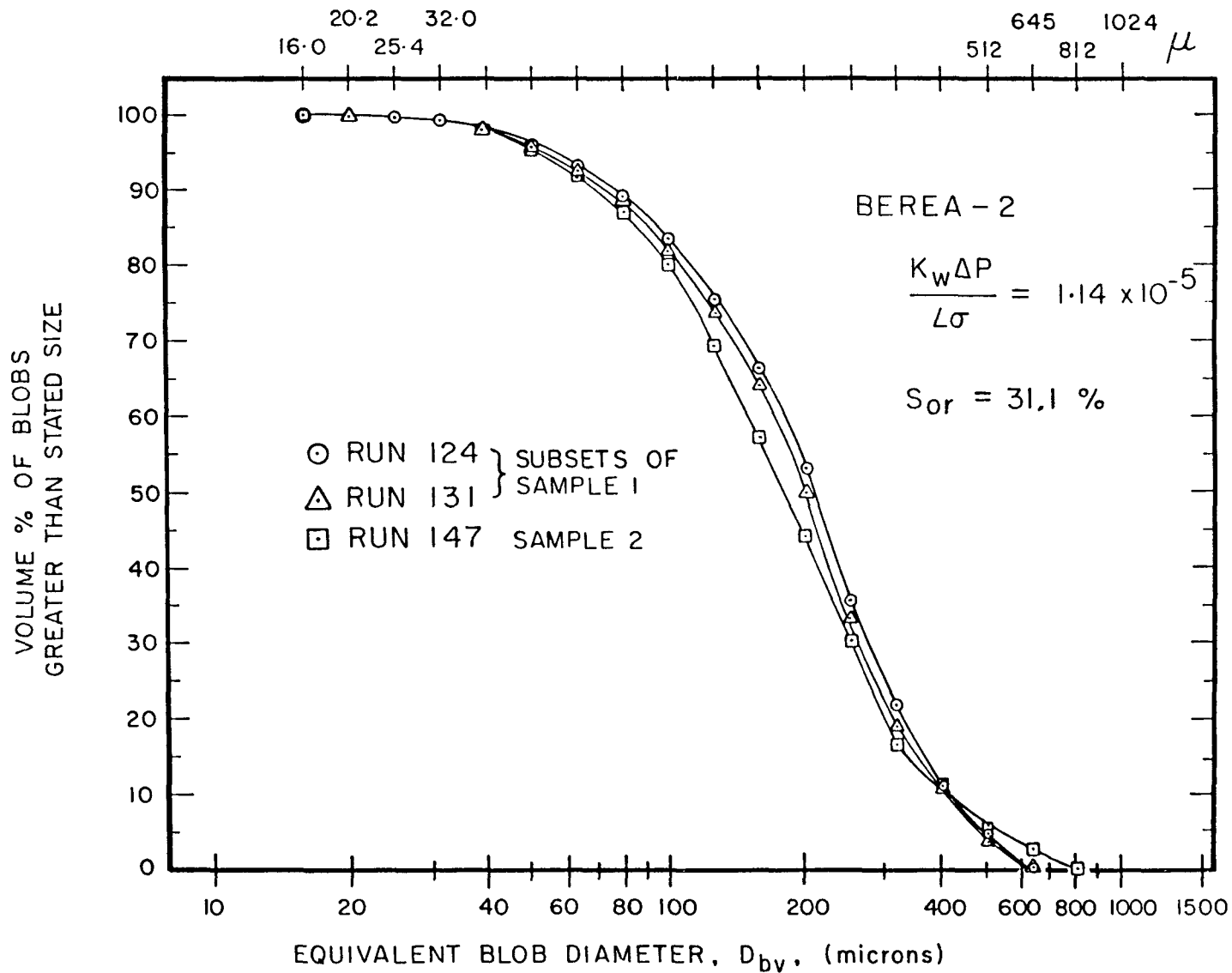
Fig. 4.15. Two-aperture size analysis for two independent samples of residual oil blobs trapped in Berea-2. (Curves shown for each run are the averaged results from at least three passes of a sample subset.)

$$\left(\frac{K_w \Delta P}{L\sigma} = 4.78 \times 10^{-6} \right)$$
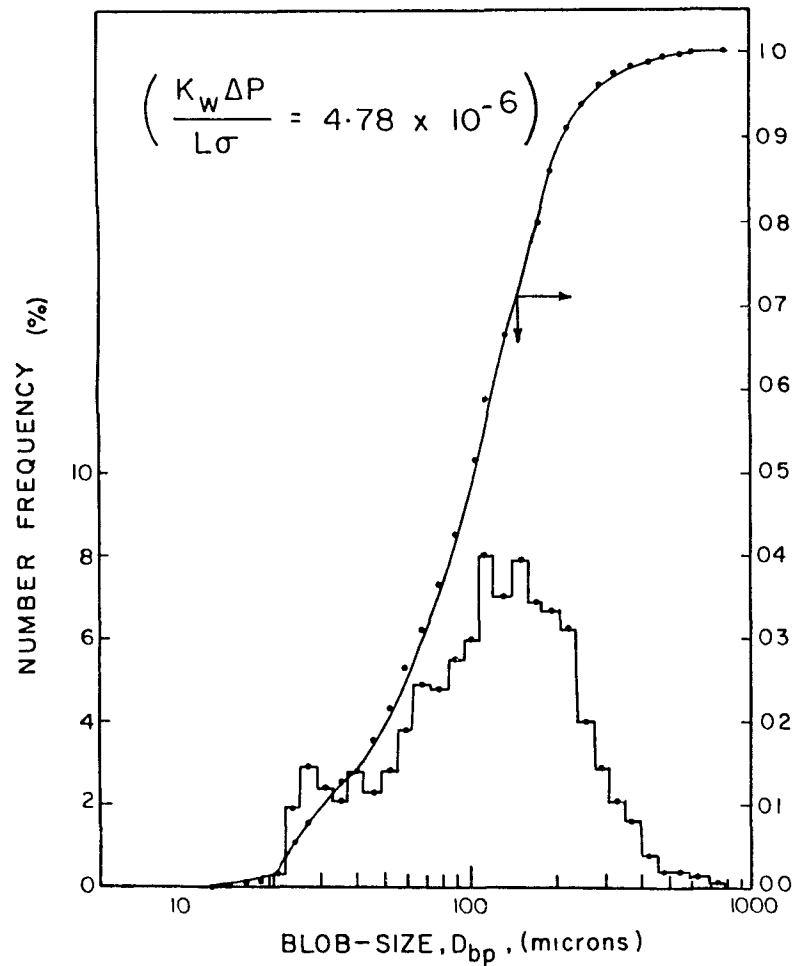
a) By projected diameter
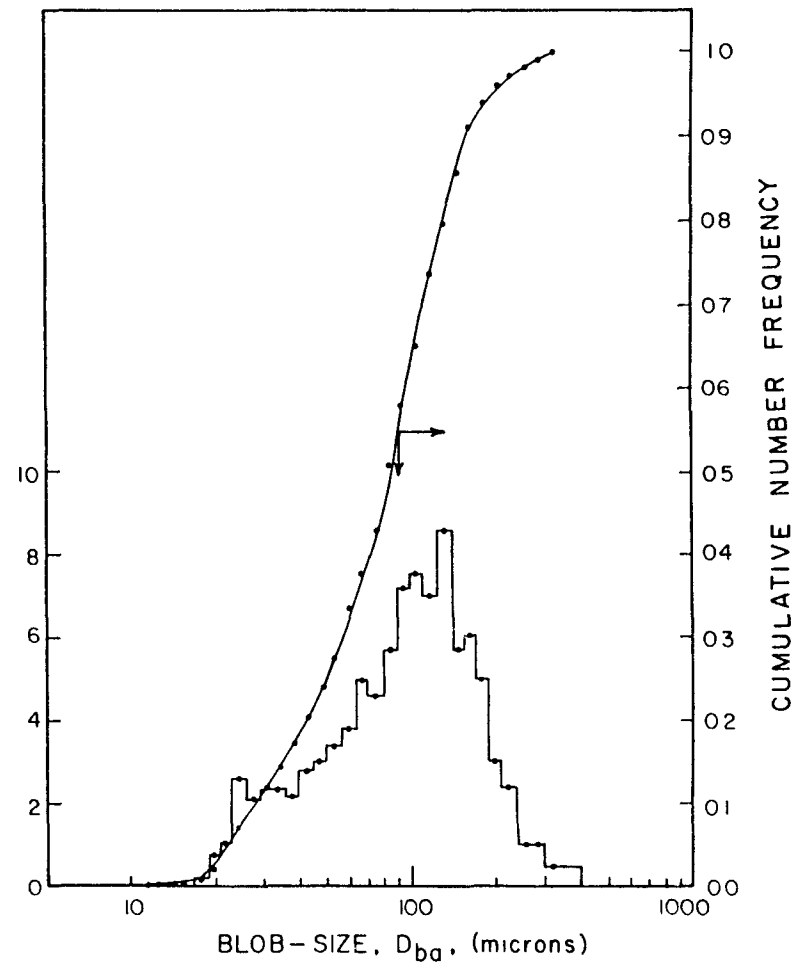
b) By projected area

Fig. 4.16. Photomicrographic blob-size distribution for Berea-I sandstone sample.
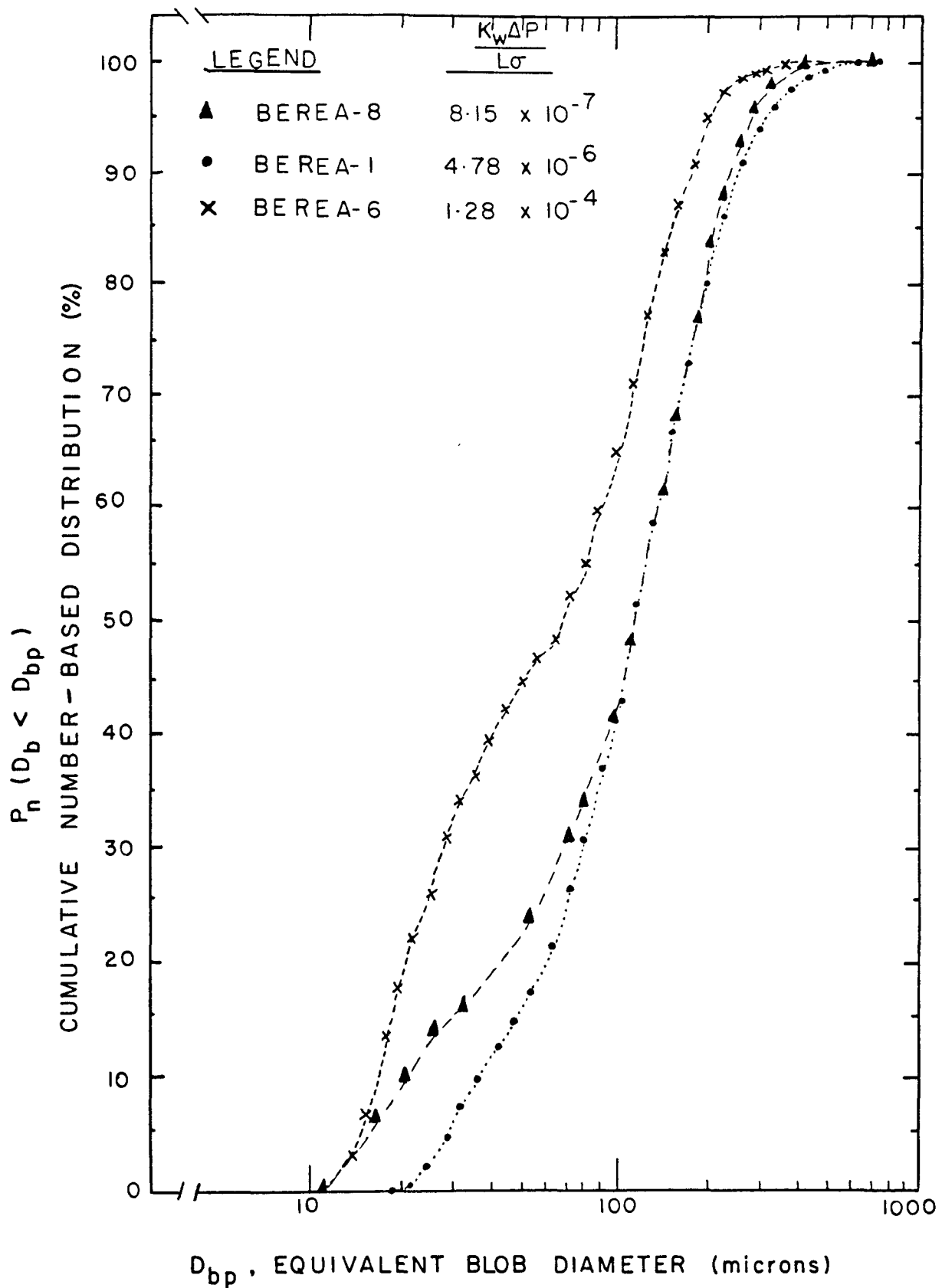
Fig. 4.17. The effect of capillary number on blob-size distributions obtained by image analysis.

172

CHANNEL NUMBER →

$$\frac{K_W \Delta P}{L\sigma} = 4 \cdot 78 \times 10^{-6}$$

⊙ RUN 17

△ RUN 120

⊡ RUN 123

$P_v (D_b > D_{bv})$

VOLUME % OF BLOBS GREATER THAN STATED SIZE

D_{bv}, EQUIVALENT BLOB DIAMETER (microns)

173
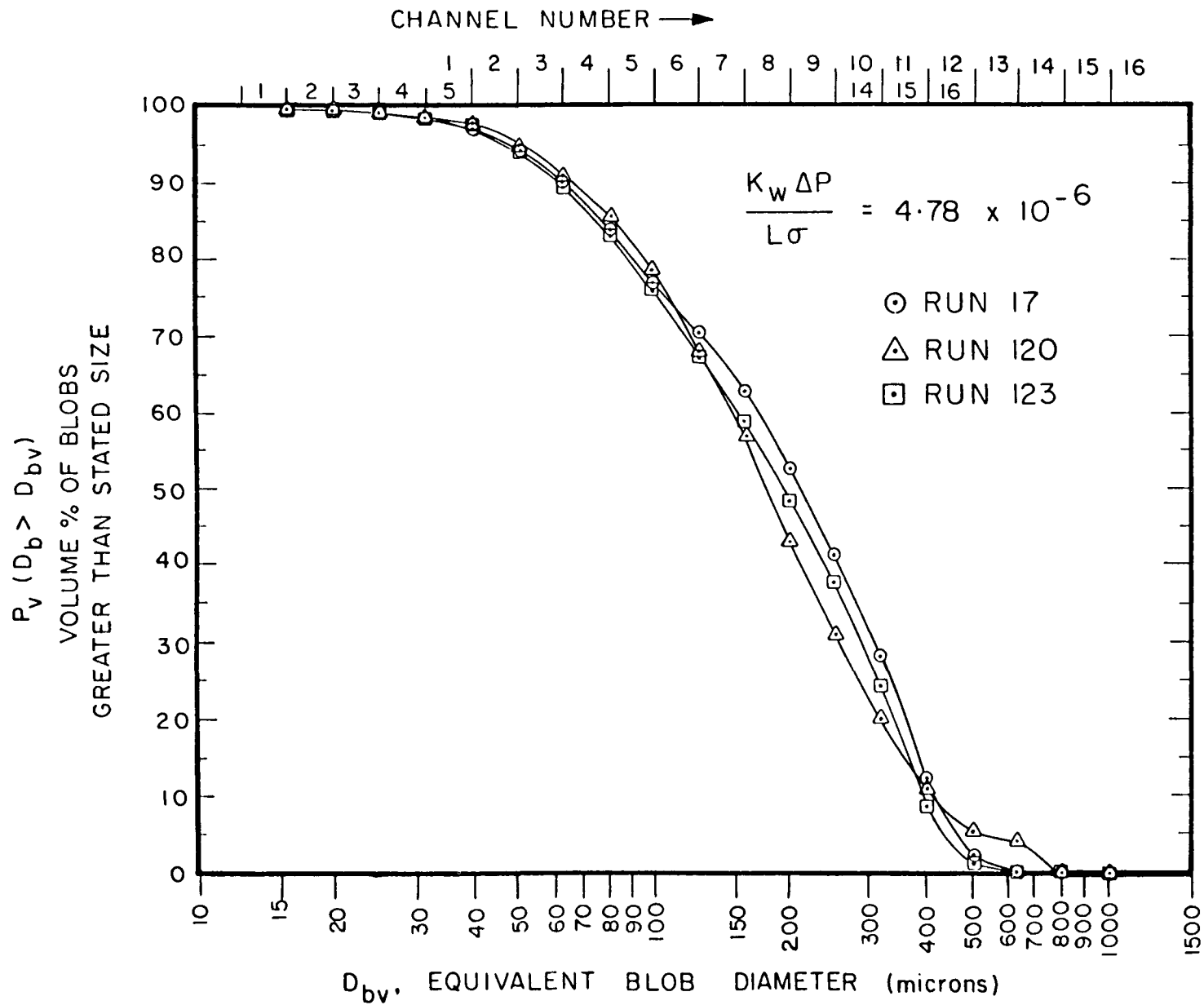
Fig. 4.18. Volume-based, blob-size distributions obtained by Coulter Counter technique for Berea-1 sample.
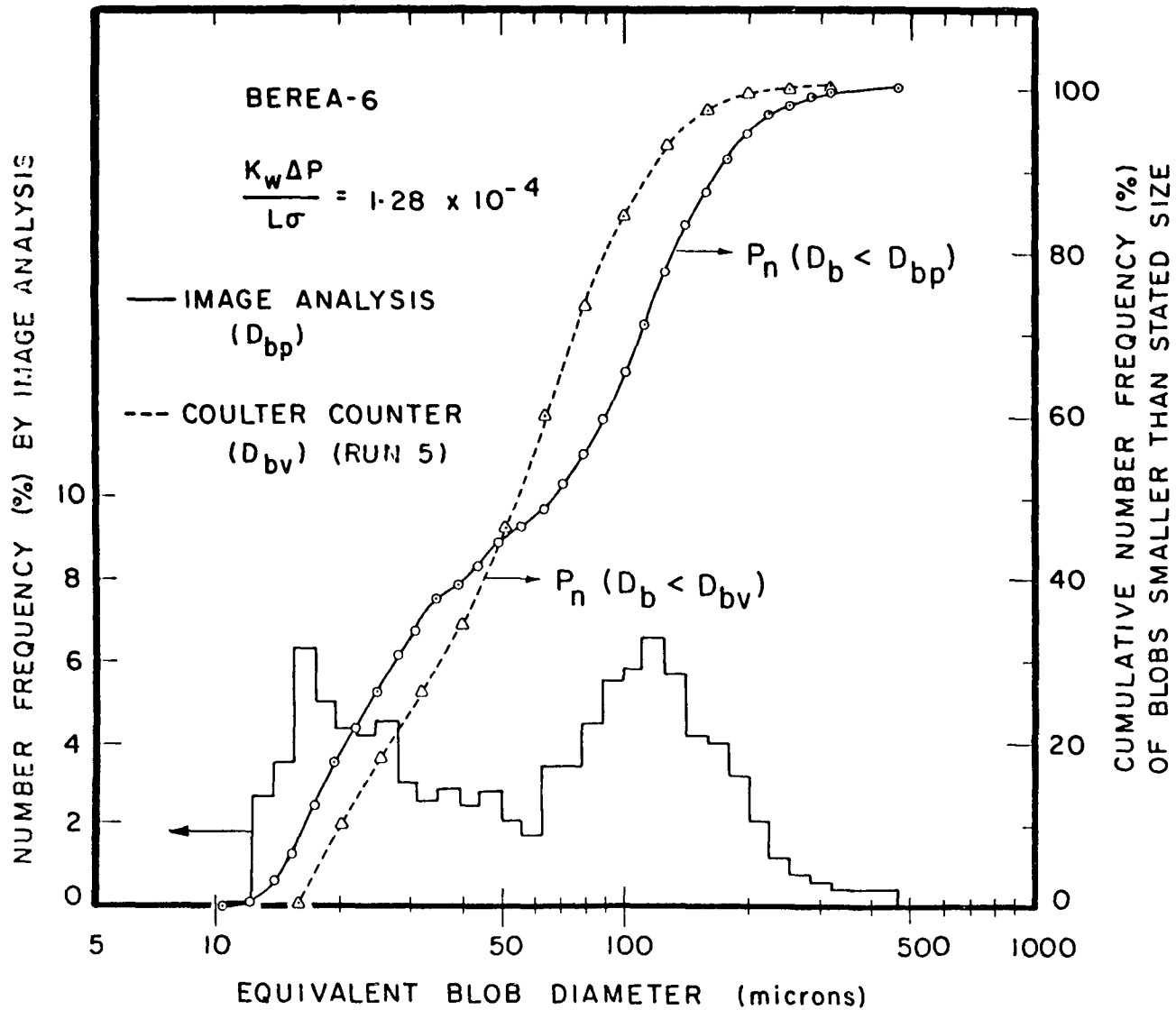
Fig. 4.19 a. Blob-size distributions determined by image analysis and by Coulter Counter methods for Berea-6 sample. Number distributions based on D_{bp} and D_{bv}.
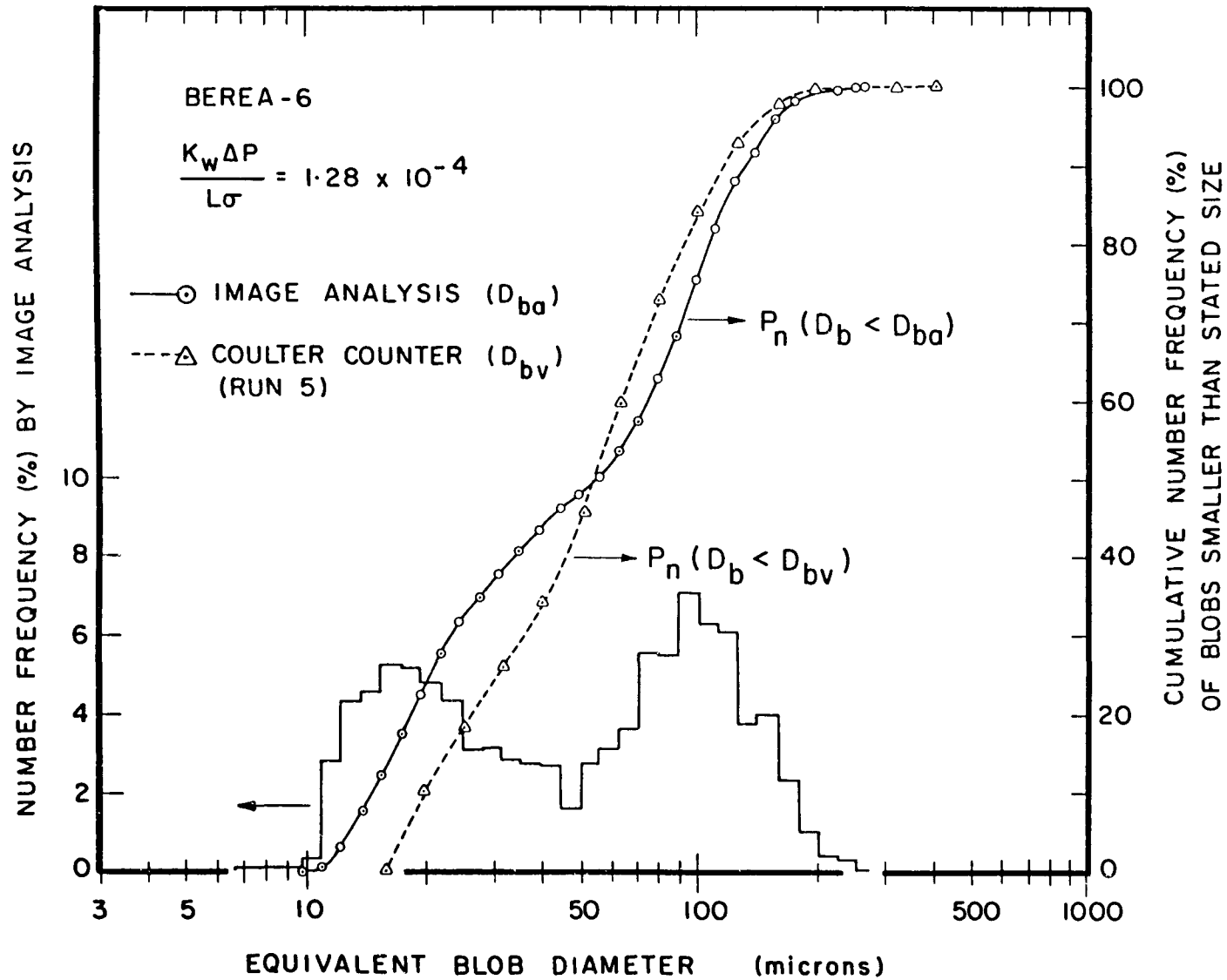
Fig. 4.19 b. Blob-size distributions determined by image analysis and by Coulter Counter methods for Berea-6 sample. Number distributions based on D_{ba} and D_{bv}.
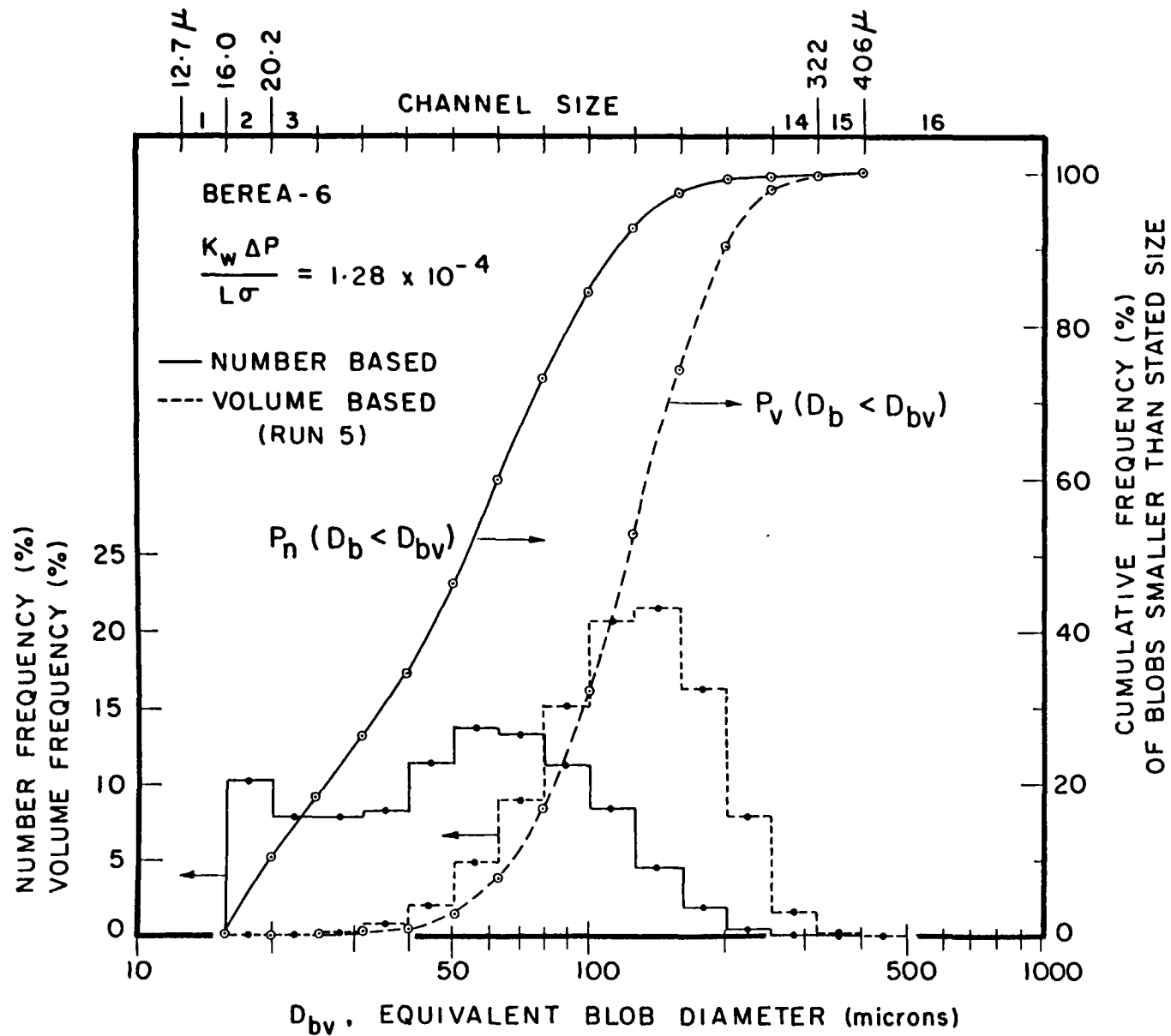
Fig. 4.19 c. Blob-size distributions determined by Coulter
Counter method for Berea-6 sample. Number
and volume distributions based on D_{bv}.
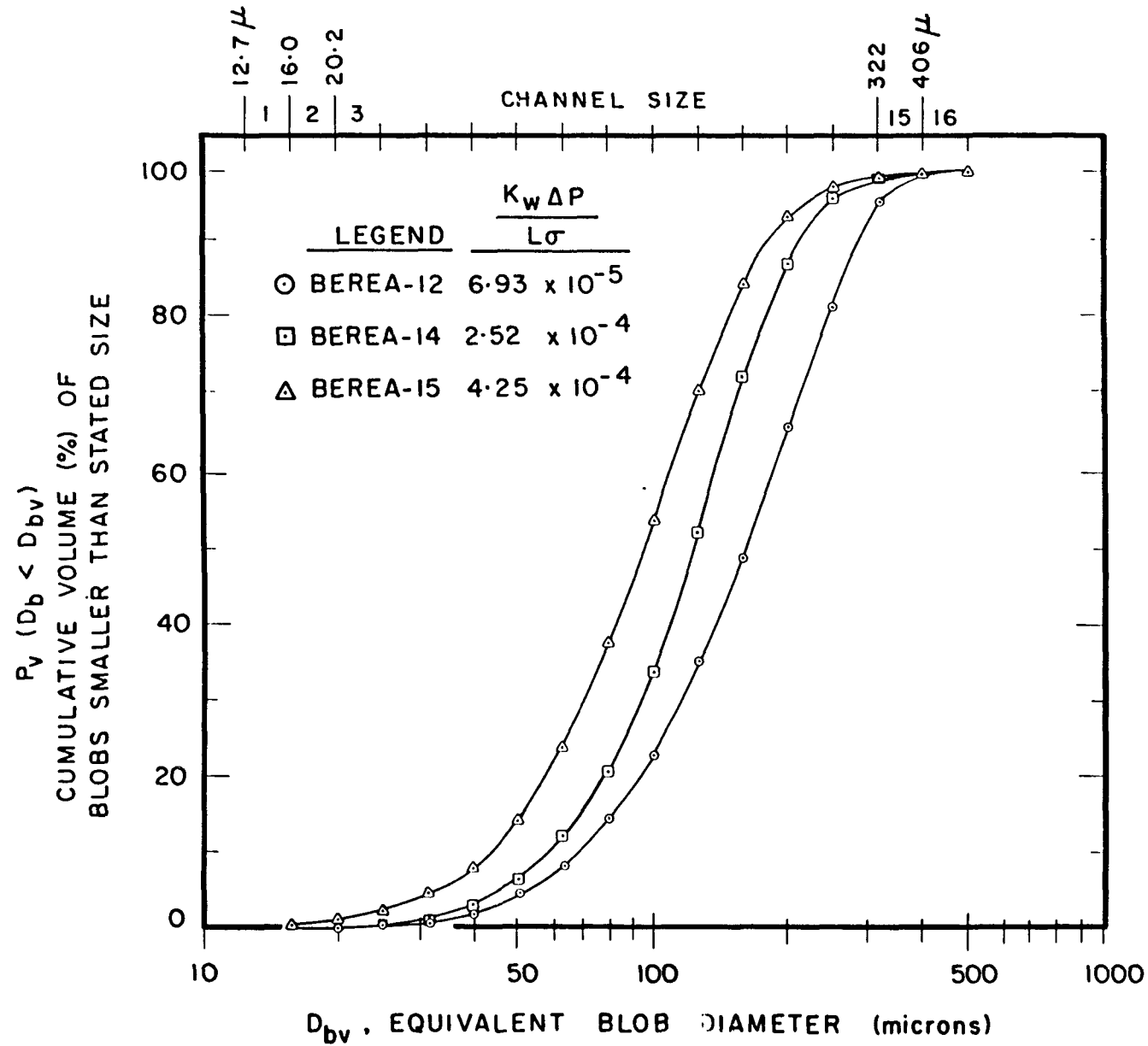
Fig. 4.20. Effect of capillary number on blob-volume distributions of residual oil in Berea sandstone samples.

Fig. 4.21. Effect of capillary number on scaled volume distributions of residual oil blobs trapped in Berea cores of similar properties.
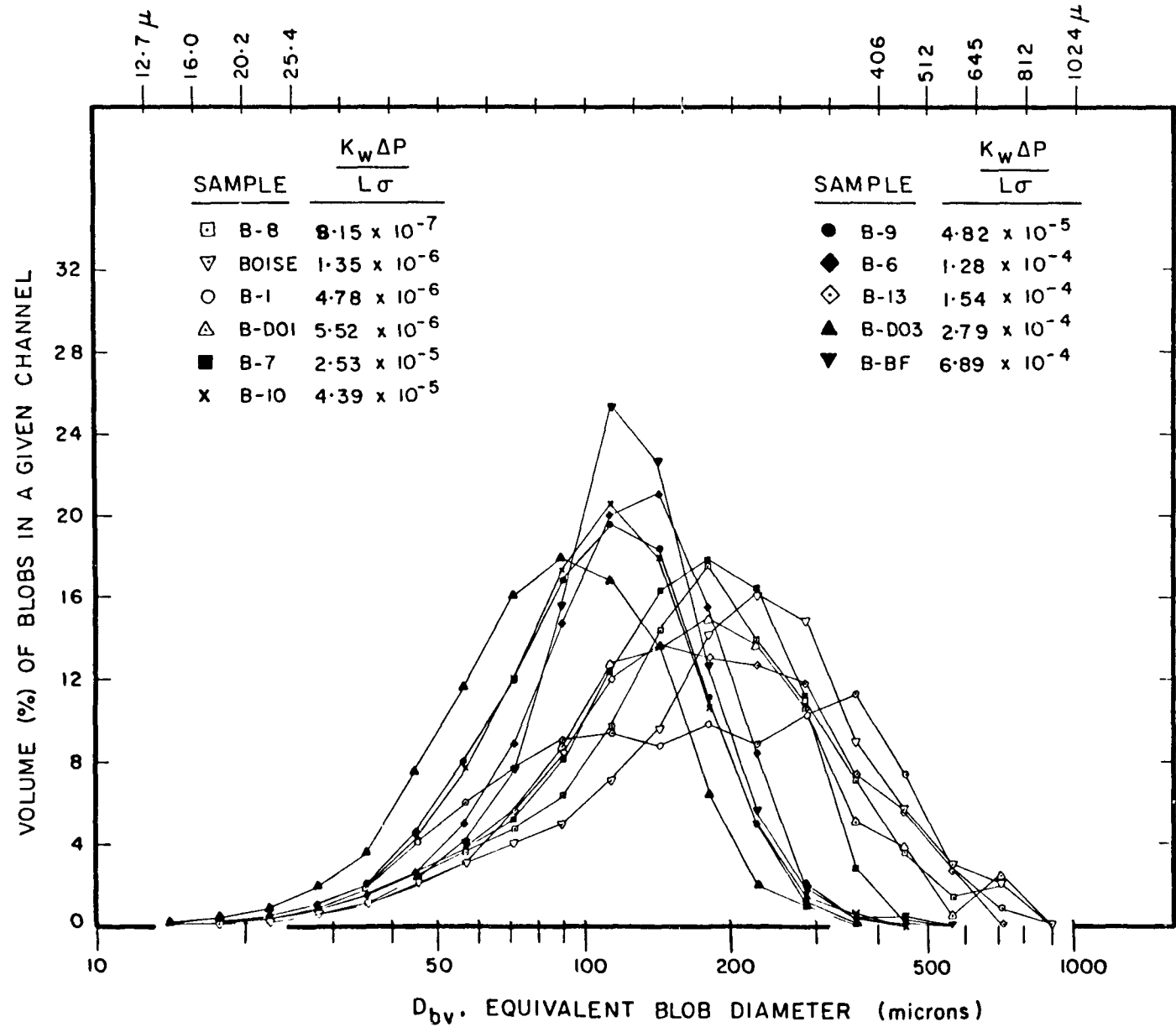
Fig. 4.22. Differential volume distributions of residual oil blobs trapped in several sandstone cores.

ACKNOWLEDGEMENT